Ref. Ares(2025)5062245 - 25/06/2025

CrossEU

D2.2- Key findings in CCHs and STLs

WP2 - Task 2.2
June 2025

Funded by the European Union

Disclaimer

Funded by the European Union. Views and opinions expressed are however those of the author(s) only and do not necessarily reflect those of the European Union or European Climate, Infrastructure and Environment Executive Agency (CINEA). Neither the European Union nor the granting authority can be held responsible for them.

UK participants in this project are co-funded by UK Research and Innovation

Project Acronym	CROSSEU
Project Name	Cross-sectoral Framework for Socio-Economic Resilience to Climate Change and Extreme Events in Europe
Grant Agreement Number	101081377
Project Coordinator	Administrația Națională de Meteorologie R.A. (MeteoRo)
Project Duration	January 2024 – December 2026
Website	www.crosseu.eu

Deliverable No./Milestone No	D2.2
Dissemination Level	Public
Work Package	W2
Lead beneficiary	Technical University of Denmark (DTU)
Author(s)	DTU: Kirsten Halsnæs, Katrine Ødum Nielsen, Kaija Jumppanen Andersen MeteoRo: Roxana Bojariu, Argentina Nertan, Liliana Velea, Irina Ontel, Dana Micu, Monica Paraschiv, Vlad Amihaesei UNIPD: Cristiano Franceschinis, Giovanna Piracci EDF: Sandrine Charousset, Boutheina Oueslati UB: Mihai Adamescu, Relu Giuca CZU: Falak Naz, Tugba Dogan HEREON: Oliver Bothe, Paul Bowyer BOKU: Erwin Schmid, Hermine Mitter, Katrin Karner, Verena Kröner UCL: Alvaro Calzadilla, Zein Khraizat WEMC: Kristian Nielsen
Reviewed by	DTU: Per Skougaard Kaspersen, Shreya Some

Funded by the European Union

	MeteoRo: Sorin Cheval, Laurentiu Ciuhu, Cristina Plescan UNIPD: Mara Thiene, Marco Borga K&I: Gabriele Quinti BOKU: Katharina de Melo UB: Constantin Cazacu, Denisa Igescu CZU: Aleš Urban
Date	25 June 2025
File Name	CROSSEU_ D2.2 – Key findings in CCHs and STLs _v01_25062025_DTU

Table of Contents

List of figures

Funded by the European Union

Funded by the European Union

List of Tables

Executive Summary

This deliverable (D2.2) applies the methodological framework developed in D2.1 to eight Case Study Areas (CSAs), in order to assess the socio-economic risks and impacts of climate change across geographical areas in Europe. These geographical areas, referred to as Climate Change Hotspots (CCHs) exhibit pronounced vulnerability to climate-induced physical, economic, and social pressures. In combination with the hotspots, Event-Based Storylines (STLs) provide a narrative of the plausible future events that combine projected climate change trends with socio-economic developments. As such, using the framework, each CSA dive into different risks - such as heatwaves or flooding - and consider how these risks might develop over the period 2000-2100. These findings inform the strategic directions for climate-change mitigation while enhancing the understanding of the near-term hazards facing Europe.

Keywords

Capability approach, Climate change, climate change hotspots, climate resilience, climate adaptation and mitigation, cross-sectoral, climate change impact, consequences, event-based storylines, methodology, socio-economic impacts and risks, vulnerability

Abbreviations and acronyms

Acronym	Description
AHP	Analytical Hierarchy Process
AWU	Annual Work Unit
CCHs	Climate Change Hotspots
CE	Choice Experiment
CHI	Composite Climate Hazard Index
CINEA	European Climate, Infrastructure and Environment Executive Agency
CMIP	Coupled Model Intercomparison Project
CPM	Convection-Permitting Model
CSA	Case Study Area
ENGAGE	Environmental Global Applied General Equilibrium
EPIC	Environmental Policy Integrated Climate
ESPON	European Spatial Planning Observation Network
EU	European Union
FIGARO	Full International and Global Accounts for Research in Input-Output Analysis
GCM	Global Climate Model
GTAP	Global Trade Analysis Project
IMF	Integrated Modelling Framework

MEV	Metastatistical Extreme Value
MNL	Multinomial Logit
NUTS	Nomenclature of Territorial Units for Statistics
OECD	Organisation for Economic Co-operation and Development
RCM	Regional Climate Model
RCP	Representative Concentration Pathway
SDGs	Sustainable Development Goals
SMEV	Simplified Metastatistical Extreme Value
SSP	Shared Socioeconomic Pathway
STLs	Storylines
WMO	World Meteorological Organization
WP	Work Package
WTP	Willingness-To-Pay
scPDSI	Self-calibrating Palmer Drought Severity Index

Graphical abstract

Deliverable 2.2. Key findings in CCHs and STLs

Scope

The purpose is to address the socio-economic risks of climate change by means of sectoral climate change hotspots and event-based storylines.

Focus

- Application of the methodological framework developed in CROSSEU Deliverable 2.1
- Each case study area (CSA) addresses a climate change hazard in one or more selected regions across Europe (i.e. the CCHs). These hazards are analysed in connection with an extreme event (STL)
- The CSA will consider the physical climate-related and socio-economic projections of an event

Climate Change Hotspots (CCHs)

The deliverable takes departure in geographical hotspots that are especially vulnerable to extreme events and which provide indications of the multifaceted consequences of climate change.

Highlights

- The CSAs imply a substantial increase in climate hazard impacts in the period 2025-2100.
- D2.2. highlights spatial heterogeneity in projected changes as well as heterogeneity in willingness-to-pay
- Extremities of today likely becomes a new normal in the future

Case studies

The deliverable considers 8 primary CSAs that pose a risk for each CCH.

1. Heat
2. Drought
3. Storm
4. Flood
5. Snow
6. Cross-sectional
7. Power systems
8. Global agriculture

Conclusions

CROSSEU CSAs undertake a detailed climate hazard risk assessment at NUTS 3 levels for Europe. They provide information about how physical and socioeconomic risks could develop from the present to 2100 in areas that have been identified by IPCC AR7 as high risk.

Links to other deliverables

- Task 1.5 (D1.6 and D1.7)
- Tasks 2.1, 2.3 and 2.4 (D2.1, D2.3-D2.6)
- Tasks 4.1 and 4.5 (D4.1, 4.7-4.9)

Funded by the European Union

1. Introduction

The purpose of Deliverable 2.2. is to address the socio-economic risks of climate change by means of sectoral climate change hotspots and event-based storylines. Deliverable 2.2. builds on the methodological framework presented in Deliverable 2.1, which is shortly reintroduced in section 1.1. Deliverable 2.2. considers the CROSSEU Case Study Areas (CSAs) that provide a detailed climate hazard risk assessment at NUTS 3 levels for Europe. The CSAs will provide information on the physical and socioeconomic risks that can arise over the period 2000-2100. Hence, the findings go beyond the IPCC Seventh Assessment Report AR7 Working Group II Climate risks and Adaptation (IPCC, 2022). The CSAs are described in Table 0. Each CSA will take account of specific geographical areas and socio-economic sectors, referred to as Climate Change Hotspots (CCHs) using Storylines (STLs).

***Table 0**: Overview of case study areas and chosen hotspots.*

Case Study	Area	Description of CCHs and STLs
1 Heat	Czech Republic	The CCHs are Prague and the Southern Moravia Region of the Czech Republic. The STL context is the record-breaking heatwave period (2010-2019), which highlights the importance of assessing the adaptive capacity of health sectors.
2 Drought	Austria	CCHs are narrowed down to five regions within Germany, the Czech Republic, Poland, Romania, and Austria. The STL relates to the increased frequency and intensity of drought in Central and SE Europe, which pose severe environmental and economic challenges.
3 Storm	Denmark and Germany	The CCHs are located in the regions of Southern Denmark and Northern Germany. The STL relates to very high exposure to coastal hazards, both flooding and coastal erosion, which are regularly occurring in the cities and regions located in the Northern part of Europe.
4 Flood	Italy	The CCH is located in the valley areas of the Trentino-Alto Adige region in northeastern Italy. The storyline is based on Storm Vaia, which created extended dry periods and extreme hydrological responses.
5 Snow	European Alps and Carpathians	Six CCHs are chosen of which 3 are in the European alps, and 3 are located in the Carpathian Mountains. The CCHs spread across several countries including e.g. France, Italy, Slovakia, and Poland. Seven major STL events were selected for this case study based on their fatalities and significant impacts on communities, tourism infrastructure, transport routes, and forest areas.
6 Indirect	Romania	The CCH is the lower Danube region of Romania, which experienced extreme floods and droughts, causing

		damages of above 343 mEUR (STL). The STL gives insights into cross-sectoral multi-hazard risks.
7 Indirect	France	The CCH is the geographical area of France, while the STL is focusing on the prolonged events of extreme weather that affects the power system including relationships to the European power systems.
8 Spillover	United Kingdom	The CCH of this study relates to how climate change impacts the global agricultural system and the effects it has on the UK and EU27, with a focus on subnational-level analysis. The STL considers the projected effect of climate change on agricultural systems and the inherent uncertainty related to these effects.

1.1. D2.1 The common methodological framework for case studies

By means of D2.1, each CSA will assess the socio-economic risks and impacts using a 6-step method. The method is depicted in Figure 0. The methods and assumptions that are deployed in this delivery have been described in relation to the four primary steps of the methodological framework, namely:

Step 1 Climate and socioeconomic scenario

Step 2 Spatial data integration

Step 3 Impact assessment

Step 4 Risk assessment

Step 1 captures both the physical climatic projections as well as the socio-economic projections using climate models and scenario analysis. Based on the results of step 1, step 2 develops a geographical representation of the socio-economic activities and land use for instance using GIS modelling. Step 3 studies the physical and socio-economic impact on sectors and geographical location, based on the information generated in step 1 and 2. The impact assessment can be conducted using different analytical approaches such as a cost-benefit analysis or a cost effectiveness analysis. Finally, step 4 measures the overall climate risk associated with each CSA and thus lays the foundation for the adaption options and decisions support of step 5 and 6.

Funded by the European Union

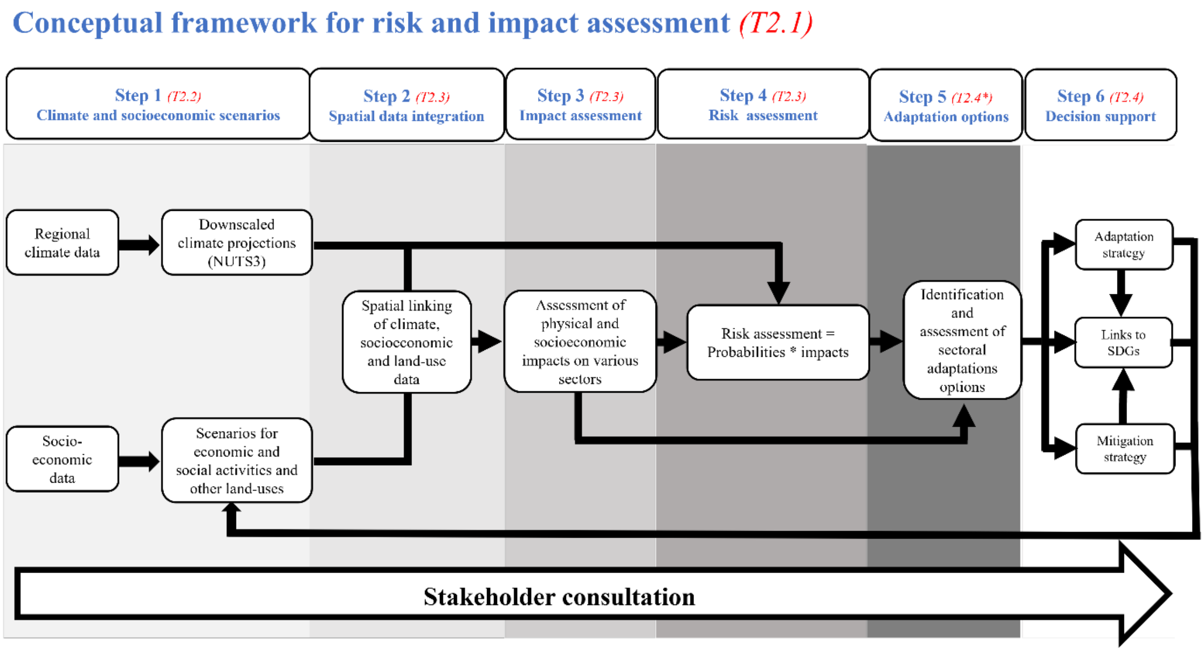

Figure 0: *Conceptual framework for risk and impact assessment as described in Deliverable 2.1 (ref).*

1.2. Case study results were reported in relation to STLs and Hot Spots

Climate Change Hotspots (CCHs) represent specific geographical areas experiencing significant climate change impacts in terms of physical, economic, and social impacts within storylines. Storylines (STLs) are narratives of plausible future events that combine projected climate change trends with socio-economic developments. The STLs answer the following questions (i) what would be the local socio-economic, social, and bio-geophysical impacts if the specific observed high-impact extreme events happened and were amplified by different pre-conditions or contexts; (ii) What are the potential consequences of similar extreme events occurring in different CCH areas; (iii) What could be the impact of similar future extreme events under different socioeconomic scenarios. STLs help to explore the potential consequences of climate change within the CCHs in a tangible and relatable way. Evaluating the socio-economic risks and impacts within CCHs and through the lens of STLs is crucial for understanding the multifaceted consequences of climate change. This includes identifying vulnerable sectors, populations, and regions, and ultimately informing effective adaptation and mitigation strategies. Please refer to Table 0 for an overview of the CCHs and STLs for each CSA. Note that the overview only accounts for the CCHs that are considered in this delivery. The CCHs are chosen in order to capture the implications for areas most vulnerable to climate risks, thus accounting for the hotspots that have been subject to risk-related events in the past years.

Funded by the European Union

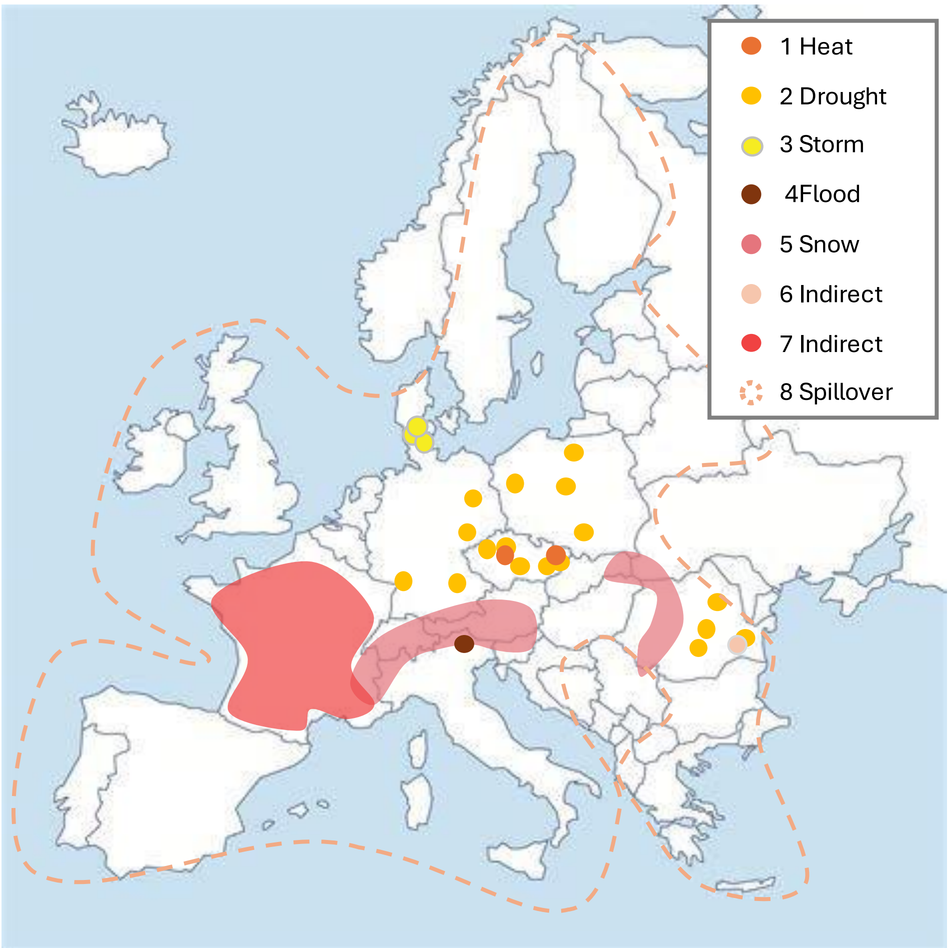

Figure 1: *Overview of Climate Change Hotspots (CCHs). Note that 7Indirect considers both France as its primary hotspot as well as EU27 on a general basis.*

2. Results of the CSA's

2.1. CSA 1 HEAT

2.1.1. Summary of climate change hotspot and event-based storyline

The STL context of the extreme heat case is the record-breaking heatwave period that has been observed across Europe during the recent decade (2010-2019). Attributional studies suggest that the likelihood of occurrence of European heatwaves like the one in 2019 has been 2 to 10 times higher due to climate change (Vautard et al., 2020). These studies compare the contribution of CC to specific events, e.g. by comparing the probability of the occurrence of 2019 EU heatwaves in the present climate compared to a counterfactual scenario (without anthropogenic CC). Increasing frequency and intensity of heatwaves affect human health across Europe, with differences between local areas (van Daalen et al., 2024). For example, a case study from Prague, Czech Republic, suggests that the risk of heat-related mortality in 2010–2019 was twice as high as in the previous three decades (Urban et al., 2022). This finding highlights the importance of assessing the adaptive capacity of health sectors in individual countries while using as recent as possible datasets.

Prague and the Southern Moravia Region of the Czech Republic (both NUTS 3-level regions) are current CCHs regarding the overall heat-related mortality risk relative to other regions in the Czech Republic (Figure 2), based on a study by Jánoš et al. (2023). In addition, recent studies suggest that women and the elderly are most at risk of extreme heat (Figure 3) (Jánoš et al., 2023; Vésier and Urban, 2023).

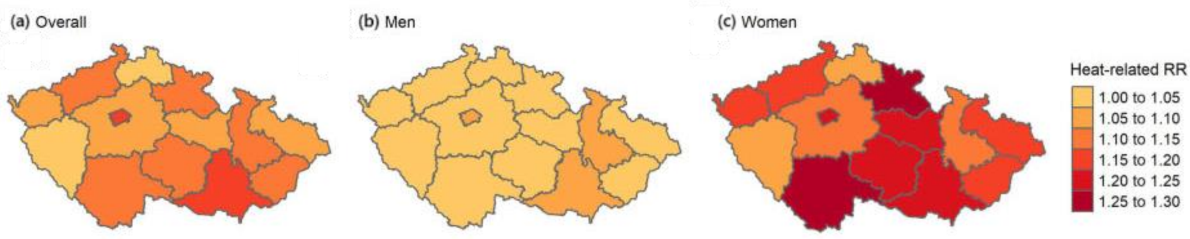

Figure 2: *Spatial variation in heat-related mortality risk in the Czech Republic for (a) overall population, (b) men, and (c) women, 1994–2019 (Jánoš et al. 2023).*

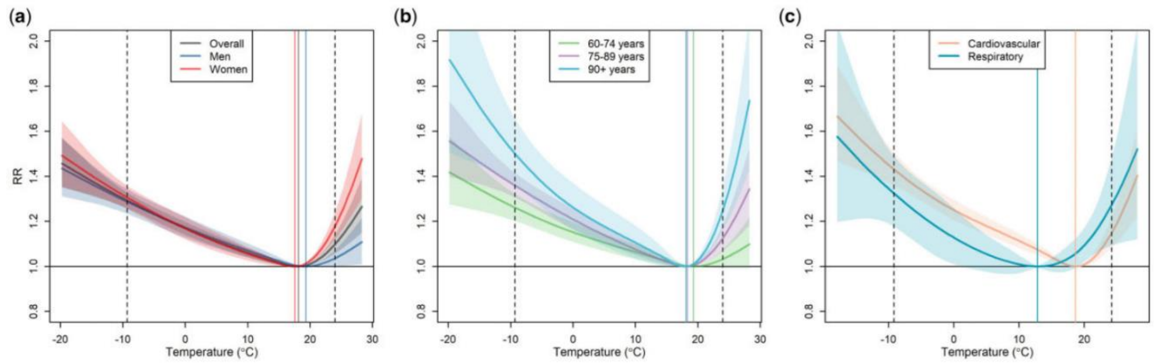

Figure 3: *Temperature–mortality relative risk (RR) associations in the Czech Republic 1994–2019 stratified by (a) sex, (b) age category and (c) cause of death. Dashed vertical lines denote the 1st (cold) and 99th (heat) percentiles of the study period-specific temperature.*

2.1.2. Objectives

The objectives of the case study are as follows:

- Assess historical associations between temperature and mortality in selected population groups at the regional level (NUTS 3) of the Czech Republic.
- Analyze regional spatial differences in the patterns with respect to spatial variations in meteorological and demographic factors.
- Investigate the impact of climate change on regional differences in heat mortality under different climate change and demographic scenarios.

2.1.3. Application of the methodological framework

Step 1 Climate and socioeconomic scenarios

Future changes in associations between daily mean temperature and mortality were studied based on the ensemble mean of high-resolution RCM simulations from the EURO-CORDEX [1] as listed in Table 1. The Representative Concentration Pathways (RCP) 4.5 and 8.5, based on the RCM simulations (Figure 4a), were coupled with population projections (Figure 4b) to consider population aging in the future impact of heat on mortality. Projected population and projected deaths at the NUTS 3 regional level were obtained from the baseline projection of the EUROPOP2019 product by EUROSTAT[2]. The baseline projection assumes no migration, i.e., it includes only region-specific fertility and mortality

[1] https://euro-cordex.net/

[2] https://ec.europa.eu/eurostat/web/population-demography/population-projections/database

Funded by the European Union

projections, while the net migration is set to zero in each year of the entire horizon of projections.

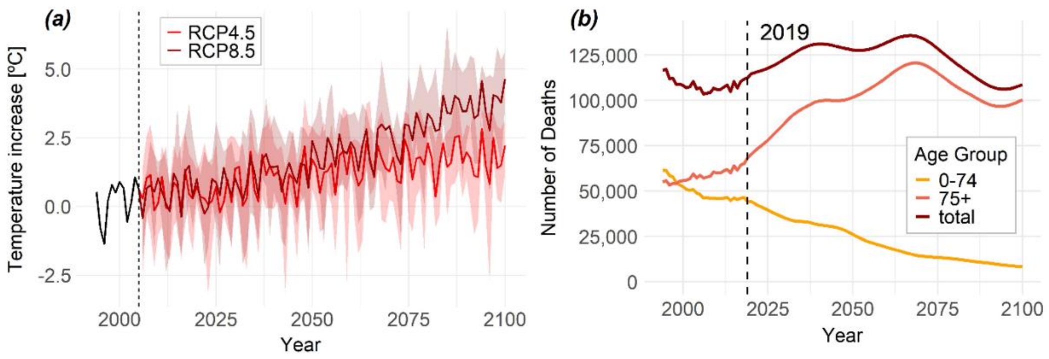

__Figure 4:__ (a) Deviation of annual daily mean temperature development in the Czech Republic under RCP 4.5 and RCP 8.5 scenarios compared to the historical period (1994–2003); (b) The annual number of deaths in the Czech Republic, according to observed data (1994—2019) and the EUROPOP2019 regional population projections (2020–2100).

Combining the two RCP scenarios with the EUROPOP2019 projections, we compared four different scenarios: RCP4.5 - constant population (i.e., no change in the demographic structure), RCP4.5—changing population (based on EUROPOP2019 projections), RCP8.5 - constant population, and RCP8.5—changing population. All scenarios were calculated for four future periods: 2030 (2025–2034), 2050 (2045–2054), 2070 (2065–2064), and 2090 (2085–2094).

__Table 1:__ Characteristics of CMIP5 EURO-CORDEX RCMs simulation ensemble for the selected scenarios (RCP4.5 and RCP8.5)

Driving GCM	Ensemble member	RCM	version-tag
CNRM-CERFACS-CNRM-CM5	r1i1p1	KNMI-RACMO22E	v2
ICHEC-EC-EARTH	r12i1p1	KNMI-RACMO22E	v1
ICHEC-EC-EARTH	r1i1p1	KNMI-RACMO22E	v1
ICHEC-EC-EARTH	r3i1p1	DMI-HIRHAM5	v2
MOHC-HadGEM2-ES	r1i1p1	DMI-HIRHAM5	v2
CNRM-CERFACS-CNRM-CM5	r1i1p1	CNRM-ALADIN63	v2
MOHC-HadGEM2-ES	r1i1p1	KNMI-RACMO22E	v2
NCC-NorESM1-M	r1i1p1	DMI-HIRHAM5	v3
NCC-NorESM1-M	r1i1p1	SMHI-RCA4	v1

Step 2 Spatial data integration

We employed up-to-date mortality datasets from the Czech Republic, providing individual records with information about sex, age, cause of death, and place of residence of the deceased at the NUTS 3 level during the period 1994–2020 (provided by the Institute of Health Information and Statistics and the Czech Statistical Office). Daily mean temperature time series for each NUTS 3 region during the observational period were calculated as a spatial mean of relevant grid points of the ERA5 reanalysis (Hersbach et al., 2023). Regional-specific daily mean temperature in the future scenarios was calculated as a spatial mean of relevant grid points of the EURO-CORDEX datasets.

Step 3-4 Impact and risk assessment

The analysis was conducted using a three-stage study design following the state-of-the-art methodology (Sera et al. 2019, Vicedo-Cabrera et al. 2019). Each stage is described separately below. To analyze the effect of demographic changes on the projections of heat-attributable mortality risk, mortality data were divided into two age groups: 0-74 and 75+ years old.

Stage 1

In the first stage, the relative risk of temperature-related mortality for individual NUTS 3 regions and selected population groups (e.g., 0-74 and 75+ yrs.) in the reference historical period (1994–2003) was identified using generalised additive models with a quasi-Poisson distribution family (Wood 2006; the R package mgcv) adjusted for non-meteorological factors such as the long-term, seasonal, and weekly mortality patterns. The short-term association between temperature and mortality adjusted for the non-meteorological effects was modelled via a distributed lag non-linear modelling framework (Gasparrini, Armstrong, & Kenward, 2010). The model specification and parametrization were based on previous studies (e.g., Sera et al. (2019) or Vicedo-Cabrera et al. (2019)).

Briefly, the temperature-mortality relationship was modelled with a cross-basis function, using a quadratic B-spline with three internal knots placed at the 10th, 75th, and 90th percentiles of the region-specific temperature distribution and a natural cubic spline with three internal knots equally distributed on a logarithmic scale over 21 days of lags. The overall exposure-response function was then reduced into a one-dimensional overall cumulative exposure-response curve, which expresses the region-specific relative risk (RR) of mortality vs. the region- and/or population-group-specific minimum mortality temperature (MMT).

Stage 2

In the second stage, the exposure-response associations from individual regions were pooled to an overall temperature-mortality association for the whole country (and selected population groups), using a multivariate meta-regression framework (Sera et al., 2019). This approach enables us to capture the heterogeneity between the study locations given by the different sizes of statistical samples and thus obtain robust country-wide effects. The meta-regression modelling framework also allows for modelling temperature-mortality associations in multiple locations while considering the effects of potential geographical, socioeconomic, and demographic characteristics in one model. Thus, areas with small mortality counts can borrow information from larger populations with similar characteristics, which allows for improved estimates of the temperature–mortality associations (exposure-response functions - ERFs) in each region and population group (Gasparrini et al., 2012), called best linear unbiased predictions (BLUPs).

Stage 3

In the third stage, the region-specific BLUPs from Stage 2 were combined with climate and population scenarios in order to estimate the spatio-temporal changes in the impact of high temperature on mortality in the Czech Republic. Specifically, the heat-attributable mortality fraction (excess mortality) associated with climate and demographic changes in the Czech Republic was calculated as the percentage of deaths on days hotter than the region-specific MMT attributable to the temperature effect. Finally, the heat-attributable fraction was used to calculate annual heat-attributable deaths for each of the 14 NUTS 3 regions, RCP scenarios (RCP 4.5 and 8.5), and periods (historical, 2030s, 2050s, 2070s, and 2090s) as defined above. The future RCP scenarios were combined with two demographic scenarios, without (future constant pop) and with (future changing pop) consideration of the changing demographic structure. To ensure that the trend and variability of the original data are preserved by adjusting the cumulative distribution of the simulated data to the observed one, the temperature time series obtained from the RCP scenarios were calibrated with the observed data using the bias-correction method developed within the Inter-Sectoral Impact Model Intercomparison Project (Hempel et al., 2013).

2.1.4. Results

Czech Republic overall

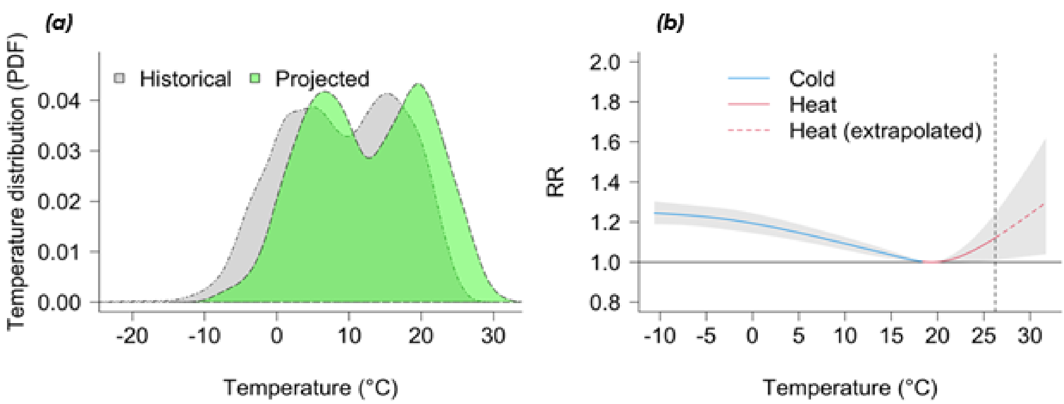

Figure 5: *(a) Change in the distribution of daily mean temperature between and (b) The relative risk (RR) of mortality in the Czech Republic for the historical (1994–2003) and projected (2091–2100, RCP 8.5) periods in the Czech Republic for the constant population demographic scenario. The red*

part of the exposure-response curve indicates heat-attributable RR (above the minimum mortality temperature threshold) for the historical and projected (extrapolated) periods.

Figure 5a suggests that, based on the ensemble mean of the RCMs defined in Table 1, the annual mean temperature will increase by approximately 4.1 °C in the Czech Republic by the end of the century (2091–2100, RCP 8.5). This warming will be associated with a more than threefold increase (from 5 to 17%) in the proportion of hot days (days with daily mean temperature above the 95th percentile of its distribution over the reference period; 21.3 °C) compared to the present climate (historical). This will also result in a shift in the pooled temperature-mortality association (RR) when comparing the present (full line) and future (dashed line) climate (Figure 5b). Specifically, under the RCP 8.5 pathway combined with the constant population demography scenario, the model estimates an 11.1% increase in the RR at the 99th percentile of the daily mean temperature distribution (from RR = 1.05 [95 % CI 1.00–1.10] historically to RR = 1.17 [95 % CI 1.02–1.34] in the future) relative to the historical MMT.

Figure 6 presents the future heat-related mortality burden estimates for the Czech Republic as a whole. Our results suggest that, by the end of the century (2090s), the annual heat-attributable burden will be equal to approx. 1500 annual deaths (for RCP 8.5, changing population), compared to 290 heat-attributable deaths in the present climate (historical). This is equivalent to the 1.5% heat-attributable mortality fraction (AF%) by the end of the century in comparison to 0.9% in the present climate. The burden of the RCP 4.5 scenario is approximately half compared to RCP 8.5.

A comparison of the two demographic scenarios (future constant vs. future changing population) indicates that the countrywide burden of heat-attributable mortality due to climate change will be aggravated by 20% as a result of population aging, averaged over the four future periods. The additional burden of demographic changes is projected to be largest in the 2070s, which is in line with the peak of projected deaths in the Czech Republic (Figure 4b).

Funded by the European Union

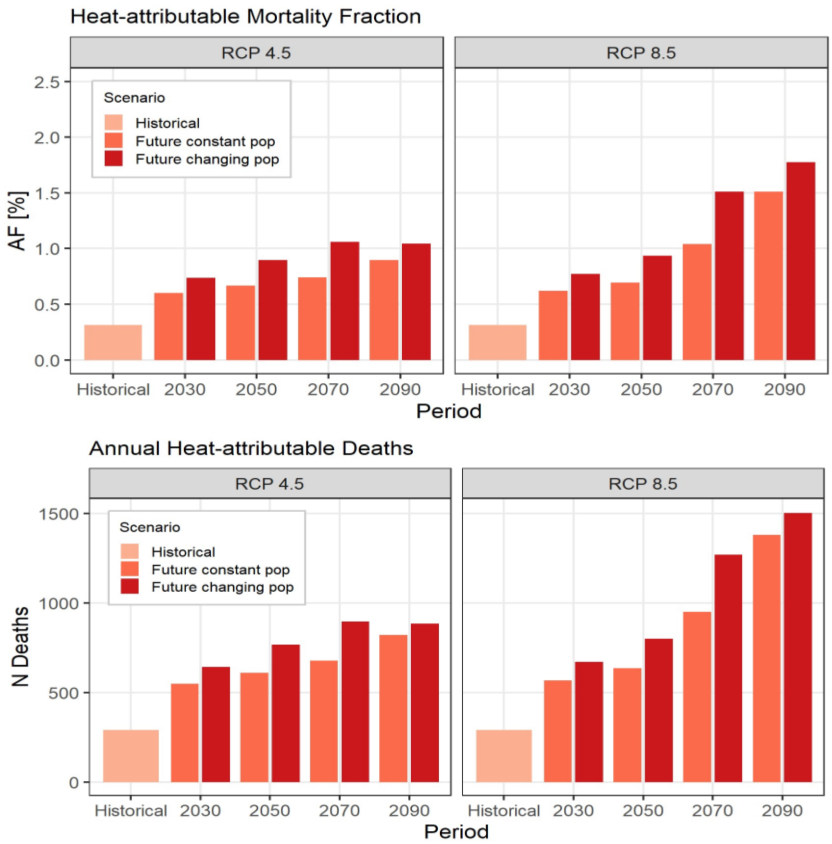

Figure 6: *Historical and future distribution of heat-attributable mortality fraction (AF in % - top row) and heat-attributable deaths (bottom) in the Czech Republic under RCP 4.5 (left) and RCP 8.5 (right) scenarios, with (future constant pop) and without (future changing pop) population aging, respectively.*

Spatial distribution in heat-attributable mortality

In Figure 7, according to a comparison mapping of the heat-attributable percentage (AF%) across historical, constant, and changing population scenarios, heat-related mortality is projected to increase across the Czech Republic, with notable regional variations. With most regions observing record values around 1.0%, the historical AF% shows a comparatively modest baseline burden, indicating minimal previous mortality attributed to heat (Figure 7a). AF% rises somewhat in the constant population scenario, which assumes solely climatic change, with several regions, particularly in the southeast, reaching between 1.5% and 2.0% (Figure 7b). The AF% increases more noticeably when shifting population dynamics, such as aging and regional demographic trends, are considered; in some regions, it is currently more than 2.5% (Figure 7c). The ratio maps further illustrate these changes, showing that under the constant population scenario, AF% increases by up to a factor of 5 compared to historical levels (Figure 7d). In contrast, under the changing population scenario, AF% rises by a factor of 10, particularly in the central and northern regions of the country (Figure 7e). In certain regions, population aging alone can nearly triple the burden of heat-related events, as evidenced by the changing-to-constant ratio results (Figure 7f).

Moreover, according to future projections (2070), Prague and South Moravia (highlighted in Figure 7) stand out as severe hotspots that are consistent in this regard. When compared to its historical value of only 0.8%, Prague's heat AF% rises significantly to about 2.7% under the changing demographic scenario, signifying a more than twofold increase in attributable mortality. Likewise, South Moravia's AF% is 2.6%, which is about 2.3 times higher than its historical rate of 0.9%. This increase is supported by the shifting population ratio results: compared to their constant population scenarios, heat-mortality burden is aggravated by 7 and 38% in Prague and South Moravia, respectively, due to population aging (Table 2).

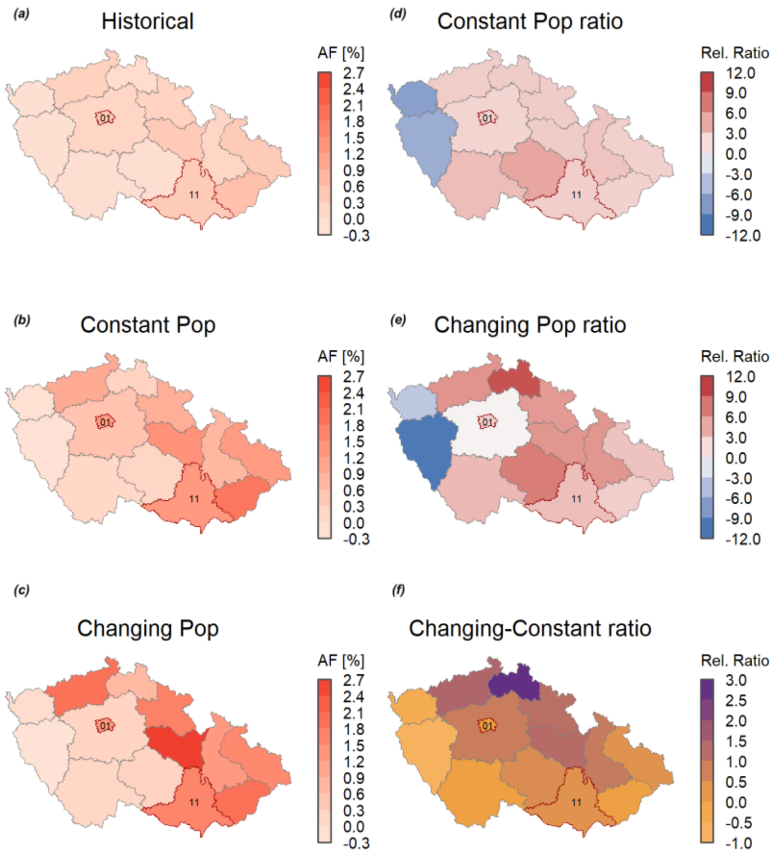

Figure 7: *Left-hand panels (a-c): Historical and future (2070s) spatial distribution of heat-attributable fraction in the Czech Republic under RCP 8.5 scenarios, with and without population aging, respectively. Right-hand panels (d-f) represent relative ratios between Historical and Constant Pop (Constant Pop ratio), Historical and Changing Pop (Changing Pop ratio), and between Changing and Constant Pop (Changing–Constant ratio). 01 = Prague, 11 = South Moravia*

Heat-attributable mortality patterns in CCHs

Figures 8 and 9 and Table 2 present the future patterns in heat-attributable mortality in Prague and South Moravia in more detail. The regional patterns follow the countrywide heat-related mortality burden as presented in Figure 6. However, additional results on the heat-related risk in individual age groups (0–74 and 75+ yrs.) highlight the important role of demographic changes in future projections. While the younger population group (0–74 yrs.) showed an increased mortality burden associated with both RCP 4.5 and RCP 8.5 if the future constant pop scenario was considered, the future changing pop scenario suggests a decreasing impact of heat on mortality in this age group. For the older population group (75+ yrs.), on the contrary, the changing population scenario estimates a gradually increasing mortality burden due to heat compared to the constant population scenario. However, the sum of these two age groups resulted in different trends, depending on the population projections in the given regions. Therefore, while results for Prague suggested a weakened heat-mortality burden due to population aging by 10% (averaged over the four future periods), heat-related mortality in South Moravia is estimated to be aggravated by 26%. Nevertheless, results for both confirm the peak in the effect of population aging on heat-related mortality in the 2070s (Figure 7).

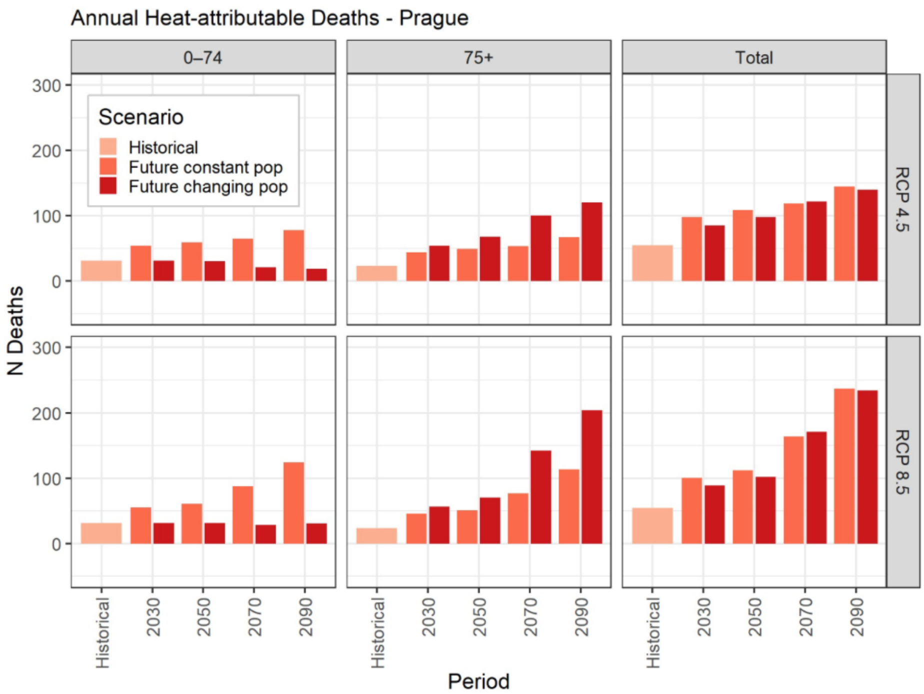

Figure 8: *Historical and future distribution of annual heat-attributable deaths in Prague, Czech Republic, under RCP 4.5 and RCP 8.5 scenarios, with (future constant pop) and without (future changing pop) population aging, stratified by age (0-74 yrs., 75+ yrs., and total population).*

Funded by
the European Union

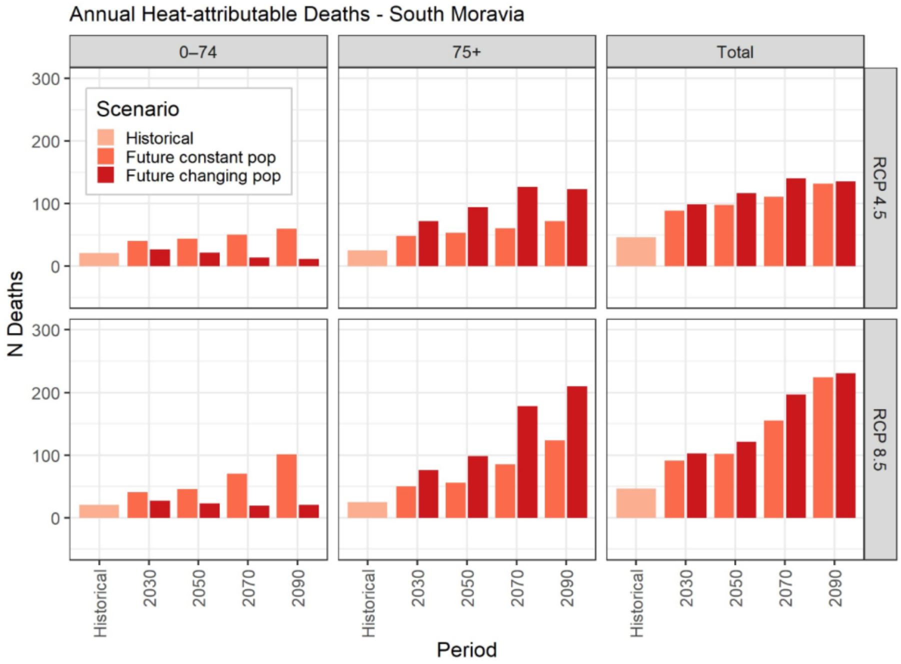

Figure 9: *Historical and future distribution of annual heat-attributable deaths in South Moravia, Czech Republic, under RCP 4.5 and RCP 8.5 scenarios , with (future constant pop) and without (future changing pop) population aging, stratified by age (0-74 years old, 75+ years old, and total population).*

Funded by the European Union

Table 2: *Historical and future distribution of annual heat-attributable deaths (AN), absolute change (AN change vs. Hist.), relative change (AN [%] change vs. Hist.), and relative change (AN change [%]) in AN between scenarios with changing (future changing pop) and constant (future constant pop) population in Prague and South Moravia, under the RCP 8.5 scenario, for four future periods.*

Total									
Variable	**Scenario**	**Prague**				**South Moravia**			
		2030	**2050**	**2070**	**2090**	**2030**	**2050**	**2070**	**2090**
AN	Historical	55	55	55	55	46	46	46	46
	Future constant pop	101	112	164	237	91	102	155	224
	Future changing pop	89	102	171	234	103	121	197	230
AN change vs Hist.	Future constant pop	46	58	109	182	45	56	109	178
	Future changing pop	34	47	116	180	57	75	151	184
AN change [%] vs Hist.	Future constant pop	84	105	199	334	97	120	236	385
	Future changing pop	62	86	213	329	123	162	326	398
AN change [%]	Future changing vs Future constant	-26	-18	7	-2	26	35	38	4
0–74 yrs.									
Variable	**Scenario**	**Prague**				**South Moravia**			
		2030	**2050**	**2070**	**2090**	**2030**	**2050**	**2070**	**2090**
AN	Historical	31	31	31	31	21	21	21	21
	Future constant pop	55	61	87	124	41	46	70	101
	Future changing pop	32	32	29	30	27	23	19	21
AN change vs Hist.	Future constant pop	24	30	56	93	20	25	49	80
	Future changing pop	0	0	-2	-1	6	2	-2	0
AN change [%] vs Hist.	Future constant pop	75	95	178	295	97	118	234	382
	Future changing pop	1	1	-8	-3	31	9	-8	-2
AN change [%]	Future changing vs Future constant	-98	-99	-104	-101	-68	-93	-104	-100
75+ yrs.									
Variable	**Scenario**	**Prague**				**South Moravia**			
		2030	**2050**	**2070**	**2090**	**2030**	**2050**	**2070**	**2090**
AN	Historical	23	23	23	23	25	25	25	25
	Future constant pop	46	51	76	113	50	56	85	123
	Future changing pop	57	70	142	204	76	98	178	210
AN change vs Hist.	Future constant pop	22	28	53	90	25	31	60	98
	Future changing pop	34	47	119	181	50	73	153	185
AN change [%] vs Hist.	Future constant pop	96	120	228	386	98	122	237	387
	Future changing pop	144	202	510	775	199	288	602	729
AN change [%]	Future changing vs Future constant	50	69	124	101	103	137	154	88

2.1.5. Challenges and conclusions

Climate change impacts like the escalating intensity, frequency, and duration of warm extremes (i.e., heatwaves) have been identified as a direct and potent threat to human health that require to urgently quantify the associated health burdens. The results of our present analysis suggest that the recently observed trend in increasing heat-related mortality burden (Urban et al. 2022) will continue if no adaptation takes place. Specifically, in Prague our findings indicate that by the end of the century (2090s, RCP 8.5), we can expect more than 230 heat-attributable deaths annually, compared to 55 annual heat-related deaths in the 2000s (Historical in Table 2). In some regions of the Czech Republic, such as South Moravia, the burden of heat-related mortality will be substantially aggravated by demographic changes. Therefore, the nationwide heat impact is projected to increase from the current 290 to as many as 1500 annual heat-related deaths by the 2090s (RCP 8.5). In addition to climate change, these shifts are caused by aging populations, making the health effects of heat more serious.

Our findings suggest that estimates of the future mortality burden associated with extreme temperature events are highly sensitive to demographic changes within regions. In addition, both intra- and inter-national migration will likely alter future population distributions and exposure patterns. To account for these dynamics, follow-up analysis will integrate alternative population scenarios based on migration storylines informed by the Shared Socioeconomic Pathways (SSPs), allowing for more nuanced and policy-relevant projections.

Several research steps are being planned to continue this work:

- Finalizing the current modelling framework, making it transferable to other case studies.
- Incorporating additional socioeconomic indicators into the modelling framework, to better capture the regional differences in heat–vulnerability.
- Extending the approach to additional geographic regions, particularly in London (UK), and upscaling it to the European level to support comparative risk assessment and adaptation planning.

The results and improvements to the analysis will be part of follow-up deliverables, namely Deliverable D2.3 (with a due time in Month 24 of the project). This will assist evidence-based initiatives for climate adaptation and public health resilience in Europe by advancing a more comprehensive understanding of the human and social dimensions of climate-related vulnerabilities.

2.1.6. References

Gasparrini, A., Armstrong, B., & Kenward, M. G. (2010). Distributed lag non-linear models. Statistics in medicine, 29(21), 2224-2234.

Gasparrini, A., Armstrong, B., & Kenward, M. G. (2012). Multivariate meta-analysis for non-linear and other multi-parameter associations. Statistics in medicine, 31(29), 3821-3839.

Hempel S, Frieler K, Warszawski L, Schewe J, Piontek F. (2013). A trend-preserving bias correction – the ISI-MIP approach. Earth Syst Dynam. 4, 219–236.

Hersbach, H., Bell, B., Berrisford, P., Biavati, G., Horányi, A., Muñoz Sabater, J., Nicolas, J., Peubey, C., Radu, R., Rozum, I., Schepers, D., Simmons, A., Soci, C., Dee, D., Thépaut, J-N. (2023): ERA5 hourly data on single levels from 1940 to present. Copernicus Climate Change Service (C3S) Climate Data Store (CDS).

Jánoš, T., Ballester, J., Čupr, P., & Achebak, H. (2024). Countrywide analysis of heat- and cold-related mortality trends in the Czech Republic: growing inequalities under recent climate warming. 53(April 2023), 1–11.

Sera, F., Armstrong, B., Blangiardo, M., & Gasparrini, A. (2019). An extended mixed-effects framework for meta-analysis. Statistics in Medicine, 38(29), 5429–5444.

Urban, A., Fonseca-Rodríguez, O., Di Napoli, C., & Plavcová, E. (2022). Temporal changes of heat-attributable mortality in Prague, Czech Republic, over 1982–2019. Urban Climate, 44, 101197.

Vésier, C., & Urban, A. (2023). Gender inequalities in heat-related mortality in the Czech Republic. International Journal of Biometeorology, 67(8), 1373–1385.

Vautard, R., Van Aalst, M., Boucher, O., Drouin, A., Haustein, K., Kreienkamp, F., Van Oldenborgh, G. J., Otto, F. E. L., Ribes, A., Robin, Y., Schneider, M., Soubeyroux, J. M., Stott, P., Seneviratne, S. I., Vogel, M. M., & Wehner, M. (2020). Human contribution to the record-breaking June and July 2019 heatwaves in Western Europe. Environmental Research Letters, 15(9).

Vicedo-Cabrera, A. M., Sera, F., & Gasparrini, A. (2019). Hands-on Tutorial on a Modeling Framework for Projections of Climate Change Impacts on Health. Epidemiology, 30(3), 321–329.

Vicedo-Cabrera, A. M., Scovronick, N., Sera, F., Royé, D., Schneider, R., Tobias, A., Astrom, C., Guo, Y., Honda, Y., Hondula, D. M., Abrutzky, R., Tong, S., Coelho, M. de S. Z. S., Saldiva, P. H. N., Lavigne, E., Correa, P. M., Ortega, N. V., Kan, H., Osorio, S., … Gasparrini, A. (2021). The burden of heat-related mortality attributable to recent human-induced climate change. Nature Climate Change, 11(6), 492–500.

Wood, S. (2006). Generalized additive models: an introduction with R. Chapman & Hall, London

2.2. CSA 2 DROUGHT

2.2.1. Summary of climate change hotspot and event-based storyline

Event-based storyline (STL)

The STL of the DROUGHT case study relates to the increased frequency and intensity of drought in Central and SE Europe, which pose severe environmental and economic challenges. Significant droughts during the period 2018–2023 lead to impacts on agriculture (e.g., notable yield reductions in key crops such as maize and sunflower (Pinke et al., 2023), forests (defoliation, pest outbreaks, decreased timber yields) (Conradt et al., 2023; Knutzen et al., 2023), and water availability (Hanel et al., 2018), or desertification). These impacts further extended to socio-economic impacts with negative effects on local/national economies, contributing to inflation in food prices and thus affecting food security.

Thus, the activities within this case study focused on analysing in more detail the drought characteristics and impacts in the present and especially in the future climate, aiming to enhance the understanding of the drivers generating bio-physical, economic and societal risks associated with different climate scenarios.

The specific objectives were to (1) assess the features of the physical risks of the 2018–2023 multi-year drought and its potential socio-economic implications in a changing climate; (2) examine socio-economic fluxes that increased competition for land, groundwater resources and rare ecosystems; (3) identify the range of socio-economic drought-related risks and societal interventions that were applied to secure food supply during the post-COVID-19 transformation and geopolitical crises.

Climate change hotspots (CCH)

Although several regions in Central and SE Europe suffered consequences of drought, four regions located in the Czech Republic, Poland, Germany and Romania (Table 3) have been selected as CCH hotspots in CSA 2. These regions have been defined in D2.1 based on the socioeconomic impacts reported in scientific literature and media reports. The climate change signal for these hotspots in the current climate have been further investigated within a new analysis to assure a consistent, homogenous approach for grounding the findings on changes in the context of future climate scenarios. An additional hotspot located in Austria has been introduced (Table 3), providing the opportunity to address in a more comprehensive manner the impact of climate changes on agriculture sector through the inclusion of land management options.

***Table 3:** Selected drought-related hotspots and main impacts of the 2018-2023 drought.*

No.	Country	Regions	Main impacts of the 2028-2023 drought
1	Germany	Brandenburg, Saxony, Bavaria, and Baden-Württemberg	Reduced crop yields, economic losses and environmental degradation
2	Czech Republic	South Moravia, Vysočina Region, Central Bohemia and Ústí and Labem and Pardubice	Water rationing, environmental degradation, reduced crop yields
3	Poland	Central Poland (Łódź and Greater Poland), Western Poland (Lubusz and Lower Silesian), Northern Poland (West Pomeranian), and Southern Poland (Lesser Poland and Silesian)—	High exposure to extreme events, economic reliance on water-dependent sectors, stressed ecosystems and local economies
4	Romania	Dobrogea, Bărăgan Plain, Oltenia Plain and Moldavia	Vulnerability of agricultural systems, limited water supplies
5	Austria	Seewinkel region (Figure 10)	Decline of groundwater table, increased distance to the groundwater table, water quality issues

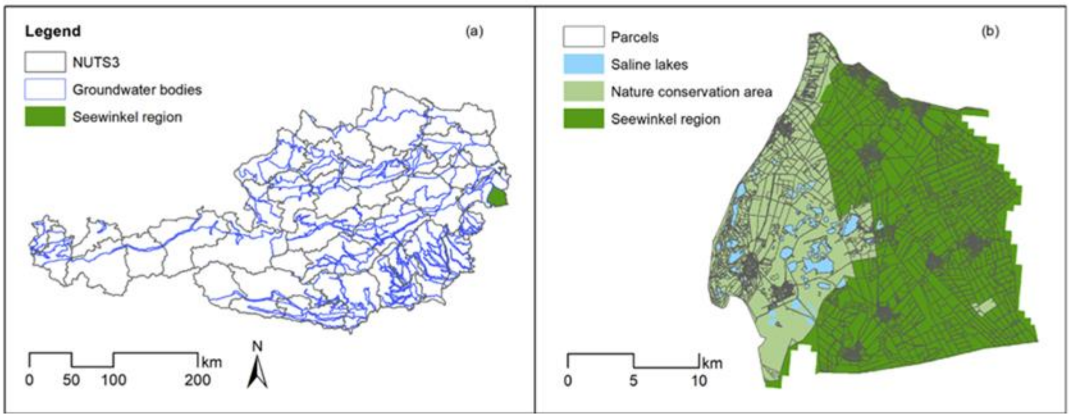

***Figure 10:** Location of the Seewinkel region in Austria (a) and overview of the Seewinkel region (b). Note: The National Park Neusiedler See – Seewinkel is part of the nature conservation area. Source: Own illustration based on BMLFUW (2017), Statistik Austria (2019), Amt der Burgenländischen Landesregierung (2021) and Nationalpark Neusiedler See Seewinkel (2021) (CC BY 3.0 AT).*

The analysis for the present climate scenario aimed to document the drought hazard over the selected hotspots; due to the small area of the Austrian hotspot compared with the other hotspots, the analysis targeted only the hotspots located in the Czech Republic, Poland, Germany and

Romania. This has been performed by using the following climate-related and remote sensing data:

- *Observation-based data*: The self-calibrating Palmer Drought Severity Index (scPDSI; Wells et al, 2004) provided by the Climate Research Unit (CRU) of the University East Anglia (van der Schrier et al., 2013; Barichivich et al., 2024) has been used to characterise the drought-related hazard in the present climate. The drought intensity classes associated with scPDSI values are presented in Table 4. The monthly values from the CRU TS4.08 scPDSI data cover the global land surface, spanning the period 1901–2023 with the spatial resolution of 0.5 x 0.5 degrees. The calibration is made over the complete period 1901–2023 to ensure the representativeness of the full range of climate variability in the context of observed climate change. In this analysis, the hazard metrics used is the linear trends of annually averaged scPDSI, computed in each grid point.

Table 4: *Drought conditions classification using scPDSI values.*

scPDSI values	Drought conditions
0 to -0.5	normal
-0.5 to -1.0	incipient drought
-1.0 to -2.0	mild drought
-2.0 to -3.0	moderate drought
-3.0 to -4.0	severe drought
< -4.0	extreme drought

- *Remote sensing data* in the form of the CDI (Combined Drought Index) (Sepulcre-Canto et al., 2012), developed by the Copernicus European Drought Observatory (EDO https://www.copernicus.eu/en/european-drought-observatory). The data covers the period 2012–2024, with a 10 days temporal frequency and at 5km spatial resolution. The analysis focused on three drought intensity levels "Watch" (early signs of precipitation deficits), "Warning" (significant soil moisture anomalies), and "Alert" (visible vegetation stress) (JRC, 2020) and two periods (2012–2024 and 2019–2024).

The analysis of long-term (1901–2024) scPDSI index shows tendencies for droughty conditions over a large part of the selected hotspots, more pronounced over the central Europe (Figure 11). Focusing on the selected period 2018-2023, the multiannual drought conditions are clearly shown in the map with averaged scPDSI suggesting the presence of droughts from incipient to severe (Table 4) in the four hazard-related hotspots (Figure 12).

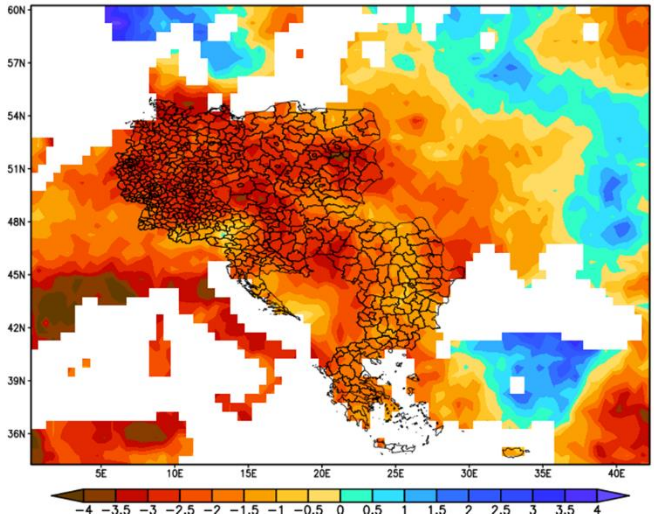

Figure 11: *The tendencies for droughty conditions expressed as the slope coefficients from the linear trend of annual scPDSI multiplied by the number of years (in standardised units; color-shaded) in the period 1901–2023. Black lines illustrate the area of interest at the NUTS 3 level.*

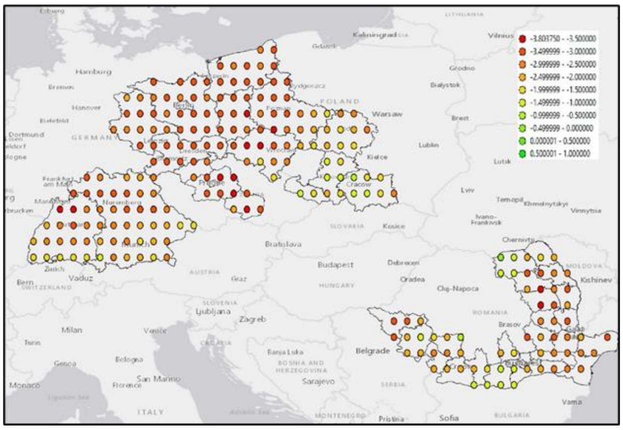

Figure 12: *The multiannual averaged scPDSI values for the period 2018–2023 (standardised units; colored circles) over the selected hazard-driven hotspots. Black lines illustrate the selected hotspots.*

The remote sensing data brings additional support for identifying the drought-related hazard. The analysis highlights the evolution of drought conditions in the selected area, focusing on three drought severity level (CDI 1, CDI 2, and CDI 3) corresponding to the 'Watch', 'Warning' and 'Alert' states (JRC, 2020). The drought frequency map for the period 2012–2024 (Figure 13) points out the areas from the Central and South - Eastern Europe, highlighting limited areas from Romania, Bulgaria, Austria and Germany significantly affected by drought conditions.

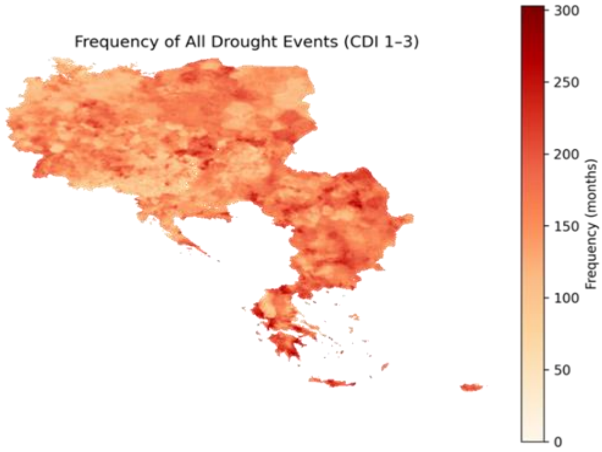

Figure 13: *Drought frequency considering the sum of all intensity levels ('Watch' (CDI=1), 'Warning' (CDI=2), 'Alert' (CDI=3)) in each grid point, expressed as the total number of months during the period 2012-2024.*

The focus at seasonal scale on the recent period 2018-2023 (Figure 14) emphasises a higher frequency occurrence of drought conditions (all intensity levels) during spring and autumn, while in summer the area affected by drought conditions expands in almost the entire study area.

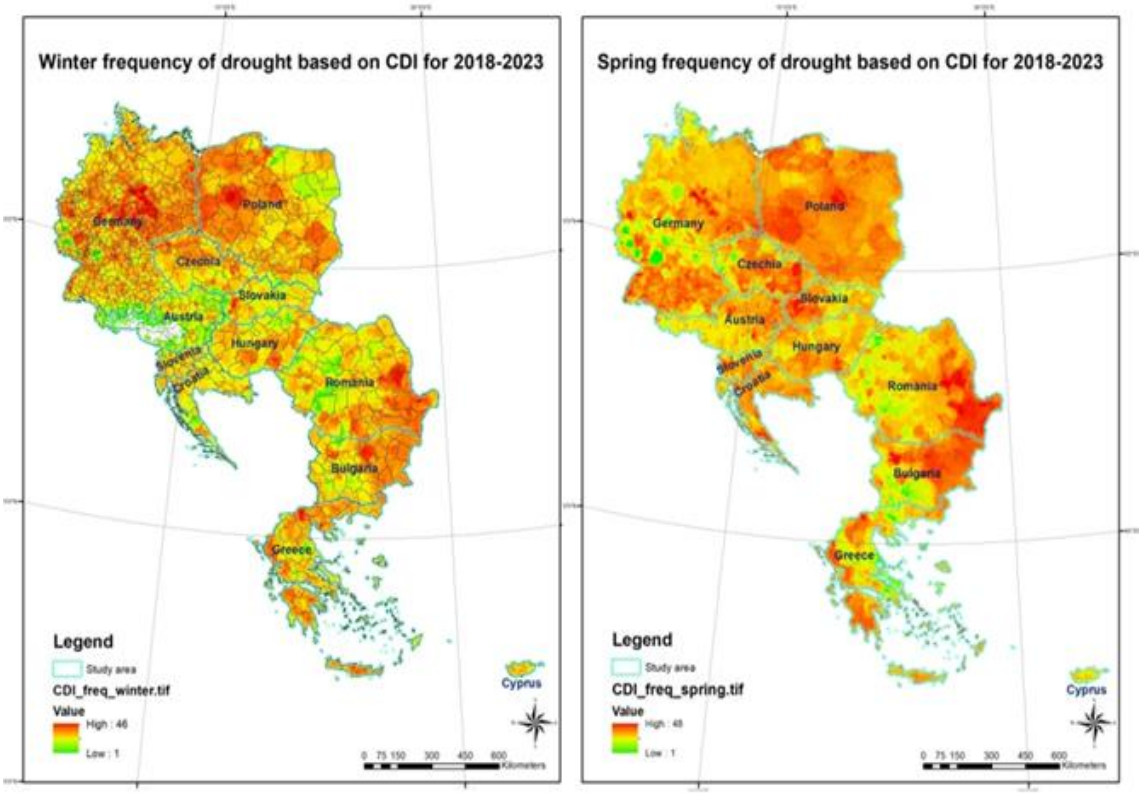

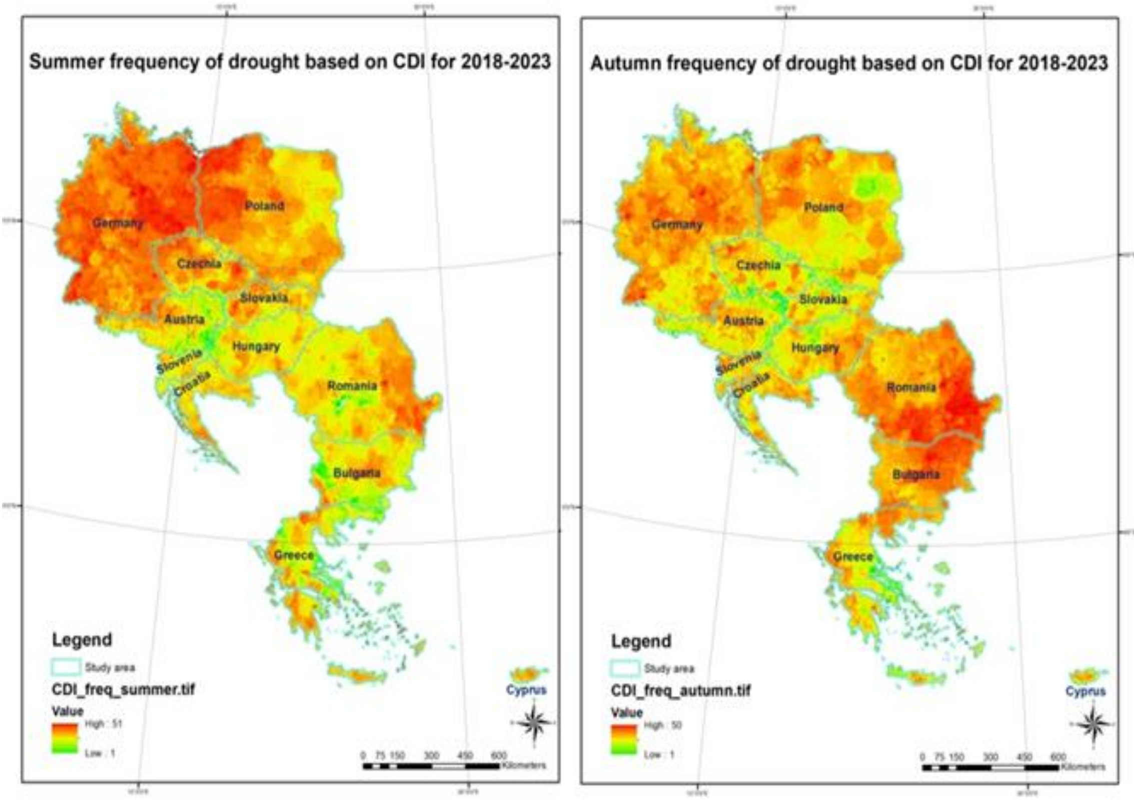

Figure 14: *Seasonal drought frequency considering the sum of all intensity levels ('Watch' (CDI=1), 'Warning' (CDI=2), 'Alert' (CDI=3)) in each grid point, expressed as the total number of months during the period 2018-2023.*

2.2.2. Application of the methodological framework

The project methodology framework is applied in CSA 2 focusing mainly on the agriculture sector, and it is the result of two implementation approaches.

1. The first implementation approach (IMP1) is applied to the four hotspots located in the Czech Republic, Poland, Germany and Romania (Table 3) and selected in D2.1 and it has as final product a risk analysis based on the risk matrix method.
2. The second approach (IMP2) regards exclusively the new Austrian hotspot, introduced in D2.2 and it is based on an integrated modelling framework, which produce information on the drought impacts on agriculture and adaption through crop management options.

The implementation of each approach is detailed in the following.

Step 1 Climate and socioeconomic scenarios

The key research objectives of this step were: (i) understanding the regional climate change (CC) signals under both current and future climate conditions, (ii) elaborating maps of drought-related hazard for the selected time slices in the future climate using specific climate indicators and (iii) understanding the expected socioeconomic effects on some elements at risk (e.g., farmers).

CSA 2 integrates various climate datasets for achieving these research objectives. The data used for future climate is presented in the following.

IMP1: Application for the hotspots located in the Czech Republic, Poland, Germany and Romania

- **Climate scenarios**
  The climate data employed for assessing the hazard component of the risk in the future climate is provided by CMIP5 EURO-CORDEX; the list of CMIP5 EURO-CORDEX simulations used in analysis is shown in the deliverable D6.2. (Data Management Plan – version 2). This data has a horizontal spatial resolution of ~12.5 km (EUR-11) and daily frequency. Two representative concentration pathways (RCP) scenarios have been used, namely RCP4.5 and RCP8.5. The hazard metrics used are: (1) the median changes in the scPDSI index (Wells et al., 2004; Bojariu et al., 2018; Bojariu et al., 2021); (2) changes in the drought intensity classes (i.e., scPDSI < -1). The analysis covers three time periods of interest (2011-2040, 2041-2070, and 2071-2100) for both RCPs, using 1971-2000 as the baseline.
- **Socio-economic scenarios**
  The methodological framework for assessing socioeconomic exposure to drought in the four hotspots selected in D2.1 is based on the current socioeconomic context, with the climate hazard indicator scPDSI representing the only dynamic component.

IMP2: Austrian hotspot introduced in D2.2

The main output of the analysis over the Austrian hotspots relates to the assessment of trade-offs between the regional goal indicators. Climate risk management interacts with other policies framing agricultural policies; consequently, drought risk management can have benefits or costs related to other policy goals. Recognizing trade-offs allows balancing competing priorities (e.g., economic prosperity) and avoiding unintended consequences (e.g., environmental damages, socially not acceptable solutions).

For Seewinkel region an integrated modelling framework (IMF), which uses two stochastic climate scenarios, has been developed based on the work of Karner et al. (2019b) and Mitter and Schmid (2021). The regional goal indicators include (i) economic prosperity by maximizing net benefits of agricultural production (NB), (ii) preserving groundwater resources by minimizing groundwater extraction for irrigation (GWEX), (iii) improving water quality by minimizing nitrate leaching in the percolate (NO3), and (iv) increasing topsoil organic carbon stocks by maximizing carbon sequestration (SOC).

The IMF makes use of the following data:

- observed daily weather station data (minimum and maximum temperatures, wind speed, relative humidity, solar radiation, precipitation) for the period 1975-2007
- land use data from the Integrated Administration and Control System for 2015-2017; agronomic constraints for pre-crop/main-crop combinations
- statistically projected daily weather data from 2010 to 2040, using monthly block bootstrapping.

The IMF chain, schematically presented in Figure 15, consists of:

- a statistical climate model for Austria (Strauss et al., 2013a, 2013b), which provides two stochastic climate scenarios. The model uses observed daily weather station data as described before. The two stochastic climate scenarios developed are as follows: (i) SIMILAR scenario, which resembles past precipitation until 2040, and (ii) DRY scenario, which is drier compared to the past with more frequent sampling from drier blocks. Hence, the two climate scenarios differ mainly by the precipitation volume and seasonal distribution. For the case study region, average annual precipitation volumes are 20% lower in DRY compared to SIMILAR. The derived daily weather data are input to the bio-physical process model EPIC.
- a crop rotation model (CropRota; Schönhart et al., 2011). In this study, 24 crops are taken into account to model up to 23 alternative, typical, crop rotations with their relative shares on cropland per municipality. One crop rotation includes up to six crops in a sequence and crop rotations are assigned proportionally to the 500 m pixels, which are input to EPIC.
- a bio-physical process model (EPIC; Williams, 1995), which is used to simulate crop yields and environmental outcomes for the stochastic climate scenarios. The model was used to provide outputs at spatial resolution of 500 m and a period of 31 years. Five land use classes (cropland, intensive grassland, extensive grassland, vineyards, and other land) are considered as well as a set of alternative management practices (i.e., combinations of different fertilization intensities and irrigation on cropland).
- a bottom-up economic land and water use optimization model (BiomAT; Karner et al., 2019b; Mitter and Schmid, 2021). BiomAT is calibrated to statistical reports of past land use and results show the trade-offs between the regional goal indicators.

Funded by the European Union

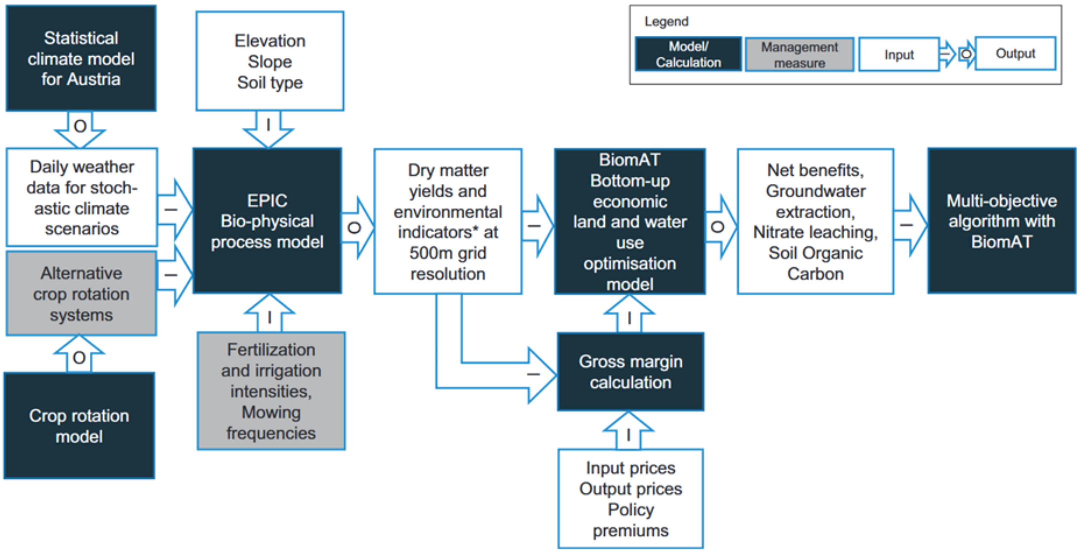

Figure 15: *Overview of the integrated modelling framework for the Seewinkel region (Austria).*

Step 2: Spatial data aggregation

This step is applied only in IMP1 (i.e., over the hotspots located in Czech Republic, Poland, Germany and Romania) to two types of data:

- Climate hazard analyses –conducted at grid level and NUTS3 level;
- Socio-economic (SE) analysis – based on data available from EUROSTAT such that assure a coherent coverage of all four selected hotspots.

Step 3: Impact assessment

IMP1

For the hotspots selected in D2.1, the impact of drought is evaluated using three indicators available from EUROSTAT level, namely:

- Population density. This indicator is calculated as the annual average population divided by the land area and refers to the number of inhabitants per km2 (https://agridata.ec.europa.eu/Qlik_Downloads/InfoSheetSocioEconomic/infoC4.html). It is linked to sensitivity component of vulnerability in relation to natural hazards, reflecting the social component of the impact. This indicator is used at NUTS2 and NUTS3 level, for 2023.
- Main agricultural labour force, for 2016. Labour force is expressed in persons and in Annual Work Units (AWUs) where one AWU corresponds to the work performed by one person occupied on a full-time basis. This indicator is linked to the 'Dependency on agriculture for livelihood' indicator considered as one of the most important indicators in the social susceptibility dimension regarding the vulnerability in relation to drought in agriculture (Meza et al., 2019).
- The maximum share of irrigable areas in utilised agricultural area, for 2016. According to EUROSTAT, 'total irrigable area is the maximum area which could be irrigated in the reference year using the equipment and

the quantity of water normally available on the agricultural holding.'; however, crops under glass and kitchen gardens are not considered within this data set. This sectoral indicator relates to the 'irrigated land' indicator, appreciated as being one of the most important indicators for characterizing coping capacity in relation to drought (Meza et al., 2019).

IMP2

The impact on agriculture in the Austrian region Seewinkel has been investigated along with the evaluation of risk/trade-offs and adaptation options within the IMF modelling chain. The analysis aims to assess the impacts on and trade-offs between the regional goal indicators described above (i.e., maximizing net benefits of agricultural production (NB), minimizing groundwater extraction for irrigation, minimizing nitrate leaching in the percolate (NO3), maximizing carbon sequestration (SOC)) in the context of two stochastic climate scenarios, taking into account 5 land use classes and 15 land management practices.

Step 4 Risk assessment

IMP1

The approach used for drought-related risk assessment in the hotspots located in Czech Republic, Poland, Germany and Romania is based on the risk matrix method, which is a comprehensive yet simple risk evaluation technique (Dolge and Blumberga, 2021). In this approach, the risk is generally defined as the combination between an indicator illustrating the probability of the phenomenon (i.e., hazard) and its impact; by classifying each of the terms in categories (e.g., very low, low, moderate, high, very high) it allows to rank and compare the risk levels (Peace, 2017). This approach has been previously used in climate-related risk assessment studies, for instance in adaptation of agriculture to climate changes (Cobon et al., 2016), assessing climate risks in urban areas (Papathoma-Koehle et al., 2016; Szymalski and Kassenberg, 2022), community resilience analysis in relation to climate changes (Li and van de Lindt, 2025). The risk matrix method is an approach in-between quantitative and qualitative ones and the choice to use it in the current analysis is driven by the availability of data covering all hotspots, especially in the case of the impact indicators.

In this analysis, the risk is defined by the five categories of drought-related hazard and impact indicators, resulting four risk levels of interest- low, moderate, high and very high - illustrated through a colour scheme (i.e., green, yellow, orange, red; Figure 16) widely accepted in the implementation of this approach (Proto et al, 2023)

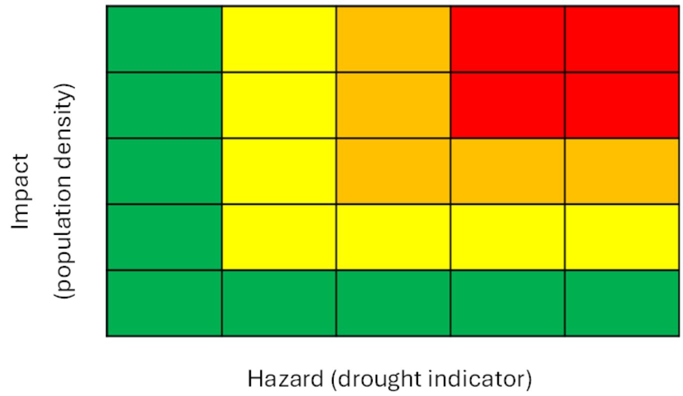

Figure 16: *Risk matrix defined for the analysis of the four selected hotspots.*

The risk matrix approach has been applied for future climate vs. historical one; the hazard metrics used is the share of NUTS3 area affected by at least mild drought (i.e., scPDSI < -1) in RCP45 and RCP85 climate change scenarios, for three time horizons: near present (2011-2040), mid-century (2041-2070) and end-century (2071-2100); the reference/historical period is 1981-2010; as impact indicator, the population density at NUTS3 is used, assuming this remain unchanged in the next decades.

For risk assessment purposes, both the hazard and the impact are classified into five categories, considering that the category with the highest impact is associated with the highest population density. As for the hazard, the common five categories are defined by the differences between future and historical periods of NUTS3 area shares affected by droughts under the two scenarios (RCP 4.5 and RCP 8.5). Only the positive values of these differences are further considered for the risk analysis. The category with highest hazard is that with the highest positive difference between future and historical periods. The range of both hazard and impact components cover all the selected hotspots, leading to an assessment of relative risk levels among the selected areas.

IMP2

For the Seewinkel region, this step of the methodology framework has been applied in the form of the trade-off analysis between the net benefits of agricultural production (NB) and three environmental indicators related to land management practices, namely groundwater extraction (GWEX), nitrate leaching in the percolate (NO_3) and soil carbon sequestration (SOC).

A synthesis of the implementation approaches used for steps 3 and 4 of the methodological framework is schematically presented in Figure 17.

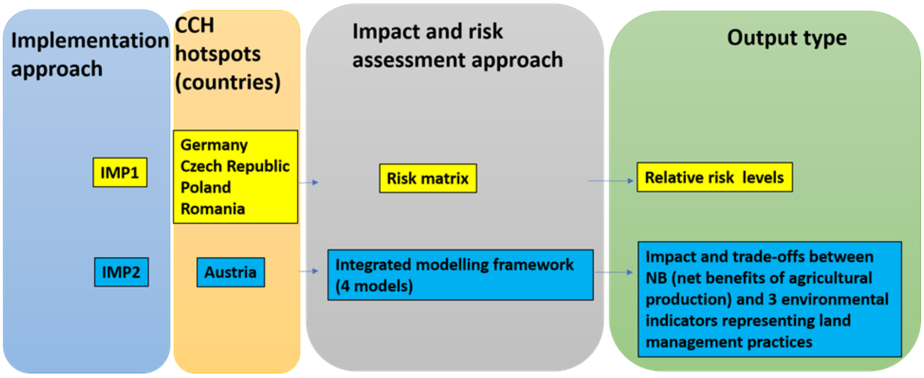

***Figure 17:** Schematic representation of impact and risk assessment approaches implemented in CSA 2.*

2.2.3. Results

IMP1

A. Drought-related hazard in the future climate

The scPDSI indicator is used to investigate drought-related hazard in the context of climate change scenarios. The analysis at seasonal scale of median change of scPDSI at the grid-point level across the 9 simulation sets for RCP45 and RCP85 respectively, indicates similar patterns across seasons for both scenarios; Figure 18 and Figure 19 show patterns of these changes for summer season (other seasons are not shown)

Considering RCP45, changes are small over wide regions from the base period to the near present. Wetting is notable in the Alpine region, central Germany, northern and eastern Poland, and parts of Romania. Drying is particularly prominent in Greece, Turkey and southern Italy. Slight wetting is still visible in changes from the base period to the mid-21st century in Austria. Drying is prominent across the western parts of Central Europe, Italy, Greece, Turkey, Bulgaria, parts of Hungary, and parts of Romania among others. Changes between the end of the 21st century and the base period are in parts a reversal of the changes to the middle of the 21st century. Some wetting is seen, e.g., in Austria and Poland. Drying is still prominent in western Europe, Italy, Greece, and Turkey.

The median changes in scPDSI differ in prominent aspects for RCP85. Again, changes are small over wide regions from the base period to the near present. Some regions become wetter in Germany, Poland and Austria, while the southern parts of the shown domain dry from Sardinia across southern mainland Italy to Greece and Bulgaria.

Regional wetting is still visible in the mid-century in Austria and Poland, while western central Europe shows drying and drying intensifies in the south of the shown domain. At the end of the century there is still some wetting visible across the Alps, while drying is severe in western central and southern Europe and becomes prominent in south-eastern Europe.

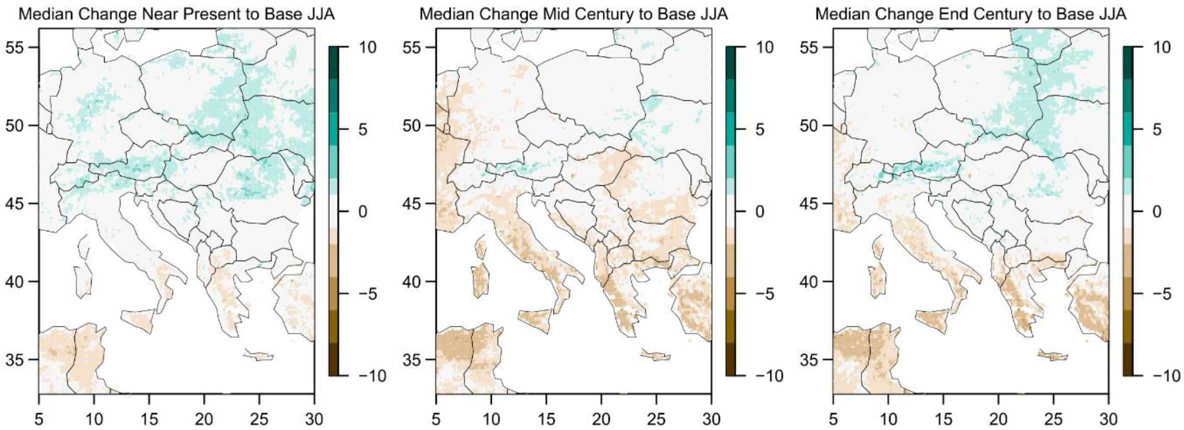

Figure 18: *Median change at the grid-point level in scPDSI-values for RCP45 in summer. Columns are from left to right for Near Present (2011-2040) to Base Period (1971-2000), Mid Century (2041-2070) to Base Period, and End Century (2071-2100) to Base Period. Other seasons are not shown.*

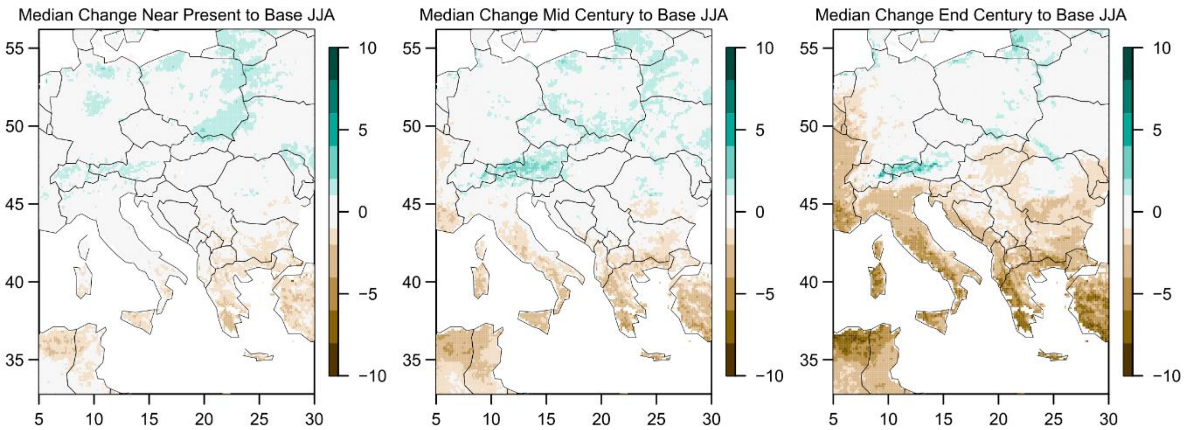

Figure 19: *Median change at the grid-point level in scPDSI-values for RCP85 in summer. Columns are from left to right for Near Present to Base Period, Mid Century to Base Period, and End Century to Base Period. Other seasons are not shown.*

Focusing on the selected hotspots, the drought-related hazard is further analysed to highlight the relative hazard level over the hotspots, following the approach used for risk assessment. For this, using the mean of the ensemble simulations presented in Table 4, we consider only changes in scPDSI with values below -1 (i.e., ‘mild’, ‘moderate’, ‘severe’ and ‘extreme’ drought intensity classes, Table 4); additionally, the magnitude of hazard indicator is assessed through the share of NUST3 area affected by any of these drought classes. This is further divided in 5 classes emphasizing the hazard intensities from ‘very low’ (i.e., small share of NUTS3 area affected by drought) to ‘very high’. The results are presented in Figure 20 for the three time horizons of interest (2011-2040 vs. 1981-2010; 2041-2070 vs. 1981-2010; 2071-2100 vs. 1981-2010) and for the two climate change scenarios (RCP45, RCP85).

The drought analysis for the future climate suggests that in the “model world” the climate change signal clearly emerges under the scenario RCP 8.5. In this case, the differences in the share of NUTS 3 area relative to the reference period is progressing in time becoming the largest at the end of century (Figure 20 b, d, f). The climate variability in the models seems to be larger under the scenario RCP 4.5, even though we could still identify the increase of the share in NUTS3 areas affected by droughts especially between the near term and the mid and end of the century (Figure 20 a, c, e). The higher internal variability in hazard under the scenario RCP 4.5 is what is expected considering the less pronounced climate change forcing. The conclusion is that one could expect larger shares of NUTS3 areas to be affected by drought (more pronounced drought-related hazard) under climate change especially in the southern hotspot, but also in some other regions from central Europe (Figure 20 f).

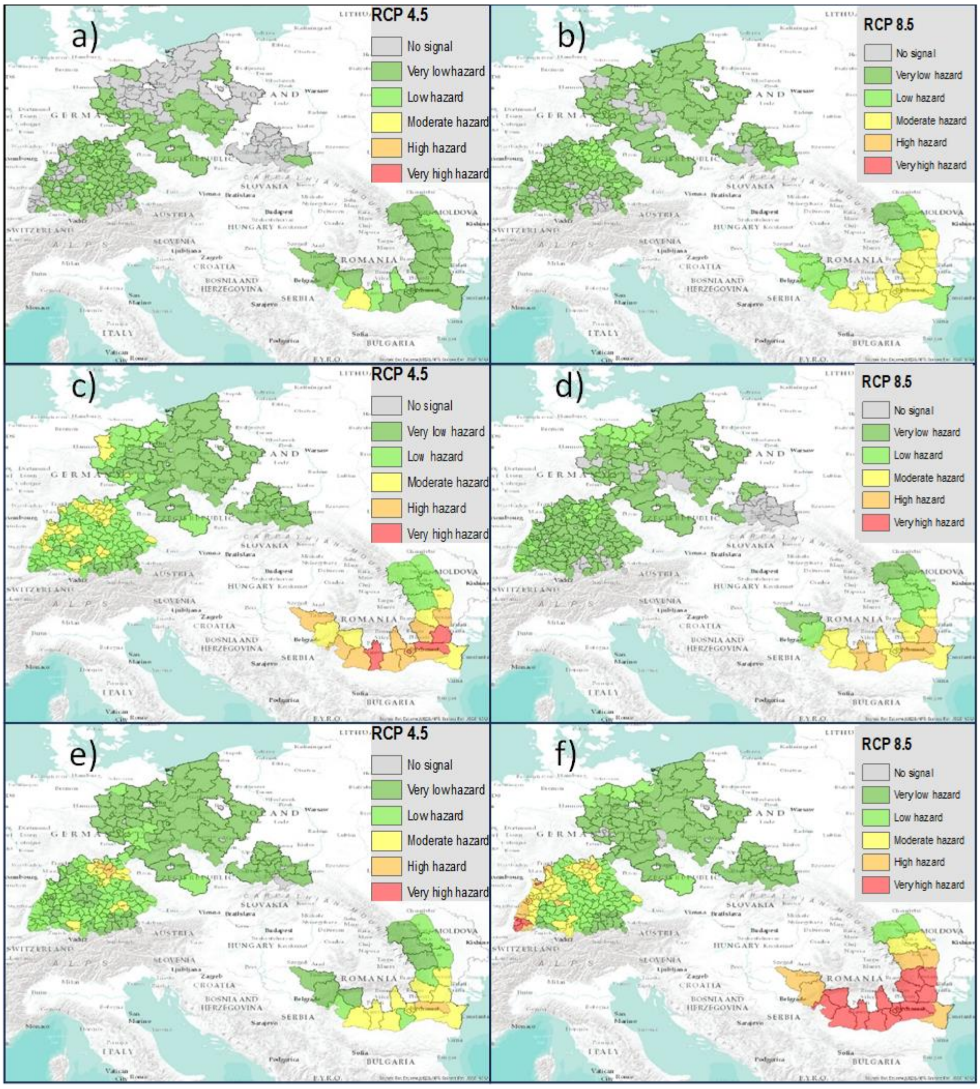

Figure 20: *Hazard levels in the future climate relative to the present climate, related to drought intensity classes 'mild', 'moderate', 'severe', and 'extreme', expressed through the share of NUTS3 area affected by any of these drought classes, for the periods near-term (a and b), (b) mid century (c and d) and end of century (e and f) under scenarios RCP 4.5 and RCP 8.5. The grey areas (no signal) are those in which the differences in share of NUTS3 areas between the future and reference period are less than 0.*

B. Drought-related impact

Population density is used as a first sensitivity indicator for investigating the socio-economic impact of drought, as 'highly dense population areas tend to be more vulnerable due to an increase of both the population exposed to hazards and their sensitivity'[3]. The EUROSTAT data for 2023 (Figure 21) show that the selected NUTS2 regions in Romania present in general the lowest population density (less than 100 inhabitants/km2), along with some regions in Germany and Poland. At the opposite end, most of selected NUTS2 regions in Germany present a population density over 200 inhabitants/km2, up to 413 inhabitants/km2 in Karlsruhe. The impact expressed through a 5-quantile classification of population density at NUTS3 level (Figure 22) allows a more detailed assessment. These provide a first view on the sensitivity of selected hotspots to drought, potentially reflected in a cross-sectoral path of impact, as for example on water availability for households- of particular interest in highly densely populated regions, or tourism sector - due to increased competition on water resources with other sectors. However, a lower population density does not necessarily imply a lower vulnerability; an update of this investigation will follow in the next months, using a larger selection of indicators to assure a more comprehensive assessment of vulnerability of the general population in relation to drought hazard.

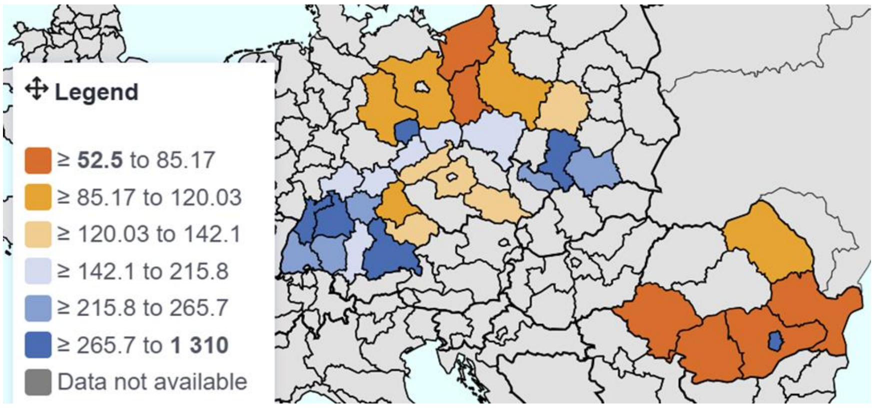

Figure 21: *Population density in selected hotspots, at NUTS2 level, in 2023.*

[3] https://drmkc.jrc.ec.europa.eu/risk-data-hub/media/vulnerability/Indicators_and_References.pdf

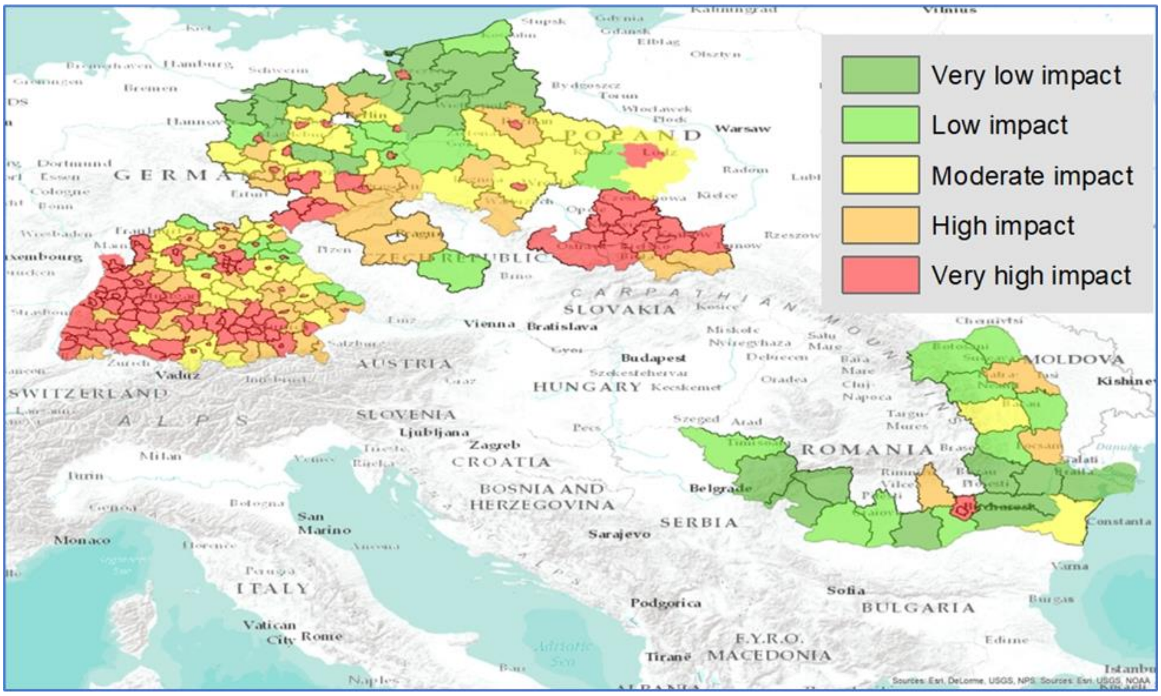

Figure 22: *Impact map based on a 5-quantile classification of population density (reference year 2023) at NUTS 3 level.*

Focusing on the agriculture sector, the socio-economic sensitivity to drought is assessed through the number of people working in this sector. The sectoral data indicates that Romania and Poland present the highest degree of sensitivity (Figure 23). The hotspots located in these countries present an agricultural labour force significantly larger than the other hotspots, suggesting a stronger dependency on agriculture. This population segment is expected to be directly affected by drought (Edwards et al, 2019) through economic loss, due the lower agricultural productivity and risk of losing their jobs. The socio-economic impact might be even larger considering other sectors directly affected like forestry and fishery; for example, in Romania about 21% from total employees in the selected hotspots worked, in 2016, in agriculture, forestry and fishing, according to the National Institute for Statistics.

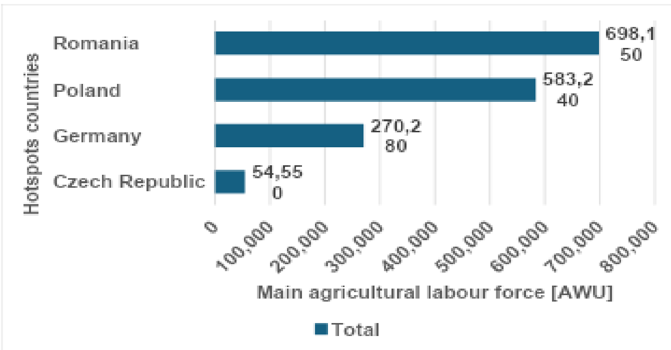

Figure 23: *Main agricultural labour force, in 2016, expressed in Annual Working Units (AWU).*

As an indicator for adaptive capacity, the share of irrigable agricultural land is considered. The EUROSTAT data for 2016 (Figure 24) shows that selected hotspots in Germany are better equipped to mitigate the short-term effects of drought, having the largest share of irrigable areas, while at the opposite end of the spectrum Czech Republic is found. It should be considered, however, that the usability of irrigation infrastructure depends not only on its existence, but also on its technical functionality (e.g., in 2016 in Romania about 75% of the irrigation infrastructure was already too old to be used (MARD, 2016)) and on the real capacity to use it (e.g., water and energy availability; funds for operational and maintenance costs; energetic and water-related efficiency).

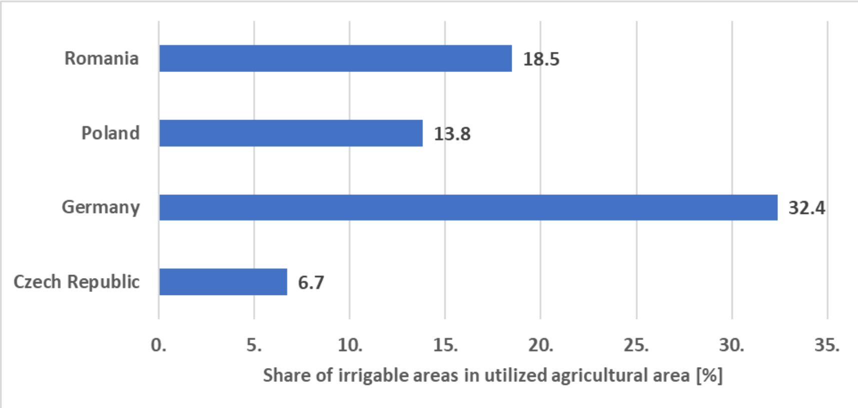

Figure 24: *Share of irrigable areas in utilised agricultural area, aggregated as sum over the hotspots in each country, for 2016, expressed as percentage of total utilised agricultural area*

C. Drought-related risk assessment

The local response to climate change in drought conditions is most pronounced at the NUTS3 areas from the Southern Romanian and, to a smaller extent, from the Southern and central Germany under the scenario RCP 8.5 at the end of this century (Figure 20). The local hazard-related response considered together with the population density at the NUTS3 level (Figure 22) and the risk matrix (Figure 16) led to the identification of areas with higher relative risks in a cross-sectorial water-relevant framework (Figure 25). In this context, regions from Eastern Romania and Southern and central Germany are prone to increasing drought-related risks in the future compared to the historical period (Figure 25). This risk is mostly reflecting the competition for water resources between different sectors (i.e. households against non-household customers from tourism, agriculture, energy) under climate change as population density is related to water supply and demand in a cross-sectoral framework. Different types of risk assessment start with or include the population density to give further sectoral insights in drought-related risks. Regional and local projections of population density are essential in assessing the future risks related to water resources at the European level. In addition to the sectoral competition for water resources, regional and national imbalances are expected. Our approach highlights regions at NUT3 level either prone to increasing water scarcity and drought (areas from the Eastern and Southern Romania, and Southern and central Germany) or free of such risks under future climate change (e.g., some Poland and Czechs NUTS3 areas).

More analysis is needed for a more robust and detailed drought-related risk assessment. Such analyses need better impact data in granularity and coverage at the European level which are not available now.

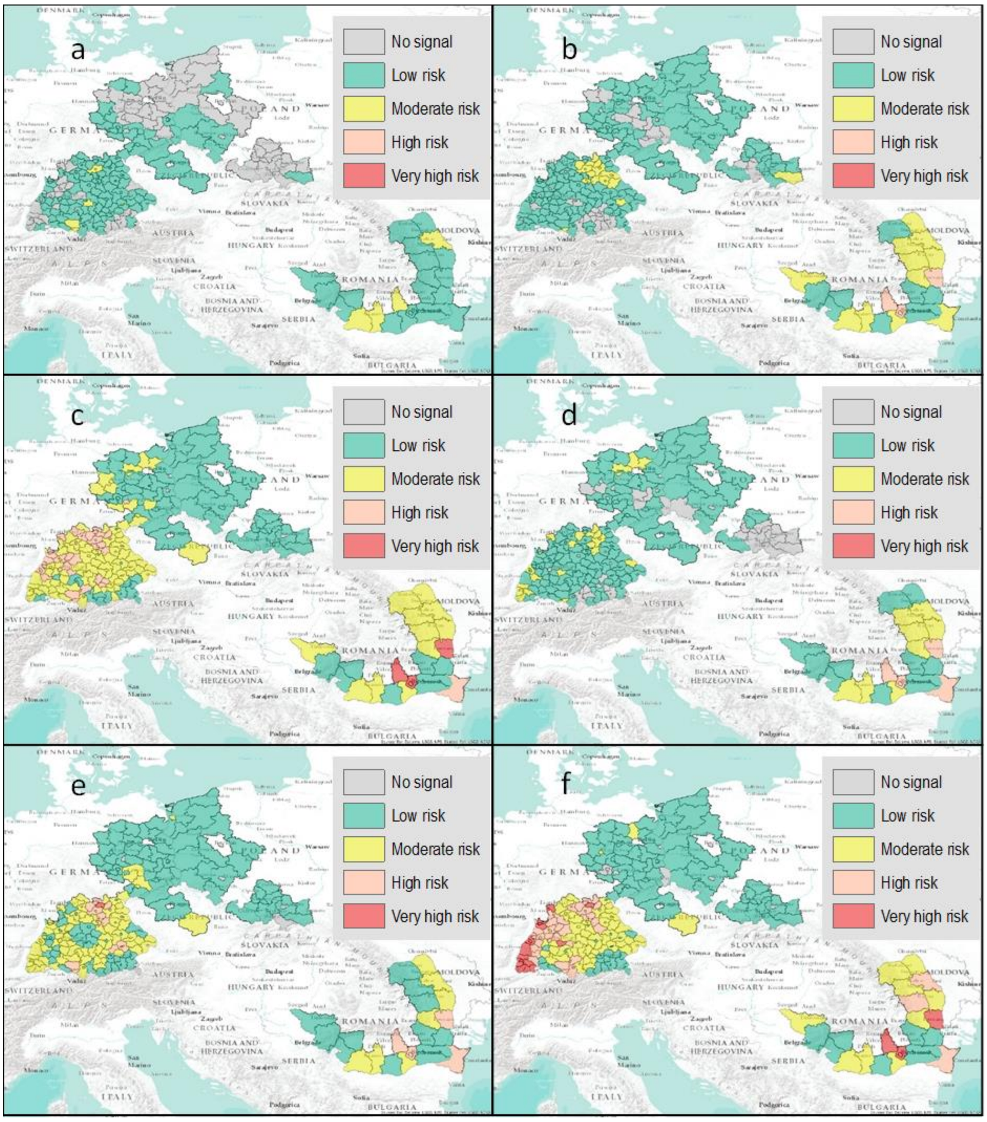

Figure 25: *Future risk levels relative to the reference period for drought intensity classes 'incipient', 'moderate', 'severe' and 'extreme', expressed through the share of NUST3 area affected by any of these drought classes, for the periods near-term (a and b), mid-century (c and d), and end of century (e and f) under scenarios RCP 4.5 (a, c, and e) and RCP 8.5 (b, d, and f). The grey areas (no signal) are those in which the differences in share of NUT3 areas between the future and reference period are equal or less than 0.*

IMP2

A. Trade-off assessment of regional goal indicators in the agriculture sector – Seewinkel region (Austria)

The results of the IMF modelling chain highlight the relative improvements for the environmental goal indicators compared to the reference situation for each climate scenario (DRY & SIMILAR; see data description) as well as the trade-offs between net benefits of agricultural production (NB) and the environmental goal indicators GWEX, as depicted in Figure 16. The results reveal that groundwater extraction (GWEX) is reduced by 19.5% (11%), on average, at NB reduction levels of 1% compared to the reference situation (Figure 26). In DRY scenario, a maximum decline of 92% of GWEX is achieved at 50% NB reduction levels. Trade-offs between NB and GWEX are non-linear, i.e. relative reductions of GWEX are largest for small NB reduction levels and decline with higher NB reduction levels in SIMILAR and DRY, as shown in Figure 26.

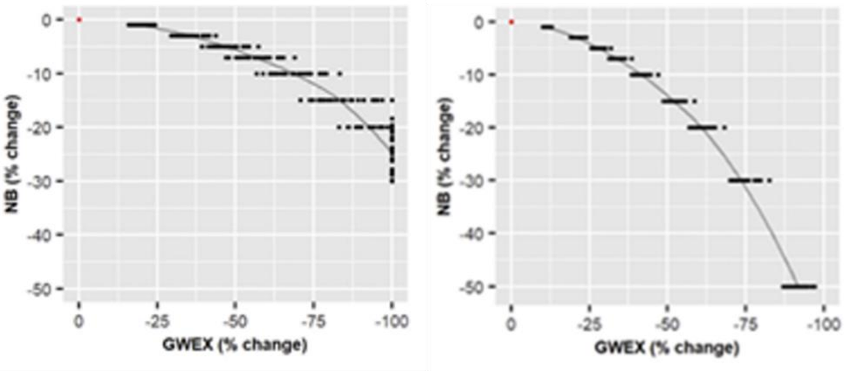

Figure 26: *Modelled impacts and trade-offs between net benefits of agricultural production (NB) and environmental goal indicator GWEX (x-axis) by NB reduction levels, for (left) SIMILAR and (right) DRY climate scenario; the relative changes always relate to the same realization of a climate scenario.*

Two other environmental indicators - nitrate leaching (NO3) and topsoil organic carbon stock (SOC) - have been also investigated. The results show that compared to the reference situation, nitrate leaching is lower in DRY compared to SIMILAR scenario (by 10% on average). Trade-offs between NB and NO3 are smaller in DRY, however, they do not vary substantially between the climate scenarios, although these still influence NO3 levels. For instance, NO3 is by 7-13% lower, on average, in DRY compared to SIMILAR if NO3 is minimised, depending on the NB reduction level. For topsoil organic carbon stock (SOC), the results indicate that at a 50% reduction level of NB, SOC would increase by 8.1% (7.6%) in SIMILAR (DRY), on average. Again, trade-offs between NB and SOC are non-linear and relative improvements of SOC decline with higher NB reduction levels. Such trade-off analyses support climate risk management by revealing synergetic and antagonistic effects of management options on regional goal achievements.

2.2.4. Challenges

IMP1

The drought-related risk assessment conducted in IMP1, while offering a structured and spatially explicit perspective, faces several challenges that reflect both methodological limitations and data constraints. One of the main difficulties lies in the uncertainty associated with climate projections. Despite the use of high-resolution regional climate models (RCMs) from the EURO-CORDEX initiative, the spread between models and emission scenarios (RCP4.5 vs. RCP8.5) results in significant variability in future drought patterns, especially across different time horizons. This uncertainty can affect the robustness of the hazard classification based on scPDSI, particularly when quantifying the frequency and severity of future droughts at the NUTS3 level.

Another major challenge stems from the static nature of the socio-economic indicators used to assess impact and vulnerability. While data such as population density, agricultural labour force, and irrigable land share offer valuable insights into current exposure and adaptive capacity, they do not capture dynamic trends or future socio-economic developments that could alter risk profiles. Moreover, the granularity of the available socio-economic data often limits the precision of the analysis, especially in rural and transboundary regions where agricultural practices and vulnerabilities vary significantly over short distances.

Methodologically, integrating hazard and impact components into a risk matrix framework poses its own set of challenges. One of the main applications of this approach is to help 'decision-making about the acceptance of risk' (Duijin, 2015); however, there are limitations stemming from several sources, like the use of discrete categories, which may lead to simplifications that overlook nuanced regional differences or the difficulties in translating the outputs into recommended risk management decisions (Cox, 2008). Additionally, the lack of temporally harmonised datasets for some impact indicators may introduce biases or inconsistencies when comparing across hotspots or timeframes.

Finally, translating relative risk levels into actionable policy recommendations requires further efforts in stakeholder engagement and cross-sectoral integration, along with more sophisticated assessments of economic and social impacts. The risk matrix approach offers a strong scientific foundation, providing, in a structured way, semi-quantitative sectoral information to identify and prioritise adaptation actions by assessing the likelihood and potential impact of climate change risks. Nevertheless, aligning the results of the risk assessment with local agricultural realities, institutional capacities and climate adaptation planning processes remains an ongoing challenge.

IMP2

An adapted study design of the presented IMF might reveal different trade-offs and co-benefits between net benefits and environmental goal indicators (EI). Hence, in a next step, we aim to develop the presented methodology further. By integrating additional land and water management practices, modelled trade-offs between NB and EI will be revealed in order to support regional climate risk management. For instance, additional management practices have been identified as relevant to decrease trade-offs between NB and EI such as increasing water productivity, fertilizer use efficiency, plant species diversity, crop residue retention and soil water holding capacity or if liming or biochar is applied. Moreover, we have not yet discussed the model results with stakeholders to understand whether they perceive the modelled solutions as socially optimal or acceptable. As studies have pointed out, the integration of stakeholders is key in land use and climate research. The presented modelling approach could be combined with stakeholder preferences on land and water use to analyze how certain socially optimal environmental outcomes can be achieved.

2.2.5. Conclusions

The assessment of drought risk across the hotspots located in Czech Republic, Poland, Germany and Romania, based on the EURO-CORDEX CMIP5 climate projections under RCP4.5 and RCP8.5 scenarios, reveals a significant increase in drought hazard intensity, especially towards the late 21st century. The analysis highlights spatial heterogeneity in projected changes: while certain areas in Austria and Poland may experience slight increases in precipitation and thus a minor wetting trend, southern and western Europe—including Greece, Italy, and regions in Romania—are expected to face more frequent, longer-lasting, and intense drought events. Socio-economic vulnerability factors differ notably among these hotspots. For example, agricultural labour force participation is higher in Romania and Poland, suggesting a greater dependence on agriculture and hence increased sensitivity to drought impacts on livelihoods; however, in the future this will tend to decrease over time with efficiency improvements in agriculture following the trend in other countries around the world. Conversely, Germany exhibits higher population densities and better-developed irrigation infrastructure, which could enhance its capacity to adapt and reduce vulnerability. Combining climatic hazard projections with socio-economic indicators in a risk matrix shows that drought risk is unevenly distributed, with some hotspots—particularly in southeastern Europe—facing extreme risks due to the convergence of high hazard levels and socio-economic sensitivity. These findings underscore the critical need for regionally tailored adaptation and mitigation strategies integrating both climatic projections and local socio-economic realities to effectively reduce drought risk and enhance resilience.

The trade-off analysis for the Austrian hotspot Seewinkel shows that adaptation of land use and management practices significantly improves the environmental performance for fairly small reductions in agricultural net benefits. Such trade-off analysis support regional climate risk management by tailoring land and water use practices and their effects on economic and environmental domains Thus, tailored climate risk management would allow considerable improvements of EI at relatively low costs. However, improvements of EI beyond a particular level can quickly lead to higher costs. In fact, improvements of EI per percentage point reduction of net benefits are always highest for the first percent and decrease continuously with higher NB levels.

The model results indicate that climate change might alleviate or intensify trade-offs in the region, depending on the realised climate scenario and the analysed EI. This emphasises the importance to account for multiple EI and stochastic climate information. In particular, a dry climate scenario would increase the costs to reduce groundwater extraction for irrigation and increase topsoil organic carbon stocks, hence, leading to higher trade-offs with net benefits of agricultural production.

The model results provide useful insights for developing regional climate risk management plans by accounting and visualizing synergistic and antagonistic effects of agricultural practices on economic and environmental indicators at high spatial resolution. Hence, tailored adaptation strategies can be developed.

2.2.6.References

Barichivich J, Osborn TJ, Harris I, van der Schrier G and Jones PD (2024). Monitoring global drought using the self-calibrating Palmer Drought Severity Index in "State of the Climate in 2023"]. Bull. Amer. Meteor. Soc., in press.

Boere, E., Valin, H., Bodirsky, B. Baier, F., Balkovic, J., Batka, M., Folberth, C., Karstens, K., Kindermann, G., Krasovskii, A., Leclere, D., Wang, X., Weindl, I., Havlik, P., LotzeCampen, H. (2019). D2.2 Impacts on agriculture including forestry & fishery. Deliverable of the H2020 COACCH project.; available online from https://www.coacch.eu/wp-content/uploads/2020/05/ D2.2_after-revision-to-upload.pdf

Bojariu R, Chitu Z., Dascălu SI, Gothard M, Velea L, Burcea R, Dumitrescu A, Burcea S, Apostol L., Amihaesei V., Marin L, Crăciunescu VS, Irimescu A, Mătreata M, Niţă A., Bîrsan MV (2021). Schimbările climatice – de la bazele fizice la riscuri și adaptare (Climate change – from physical bases to risks and adaptation, in Romanian with Summary in English), editie revăzută si adăugită. Editura Printech, București, 222 p, ISBN: 978-606-23-1275-6, https://doi.org/10.5281/zenodo.10517336

Bojariu R, Dascălu SI, Gothard M, Dumitrescu A, Crăciunescu V, Mătreață M, Chendeș V, Burcea S, Cică R, Birsan M, Boincean B, Velea L, Niță A, Irimescu A, Potopová V, Cazac V, Niță A. (2018). Variability and change in water cycle at the catchment level. In: Engineering and mathematical topics in rainfall, vol 7, pp 115–129. https://doi.org/10.5772/67933

Busschaert, L., de Roos, S., Thiery, W., Raes, D., and De Lannoy, G.J.M. (2022). Net irrigation requirement under different climate scenarios using AquaCrop over Europe, Hydrology and Earth System Sciences (HESS), 26, 3731–3752, https://doi.org/10.5194/hess-26-3731-2022.

Cobon, D.H., Williams, A.A.J., Power, B. *et al.* (2016). Risk matrix approach useful in adapting agriculture to climate change. *Climatic Change* 138, 173–189. https://doi.org/10.1007/s10584-016-1732-z.

Conradt, T., Engelhardt, H., Menz, Ch., Vicente-Serrano, S., Farizo, B., Peña-Angulo, Dh., Domínguez-Castro, F., Eklundh, L., Jin, H., Boincean, B., Murphy, C., López-Moreno, J.. (2023). Cross-sectoral impacts of the 2018–2019 Central European drought and climate resilience in the German part of the Elbe River basin. Regional Environmental Change. 23. 10.1007/s10113-023-02032-3.

Cox, L.A. (2008). What's wrong with risk matrices? Risk Anal 28(2):497–512. https://doi.org/10.1111/j.1539-6924.2008.01030.x

Dolge, K. and Blumberga, D. (2021). Composite risk index for designing smart climate and energy policies, Environmental and Sustainability Indicators, 12, 100159, https://doi.org/10.1016/j.indic.2021.100159

Duijm, N.J. (2015). Recommendations on the use and design of risk matrices. Saf Sci 76:21–31. https://doi.org/10.1016/j.ssci.2015.02.014

European Commission, Joint Research Centre (JRC) (2020). EDO Combined Drought Indicator (CDI) (version 1.6.1, dismissed). European Commission, Joint Research Centre (JRC) [Dataset] PID: http://data.europa.eu/89h/e83b19ce-08c2-4e0c-b93a-5fd62be21e5e

European Parliament, Council of the European Union (2013). Regulation (EU) No 1308/2013 of the European Parliament and of the Council of 17 December 2013 establishing a common organisation of the markets in agricultural products and repealing Council Regulations (EEC) No 922/72, (EEC) No 234/79, (EC) No 1037/2001 and (EC) No 1234/200, COD 2011/0281.

Feyen L., Ciscar J.C., Gosling S., Ibarreta D., Soria A. (editors) (2020). Climate change impacts and adaptation in Europe. JRC PESETA IV final report. EUR 30180EN, Publications Office of the European Union, Luxembourg, ISBN 978-92-76-18123-1, doi:10.2760/171121, JRC119178.

George, J.-.-P., Bürkner, P.-.-C., Sanders, T.G.M., Neumann, M., Cammalleri, C., Vogt, J.V. and Lang, M. (2022). Long-term forest monitoring reveals constant mortality rise in European forests. Plant Biol J, 24: 1108-1119. https://doi.org/10.1111/plb.13469.

Hanel, M., Rakovec, O., Markonis, Y. et al. (2018). Revisiting the recent European droughts from a long-term perspective. Scientific Reports 8, 9499. https://doi.org/10.1038/s41598-018-27464-4

Harris, I., Osborn, T.J., Jones, P. et al. Version 4 of the CRU TS monthly high-resolution gridded multivariate climate dataset. Sci Data 7, 109 (2020). https://doi.org/10.1038/s41597-020-0453-3.

Heinzel, C., Fink, M., Höllermann, B. (2022). The potential of unused small-scale water reservoirs for climate change adaptation: A model- and scenario based analysis of a local water reservoir system in Thuringia, Germany, Front. Water, 4, https://doi.org/10.3389/frwa.2022.892834.

Karner, K., Mitter, H., Schmid, E., 2019. The economic value of stochastic climate information for agricultural adaptation in a semi-arid region in Austria. Journal of Environmental Management 249, 109431. https://doi.org/10.1016/j.jenvman.2019.109431

Knutzen, F., Averbeck, P., Barrasso, C., Bouwer, L. M., Gardiner, B., Grünzweig, J. M., Hänel, S., Haustein, K., Johannessen, M. R., Kollet, S., Pietikaeinen, J.-P., Pietras-Couffignal, K., Pinto, J. G., Rechid, D., Rousi, E., Russo, A., Suarez-Gutierrez, L., Wendler, J., Xoplaki, E., and Gliksman, D. (2025). Impacts and damages of the European multi-year drought and heat event 2018–2022 on forests, a review, Natural Hazards and Earth System Sciences, https://doi.org/10.5194/nhess-25-77-2025

Li, J. and van de Lindt, J. (2025). Climate Adaptation Matrix Concept for Multidisciplinary Community Resilience in a Changing Climate, Natural Hazards Review, 26(2) https://doi.org/10.1061/NHREFO.NHENG-2122

Meza, I., Hagenlocher, M., Naumann, G., Vogt, J. and Frischen, J., Drought vulnerability indicators for global-scale drought risk assessments, EUR 29824 EN, Publications Office of the European Union, Luxembourg, (2019). ISBN 978-92-76-09210-0, doi:10.2760/73844, JRC117546.

MARD (Ministry of Agriculture and Rural Development) (2016). National Program for the Rehabilitation of the Main Irrigation Infrastructure in Romani, available online from https://www.madr.ro/docs/agricultura/programul-national-reabilitare-irigatii-update.pdf (in Romanian); accessed on 27 may 2025.

Mitter, H., Schmid, E., (2021). Informing groundwater policies in semi-arid agricultural production regions under stochastic climate scenario impacts. Ecological Economics 17.

Palmer WC (1965). Meteorological drought. Research Paper No. 45, U.S. Department of Commerce, Weather Bureau, Washington, D.C. 12.

Papathoma-Koehle M,, Promper C, Bojariu R, Cica R, Sik A, Perge K, Laszlo P, Czikora EB, Dumitrescu A, Turcus C, Birsan MV, Velea L, Glade T. (2016). A common methodology for risk assessment and mapping for south-east Europe: an application for heat wave risk in Romania, Nat Hazards, 82, pp. 89-109, doi 10.1007/s11069-016-2291-3.

Peace, C. (2017). The risk matrix: uncertain results? *Policy and Practice in Health and Safety*, *15*(2), 131–144. https://doi.org/10.1080/14773996.2017.1348571

Potopová, V., Trnka, M., Vizina, A., Semerádová, D., Balek, J., Chawdhery, M.R.A., Musiolková, M., Pavlík, P., Možný, M., Štěpánek, P., Clothier, B. (2022). Projection of 21st century irrigation water requirements for sensitive agricultural crop commodities across the Czech Republic, Agricultural Water Management, 262, 107337, https://doi.org/10.1016/j.agwat.2021.107337

Reisner, G. (2014). Datenerhebung, Datenaufbereitung und fachliche Darstellung des Bewässerungsbedarfs der landwirtschaftlichen Beregnung (No. 9- W- 1099/315-2014). Amt der Burgenländischen Landesregierung Abteilung 9 – Wasser- und Abfallwirtschaft, Eisenstadt.

Reynaert, S., De Boeck, H.J., Verbruggen, E., Verlinden, M., Flowers, N. and Nijs, I. (2021), Risk of short-term biodiversity loss under more persistent precipitation regimes. Glob. Change Biol., 27: 1614-1626. https://doi.org/10.1111/gcb.15501

Schönhart, M., Schmid, E., Schneider, U.A. (2011). CropRota - A crop rotation model to support integrated land use assessments. European Journal of Agronomy 34, 263–277. https://doi.org/10.1016/j.eja.2011.02.004

Sepulcre-Canto, G., S. Horion, A. Singleton, H. Carrão, and J. Vogt (2012). Development of a Combined Drought Indicator to detect agricultural drought in Europe. Natural Hazards and Earth System Sciences, 12, 3519-3531

Strauss, F., Formayer, H., Schmid, E. (2013a). High resolution climate data for Austria in the period 2008-2040 from a statistical climate change model. International Journal of Climatology 33, 430–443. https://doi.org/10.1002/joc.3434

Strauss, F., Moltchanova, E., Schmid, E. (2013b). Spatially Explicit Modeling of Long-Term Drought Impacts on Crop Production in Austria. American Journal of Climate Change 02, 1–11. https://doi.org/10.4236/ajcc.2013.23A001

Szymalski, W. and Kassenberg, A. (2022). Determining the Climate Risk in the City Using the Risk Matrix Method – Examples from Poland, *Studia Ecologiae Et Bioethicae*, 20(3), 75–90. https://doi.org/10.21697/seb.2022.16

van der Schrier G, Barichivich J, Briffa KR and Jones PD (2013). A scPDSI-based global data set of dry and wet spells for 1901-2009. J. Geophys. Res. Atmos. 118, 4025-4048 (10.1002/jgrd.50355).

Weiss, F., von Wehrden, H. and Linde, A. (2024). Long-term drought triggers severe declines in carabid beetles in a temperate forest. Ecography, 2024: e07020. https://doi.org/10.1111/ecog.07020

Wells, N., Goddard, S. and Hayes, M. J. (2004). A Self-Calibrating Palmer Drought Severity Index, J. Climate 17, 2335-2351.

Williams, J.P., (1995). The EPIC Model, in: Singh, V.P. (Ed.), Computer Models of Watershed Hydrology. Water Resources Publications, Colorado, pp. 909–1000.

2.3. CSA 3 STORM

2.3.1. Summary of climate change hotspot and event-based storyline (STL)

The case study area is characterised by very high exposure to coastal hazards, both flooding and coastal erosion, which are regularly occurring in the cities and regions located in the Northern part of Europe. Figure 27 shows the STL area with a similar risk profile. See also the European climate risk typology system[4], which is characterising the area as a high-risk area for storms. The region is characterised by cities and relatively high population densities, high intensity of transport- and critical infrastructure, such as road, rail and port infrastructure as well as socioeconomic activities, which can be severely affected during flooding events. Socioeconomic indicators suggest that the regions are among the regions in Europe with relatively high GDP per capita, which may positively impact the ability to recover from extreme events and adapt to future climate change impacts.

Approximately 80 different NUTS 3 regions with similar characteristics are identified within the focal STL storyline region. They are located in Denmark, the Northern coast of Germany, The Netherlands, Belgium and the North-western part of France (Figure 27).

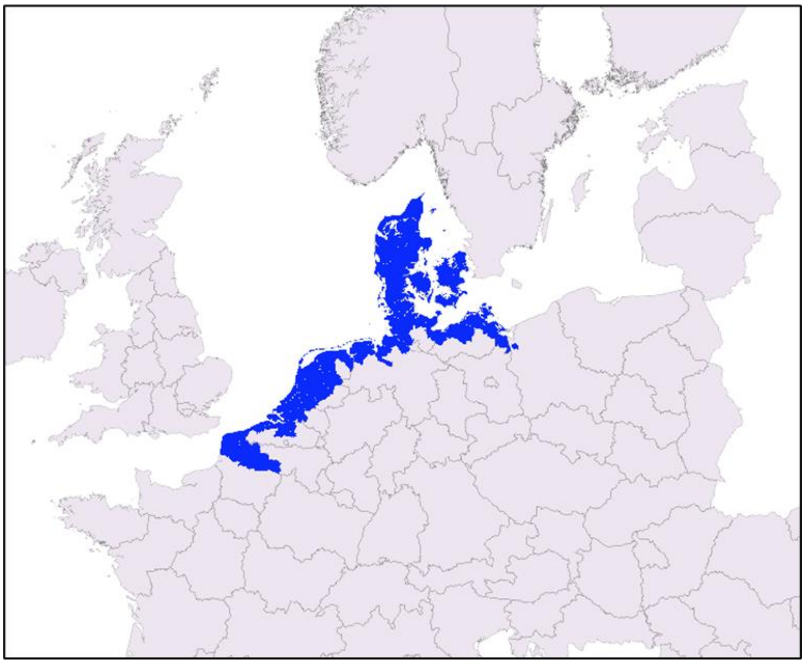

Figure 27: *Storms, NUTS 3 regions with similar climate risk typology as the CSA3.*

[4] European Climate Risk Typology | Typology Methodology.

The Climate Change Hotspots (CCHs) were selected within the region based on a storm surge in southern Denmark and north-eastern Germany in October 2023, where many urban areas were flooded.

The CCHs are highly exposed and vulnerable towards the occurrences and impacts of storm surges from the Baltic Sea. The regions of Southern Denmark and Northern Germany have low lying coastlines, and cities in this region are often positioned at the head of fjords, next to the sea. The combination of a low-lying coastline with a high degree of human and economic activities next to the sea makes this region particularly exposed and vulnerable to the occurrences and consequences of flooding during storm surges. The region has experienced serious flooding events in the last decades and most recently in October 2023, which in several locations had larger storm surge levels than a 100-year flood event. Water levels during the event are presented in Figure 28 below along with pictures illustrating some of the damages.

***Figure 28:** (A) Water levels and (B) images from the October 2023 storm surge.*

The EU green transition plans and national policies include a large expansion of existing large harbours and facilities supporting renewable energy such as power-to-x production plants, which could be at risk in the case of storms. The region has already experienced many severe flooding events in the past decades and will be even more exposed to such events in the future as sea levels rise as consequence of climate change.

Decision makers and private investors in the region are in the process of planning for future city development, infrastructure and economic development, including disaster risk management plans, and adaptation.

Extensive stakeholder engagement is also already included in this process. The focus of decision makers is now to prepare and adapt to the storm surge climate risks, and extensive plans are already adopted by local governments and projects are implemented.

The CCH focus within the areas includes the municipalities of Aabenraa and Haderslev in Denmark, and Flensburg and Kiel in Germany as shown in Figure 29. The Danish cities are part of the first study phase, and the German cities will follow in a second phase.

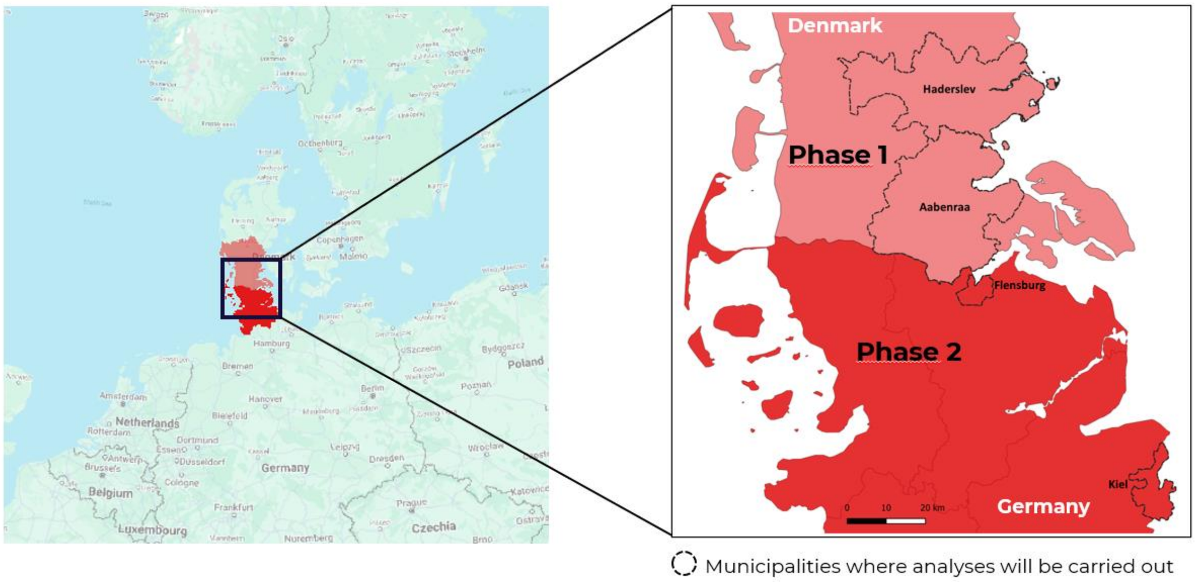

Figure 29: *The Climate Change Hotspot with focus on the municipalities of Aabenraa and Haderslev in Denmark, and Flensburg and Kiel in Germany.*

2.3.2. Application of the methodological framework

The case study investigates the impacts of storm surge events on sectors and assets based on detailed geographical information on flood hazards, land use and damage cost, which are used as input to an assessment of storm surge damages and adaptation options.

The assessment of damages from coastal flooding is based on an integrated analysis of climate scenarios, flood inundation modelling, impact mapping, damage cost modelling, and socioeconomic impact assessment. Figure 30 shows the analytical structure of the analysis. As demonstrated in Halsnæs et al. (2015, 2023, 2025), key methodological issues and assumptions including damage cost functions for flooding play important roles when estimating the socioeconomic consequences of urban flooding.

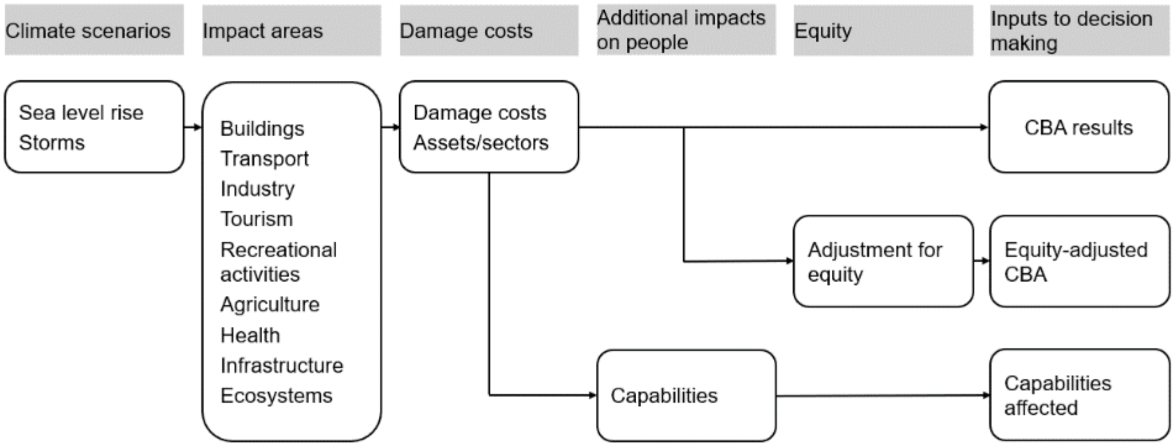

Figure 30: *Analytical structure of the integrated analysis of climate impacts from coastal flooding with extensions representing well-being. Figure from Halsnæs et al. (2025).*

Detailed local digitalised information is used to explore storm surge risks in relation to context specific assets and sectors including buildings, industry, harbour- and energy infrastructure, cultural/historical values, health, transportation, tourism, and ecosystems. This is done in a joint process with local stakeholders to provide inputs for decision-making on adaptation. The DTU DamageCost Model is applied to a quantitative assessment of the socioeconomic consequences of floods based on the observations from the flooding in October 2023 and ongoing research by DTU. The sectors included in the current version of the DTU DamageCost Model are presented in Figure 31.

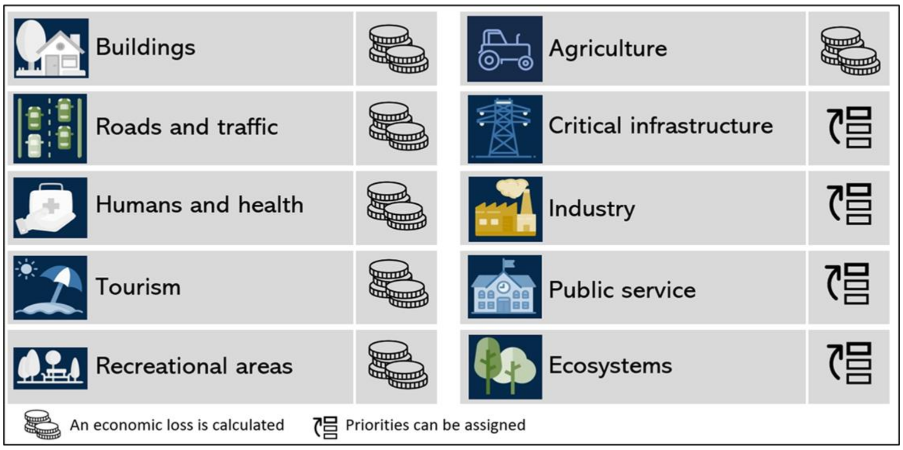

Figure 31: *Sectors on DTU DamageCost Model. Sectors marked with coins include monetary damage estimates and sectors with stacked boxes include other indicators.*

The analytical structure in Figure 30 represents a conventional cost-benefit analysis (CBA) related to coastal flooding but extended with indicators representing wellbeing to better represent social issues. The focus is how people and households are affected by flooding with adjustment for equity. The first two columns in Figure 30 represent the sectors and assets which can be affected by flood events given different climate scenarios. Associated damages of this are measured by monetary value estimates in column 3. In columns 4 and 5, additional impacts on people and equity are then added as an extra dimension of damages. Measures are here included, which represent a wider range of socioeconomic impacts. Examples of measures included here are the households' income, age, and education.

Based on Halsnæs et al. (2025) the assessment of wellbeing impacts of flooding events is inspired by the capability approach (Sen, 1987), which conceives a person's life as a combination of various "doings and beings" (functionings) and of his or her freedom to choose among these functionings (capabilities). Some of these capabilities may be quite elementary, such as being adequately nourished and escaping premature mortality, while others may be more complex, such as having the literacy required to participate actively in political life (Stiglitz et al., 2009). In terms of storm surge hazards, individuals' freedom can be constrained if i) damages for example occur on the homes of people, ii) impacts occur on workload and lost leisure time due to a burden of managing building refurbishment and limited possibilities for moving, or iii) from mental stress, etc. In addition to representing wellbeing in terms of people's capabilities affected by flooding, the damage cost assessment is also adjusted to reflect equity aspects. A diminishing marginal utility of income is assumed (Atkinson, 1970), which implies that additional income gains or losses through flood damage will increase or decrease wellbeing more for people with low incomes than for people with high incomes.

To account for income differences in the flood damage cost assessment, we utilise the methodological approach developed by Kind et al. (2017), which follows the ideas introduced by Atkinson (1970) and further introduced and discussed by Adler (2016).

We assume that individuals receive utility from income based on a utility function with constant relative risk aversion:

$$U(Y) = \frac{Y^{1-\gamma}}{1-\gamma} \quad for\ \gamma \geq 0,\ \ \gamma \neq 1$$

, where U is utility, Y is income, and γ is the elasticity of marginal utility of income, which is assumed to be the same for all individuals. Marginal utility of income is given by $U'(Y) = Y^{-\gamma}$. For $\gamma > 0$ marginal utility of income decreases with income.

Equity weights, ω_i, are defined as the incremental change in the utility of individual *i* caused by a change in income, relative to that of an individual with the average income:

$$\omega_{Yi} = \left(\frac{Y_i}{Y_{avg}}\right)^{-\gamma}$$

The equity weighted damage cost is given by

$$EWD = \sum_{i=1}^{I} \omega_{Yi} * D_i$$

, where D_i is the total damage cost of flooding hazards for individual *i*.

Step 1 Climate and socioeconomic scenarios

The climate scenarios are based on downscaled scenarios from the Klimaatlas from the Danish Meteorological Institute, DMI [Introduction to Klimaatlas | DMI.](#) Scenarios for sea level rise follow SSP1-2.6, SSP2-4.5 and SSP3-7.0. The latter is comparable to the corresponding SSP3-8.5 in terms of sea level rise in the case of Denmark). The Klimaatlas includes data on sea level rise in Danish coastal areas. Projections of sea level rise for SSP scenarios are added to present-day storm surge statistics as a basis for calculating event return periods (RP).

Table 5 and Table 6 show the sea level rise associated with storm surge return periods in Aabenraa and Haderslev based on the Klimaatlas. The present-day reference period covers 1981-2010.

Table 5: *Sea levels in cm for specific return periods (rp) for different climate scenarios for 2024 to 2100 In Aabenraa.*

Present day	2050			2100		
	SSP1-2.6	SSP2-4.5	SSP3-7.0	SSP1-2.6	SSP2-4.5	SSP3-7.0
159	176	175	178	199	202	217
170	187	186	189	210	213	228
181	198	197	201	221	224	239
200	217	216	220	240	243	258
214	231	230	234	254	257	272
227	244	243	247	267	270	285
250	267	266	269	290	293	308

Table 6: *Sea levels in cm for specific return periods (rp) for different climate scenarios for 2024 to 2100 for Haderslev.*

Present day	2050			2100		
	SSP1-2.6	SSP2-4.5	SSP3-7.0	SSP1-2.6	SSP2-4.5	SSP3-7.0
160	177	176	179	200	203	218
170	188	187	190	211	214	229
181	198	197	201	221	224	239
199	216	215	219	239	242	257
212	229	228	232	252	255	270
224	241	240	244	264	267	282
245	262	262	265	285	288	303

There are very small differences between sea level rise between the different climate scenarios in 2050 both for Aabenraa and Haderslev, but the differences increase in 2100. The damages and risk thereby vary more in the long term.

The socioeconomic scenarios used for the assessment of storm surge damages utilise a static continuation of the current land use including economic data as well as population data. This is because the future development trends are not available at the detailed local scale of the analyses in the CSA. Examples of how local development plans influence climate risks will be evaluated in collaboration with decision makers. Local development plans for Aabenraa and Haderslev are used, e.g., urban plans for Haderslev for adaptation assessment. A major issue here is planning for industry, settlements, open city space and ecosystems in flood prone old industrial harbour areas.

Step 2 Spatial data integration

Flood maps for the climate and socioeconomic scenarios are shown in the following Figure 32 and Figure 33. The maps show the extend of a flood with a 100-year return period at different time horizons using climate scenario SSP3-7.0.

In the city of Aabenraa, Figure 32, the map illustrates that there are certain thresholds in storm surge levels, which when exceeded, can result in significantly larger flooded areas, impacting the city centre and residential and recreational areas. This is due to the topography of the city with a steeply increasing moraine landscape.

In the city of Haderslev, Figure 33, the increase in flooded areas and flood risk areas is more gradual over time due to the rising terrain and without thresholds as in Aabenraa. In Aabenraa, a higher climate scenario, with faster rising sea level means that the city can experience significant increased risk by mid-century compared to a lower climate scenario.

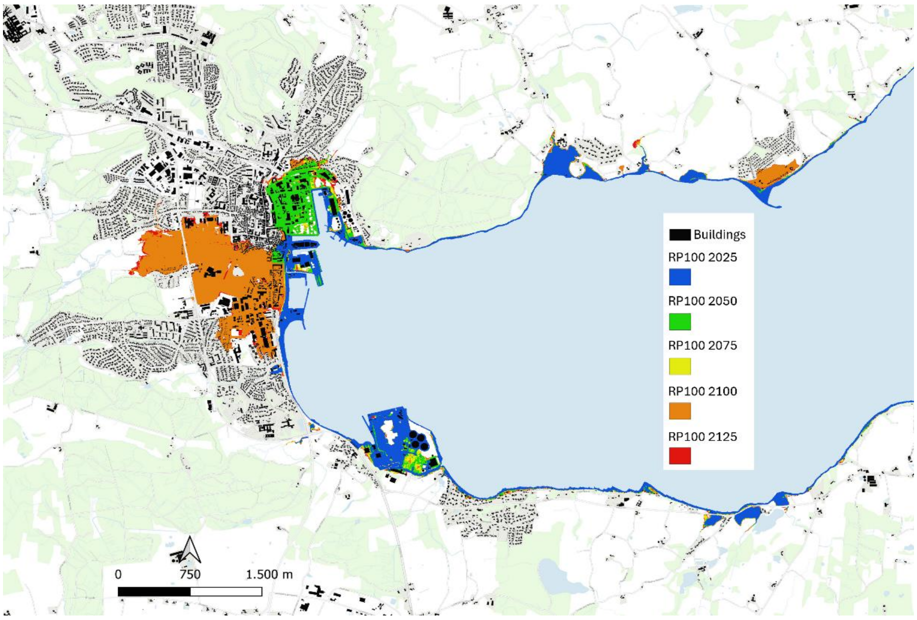

Figure 32: *Flood map for Aabenraa showing a 100-year flood at different time horizons using climate scenario SSP3-7.0. The colours show the additional areas, which will be flooded over time.*

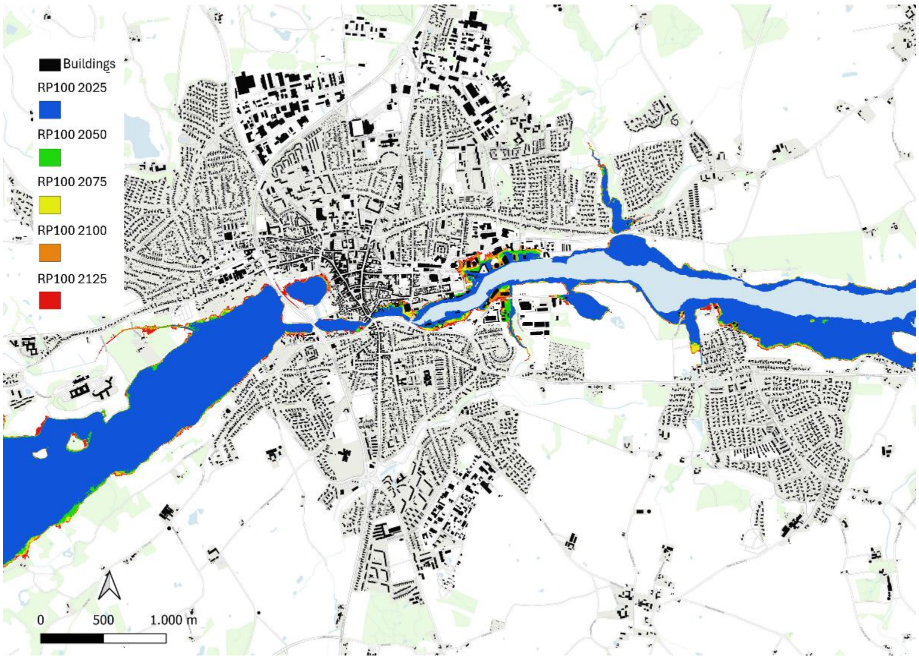

Figure 33: *Flood map for Haderslev showing a 100-year flood at different time horizons using climate scenario SSP3-7.0. The colours show the additional areas, which will be flooded over time.*

Step 3 Impact assessment

Figure 34 left shows the development in the land area being flooded in a 100-year event for different climate scenarios. Top is Aabenraa and bottom is Haderslev. As also illustrated in Figure 32 and Figure 33, in Haderslev the flood extent increases gradually with the increased expected storm surge levels, due to the topography of the area. In Aabenraa, there are specific thresholds of storm surge levels, which if passed result in a steep increase in the city area flooded.

Funded by the European Union

Figure 34 right shows the number of people living in areas, who potentially could get flooded by the same events as above. These figures illustrate that in Aabenraa around 150 people are at risk of flooding from a 100-year event today, and this could increase to between 2,000 and 2,300 by the end of the century, dependent on the climate scenario. In Haderslev, about 300 people are at risk of flooding from a 100-year event today, and the number will gradually increase with climate change, but the increase over time is more moderate than in the case of Aabenraa. The large blue flooded area on the figure is a low-lying area with no settlements.

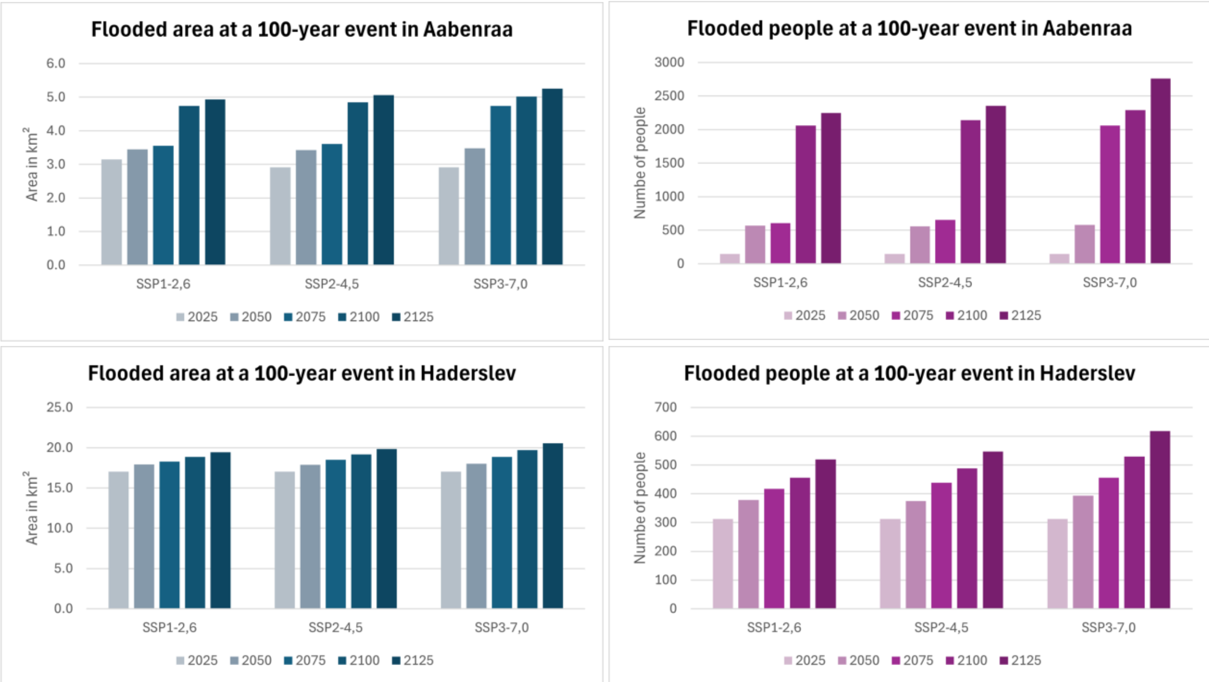

Figure 34: *(Left) Area flooded for a 100-year flood at different time horizons for three SSP-scenarios and (Right) number of people flooded at same events. Aabenraa municipality at top and Haderslev municipality at bottom.*

The impacts in terms of economic damages of different return period storm surges are shown in Figure 35 and Figure 36 for Aabenraa and Haderslev respectively using climate scenario SSP3-7.0 for the time horizons 2025, 2050, 2075, 2100 and 2125.

For both areas, damages to buildings are by far the largest damage cost, for Aabenraa approx. 86%-91% of total damage cost, dependent on scenario, and for Haderslev 70-77%. However, in Aabenraa, the second largest damage cost is human and health amounting to 2-10%, while for Haderslev it is tourism amounting to 19-25%, which is related to large summerhouse areas at risk.

The building damage costs are assessed for the following categories:

- Permanent residence
- Holiday home
- Commercial buildings
- Garage etc.
- Annex

- Utility
- Culture
- Public
- No data/Other

For Aabenraa, commercial buildings are the category with largest expected damage costs (approx. 55% of building damage cost), with holiday homes second for low storm surge levels, and with permanent residences second for higher storm surge levels, when the central city area is imposed to flooding. Public buildings are another large category for high storm surge levels.

Holiday homes contribute about 60% of the total building damage cost of flooding in Haderslev, while damages on permanent residential buildings are only about 10-14% of the flood damages, and business buildings about 15-27% of the damages.

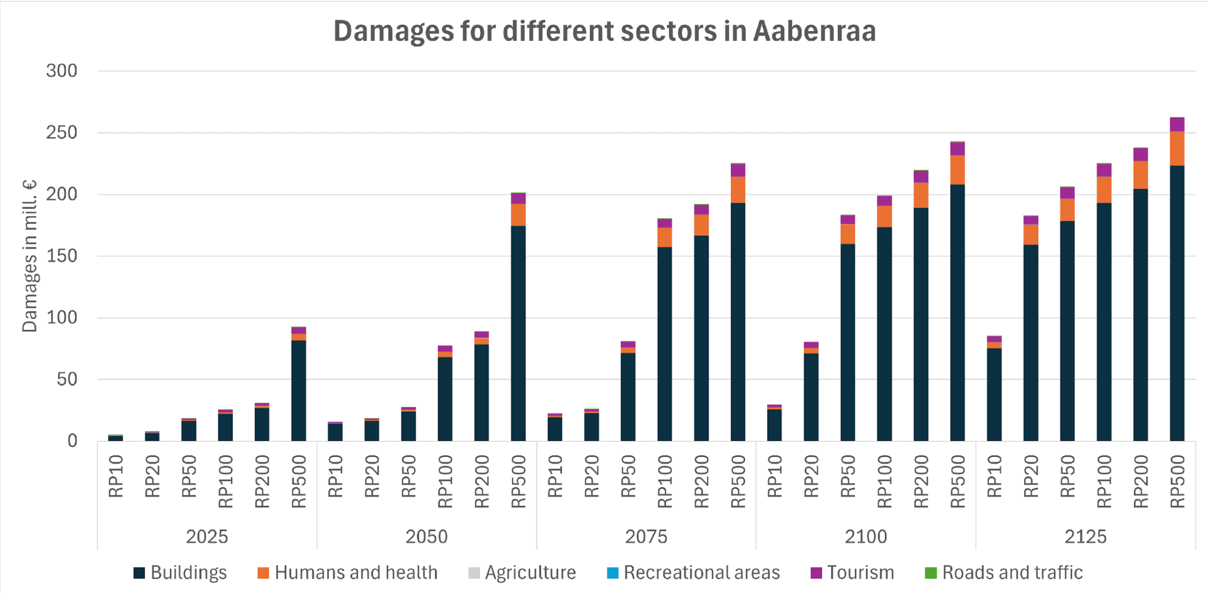

Figure 35: *Damage cost of Aabenraa for floods of different return periods at five time horizons with climate scenario SSP3-7.0.*

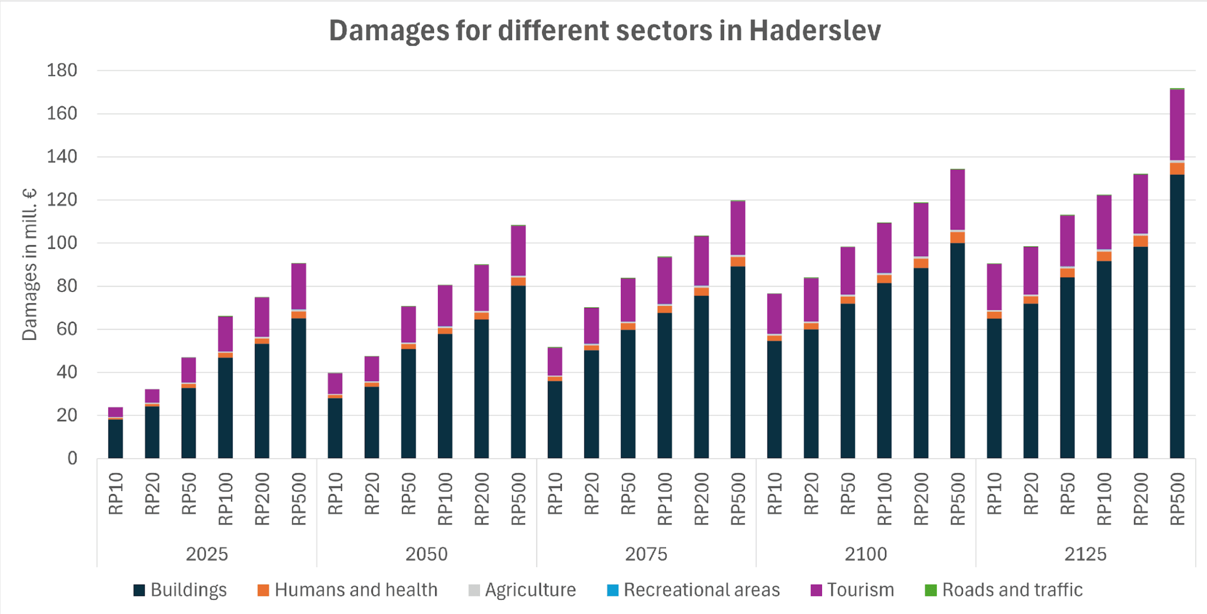

***Figure 36**: Damage cost of Haderslev for floods of different return periods at five time horizons with climate scenario SSP3-7.0.*

In addition to the monetary flood damage costs reported for Aabenraa and Haderslev, there are several social impacts of flooding including equity impacts on low-income households. In order to assess equity impacts on households with flooding risk, detailed spatial flood risk data and household income data have been collected and inequality aversion parameters have then been used to adjust damage costs from an equity perspective (see the methodology section).

Figures 37 and 38 show the results of the application of equity weights to household incomes in flooded risk areas relative to average household incomes in the cities.

Funded by the European Union

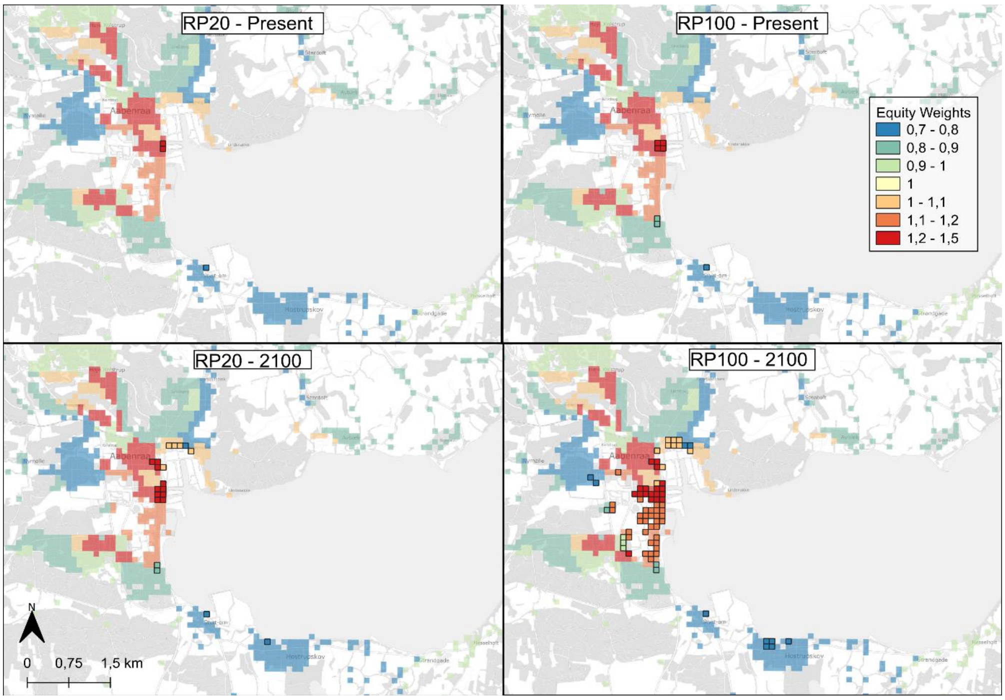

Figure 37: *Equity weights on household incomes in Aabenraa. Colours show the equity weight in grid cells. The grid cells with a marked boarder are flooded at the specific event. That data shows a 20- and 100- year event today and in 2100 using climate scenario SSP3-7.0.*

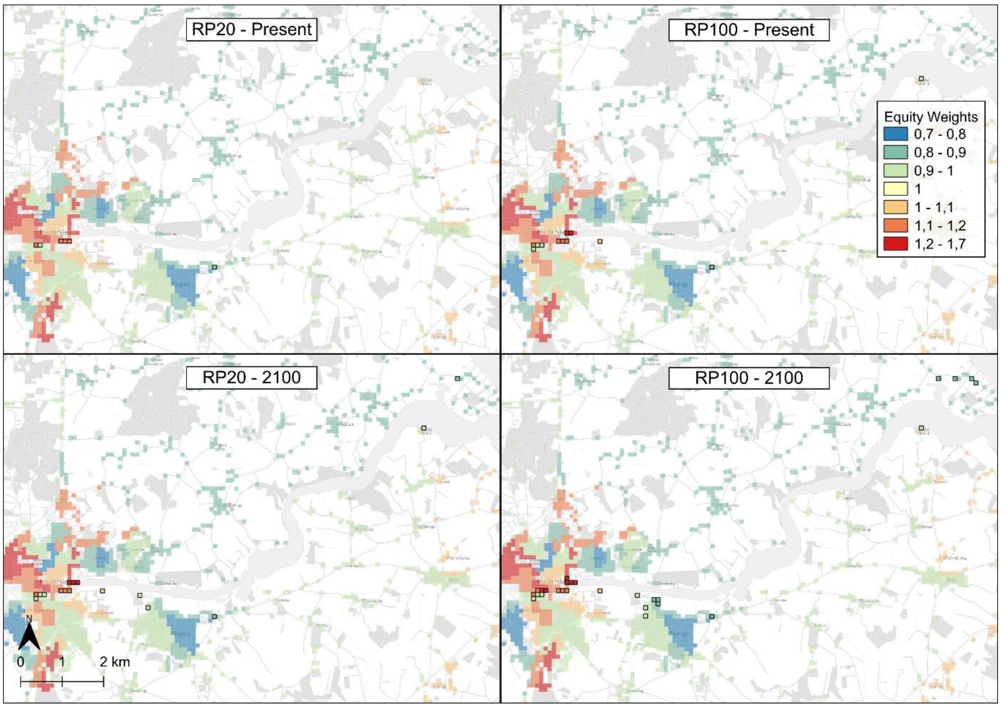

Figure 38: *Equity weights on household incomes in Haderslev. Colours show the equity weight in grid cells. The grid cells with a marked boarder are flooded at the specific event. That data shows a 20- and 100- year event today and in 2100 using climate scenario SSP3-7.0.*

It can be seen from Figure 37 that in 2100 in Aabenraa large parts of the flooded area affected by a 100 years flooding event in the SSP3-7.0 scenario will be areas, where, today, households are living with a relatively low income. Following our methodology, flood damages could be adjusted upwards to reflect this incidence from an equity perspective, and this could also be an argument to prioritise adaptation investments in such areas. Haderslev similarly has some flooding related equity impacts (Figure 38), but the area with flood risk where low-income households are located today is a smaller share of the flood risk area than in Aabenraa.

Step 4 Risk assessment

The expected net present values of flood risks for Aabenraa and Haderslev have been calculated by multiplying the monetary damages and the likelihood of flooding events over time for three different climate scenarios SSP1-2.6; SSP3-4.5; and SSP3-7.0.

For Aabenraa (Figure 39), the risk is relatively low in the beginning of the century, increasing to around €5 mill. annually in 2050 for all climate scenarios. Later in the century and in the beginning of the 22nd century, the difference between SSP3-7.0 and the two lower climate scenarios increases sharply. The annual risk is estimated to be €16 mill. in 2100 which is 60% larger than the two lower climate scenarios, and in 2125 the risks of the high climate scenario are 2-3 times larger than the two lower climate scenarios. This illustrates how sensitive Aabenraa is towards sea level rise in high climate scenarios over a long time horizon.

The risk in Haderslev is €7 mill. annually at present and increases gradually over time to be between €20 mill. and €30 mill. annually by 2100 from the low to the highest climate scenario (Figure 40). The development in the risk for the three climate scenarios exhibits smaller variations than for Aabenraa. The accumulated net present value (NPV) risk values are however significantly larger for Haderslev than for Aabenraa, which reflects that Haderslev in the near term has a high exposure to flooding risks in low laying areas with holiday homes.

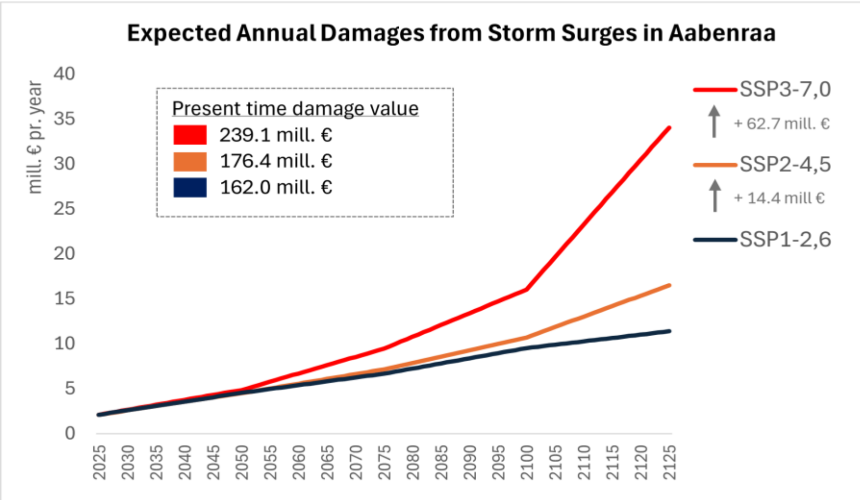

Figure 39: *Expected annual damages from storm surges in Aabenraa municipality for the three climate scenarios used and accumulated damages for the 100-year period in present day values.*

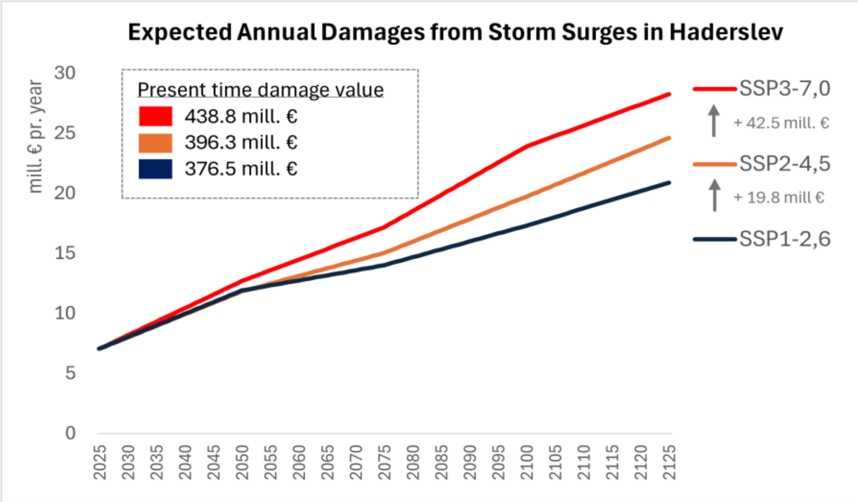

Figure 40: *Expected annual damages from storm surges in Haderslev municipality for the three climate scenarios used and accumulated damages for the 100-year period in present day values*

2.3.3. Results

Economic damages of coastal flooding have been assessed for the two Danish cities of Aabenraa and Haderslev, which are located in the South East of Jutland. The cities have been exposed to flooding events several times and most recently in October 2023, when large areas of the Aabenraa harbour with industrial buildings and services as well as areas with holiday homes in Haderslev were flooded.

In particular Aabenraa could risk a very steep increase in flood risks after 2050 if a high climate scenario is materializing, where the city area and large population groups could be affected. It is estimated that around 150 people could be impacted by a 100-year flooding event today, but this could increase to between 2,000 and 2,300 by the end of the century, dependent on the climate scenario. Large damage costs are associated with flooding risks, but on the top of these, there is also a negative incidence on equity since households with a relatively low income living in the city centre of Aabenraa could be at risk.

In Haderslev, flood damage costs are developing very gradually from today and into the future, and holiday homes are a high share of the assets at risk. 300 people are today expected to be at risk from flooding from a 100-year event, and climate change will gradually increase this number over time, but the increase will be more moderate than in the case of Aabenraa. Low-income households could suffer from flooding risks in Haderslev like for Aabenraa, but the equity impacts of flooding in Haderslev are smaller than in the case of Aabenraa.

The results from the case study will be compared with the results from the COACCH and PESETAS projects at regional level, and this comparison will also be a main element in the upscaling to sectoral level based on regional analogies in Europe. The damage cost model will here be supplemented

Funded by the European Union

with geographical activity-based information drawing on EUROSTAT NUTS3 information and CORINE land use data. The sectoral upscaling is based on data on the economic turnover of sectors, population and flooded areas which could be exposed to similar climate events around Europe.

2.3.4. Challenges and conclusions

The two cities Aabenraa and Haderslev have been exposed to flooding events several times and most recently in October 2023. Aabenraa could expect a steep increase in flood risks after 2050 if a high climate scenario is materializing, with the people exposed during a 100-year event rising from roughly 150 affected to more than 2,000 by 2100. The concentration of lower-income residents in the vulnerable city core compounds both the economic and equity impacts. By contrast, Haderslev faces a steadier, more moderate cost curve: holiday homes dominate the asset base at risk, and the exposed population grows only gradually from today's appr. 300 people, leaving distributional effects less pronounced than in Aabenraa. Moreover, the accumulated NPV risk values are significantly larger for Haderslev than for Aabenraa, reflecting that Haderslev is currently more exposed to flood risk in low laying areas.

2.3.5. References

Adler MD (2016) Benefit-Cost Analysis and Distributional Weights: An Overview. Review of Environmental Economics & Policy 10:264-285. https://doi.org/10.1093/reep/rew005

Atkinson AB (1970). On the Measurement of Inequality. Journal of Economic Theory 2:244-63. https://doi.org/10.1016/0022-0531(70)90039-6

Carter, J.G, Hincks, S, Vlastaras, V, Connelly, A and Handley, J. 2018. European Climate Risk Typology. [ONLINE] Available at: http://european-crt.org/index.html.

Danish Meteorological Institute (2024). Klimaatlas. Danish Meteorological Institute. https://www.dmi.dk/klimaatlas. Accessed 16 December 2024.

Halsnæs, K., Dømgaard, M.L., Larsen, M.A.D., & Kaspersen, P.S. (2021). Modeldokumentation og –vejledning for DTU SkadesØkonomi model (in Danish). Department of Technology, Management and Economics, DTU.

Halsnæs, K., Kaspersen, P. S., & Drews, M. (2015). Key drivers and economic consequences of high-end climate scenarios: uncertainties and risks. Climate Research, 64(1), 85-98. https://doi.org/10.3354/cr01308.

Halsnæs, K., Larsen, M. A. D., Sunding, T.P., & Dømgaard, M. L. (2023). The value of advanced flood models, damage costs and land use data in cost-effective climate change adaptation. Climate Services, 31(1). https://doi.org/10.1016/j.cliser.2023.100424.

Kind, J., Botzen, W.J.W., & Aerts, J.C.J.H. (2016). Accounting for risk aversion, income distribution and social welfare in cost - benefit analysis for flood risk management. WIREs Climate Change 8:e446. https://doi.org/10.1002/wcc.446.

Sen, A. (1986). Commodities and Capabilities. The Economic Journal, Volume 96, Issue 383, 1 September 1986, Pages 820–822, https://doi.org/10.2307/2232999.

Stiglitz, J., Sen, A., & Fitoussi, J-P. (2009). Report by the Commission on the Measurement of Economic Performance and Social Progress. Commission on the Measurement of Economic Performance and Social Progress, Paris.

2.4. CSA 4 FLOOD

2.4.1. Summary of climate change hotspots and event-based storyline

Climate Change hotspots (CCH)

The selected Climate Change Hotspot (CCH) is located in the valley areas of the Trentino-Alto Adige region in northeastern Italy. Recent evidence (e.g. Libertino et al., 2019; Dallan et al., 2022) shows that this Alpine territory is increasingly exposed to short-duration extreme precipitation events, a trend driven by climate change. The combination of complex orography and geomorphological fragility makes the region particularly susceptible to hydrogeological hazards, especially flash floods and debris flows, whose frequency and intensity are expected to rise under future climate scenarios. Among others, the high concentration of alluvial fans across the territory significantly contributes to hydrogeological vulnerability. These geomorphological formations are highly susceptible to flash flood events, as they tend to accumulate debris flows and channel sudden water surges during episodes of intense rainfall. As an illustrative example, the spatial distribution of alluvial fans across the province of Trento is shown in Figure 41.

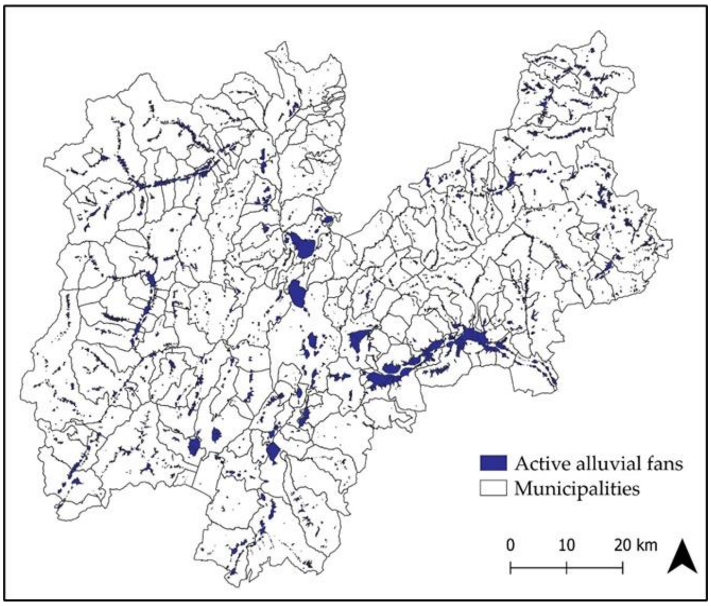

Figure 41: *Spatial distribution of alluvial fans in the province of Trento.*

Similar challenges concerning flood vulnerability, defined not only in terms of physical susceptibility, but also of exposure and potential socio-economic impacts, are found in other Alpine and pre-Alpine regions across Europe. Areas such as Bavaria in southern Germany, western Austria, and parts of eastern France present comparable combinations of steep topography, densely inhabited valleys, critical infrastructure, and climate-induced increases in precipitation extremes (Böhm et al., 2014; Boisson et al., 2021; Junger et al., 2022).

Event based storyline (STL)

The storyline anchoring the case study is based on Storm Vaia, which severely affected the Eastern Italian Alps, including Trentino-Alto Adige, between 27th and 29th October 2018. The event followed an extended dry period and resulted in extreme hydrological responses to intense and persistent rainfall. Synoptic conditions led to cumulative precipitation levels between 200 and 500 mm over 72 hours, with numerous locations exceeding historical records. The storm caused widespread flooding, landslides and slope failures, resulting in 11 fatalities and substantial socio-economic disruption.

2.4.2. Objectives

Building on the storyline and CCH characteristics, the overarching objectives of the present case study are:

- to assess the magnitude, frequency and plausibility of current and future flood-related impacts;
- to monetise the societal benefits of mitigation and adaptation (M&A) strategies under alternative impact scenarios;
- to investigate how such benefits are distributed across different population segments, with a focus on social equity dimensions.

2.4.3. Application of the methodological framework

To address the objectives, the six-step methodological framework presented in Deliverable D2.1 was operationalised to evaluate the socio-economic risks and impacts of extreme precipitation events in the CCH.

In line with Step 1, future flood scenarios were constructed using climate projections generated by a multi-model ensemble of convection-permitting regional climate models developed under the CORDEX Flagship Pilot Project. These projections were downscaled and remapped over the study area at a spatial resolution of 3.02 km. The time horizon comprised three 10-year periods (1996–2005, 2041–2050, and 2090–2099) modelled under the RCP 8.5 scenario. As per Step 2, climate and socio-economic data were integrated spatially at the NUTS3 level. Concerning socio-economic data, we assumed that population and economic variables are the same in the present and in the future, as data to build different future socio-economic scenarios are not available in our study area. The integration of climate and socio-economic data enabled a coherent representation of both hazards and exposure, thereby supporting the subsequent impact and risk analyses. As per the impact assessment (Step 3), hydrological models were used to transform precipitation inputs into flood hydrographs. These outputs were then applied to estimate physical impacts across five key domains: i) residential areas, ii) productive areas, iii) roads, iv) agricultural land and v) touristic infrastructures. The individual economic damage associated with a 1% increase in the flooded area in each of these domains was monetised through a Choice Experiment (CE) embedded in a large-scale survey. In Step 4, hazard and exposure data were integrated to construct proxy indicators of flood risk. These, combined with the valuation results derived from the Choice Experiment (CE), allowed for a first spatially disaggregated economic interpretation of flood risk, focusing on the perceived societal value of impact reductions across different land use categories. Subsequently, we estimated the average social cost of flood impacts under alternative future scenarios, by aggregating the estimates at the scale of the Trentino-Alto Adige population.

Methods: Exploiting km-scale convection-permitting climate models for projection of flash flood impacts over a range of mountainous basins in the Eastern Italian Alps

Global Climate Models (GCMs) and Regional Climate Models (RCMs) struggle to accurately represent changes in extreme sub-daily precipitation, particularly in regions with complex terrain. This limitation stems from their coarse spatial resolution (60 to 300 km for GCMs and 10 to 50 km for RCMs) and their reliance on parametrisations of convection, a known source of errors and uncertainty for the simulation of short-duration heavy precipitation (Coppola et al., 2020; Martel et al., 2020). The advent of Convection-Permitting Models (CPMs) significantly advances in addressing these limitations. CPMs, with their higher spatial resolutions (typically less than 4 km) and the explicit representation of convective processes, have demonstrated substantial improvements in representing extreme precipitation at sub-daily scales (e.g., Fosser et al. (2024)).

Such simulations are often short (10–20 model years) due to their high computational cost. The short length of these simulations challenges the applicability of extreme value analysis, which typically relies on observed or simulated extremes (Kottegoda and Rosso, 2008). To address this limitation, recent advancements in the statistical analysis of extremes based on ordinary values, such as the Metastatistical Extreme Value (MEV) (Marani and Ignaccolo, 2015) and its simplified version (SMEV) (Marra et al., 2019) offer a viable alternative. These methods can provide more reliable estimates of extreme events associated with a desired low exceedance probability from relatively short time series by using ordinary events instead of only using annual maxima (Dallan et al., 2024a, b).

Here, we take advantage of seven members from the CORDEX Flagship Pilot Project on Convective Phenomena over Europe and the Mediterranean (Coppola et al., 2020) (Table 7). To compare the different CPMs, a conservative remapping is applied to all the simulations to bring them to a regular grid with a horizontal resolution of 3 km.

Table 7: List of the CPM members used with the reference name, the original CPM name and resolution, and the coupled RCM with its resolution.

Institute	CPM name and original resolution	RCM
CMCC Euro-Mediterranean Center on Climate Change	CCLM (3 km)(Adinolfi et al., 2020; Rockel et al., 2008)	CCLM (12 km)(Adinolfi et al., 2020; Rockel et al., 2008)
CNRM Centre National de Recherches Météorologiques	CNRM-AROME41t1 (2.5 km)(Caillaud et al., 2021)	CNRM-ALADIN63 (12 km)(Nabat et al., 2020)
ETH Institute for Atmospheric and Climate Science	COSMO-crCLIM (2.2 km)(Leutwyler et al., 2016; Rockel et al., 2008)	COSMO-crCLIM (12 km)(Leutwyler et al., 2017; Rockel et al., 2008)
DMI-MET-SMHI DMI-MET Norway- SMHI HARMONIE-Climate community	HCLIM38-AROME (3 km)(Belušić et al., 2020)	HCLIM38-ALADIN (12 km)(Belušić et al., 2020)
KIT Karlsruhe Institute of Technology	CCLM5(3 km)(Baldauf et al., 2011; Rockel et al., 2008; Sørland et al., 2021)	CCLM4-CCLM5 (25 km)(Caldas-Alvarez et al., 2023; Coppola et al., 2020; Keuler et al., 2016; Sørland et al., 2021)
KNMI The Royal Netherlands Meteorological Institute	HCLIM38-AROME41 (2.5 km)(Belušić et al., 2020)	RACMO2.3 (12 km)(Noël et al., 2015)
MOHC Met Office Hadley Centre Exeter	HadREM_UM10.1 (2.2 km) (Berthou et al., 2018; Chan et al., 2020)	ERA-Interim (80km) *Directly driven by ECMWF without an intermediate nested RCM (Dee et al., 2011)

We used the Simplified Metastatistical Extreme Value (SMEV) (Marra et al., 2019) approach, a non-asymptotic method, to estimate the extreme precipitation return levels for a return period of 50 years and five durations (1, 3, 6, 12, and 24 hours). Different from extreme value theory, this type of approach estimates the distribution of extremes, assuming they are generated by finite samples from the distribution of ordinary events. In this way, all the ordinary events can be used in the statistical inference, strongly decreasing estimation uncertainties. This advantage is particularly useful in the case of the short data records of CPMs (Dallan al., 2023, 2024a). We focused on a return period of 50 years because this permits to approach extreme return levels at the same time keeping the sampling uncertainty reasonably low. The application of the SMEV technique pemitted the computation of changes in 50 years return levels between current period time slice (1996-2005), near future (2041-50) and far future (2091-2100).

Depth duration frequency (DDF) relationships were developed based on these return levels for a set of 20 mountainous basins located over the Eastern Italian Alps, with area ranging from 4 to 10 km2.

The DDF relationships were then used as an input to a modelling chain represented by the SAFER PLACE modelling tool to quantify flood impacts (extent) on:

- Residential areas;
- Productive areas;
- Roads
- Touristic infrastructures
- Agricultural land use

Methods: Choice Experiment description

CEs are a stated preference method extensively applied in environmental and resource economics to estimate the value of non-market goods and services (Mariel et al., 2021), i.e. goods for which no market prices exist, and whose economic value cannot be directly inferred from observed purchase behaviour. The theoretical foundations of the CE method lie in Lancaster's theory (Lancaster, 1966), which posits that utility is derived not from goods per se, rather from their attributes, and in random utility theory (Thurstone, 1927; Manski, 1977), which models individual choices under uncertainty. In a CE, respondents are presented with a sequence of choice tasks, each involving a set of hypothetical alternatives of goods characterised by varying combinations of attribute levels. For each task, they are asked to select their most preferred option. By analysing these choices through econometric models, specifically discrete choice models (McFadden, 1974), it is possible to estimate the marginal utility associated with each attribute. When a cost attribute is included among the characteristics, the analysis also allows for the derivation of marginal willingness to pay (WTP) estimates for specific attributes. In microeconomic terms, **WTP can be interpreted as a measure of the compensating surplus, that is the additional amount of income an individual would be willing to forgo to obtain a desirable change, holding utility constant. When aggregated across the relevant population, WTP estimates provide an indicator of the social welfare gains associated with the attribute presence**. The flexibility of the CE method, along with its capacity to handle multidimensional goods and capture preference heterogeneity, has contributed to its widespread application in the valuation of environmental goods and policy options (Hanley et al., 1998, 2001; Mariel et al., 2021).

In the context of the flood case study, a CE was designed and conducted to estimate the total economic value of the social benefits associated with reducing the impacts of extreme flood events. Each choice task presented respondents with three different hypothetical flood scenarios: two representing improved conditions resulting from the implementation or enhancement of protective measures (e.g. detention basins, levee reinforcement, infiltration trenches), and one representing a baseline scenario. This latter alternative was referred to in the experiment as the future quo scenario and reflected the expected level of flood impacts under a continuation of the current situation without the adoption of additional M&A interventions.

These scenarios were described by five impact attributes, each representing the percentage of flooded surface in key land use categories: residential areas, productive areas, roads, agricultural land and tourism-related infrastructure. The levels assigned to these attributes were informed by hydro-climatic modelling and varied according to land elevation, namely mountains, hills, and plains, reflecting spatially explicit projections of flood impacts under different M&A assumptions. The future quo alternative consistently presented always the highest impact level.

In addition to the five impact attributes, each scenario included a monetary attribute, representing an annual tax to be paid over five years as a financial contribution to implement M&A strategies to reduce flooding impacts. Tax levels varied across scenarios and were set at €20, €40, €60, or €80. Such levels were defined looking at the literature on choice experiments focusing on flood protection. The future quo option was always associated with zero cost. The attribute and corresponding levels are provided in Table 8.

Table 8: *Attributes and levels in the CE.*

Attributes	Plains Levels		Hills Levels		Mountains Levels	
	Improved scenarios	Future quo scenario	Improved scenarios	Future quo scenario	Improved scenarios	Future quo scenario
Residential areas	6%, 9%, 11%	11%	9%, 11%, 14%	14%	10%, 12%, 16%	16%
Productive areas	7%, 10%, 13%	13%	9%, 12%, 16%	16%	8%, 11%, 15%	15%
Roads	9%, 11%, 16%	16%	12%, 16%, 19%	19%	11%, 15%, 21%	21%
Agricultural land	13%, 16%, 18%	18%	13%, 18%, 20%	20%	15%, 19%, 25%	25%
Tourism infrastructure	6%, 9%, 10%	10%	9%, 11%, 14%	14%	10%, 12%, 16%	16%
Annual tax (5 years)	20€, 40€, 60€, 80€	0	20€, 40€, 60€, 80€	0	20€, 40€, 60€, 80€	0

Notes: *The levels shown under the improved scenarios reflect reductions in flooded surface, achievable through the enhancement or reinforcement of adaptation strategies and protective infrastructure. The "future quo" scenario represents the expected percentage of flooded surface in the absence of any additional mitigation or adaptation measures, that is, a continuation of the current situation without further intervention. All levels were defined on the basis of hydro-climatic modelling results specific to each land elevation class.*

The attribute levels were allocated across scenarios using a D-efficient experimental design. The final design included 48 distinct choice tasks, which were blocked into six groups. Each respondent was randomly assigned to one block and therefore completed only eight choice tasks, in order to minimise respondent fatigue. The blocking ensured approximately 333 full replications of the design across the overall sample. An example of a choice task is shown in Table 9.

Table 9: *Example of choice task provided in the CE.*

Attributes	Scenario 1	Scenario 2	"Future quo" scenario
Residential areas (%)	12	10	16
Productive areas (%)	11	15	15
Roads (%)	15	11	21
Agricultural land use (%)	19	19	25
Touristic infrastructures (%)	10	16	16
Tax (€)	20	60	0
I choose	○	○	○

Methods: Data collection and survey instrument

The questionnaire was administered online to a representative sample of 2,000 residents of the Triveneto area, in northeastern Italy. Quota sampling was applied to ensure representativeness in terms of age, gender, education, and income level. The questionnaire was distributed through a professional survey agency. The study received ethical approval from the Departmental Ethics Committee of the Department of Land, Environment, Agriculture and Forestry (TESAF) at the University of Padova. Data collection started in January 2025 and was completed in March 2025.

The questionnaire was organised into several sections. The first section investigated respondents' direct and indirect experiences with flood events. It included questions on the timing, frequency and severity of past floods, types of damage sustained, and familiarity with early warning systems. A specific focus was placed on the Vaia storm of 2018. The section concluded with questions on exposure to other extreme weather events, such as landslides, droughts, or heatwaves, experienced in the respondent's municipality over the past ten years. The second section explored flood risk perception and adaptive capacity. It covered perceived causes of floods, perceived safety of various protection measures in both urban and rural areas, subjective risk assessments, and respondents' sense of agency and preparedness. The third section focused on perceptions of political responsibility and institutional trust. Respondents were asked to report their level of familiarity with key EU, national and local flood risk management policies and instruments. This was followed by a set of statements on the perceived fairness, effectiveness and inclusiveness of public flood-related policies, including attention to gender equality and the needs of vulnerable groups. Trust in relevant institutions, such as municipalities, regional governments, national authorities, and civil protection agencies, was also assessed. Finally, this section included questions which addressed the perceived evolution of early warning systems, and the preferred channels for emergency communication. The questions of this section were included to inform the policy analysis carried out in WP4 and have informed D4.3 and D4.5. A subsequent section addressed climate change awareness and attribution beliefs. This included items on perceived long-term impacts on personal health, financial security, and the natural environment, as well as on the role of individual and collective responsibility in responding to climate challenges. To contextualise exposure and vulnerability, the questionnaire also collected information on the respondent's housing situation, including location, tenure, elevation, duration of residence, and the presence of any flood protection measures. This part was followed by the Choice Experiment. The final section gathered socio-demographic and economic background information, including gender, age, education, occupation, household size and composition, mobility habits, income level, and perceived sufficiency of income. It also included a set of items focused on the perceived economic impact of the COVID-19 pandemic on household resilience and on the ability to invest in flood protection.

In this deliverable we specifically used the CE data to estimate the economic value of flood risk mitigation across different land use categories. In addition, selected items from the section on socio-demographic information were employed to investigate variability in WTP across income and gender groups. The remaining parts of the survey primarily served to contextualise respondents' exposure and attitudes. Further analyses will be conducted to analyse how these factors influence WTP, and the results will be included in scientific publications for dissemination.

Methods: Econometric modelling approach

The econometric analysis of CE data was conducted by applying Random Utility Models (McFadden, 1974). Accordingly, the utility U_{int} that individual n derives from selecting alternative i in a given choice situation t consists of two components: a deterministic term V_{int}, which depends on observable attributes, and a stochastic component ε_{int}, which captures unobserved factors:

$$U_{int} = V_{int} + \varepsilon_{int}$$

In the current analysis, we adopted a Multinomial Logit (MNL) specification in WTP space (Train & Weeks, 2005; Scarpa et al., 2008) and specified the utility of the *i*-th flood scenario as follows:

$$U_{int} = \lambda^{*}(\beta' \mathbf{X}_{int} - p_{int}) + \varepsilon_{int}$$

where X_{int} is a vector of non-monetary attribute, in our case, the impact attributes representing the percentage of flooded surface across the different land use categories; p_{int} is the monetary attribute, in our case the annual tax and the vector β contains the marginal WTP associated with each non-monetary attribute; and λ^* is defined as $\lambda\ \delta$, where λ is the scale parameter of the independently and identically distributed (i.i.d) Gumbel error ε_{int} and δ is the coefficient for the tax attribute.

Specifically, the estimated coefficients represent the average marginal WTP to avoid a 1% increase in the flooded surface for each land use category. This model specification thus enables a direct economic valuation of the residents' WTP to prevent the social damage associated with flood risk and allows for disentangling how individuals value reductions in flood exposure across different land use of the territory under study.

The probability that individual *n* selects the flood scenario *i* in the choice task *t* is given by the MNL formula:

$$\pi_{int} = \frac{e^{V_{int}}}{\sum_j e^{V_{jnt}}}$$

, where *j* indexes the set of all available alternatives in the choice task *t*.

The models were estimated by maximum likelihood with the R package Apollo (Hess and Palma, 2019).

2.4.4. Results

Impact assessment

Flood impacts were quantified by coupling high-resolution precipitation data from climate models with hydrological simulations. Specifically, precipitation inputs were transformed into flood hydrographs, which were then used to estimate physical impacts at the scale of the entire study area across five land use categories: residential areas, productive areas, roads, agricultural land, and tourism-related infrastructures. The analysis focused on two future time horizons, 2041 – 2050 (mid-century) and 2090 – 2099 (end-century), modelled under the RCP 8.5 scenario. During the historical baseline period (1996 – 2005), flood impacts associated with a 50-year return period are expected to be null. As such, the baseline scenario serves as a comparative reference for evaluating changes in flood exposure under future climate conditions. Table 10 reports the estimated percentage of flooded surface across the five land use categories and three elevation zones (plains, hills, mountains). As expected, flood impacts are projected to intensify over time across all domains. The largest increases are observed for roads and agricultural land, particularly in mountainous areas, where flooded surfaces reach 21% and 25%, respectively, by 2090 – 2099. Residential and productive areas also experience notable increases in exposure, especially in hilly and mountainous zones.

Table 10: *Projected percentage of flooded surface by land use category and elevation zone in future time horizons.*

	Plains (%)		Hills (%)		Mountains (%)	
	2041-2050	2090-2099	2041-2050	2090-2099	2041-2050	2090-2099
Residential areas	5	11	6	14	7	16
Productive areas	6	13	8	16	7	15
Roads	8	16	9	19	11	21
Agricultural land	10	18	11	20	12	25
Touristic infrastructures	5	10	7	14	7	16

Notes: *The baseline period (1996–2005) corresponds to a scenario in which no flood impacts are recorded under a 50-year return period. This is therefore used as a reference for comparing projected flood exposure under future climate conditions.*

These projections of future flood impacts provide the foundation for the subsequent economic valuation and integrated assessment steps.

Economic valuation results

The socio-demographic characteristics of the survey sample are summarised in Table 11. The sample consists of 2,000 respondents and is representative of the target population, the residents of the Triveneto area, with respect to gender, age, education, and income distribution.

Funded by the European Union

Table 11: Socio-demographic characteristics of the sample (N = 2000).

	Frequency	Percentage (%)
Gender		
Male	942	47.10
Female	1058	52.90
Age class		
18-30	172	8.60
31-45	584	29.20
46-55	529	26.45
Over 55	715	35.75
Education		
Low	38	1.90
Medium	1276	63.80
High	686	34.30
Income		
Low	236	11.80
Medium	1388	69.40
High	376	18.80

Table 12 reports the average individual marginal WTP, expressed in euros, estimated from the MNL model in WTP space for the whole sample. The coefficient associated with the future quo alternative is negative and statistically significant. This indicates that, on average, respondents associate disutility with the baseline scenario, which entails no additional M&A measures. In other words, individuals are willing to pay, on average, €0.29 each per year to move away from the *future quo* and towards any improved scenario involving a reduction in flood impacts. **Turning to the land use attributes, the associated coefficients are positive, reflecting respondents' WTP to avoid a 1% increase in the flooded surface of each land use category, thus quantifying the perceived social economic value of flood impact reductions through M&A strategies. The larger the magnitude of the coefficient, the higher the social concern attached to that land use category**. Among the land use attributes, the highest marginal WTP is associated with residential areas, with an estimated value of €6.69 per year to avoid a 1% increase in flooded surface. This finding highlights the centrality of residential protection in residents' preferences. Damage to homes is likely perceived as the most immediate and personally relevant consequence of flooding, affecting both physical safety and overall well-being. The prominent role of private living spaces in public evaluations of flood risk mitigation is consistent with findings reported in previous studies (see for instance, Botzen et al. (2013)).

The second and third most valued categories are productive areas and roads, with WTP values of €2.30 and €2.12 per year, respectively. These results indicate that respondents assign substantial importance to the protection of economic infrastructure and transport networks. Damage to productive areas may be interpreted in terms of business disruption, employment loss, and reduced regional economic activity, while road infrastructure is likely linked to access to essential services, mobility, and public safety. Similarly, the estimated WTP for agricultural land protection is €2.03 per year, indicating that the public opinion places considerable value on safeguarding rural and food-producing landscapes. This reflects both cultural attachment to agricultural areas and recognition of their broader ecological and socio-economic functions. On the other hand, tourism-related infrastructure shows the lowest WTP, with a value of €0.76 per year, significant at the 10% level. While still perceived as worthy of protection, this category appears to be less prioritised by respondents. Possible explanations include the more indirect nature of tourism benefits, seasonal exposure, or the perception that damages in this sector may be more easily recoverable.

Table 12: *MNL estimates of marginal WTP for flood impacts.*

	WTP estimate	Standard Error
Future quo scenario	-0.29***	0.05
Residential areas	6.69***	0.55
Productive areas	2.30***	0.36
Roads	2.12***	0.31
Agricultural land use	2.03***	0.30
Touristic infrastructures	0.76*	0.41
LL	-16505.28	
N	16000	

Notes: *WTP estimates are expressed in euros per year. Significance levels: p < 0.01 (***), p < 0.10 (*). LL = Log-likelihood. N = Number of observations.*

Tables 13 and 14 presents WTP estimates across income groups and gender, allowing for an exploration of distributional differences in preferences for flood impact mitigation. As in the full sample, the ranking of land use attributes is generally consistent: residential areas command the highest economic value, while tourism infrastructure ranks lowest. However, the magnitude and statistical significance of the coefficients vary across groups. It is worth pointing out that WTP estimates reflect not only preference but also individuals' economic capacity to express those preferences. Higher WTP among wealthier respondents does not imply greater exposure to flood risk or stronger concern, but rather their enhanced ability to monetise those concerns within a stated preference framework. In this sense, WTP functions as an indicator of perceived value conditional on available resources, rather than of vulnerability per se.

Across income classes (Table 13), a clear gradient emerges for residential and productive areas. Respondents in higher income brackets report higher WTP values for avoiding a 1% increase in flooded surface in residential areas, with statistically significant coefficients of €3.91 (low income), €6.93 (middle income), and €9.86 (high income). This confirms that residential protection is consistently prioritised, and that wealthier individuals are able and willing to assign higher monetary values to its preservation. Similar trends are observed for productive areas (€1.89, €2.20, €3.46), and roads (€1.59, €2.17, €2.65), with all coefficients statistically significant across income groups. This suggests a shared concern for economic infrastructure and mobility. In contrast, for agricultural land, only the low-income (€1.29) and middle-income (€2.35) coefficients are statistically significant. The coefficient for the high-income group (€1.39) is not statistically distinguishable from zero, indicating greater heterogeneity in taste or less salience of this land use type among wealthier individuals. For tourism infrastructure, none of the estimates reach statistically significant levels. This result aligns with the full-sample findings and suggests limited perceived urgency or direct impact in this domain.

Table 13: *MNL estimates of marginal WTP for flood impacts by income group.*

	Low income		Medium income		High income	
	WTP estimate	Standard Error	WTP estimate	Standard Error	WTP estimate	Standard Error
Future quo scenario	-0.29**	0.12	-0.31***	0.06	-0.02	0.15
Residential areas	3.91***	0.92	6.93***	0.69	9.86***	1.91
Productive areas	1.89***	0.68	2.20***	0.44	3.46***	1.12
Roads	1.59***	0.59	2.17***	0.39	2.65***	0.95
Agricultural land use	1.30**	0.58	2.35***	0.38	1.39	0.87
Touristic infrastructures	1.29	0.82	0.46	0.51	1.12	1.22
LL	-3017.83		-11470.15		-1939.68	
N	3008		11104		1888	

Notes: *WTP estimates are expressed in euros per year. Significance levels: p < 0.01 (***), p < 0.05 (**). LL = Log-likelihood. N = Number of observations.*

Regarding gender (Table 14), both men and women display similar preference structures, with statistically significant coefficients for all land use categories except touristic infrastructures. However, some differences in the preference ranking for land use protection emerge. Among men, agricultural land protection is valued more highly than road infrastructure protection, whereas among women, flood risk protection for roads is prioritised over the protection of productive areas.

Funded by the European Union

Table 14: MNL estimates of marginal WTP for flood impacts by gender.

	Male		Female	
	WTP estimate	Standard Error	WTP estimate	Standard Error
Future quo scenario	-0.34***	0.08	-0.24***	0.07
Residential areas	7.31***	0.93	6.27***	0.66
Productive areas	2.67***	0.60	2.04***	0.44
Roads	1.90***	0.50	2.28***	0.39
Agricultural land use	2.10***	0.49	1.98***	0.37
Touristic infrastructures	0.71	0.68	0.81	0.51
LL	-7825.39		-8670.69	
N	7536		8464	

Notes: *WTP estimates are expressed in euros per year. Significance levels: p < 0.01 (***). LL = Log-likelihood. N = Number of observations.*

Overall, these results reinforce the importance of accounting for economic stratification in the interpretation of the socioeconomic valuation of impacts and highlight the need for equity considerations in the design of flood adaptation policies.

Integrated assessment of social costs of future flood impacts

The average individual WTP associated with total flood impact across elevation zones was computed by multiplying the marginal WTP values for a 1% reduction (Table 12) by the total projected flooded surface (as reported in Table 10). Figure 42 presents the total individual WTP values by elevation zone, whereas Figure 43 shows the disaggregation by land use category. **WTP represents the monetary value that individuals assign to a reduction in flood risk and serves as a proxy for the perceived benefit of mitigation strategies**. The results indicate an increase in perceived economic damages over time, with higher values in hilly and mountainous areas, particularly under the end-century scenario (2090 – 2099), since these are projected to be the most vulnerable to future flood impacts. Residential areas consistently represent the largest share of total estimated WTP, reflecting their central role in public preferences for flood risk mitigation.

Funded by the European Union

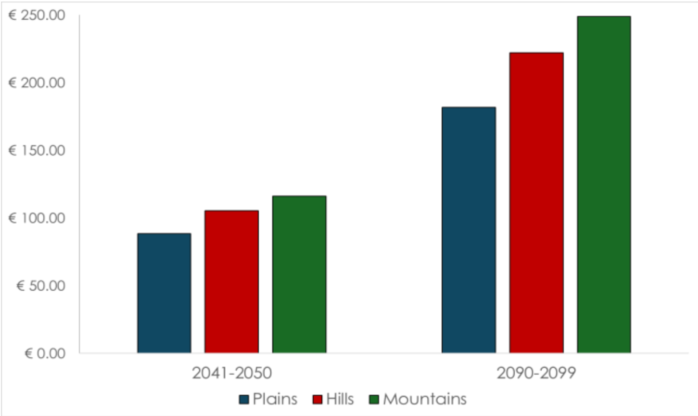

Figure 42: *Average individual economic valuation for total flood impact.*

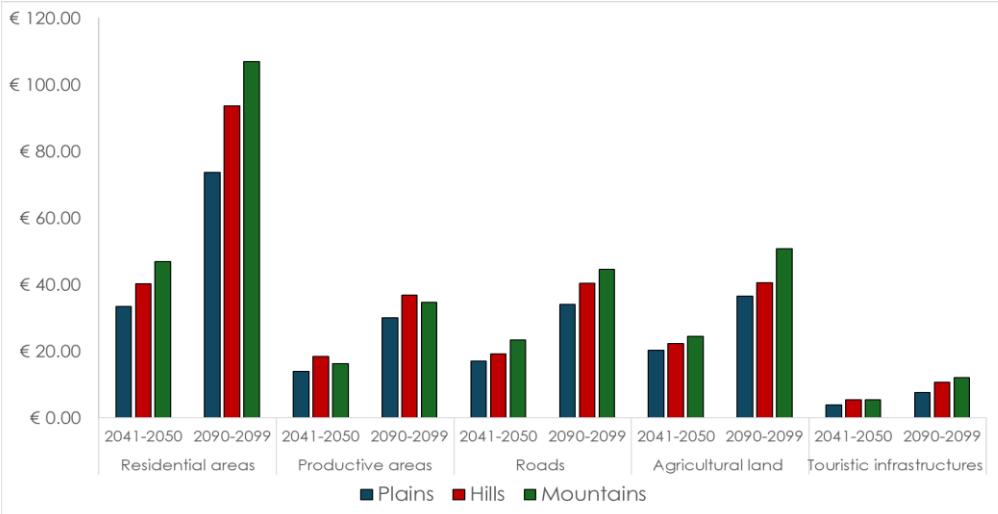

Figure 43: *Average individual economic valuation for total flood impact by land use category.*

Figures 44 and 45 present **the estimated total social benefits potentially achievable through flood risk M&A strategies, obtained by aggregating individual WTP values over the resident population of Trentino-Alto Adige.** Figure 44 shows the overall economic value per scenario, while Figure 45 breaks it down by land use category. These figures provide a quantification of the collective economic value associated with reducing future flood impacts, supporting the design of evidence-based and socially responsive adaptation strategies.

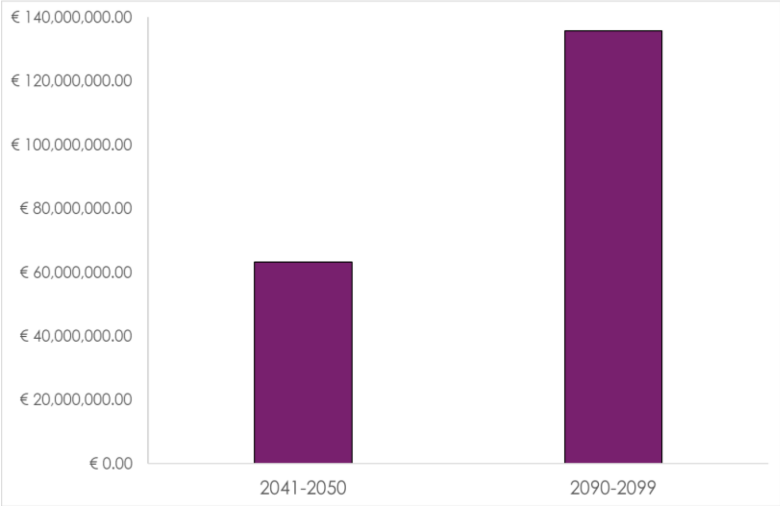

Figure 44: *Estimated total economic benefits for society of flood risk mitigation in Trentino-Alto Adige.*

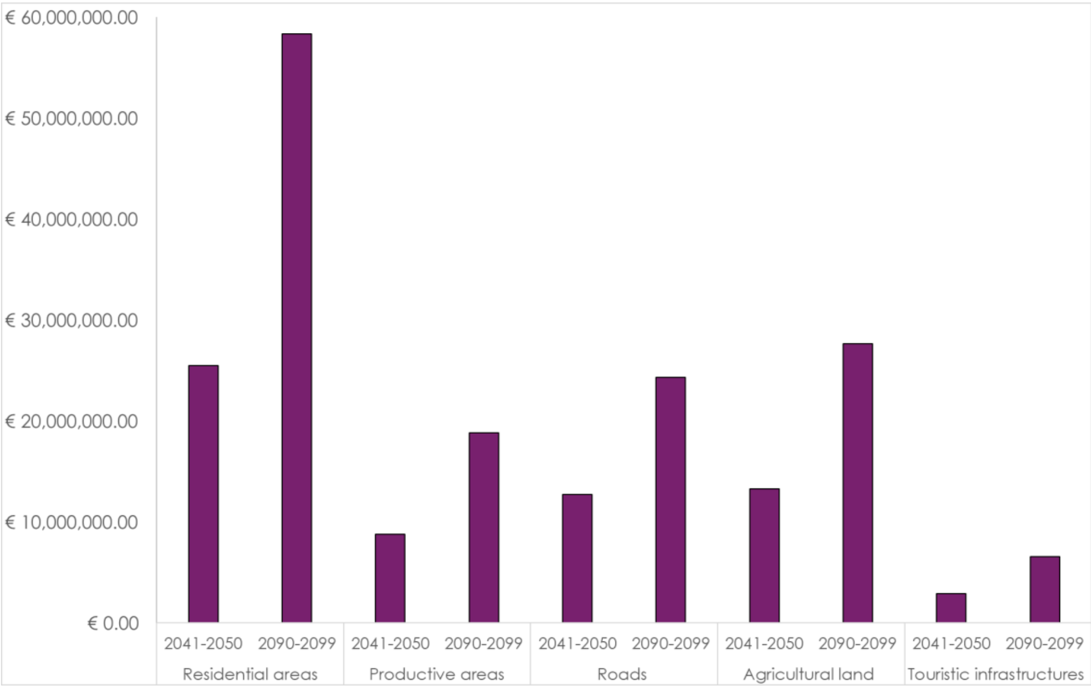

Figure 45: *Estimated total economic benefits for society of flood risk mitigation in Trentino-Alto Adige by land use category.*

2.4.5. Conclusions

This case study demonstrates the potential of combining high-resolution climate and hydrological modelling with stated preference methods to inform socially responsive adaptation strategies in flood-vulnerable regions. The results underscore the relevance of flood projections in capturing vulnerability gradients and guiding spatially targeted interventions. The analysis reveals substantial public support for M&A investments, especially when aimed at protecting residential areas and critical productive areas and infrastructure. The heterogeneity in WTP estimates across income and gender groups highlight the importance of incorporating equity and distributional concerns into policy design.

The aggregate economic estimates can serve as a benchmark for assessing the socio-economic efficiency of flood risk M&A investments. Since WTP values represents the perceived maximum benefit that individuals assign to avoiding flood damages, the aggregate measure can be interpreted as the upper bound of a socially optimal investment. In other words, any M&A strategy whose cost exceeds the corresponding total WTP would not yield net social benefits. Conversely, investment levels below this threshold remain within the bounds of collective welfare gains. Therefore, the results of this case study provide not only insights into public preferences, but also a reference point to inform cost-benefit assessments and prioritisation in flood risk management planning.

2.4.6. References

Adinolfi, M., Raffa, M., Reder, A., & Mercogliano, P. (2020). Evaluation and expected changes of summer precipitation at convection permitting scale with COSMO-CLM over alpine space. *Atmosphere*, *12*(1), 54.

Baldauf, M., Seifert, A., Förstner, J., Majewski, D., Raschendorfer, M., & Reinhardt, T. (2011). Operational convective-scale numerical weather prediction with the COSMO model: Description and sensitivities. *Monthly Weather Review, 139*(12), 3887–3905.

Belušić, D., de Vries, H., Dobler, A., Landgren, O., Lind, P., Lindstedt, D., Pedersen, R. A., Sánchez-Perrino, J. C., Toivonen, E., van Ulft, B., Wang, F., Andrae, U., Batrak, Y., Kjellström, E., Lenderink, G., Nikulin, G., Pietikäinen, J.-P., Rodríguez-Camino, E., Samuelsson, P., van Meijgaard, E., & Wu, M. (2020). HCLIM38: a flexible regional climate model applicable for different climate zones from coarse to convection-permitting scales. *Geoscientific Model Development, 13*(3), 1311–1333.

Berthou, S., Kendon, E. J., Chan, S. C., Ban, N., Leutwyler, D., Schär, C., & Fosser, G. (2020). Pan-European climate at convection-permitting scale: a model intercomparison study. *Climate Dynamics*, *55*, 35-59.

Böhm, O., Jacobeit, J., Glaser, R., & Wetzel, K. F. (2014). Flood history of the Bavarian Alpine Foreland since the late Middle Ages in the context of internal and external climate forcing factors. Hydrology & Earth System Sciences Discussions, 11(7).

Boisson, E., Wilhelm, B., Garnier, E., Mélo, A., Anquetin, S., & Ruin, I. (2021). Geo-historical analysis of flood impacts in Alpine catchments (HIFAVa database, Arve River, France, 1850–2015). Natural Hazards and Earth System Sciences Discussions, 2021, 1-24.

Botzen, W. J. W., Aerts, J. C. J. H., & van den Bergh, J. C. J. M. (2013). Individual preferences for reducing flood risk to near zero through elevation. *Mitigation and Adaptation Strategies for Global Change*, 18(2), 229–244.

Caillaud, C., Somot, S., Alias, A., Bernard-Bouissières, I., Fumière, Q., Laurantin, O., ... & Ducrocq, V. (2021). Modelling Mediterranean heavy precipitation events at climate scale: an object-oriented evaluation of the CNRM-AROME convection-permitting regional climate model. *Climate Dynamics*, *56*, 1717-1752.

Caldas-Alvarez, A., Feldmann, H., Lucio-Eceiza, E., & Pinto, J. G. (2023). Convection-parameterized and convection-permitting modelling of heavy precipitation in decadal simulations of the greater Alpine region with COSMO-CLM. *Weather and Climate Dynamics*, *4*(2), 543-565.

Chan, S. C., Kendon, E. J., Berthou, S., Fosser, G., Lewis, E., & Fowler, H. J. (2020). Europe-wide precipitation projections at convection permitting scale with the Unified Model. *Climate Dynamics*, *55*, 409-428.

Coppola, E., Sobolowski, S., Pichelli, E., Raffaele, F., Ahrens, B., Anders, I., Ban, N., Bastin, S., Belda, M., Belusic, D., Caldas-Alvarez, A., Cardoso, R. M., Davolio, S., Dobler, A., Fernandez, J., Fita, L., Fumiere, Q., Giorgi, F., Goergen, K., Güttler, I., Halenka, T., Heinzeller, D., Hodnebrog, Ø., Jacob, D., & Warrach-Sagi, K. (2020). A first-of-its-kind multi-model convection permitting ensemble for investigating convective phenomena over Europe and the Mediterranean. *Climate Dynamics, 55*, 3–34.

Dallan, E., Borga, M., Fosser, G., Canale, A., Roghani, B., Marani, M., & Marra, F. (2024a). A Method to Assess and Explain Changes in Sub-Daily Precipitation Return Levels From Convection-Permitting Simulations. Water Resources Research, 60(5). https://doi.org/10.1029/2023WR035969

Dallan, E., Marra, F., Fosser, G., Marani, M., & Borga, M. (2024b). Dynamical Factors Heavily Modulate the Future Increase of Sub-Daily Extreme Precipitation in the Alpine-Mediterranean Region. Earth's Future, 12(12), e2024EF005185.

Dallan, E., Marra, F., Fosser, G., Marani, M., Formetta, G., Schär, C., & Borga, M. (2023). How well does a convection-permitting regional climate model represent the reverse orographic effect of extreme hourly precipitation? Hydrology and Earth System Sciences, 27(5), 1133–1149.

Dee, D. P., Uppala, S. M., Simmons, A. J., Berrisford, P., Poli, P., Kobayashi, S., Andrae, U., Balmaseda, M. A., Balsamo, G., Bauer, P., Bechtold, P., Beljaars, A. C. M., van de Berg, L., Bidlot, J., Bormann, N., Delsol, C., Dragani, R., Fuentes, M., Geer, A. J., Haimberger, L., Healy, S. B., Hersbach, H., Hólm, E. V., Isaksen, L., Kållberg, P., Köhler, M., Matricardi, M., McNally, A. P., Monge-Sanz, B. M., Morcrette, J.-J., Park, B.-K., Peubey, C., de Rosnay, P., Tavolato, C., Thépaut, J.-N., & Vitart, F. (2011). The ERA-Interim reanalysis: Configuration and performance of the data assimilation system. *Quarterly Journal of the Royal Meteorological Society, 137*(656), 553–597.

Hanley, N., Mourato, S., & Wright, R. E. (2001). Choice modelling approaches: a superior alternative for environmental valuation? *Journal of Economic Surveys*, 15(3), 435–462.

Hanley, N., Wright, R. E., & Adamowicz, V. (1998). Using choice experiments to value the environment. *Environmental and Resource Economics*, 11(3–4), 413–428.

Hess, S. & Palma, D. (2019) Apollo: a flexible, powerful and customisable freeware package for choice model estimation and application. *Journal of Choice Modelling*, 32, 100170.

Junger, L., Hohensinner, S., Schroll, K., Wagner, K., & Seher, W. (2022). Land Use in Flood-Prone Areas and Its Significance for Flood Risk Management—A Case Study of Alpine Regions in Austria. Land, 11(3), 392.

Keuler, K., Radtke, K., Kotlarski, S., & Lüthi, D. (2016). Regional climate change over Europe in COSMO-CLM: Influence of emission scenario and driving global model. *Meteorologische Zeitschrift*, *25*(2), 121-136.

Kottegoda, N. T., & Rosso, R. (2008). Applied statistics for civil and environmental engineers.

Lancaster, K. J. (1966). A new approach to consumer theory. *Journal of Political Economy*, 74(2), 132–157.

Leutwyler, D., Fuhrer, O., Lapillonne, X., Lüthi, D., & Schär, C. (2016). Towards European-scale convection-resolving climate simulations with GPUs: A study with COSMO 4.19. *Geoscientific Model Development*, *9*(9), 3393-3412.

Libertino, A., Ganora, D., & Claps, P. (2019). Evidence for increasing rainfall extremes remains elusive at large spatial scales: The case of Italy. *Geophysical Research Letters*, *46*(13), 7437-7446.

Manski, C. F. (1977). The structure of random utility models. *Theory and Decision, 8*(3), 229–254.

Marani, M., & Ignaccolo, M. (2015). A metastatistical approach to rainfall extremes. Advances in Water Resources, 79, 121–126.

Mariel, P., Hoyos, D., Meyerhoff, J., Czajkowski, M., Dekker, T., Glenk, K., Jacobsen, J. B., Liebe, U., Olsen, S. B., Sagebiel, J., & Thiene, M. (2021). *Environmental valuation with discrete choice experiments: Guidance on design, implementation and data analysis* (p. 129). Springer Nature.

Marra, F., Borga, M., & Morin, E. (2020). A Unified Framework for Extreme Subdaily Precipitation Frequency Analyses Based on Ordinary Events. Geophysical Research Letters, 47(18).

Marra, F., Zoccatelli, D., Armon, M., & Morin, E. (2019). A simplified MEV formulation to model extremes emerging from multiple nonstationary underlying processes. Advances in Water Resources, 127, 280–290.

Martel, J.-L., Mailhot, A., & Brissette, F. (2020). Global and Regional Projected Changes in 100-yr Subdaily, Daily, and Multiday Precipitation Extremes Estimated from Three Large Ensembles of Climate Simulations. Journal of Climate, 33(3), 1089–1103.

McFadden, D. (1974). Conditional logit analysis of qualitative choice behaviour. In P. Zarembka (Ed.), *Frontiers in Econometrics* (pp. 105–142). Academic Press.

Nabat, P., Somot, S., Cassou, C., Mallet, M., Michou, M., Bouniol, D., Decharme, B., Drugé, T., Roehrig, R., & Saint-Martin, D. (2020). Modulation of radiative aerosols effects by atmospheric circulation over the Euro-Mediterranean region. *Atmospheric Chemistry and Physics*, *20*(14), 8315-8349.

Noël, B., Van De Berg, W. J., Van Meijgaard, E., Kuipers Munneke, P., Van De Wal, R. S. W., & Van Den Broeke, M. R. (2015). Evaluation of the updated regional climate model RACMO2. 3: summer snowfall impact on the Greenland Ice Sheet. *The Cryosphere*, *9*(5), 1831-1844.

Rockel, B., Will, A., & Hense, A. (2008). The regional climate model COSMO-CLM (CCLM). *Meteorologische zeitschrift*, *17*(4), 347.

Scarpa, R., Thiene, M., & Train, K. (2008). Utility in willingness to pay space: A tool to address confounding random scale effects in destination choice to the Alps. *American Journal of Agricultural Economics, 90*(4), 994–1010.

Sørland, S. L., Brogli, R., Pothapakula, P. K., Russo, E., Van de Walle, J., Ahrens, B., Anders, I., Bucchignani, E., Davin, E. L., Demory, M.-E., Dosio, A., Feldmann, H., Früh, B., Geyer, B., Keuler, K., Lee, D., Li, D., van Lipzig, N. P. M., Min, S.-K., Panitz, H.-J., Rockel, B., Schär, C., Steger, C., & Thiery, W. (2021). COSMO-CLM regional climate simulations in the Coordinated Regional Climate Downscaling Experiment (CORDEX) framework: A review. *Geoscientific Model Development, 14*(8), 5125–5154.

Thurstone, L. L. (1927). A law of comparative judgment. *Psychological Review*, 34, 273–286.

Train, K. E., & Weeks, M. (2005). Discrete choice models in preference space and willingness-to-pay space. In R. Scarpa & A. Alberini (Eds.), *Application of simulation methods in environmental and resource economics* (pp. 1–16). Springer, Dordrecht.

Funded by
the European Union

2.5. CSA 5 SNOW

Case Study 5 (CSA 5) examines snow avalanche hazards and risks in the European Alps and Carpathians, using selected CCHs and STLs (as introduced in Section 1.4). It explores how changing hazard conditions, influenced by socio-economic and environmental factors, may potentially affect communities, tourism, transport, and forests.

2.5.1. Summary of climate change hotspots and event-based storyline

Seven major STL events were selected for this case study based on their fatalities and significant impacts on communities, tourism infrastructure, transport routes, and forest areas. Events were sourced from European (European Avalanche Warning Service – EAWS), national and regional inventories (i.e., of the Institute for Snow and Avalanche Research – SLF, National Meteorological Administration – NMA, regional Avalanche Warning Services – LWDs in Austria, International Association for Coordination and Documentation of Snow and Avalanche Problems – AINEVA and Meteomont in Italy, Avalanseincarpati.org), media releases, mountain rescue services inventories and reports (i.e., International Commission for Alpine Rescue – ICAR, Salvamont in Romania), and scientific publications. Their geographical distribution is shown in Figure 46.

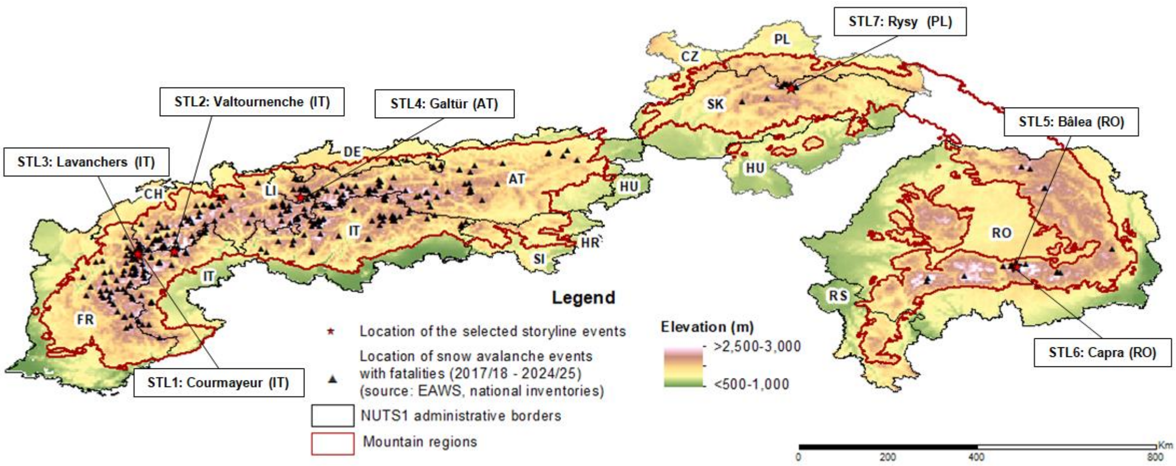

Figure 46: Spatial distribution of the selected storyline events across the European Alps and Carpathian Mountains and to the location of registered snow avalanches with fatalities (from 2017/18 to present).

Each STL event was thoroughly documented to analyse hazard conditions, impacts, and future risk potential. Key findings include:

- All events occurred in areas with complex terrain, heavy snow accumulation, high tourism activity, and recurrent avalanches.
- Most had cross-sectoral impacts, disrupting tourism, forestry, and road networks.

- A clear need for updating hazard zoning, early warning systems, and adaptive planning, especially as snow patterns shift with climate change.
- Events consistently led to severe human, infrastructural, and economic losses, with fatalities mainly among tourists and residents, particularly in the Alps.

These patterns highlight mountain regions as CCHs, with intense avalanche activity and high concentrations of vulnerable assets like ski infrastructure and alpine roads. Using a composite hazard index (1–5) that integrates seven snow hazard indicators and terrain susceptibility, six CCHs were identified across the Alps and Carpathians. Figure 47 shows their distribution from the baseline (1971–2000) to 2100 under RCP4.5 (SSP2) and RCP8.5 (SSP5), with risk peaking during winter tourism seasons, especially in the Alps and key Carpathian resorts. The identified CCHs overlap many well recognised avalanche-prone areas across both mountain regions with a significant number of reported fatalities (especially in the Alps), as well as the areas where the selected storyline events are located. The CCHs areas show similar extension and location in spring (MAM), when climate change signals are also important.

In the European Alps, CCHs areas are concentrated in:

- CCH1 (SE France and NW Italy), including parts of the Haute-Alpes, Savoie, Haute-Savoie, Drôme, Alpes-de-Haute-Provence and Valle d'Aosta NUTS3 regions, showing moderate to very high hazard levels across all timeframes.
- CCH2 (S-central Switzerland and N Italy), particularly around the Valais, Graubünden, Uri, Ticino, Oswalden and Sondrio NUTS3 regions, known for historic avalanche activity and complex terrains.
- CCH3 (W Austria and N Italy), including Tiroler Oberland, Osttirol, Pinzgau-Pongau and Bolzano NUTS3 regions, where dense tourism infrastructure overlaps with high hazard levels.

These CCHs align with reported avalanche events and STL locations, indicating a good spatial correlation between current exposure and the potential future risk.

In the Carpathian Mountains, CCHs include:

- CCH4 (N Slovakia and S Poland), notably in the High Tatra region, especially in Nowotarski and Zilinsky kraj NUTS3 regions, where high hazard levels persist from the baseline through end-century scenarios.
- CCH5 (central-SW Romania), covering the mountain areas of Brașov, Sibiu, Hunedoara, Gorj, Caraș Severin, Argeș, Prahova and Vâlcea NUTS3 regions, where hazard level is shifting from moderate to high levels.
- CCH6 (NE Romania), particularly Maramureș and Bistrița-Năsăud NUTS3 regions, where localised hazard intensification is expected.

Funded by the European Union

Across both the Alps and Carpathians, the spatial extent and intensity of CCHs increase progressively under both RCP4.5/SSP2 and RCP8.5/SSP5 scenarios by 2100. However, the RCP8.5 pathway clearly drives a more pronounced expansion and intensification of composite snow avalanche hazard levels, particularly after mid-century (after 2040). In the Alps, temporal changes in CCHs are more pronounced. Between 2011–2040, CCH1 and CCH3 begin to show localised increases in hazard levels, followed by more widespread amplification across all CCHs after 2041, especially under RCP8.5. By 2070, hazard zones shift eastward and southward in CCH1 and CCH3, with a westward and upslope expansion also visible in CCH1 toward 2100. Intensification is most notable in Valais, Ticino, and Tirol regions. Under RCP4.5, changes are moderate but still present across all three CCHs by the end of the century. In the Carpathians, hazard increases more gradually. CCH4 and CCH6 show minor intensification during 2011–2040 under RCP8.5, with stable spatial patterns. After 2040, all Carpathian CCHs exhibit clearer expansion under both scenarios, again more strongly under RCP8.5. The most substantial growth occurs in CCH5 and CCH6 after 2070, extending to higher altitudes, while CCH4 continues to focus on the High Tatra region. Overall, the Alps demonstrate higher CHI values and earlier hazard intensification compared to the Carpathians. While Alpine regions are exposed to greater risk earlier in the century, the Carpathians show a delayed but increasingly significant vulnerability under high-emission scenarios, especially in high-elevation forested and tourism-prone areas.

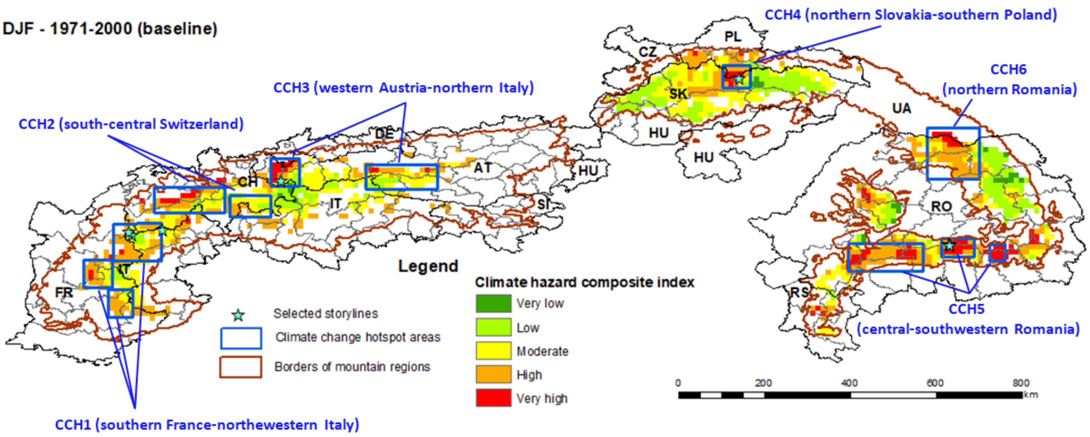

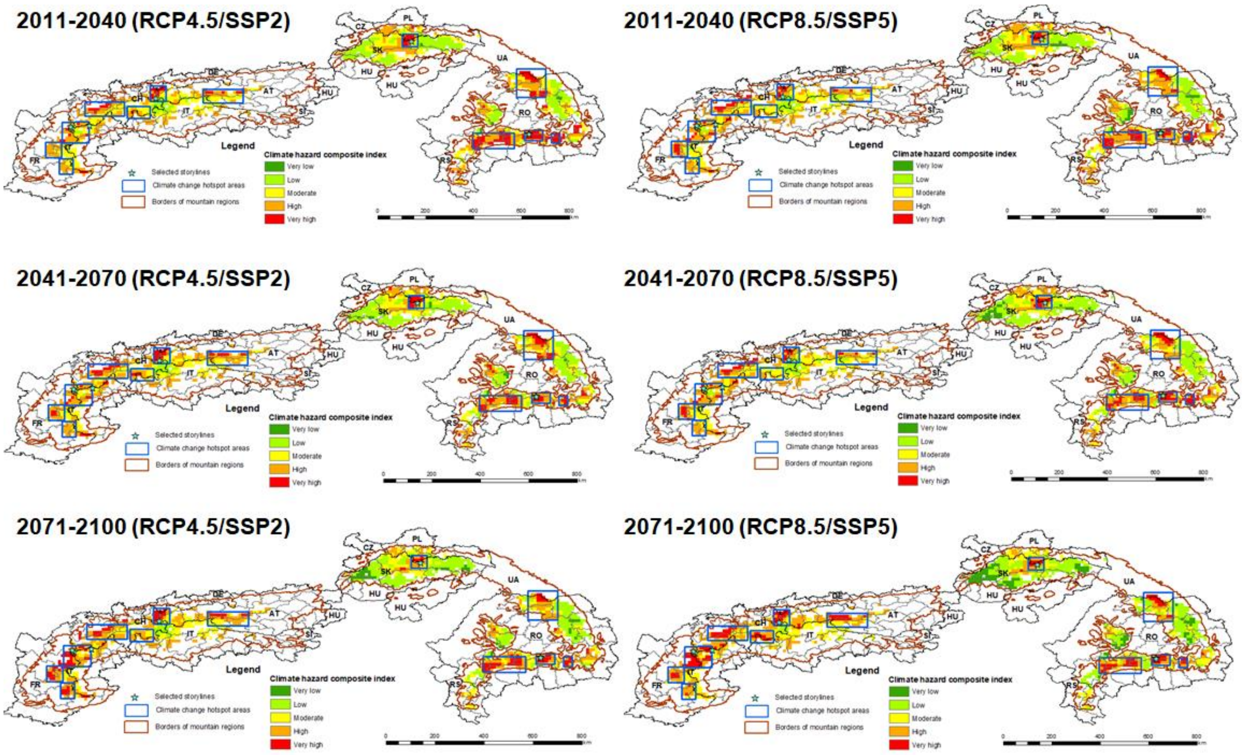

***Figure 47**: Temporal evolution of the winter CCHs from the baseline period (1971-2000) to 2100 under RCP4.5/SSP2 and RCP8.5/SSP5 scenarios across the European Alps and Carpathian Mountains.*

2.5.2. Application of the methodological framework

This case study applies the common project-wide methodological framework to assess snow avalanche risk across three sensitive sectors (tourism, forestry, and transport) at the NUTS3 level. The four-step framework integrates climate hazard indicators (for present and future conditions) with exposure and vulnerability data for the target sectors in both the European Alps and Carpathian Mountains.

Step 1: Climate and socioeconomic scenarios

The main objectives of this step were to: (i) assess regional climate change signals, (ii) map the potential snow avalanche hazard for present and future periods using specific climate indicators, and (iii) analyse projected changes in population exposure.

CSA 5 uses gridded climate datasets to meet these goals, including CERRA (5.5 km, 1984–2021) and the CMIP5 EURO-CORDEX ensemble (~12.5 km, 1971–2100) under RCP4.5/SSP2 and RCP8.5/SSP5 scenarios. The list of CMIP5 EURO-CORDEX simulations used in analysis is shown in the deliverable D6.2. (Data Management Plan – version 2). According to the CROSSEU Climate Data/Scenario Protocol (WP1), CSA 5 uses the following time slices for hazard analysis: present climate (CERRA, 1984–2021) and future climate (EURO-CORDEX, 1971–2100), including baseline (1971–2000), near-future (2011–2040), mid-future (2041–2070), and far-future (2071–2100), aligning with proposal milestones for 2030, 2050, and 2100.

To assess changes in snow avalanche hazard conditions in the Alps and Carpathians, seven climate indicators were computed (by MeteoRo and HEREON): (i) dry avalanches (H1, H2), (ii) wet avalanches (H3–H5), and slab avalanches (H6, H7) (Figure 48). The SNOW-17 model was used to estimate the snow-to-rain transition threshold for H5 (rain-on-snow). Each hazard indicator was standardised on a 1–5 scale using a quantile-based method and combined with terrain susceptibility to create a composite climate hazard index (CHI). Representing dry, wet, and slab avalanche types (H1–H7), CHI provides spatially consistent estimates of avalanche-prone conditions and identifies CCHs in the Alps and Carpathians.

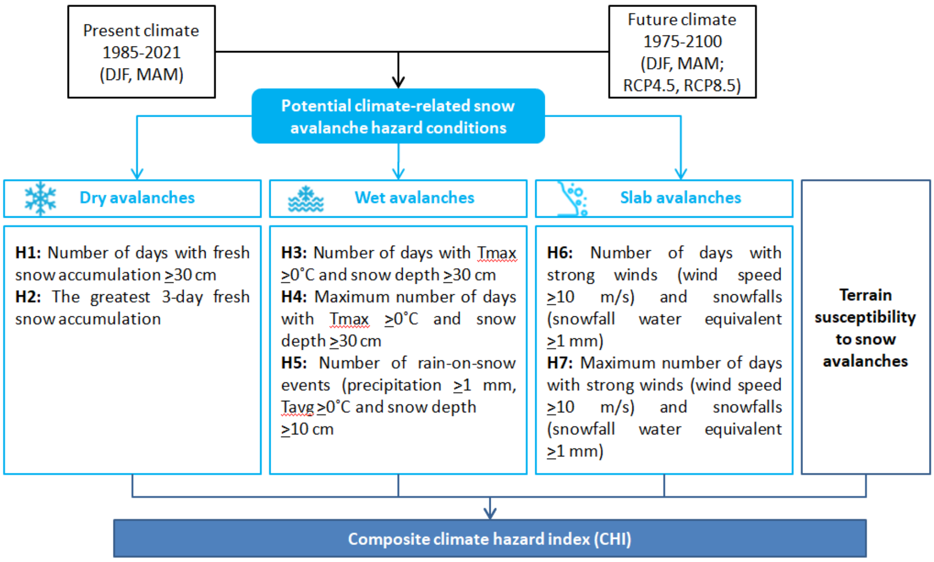

Figure 48: Derivation of the composite climate hazard index (CHI) for analyzing potential snow avalanche conditions under the present and future climate.

CSA 5 also integrates terrain susceptibility data based on the terrain conditions of the recorded fatal avalanche events since 2017/18, sourced from EAWS, national inventories, media, and rescue reports. The Analytical Hierarchy Process (AHP) was applied to weight key factors (slope, elevation, aspect, curvature, tree cover) and produce susceptibility maps (Figure 49), which served as a baseline for hazard, exposure, vulnerability, risk assessments, and CCH identification.

Socio-economic scenarios

This study assesses exposure and socio-economic vulnerability based on the current context (socio-economic indicators are listed in the Step 2), with climate hazard indicators. However, the estimations of the community's exposure incorporate EUROSTAT total population projections (by age and sex) at the NUTS3 level for 2030, 2050, and 2100 (changes are derived relative to the reference year 2019).

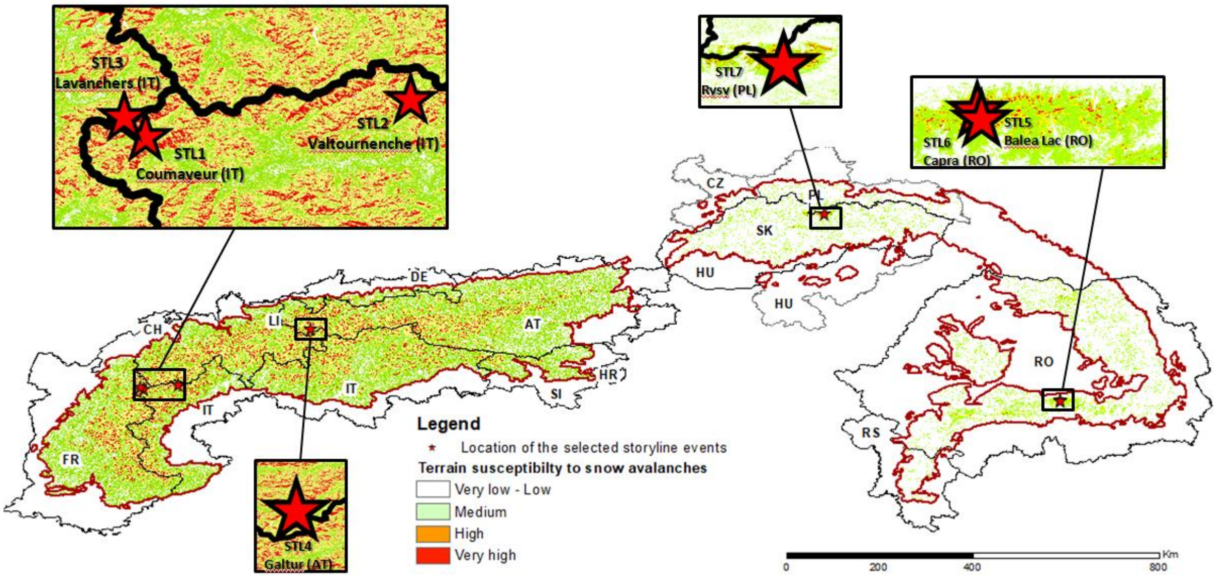

Figure 49: *AHP-derived terrain susceptibility to snow avalanches in the European Alps and Carpathian Mountains and STLs location.*

Step 2: Spatial data aggregation

CSA 5 applies a two-tiered spatial aggregation approach: (i) Climate hazard data are analysed at grid level for precise integration with terrain susceptibility and NUTS3 level, and (ii) Socio-economic data (sectoral exposure and vulnerability) are aggregated at NUTS3 level, covering tourism, transport, and forestry sectors. Twelve indicators, spanning social, economic, and environmental dimensions, were selected (post-2015). An overview is provided in Figure 50.

In CSA 5, the initial dataset included 160 Alpine and 59 Carpathian NUTS3 regions, based on the Global Mountain Biodiversity Assessment (GMBA) delineation of the two mountain regions. To improve relevance, only regions with ≥30% mountainous area were retained, resulting in 82 Alpine and 33 Carpathian NUTS3 regions for analysis.

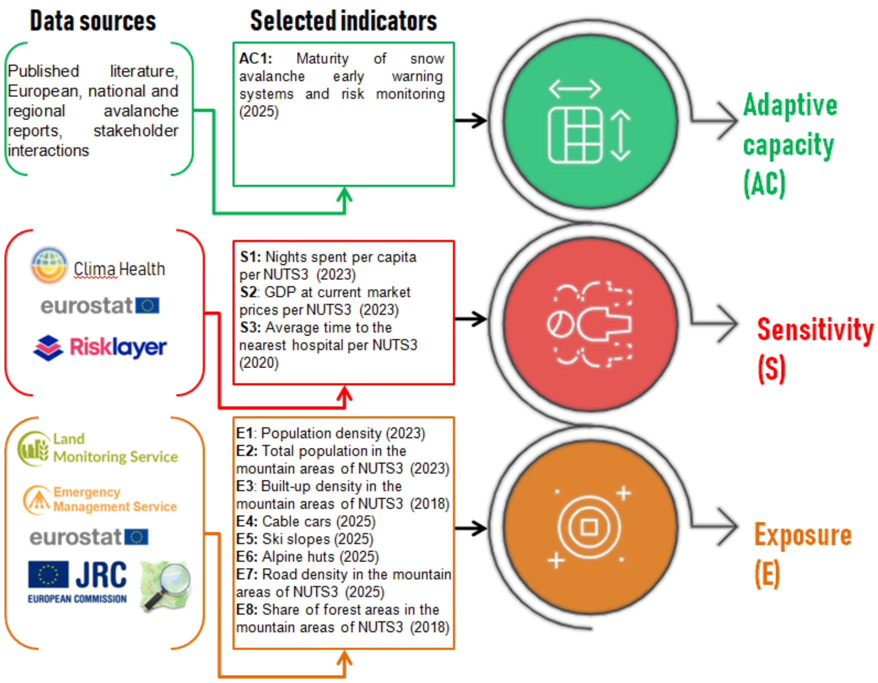

***Figure 50:** Selected socioeconomic exposure and vulnerability (sensitivity and adaptive capacity) indicators aggregated at NUTS3 level*

Composite exposure (E) and vulnerability (V) indices were computed at NUTS3 level. Values were standardised on a 1–5 scale using quantiles and aggregated via an equal-weight geometric mean.

Step 3: Impact assessment

The assessment of snow avalanche impacts on tourism, transport, and forestry in CSA 5 is shaped by the availability of sector-specific data. For the tourism sector, the analysis uses fatalities as a direct and comparable indicator, georeferenced at NUTS3 level where possible. Only events with at least one confirmed death were considered. Data sources include EAWS[5], ICAR[6], national avalanche services (e.g. SLF[7], LWD[8], AINEVA[9]), and literature. Fatalities are most frequent in tourist-heavy regions like Tyrol, Valais, Graubünden, Valle d'Aosta, and Savoie–Haute-Savoie, mainly involving tourists, recreationists, and local workers. While Alpine regions face broader disruptions to transport and tourism infrastructure, Carpathian fatalities remain lower due to limited ski tourism and underdeveloped monitoring, except in the High Tatras. For transport and forestry, due to a

---

[5] https://www.avalanches.org/

[6] https://www.alpine-rescue.org/

[7] https://www.slf.ch/en/avalanche-bulletin-and-snow-situation/

[8] https://www.lawine.at/

[9] https://aineva.it/en/

lack of direct data, proxy-based methods were applied, combining vulnerability indicators, documented avalanche events, and expert input to estimate sectoral impacts.

Step 4: Risk assessment

The risk-based assessment follows the ESPON-Climate 2022 and IPCC AR5/AR6 frameworks. Accordingly, sector-specific risk is defined as a function of hazard, exposure, and vulnerability (equation 1). Due to the localised and complex nature of snow avalanches, results reflect potential rather than observed risk. Socioeconomic vulnerability is assessed as the ratio of sensitivity to adaptive capacity (equation 2), illustrating how a system's susceptibility interacts with its ability to cope. The precise description of the parameters in the equations are provided in Step 1 and Step2

$$\text{Risk (sector)} = \text{Hazard} \times \text{Exposure (sector)} \times \text{Vulnerability} \quad \text{(Eq.1)}$$

$$\text{Vulnerability (general)} = \text{Sensitivity} / \text{Adaptive capacity} \quad \text{(Eq.2)}$$

Risk was classified on a five-level scale (1 = very low to 5 = very high) and applied across the CCHs in both mountain regions for tourism, transport, and forestry, enabling cross-regional and cross-sector comparisons.

2.5.3. Results

Climate and socioeconomic change signals across the European Alps and Carpathian Mountains

Exposure of local mountain communities (E1, E2, E3)

The European Alps show higher exposure to snow avalanches than the Carpathians, due to denser settlements, larger populations, and more infrastructure in avalanche-prone areas. Western Alpine regions, such as Isère, Savoie, Varese, Innsbruck, and Ticino, face moderate to high exposure, driven by major ski resorts and long-established communities in steep alpine valleys. In contrast, the Central and Eastern Alps have more variable exposure, shaped by lower population densities and dispersed settlements. Rural areas in eastern Austria, Slovenia, and parts of Switzerland show low exposure despite being within hazard zones (Figure 51).

The Carpathians show generally low exposure, reflecting sparse rural populations and limited tourism development. Exceptions include Trenciansky kraj (SK) and Nowosadecki and Nowotarski (PL), where tourism and clustered settlements increase local exposure.

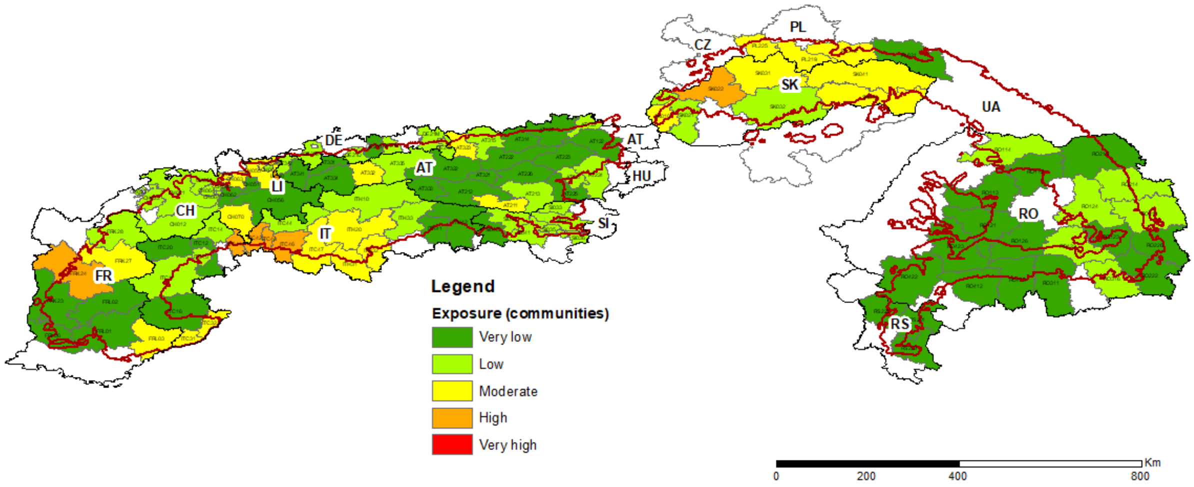

Figure 51*: Exposure of local mountain communities to snow avalanches in the European Alps and Carpathian Mountains. The dark brown line depicts the border of the two mountain regions.*

Exposure of tourism sector (tourism infrastructure) (E3, E4, E5, E6)

The exposure of the tourism sector to snow avalanches, as reflected by the distribution of tourist related built-up areas, cable cars, ski slopes, and alpine huts, is notably high in the Alps, where dense tourist infrastructure is frequently located within avalanche-prone zones. Significant concentrations of ski resorts, lift systems, and mountain lodges are in southeastern France (Savoie, Haute-Savoie), northeastern Italy (provinces of Valle d'Aosta, Bolzano, Trento), central Austria (Tiroler Oberland, Innsbruck, Tiroler Unterland), and southern Switzerland (Valais, Graubünden) (Figure 52). In such regions the exposure levels are linked to the well-developed tourism infrastructure, embedded in the steep and high-hazard alpine terrains. In the Carpathian Mountains, exposure is more localised, reflecting the clustered development of winter tourism in key resort areas. While overall exposure is lower than in the Alps, higher levels are found in regions with recent tourism growth, particularly in the Polish and Slovak Tatra Mountains and parts of the Romanian Carpathians (e.g., Bucegi Mountains, where larger ski domains and related infrastructure have been more intensively developed.

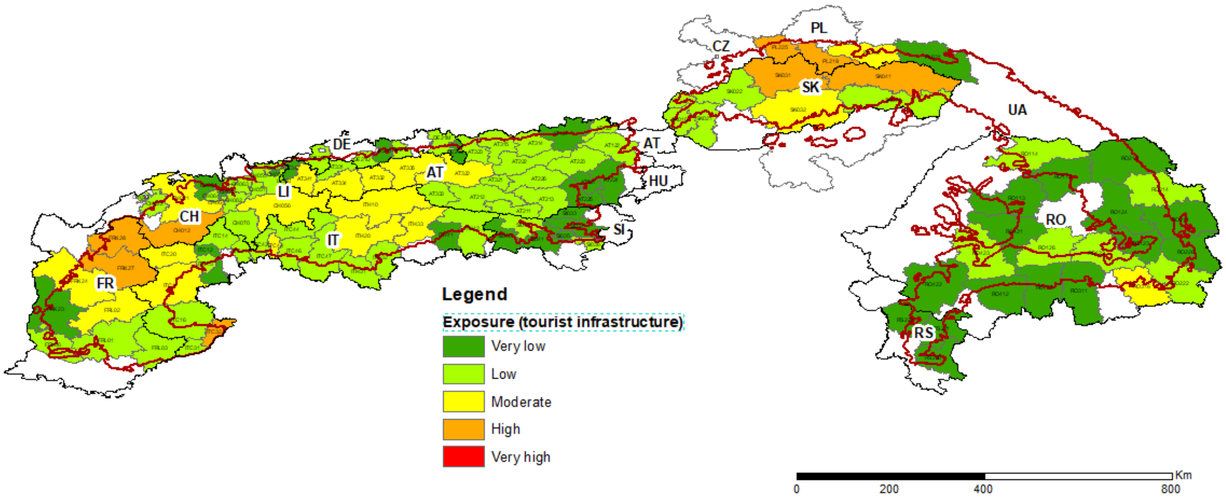

Figure 52: *Exposure of tourist infrastructure to snow avalanches in the European Alps and Carpathian Mountains. The dark brown line depicts the border of the two mountain regions*

Exposure of transport sector (road transport infrastructure) (E7)

The Alpine region generally exhibits low to moderate exposure of the road network to snow avalanches, particularly in lower-elevation peripheral areas. Moderately exposed zones include parts of southeastern France (Savoie, Haute-Savoie, Alpes-de-Haute-Provence), northern Italy (Trento, Verona, Pordenone), central and southern Austria (Innsbruck, Salzburg, Unterkärnten, Graz), and southern Switzerland (Ticino, St. Gallen, Schwyz, Nidwalden, Appenzell Ausserrhoden), where roads, often including transalpine corridors, are embedded in steep, avalanche-prone terrain and linked to high tourist activity (Figure 52). The highest exposure is found in Austrian Alpine regions such as Klagenfurt-Villach and Rheintal-Bodenseegebiet, which combine dense populations, strong economic performance, and tourism-driven infrastructure. In contrast, the Carpathian Mountains display generally low exposure, due to lower road density, particularly in high-altitude and rural areas where the transport network is more dispersed and less developed.

Funded by the European Union

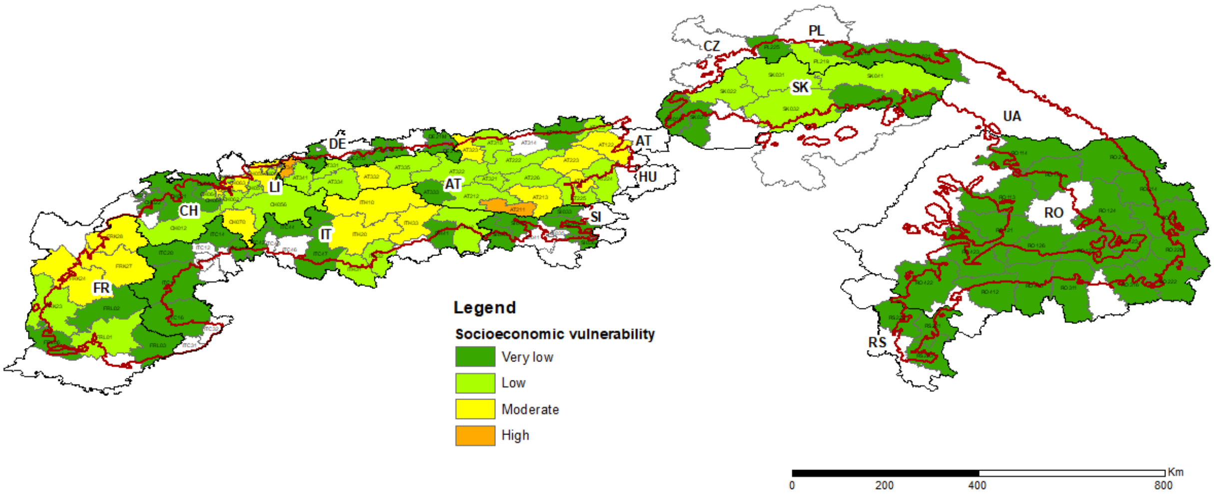

Figure 53: Exposure of road transport network in the European Alps and Carpathian Mountains. The dark brown line depicts the border of the two mountain regions

Exposure of forestry sector (forest area distribution) (E8)

The Alps exhibit moderate to high exposure of forest areas to snow avalanches, particularly in the southwestern and central regions (Figure 54). This includes mountainous zones in southeastern France (Savoie, Hautes-Alpes, Haute-Savoie, Alpes-de-Haute-Provence, Drôme), northern Italy (Valle d'Aosta, Vercelli, Cuneo, Biella, Sondrio, Varese, Bolzano, Udine), southern Switzerland (Graubünden, Uri, Valais, Ticino), and western Austria (Tiroler Oberland, Osttirol, Pinzgau-Pongau, Oberkärnten). These areas feature extensive forest cover on steep slopes intersected by active avalanche corridors. Lower exposure levels are more common in the northern rim of the Alps (e.g., southern Germany, northeastern Austria), where topography is gentler and forests lie outside main avalanche paths.

In the Carpathians, although overall forest exposure is slightly more widespread—30.3% of NUTS3 regions have ≥50% forest cover versus 29.2% in the Alps—moderate to high exposure is concentrated in regions such as Maramureș, Hunedoara, Caraș-Severin, Gorj, and Vâlcea (Romania), Prešov, Žilina, Trenčín (Slovakia), and Krosnienski, Nowosądecki, Nowotarski, Bielski (Poland). These areas are characterised by large, continuous forest tracts on rugged terrain, near or within active snow avalanche zones associated with massifs like the High Tatra, Făgăraș, Rodna, Parâng, and Țarcu Mountains.

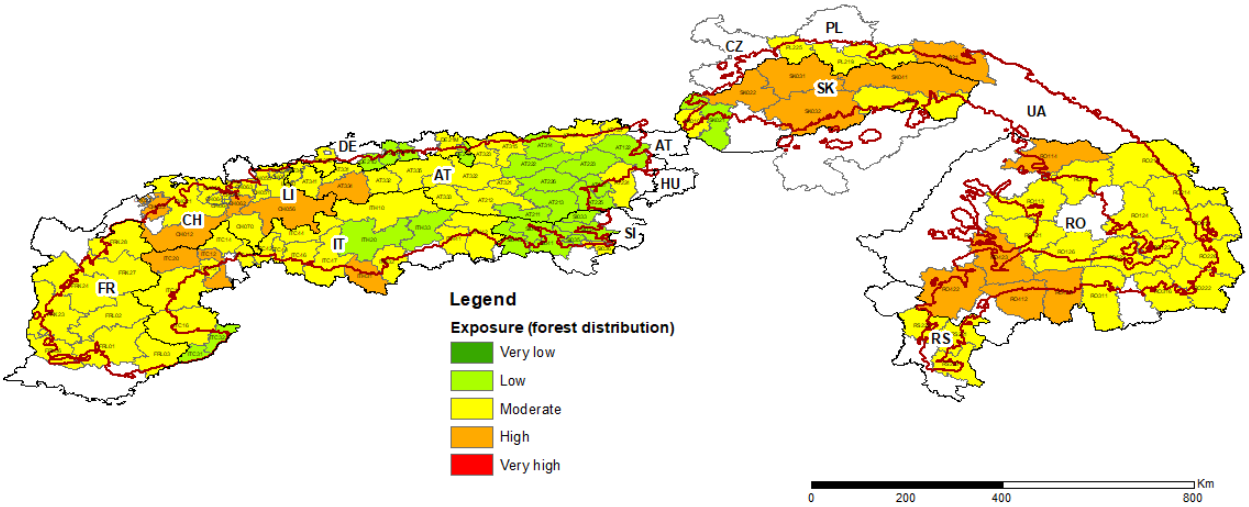

Figure 54: *Exposure of forest areas to snow avalanches in the European Alps and Carpathian Mountains. The dark brown line depicts the border of the two mountain regions.*

Socioeconomic vulnerability to snow avalanches

In CSA 5, socioeconomic vulnerability is assessed as the relationship between sensitivity, reflected by tourism intensity (S1), GDP per capita (S2), and hospital access (S3), and adaptive capacity (AC1), measured by the maturity of avalanche early warning systems based on expert judgements.

The Alps show moderate to high sensitivity, driven by intensive tourism and stronger economies. About 15% of Alpine NUTS3 regions (e.g., Savoie, Graubünden, Tiroler Oberland) report >25–50 nights spent per capita, while another 32% fall in the 8–25 range. In contrast, the Carpathians show much lower tourism intensity, with only 21% of regions (e.g., Brașov, Nowotarski) reaching 2–8 nights per capita. Economic indicators show a similar contrast, with about 12% of Alpine regions exceed €30,000 GDP per capita (e.g., Bern, Torino), while all Carpathian regions remain below €10,000, suggesting lower economic resilience.

Access to healthcare is much better in the Alps (<15 minutes in many areas), while most Carpathian regions have longer travel times (20–30+ minutes), except parts of northern Slovakia and southern Poland.

Adaptive capacity is strongest in Switzerland, Austria, France, and Italy, with advanced EWS, hazard zoning, and coordinated communication. By contrast, Slovakia has the most developed Carpathian system, while Poland and Romania maintain limited, localised monitoring, and Serbia lacks a dedicated avalanche EWS. Overall, the AC1 indicator reveals a clear divide, with Alpine countries well-equipped for avalanche risk management, and Carpathian countries facing institutional, geographic, and resource-related constraints.

The relationship between sensitivity and adaptive capacity reveals clear contrasts between the Alps and Carpathians, shaped by differences in tourism intensity, economic strength, healthcare access, and institutional readiness (Figure 55). In the European Alps, moderate to high vulnerability is primarily driven by high tourism activity, economic exposure, and variable healthcare access. The economic profile of Alpine NUTS3 regions further amplifies potential losses from snow avalanches, with about 20% of NUTS3 regions recording GDP per capita above 20,000 €. However, strong adaptive capacity, with advanced early warning systems in Switzerland, Austria, France, and Italy, helps offset these risks through well-established, well-funded institutions tailored to high-risk, high-tourism zones. In the Carpathians, socioeconomic vulnerability is generally moderate, reflecting low tourism intensity, limited economic development, and fragmented early warning systems. Although healthcare access is often more limited than in the Alps, the overall potential risk is offset by fewer assets at risk and lower seasonal population pressure. Higher vulnerability in some regions is mainly driven by low GDPs, although other factors (i.e., limited investments in protective infrastructure, limited risk education and awareness, fragmented governance structures) may be also important

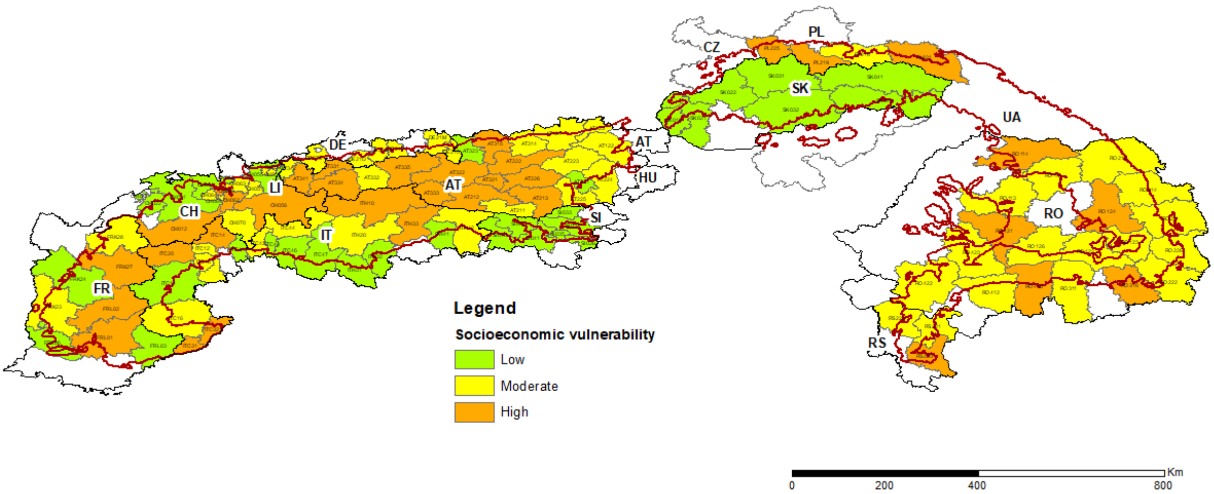

Figure 55: Socioeconomic vulnerability to snow avalanches in the European Alps and Carpathian Mountains. The dark brown line depicts the border of the two mountain regions.

Potential risk estimation

Across both mountain systems, the spatial persistence of CCHs from the baseline (1971–2000) through mid- and end-century (2041–2100) projections highlights sustained and slightly intensifying avalanche hazard potential. This is especially critical in areas where climate hazards overlap with high exposure, communities, tourism hubs, and road infrastructure, emphasizing the need for targeted adaptation, improved early warning systems, and localised risk reduction strategies.

Impact of snow avalanches

As shown in Figure 56, the number of avalanche fatalities across both regions (1988–2024) shows no clear long-term trend, though clusters of high-fatality years align with extreme snowfall events (e.g., 1999), rising backcountry activity, and periods of lower awareness or preparedness. Human-triggered avalanches, particularly by off-piste tourists during the ski seasons (generally spanning from late November to late April in the Alps and from early December to mid-March in the Carpathians), remain the leading cause of fatal incidents.

Region	Country	1986	1987	1988	1989	1990	1991	1992	1993	1994	1995	1996	1997	1998	1999	2000	2001	2002	2003	2004	2005
European Alps	IT	27	16	36	11	13	38	10	25	23	12	10	13	13	12	16	29	7	22	22	10
	FR	24	24	17	22	47	27	24	31	22	43	22	35	43	28	28	27	29	26	26	25
	CH	31	16	25	26	22	34	13	33	22	15	15	28	16	34	15	32	25	21	12	22
	AT	44	31	40	14	12	21	9	23	14	24	37	27	11	50	31	21	16	34	8	46
	SI	3	1				1			3	1	6		1					2	2	3
Carpathian Mountains	PL																				
	RO			1	5							3			4				4	8	
	SK		2	3			1		4	4	4	4	2	5	1	3	3	5	4	6	1

Region	Country	2006	2007	2008	2009	2010	2011	2012	2013	2014	2015	2016	2017	2018	2019	2020	2021	2022	2023	2024	Total number of reported avalanche fatalities
European Alps	IT	21	6	16	21	45	16	9	28	23	30	15	49	44	15	13	25	8	24	13	786
	FR	57	20	29	35	41	29	22	36	20	45	21	22	37	13	12	40	9	25	16	1099
	CH	23	23	16	23	30	29	18	26	18	31	20	15	20	24	12	25	16	24		850
	AT	22	17	29	32	39	3	10	14	7	33	14	23	10	22	14	14	18	15	14	863
	SI	2	1	1	3	7			4					1			3				45
Carpathian Mountains	PL																	2	3	2	7
	RO				4	1					1		4	7	3	1		2	1	2	51
	SK	7	1	2	4	6	1		6	1		2		5	4	1	2	5	4	2	105

Figure 56: *Temporal variability of the reported number of snow avalanches in Alpine and Carpathian countries (source: EAWS, AINEVA, ICAR, avalanseincarpati.org).*

Changing snow avalanche hazard conditions under climate change

Projections for Alpine and Carpathian CCHs under the selected scenarios show:

European Alps (CCH1–CCH3)

- Dry avalanche potential declines, especially under RCP8.5, due to fewer cold-season snow events.
- Wet avalanche risk increases, driven by more frequent rain-on-snow events.
- Slab-like avalanches remain stable or slightly increase at high elevations.

Carpathian Mountains (CCH4–CCH6)

- Dry avalanche potential stays low and declines further.
- Wet avalanche signals are mixed, with moderate increases in rain-on-snow events.
- Shorter, more variable snow seasons may intensify risk in peak periods.
- Slab-like avalanches remain rare, but possible locally under high-emission scenarios.

The emerging spatial patterns of changing snow avalanche hazard conditions suggest that: (i) in the Alps, new high-elevation risk zones may emerge (e.g., CCH2–CCH3), whereas (ii) in the Carpathians, some mountain areas of CCH4 (e.g., Călimani, Rodna, Bucegi) may face rising instability, due to climate warming and rain-on-snow events. These changes may suggest a need to update hazard zonation maps and strengthen early warning systems in the areas with underdeveloped coverage.

Estimation of the potential socioeconomic risks

A. The European Alps

Rising population exposure, moderate-to-high vulnerability, and intensifying avalanche hazards suggest that several NUTS3 regions in CCH1–CCH3 will face moderate to high risk by 2100, especially under RCP8.5, driven by wetter avalanche conditions, snowpack instability at higher elevations, population growth, and anticipated expanding tourism infrastructure.

Potential risk of snow avalanches on local mountain communities

Communities in CCH1 (SE France, NW Italy), CCH2 (S-central Switzerland), and CCH3 (W Austria, N Italy) face growing risks during peak winter tourism. While dry avalanche risk may decline, wet avalanche hazards are expected to increase at higher elevations. Regions like Savoie, Haute-Savoie, Drôme (FR), Tiroler Oberland (AT), and Obwalden (CH), with 5–15% population growth and high tourism intensity, are projected to face low to moderate risk (Figure 57), secured by existing civil protection and increase risk awareness. In contrast, Valais (CCH2) could reach moderate risk by 2100 due to 20–40% projected population growth, increased tourist presence, and persistently high hazard conditions in steep alpine zones.

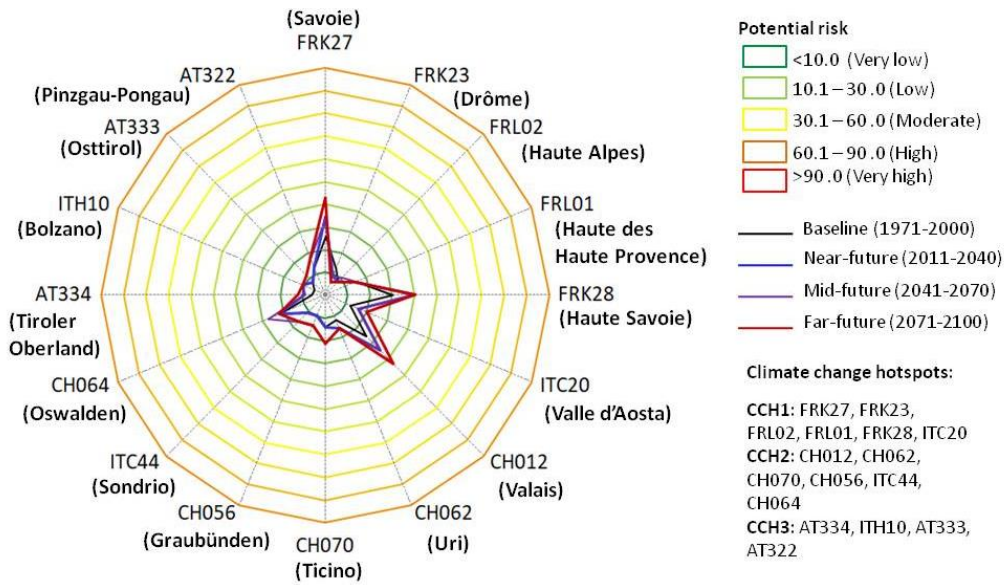

Figure 57: Potential risk to snow avalanches of local mountain communities at NUTS3 level in the climate change hotspot areas of the European Alps in the baseline and future climate conditions (scenario RCP8.5) relative to the total population living in the mountain areas of each NUTS3 region (reference year 2019, EUROSTAT).

Potential risk of snow avalanches on tourism infrastructure

Tourism infrastructure in the Alps, including huts, lifts, and ski slopes, is a key economic asset but increasingly exposed to climate-driven avalanche risk (Figure 58). Regions like Savoie and Haute-Savoie (FR, CCH1) and Valais (CH, CCH2) show moderate risk under RCP4.5, escalating under RCP8.5 due to worsening winter hazard conditions. These areas host major ski resorts like Portes du Soleil and Aletsch Arena, where high infrastructure density and seasonal tourist peaks heighten exposure. In CCH3, Pinzgau-Pongau (AT) faces moderate but rising risk by 2100 under both scenarios, as growing tourism and expanding hazard zones increase vulnerability, particularly at higher elevations.

Funded by the European Union

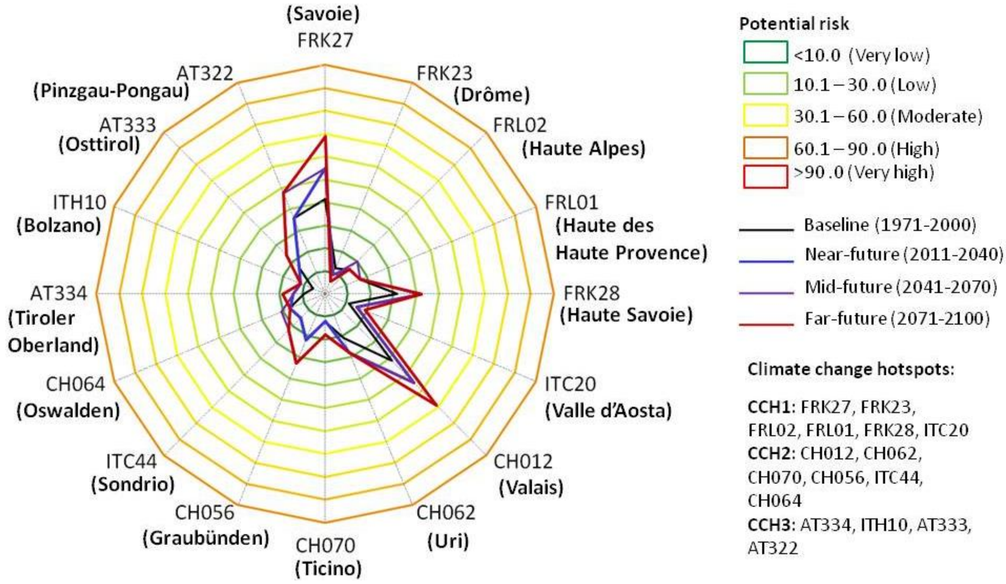

Figure 58: *Potential risk to snow avalanches of tourism infrastructure at NUTS3 level in the climate change hotspot areas of the European Alps in the baseline and future climate conditions (scenario RCP8.5).*

Potential risk of snow avalanches on road transport network

The Alpine transport network, especially mountain roads, is crucial for connectivity but increasingly vulnerable to climate-driven wet avalanche events (Figure 59). In CCH1, Savoie (FR) faces the highest transport risk, maintaining moderate risk under both RCP4.5 and RCP8.5 due to dense road networks near ski hubs like Les Trois Vallées. Haute-Savoie and Hautes-Alpes also show moderate risk from steep, infrastructure-heavy corridors. In CCH2, Valais (CH) rises from low-to-moderate to moderate risk under RCP8.5, while Uri, Graubünden, and Obwalden maintain moderate risk, due to exposed high-altitude routes. In CCH3, Pinzgau-Pongau (AT) sees a slight risk increase by 2100, staying within moderate levels, while other regions show low to low-moderate risk due to lower exposure or better protective infrastructure.

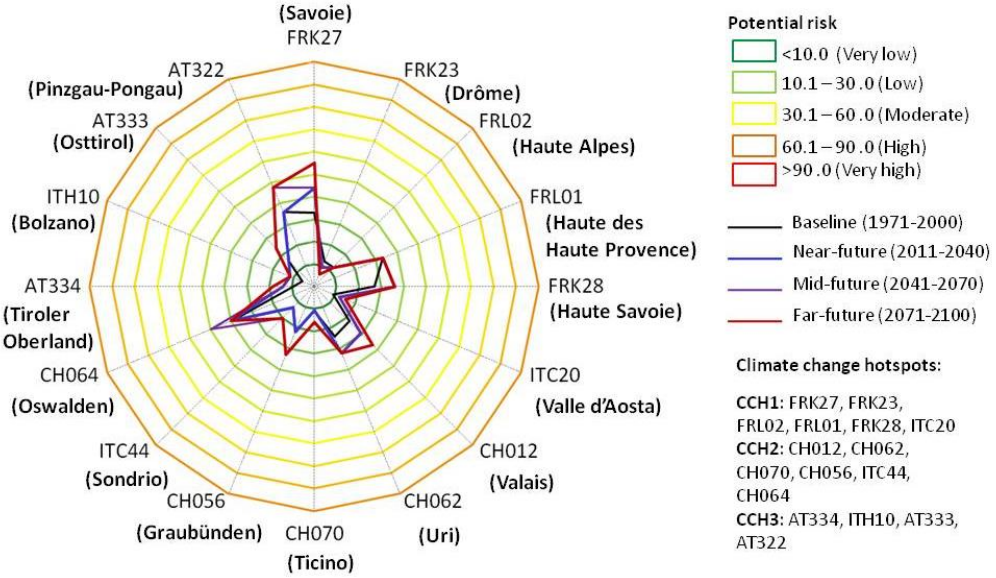

Figure 59: *Potential risk to snow avalanches of road transport network at NUTS3 level in the climate change hotspot areas of the European Alps in the baseline and future climate conditions (scenario RCP8.5).*

Potential risk of snow avalanches on forest areas

Mountain forests in the Alps provide key protective functions but face growing vulnerability to snow avalanches, especially in steep, mid-elevation zones. Under RCP4.5 and RCP8.5, moderate risk is expected to persist across most CCH1–CCH3 regions, with slight local changes depending on hazard and exposure (Figure 60). Savoie, Alpes-de-Haute-Provence, Valle d'Aosta, Obwalden, and Pinzgau-Pongau show stable moderate risk. In CCH2, Valais and Uri (CH) face notable increases, with forest risk rising to high by 2100, underscoring the need for long-term forest and slope management. Other areas are projected to maintain low to low-moderate risk due to limited forest exposure in avalanche-prone zones.

B. Carpathian Mountains

Potential risk of snow avalanches on local mountain communities

The evolution of potential snow avalanche risk for local communities in the Carpathian Climate Change Hotspots (CCH4–CCH6) shows a general pattern of low to moderate risk, shaped by climate hazard, socio-economic vulnerability, and population exposure. EUROSTAT projections indicate a widespread population decline across nearly all NUTS3 regions by 2100 (relative to 2019), contributing to a stabilization or decrease in overall risk, despite potential increases in avalanche hazard due to climate change. Population reductions are projected at 10–15% by 2030, up to 35% by 2050, and as much as 40–60% by 2100, especially in CCH5 (e.g., Gorj, Hunedoara, Argeș, Maramureș, Bistrița-Năsăud). In these areas, declining exposure and moderate vulnerability support stable or decreasing risk profiles (Figure 60). However, in regions like Sibiu, Brașov (RO), Nowotarski (PL), and Žilinský kraj (SK), where vulnerability remains high and population decline is slower

(<25%), risk levels are projected to stay low to moderate or moderate, under both RCP4.5 and RCP8.5 scenarios.

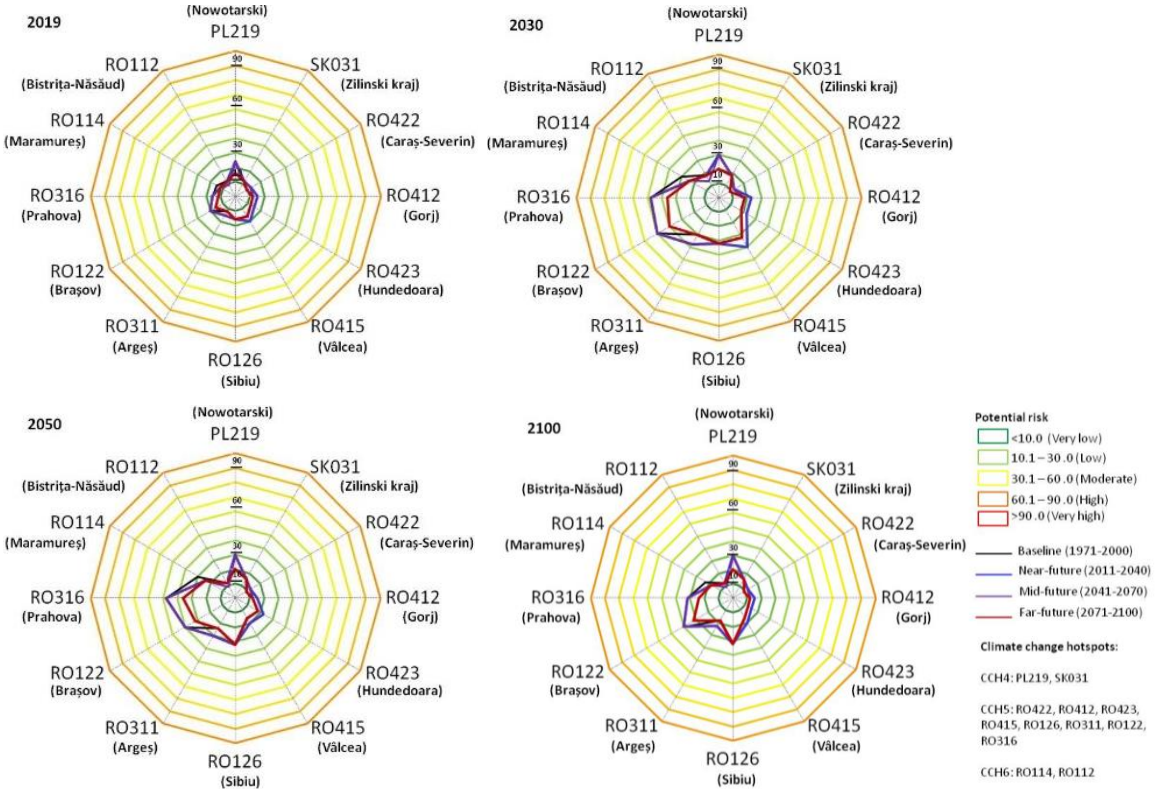

Figure 60: *Potential risk to snow avalanches of local communities at NUTS3 level in climate change hotspot areas of the Carpathian Mountains in the baseline and future climate conditions (scenario RCP8.5).*

Potential risk of snow avalanches on tourism infrastructure

Across CCH4 to CCH6, potential risk ranges from very low to moderate. CCH4, especially Nowotarski (PL), shows the most consistent moderate risk, sustained through 2100 due to active winter resorts (e.g., Zakopane – 15 km, Białka Tatrzańska – 18 km, Bukowina Tatrzańska and Czarna Góra – 8.6 km total) and persistent avalanche hazards, despite slight hazard reductions (Figure 61). CCH5 regions exhibit low to moderately stable risk, with some localised exposure in Făgăraș, Parâng, and Bucegi Mountains. Here, steep terrain and dispersed ski infrastructure create moderate vulnerability, even as overall exposure remains lower than in CCH4.

Potential risk of snow avalanches on road transport network

Road networks in the Carpathian Mountains are essential for connectivity, emergency response, and access to rural and tourist areas. While localised exposure to snow avalanche hazards exists, particularly in steep, high-altitude sections, the overall potential risk remains low across all CCHs, with only minor fluctuations projected under both climate scenarios. This low risk is largely due to the dispersed and less developed road infrastructure at higher elevations. An exception is Nowotarski (CCH4, Poland), where more extensive and exposed road networks contribute to a slight increase in risk by the end of the century (Figure 61).

Potential risk of snow avalanches on forest areas

Forest areas in the Carpathians, especially those on steep slopes or within avalanche corridors, are vulnerable to snow avalanche impacts. In CCH4–CCH6, the potential risk to forests is generally moderate, with only minor variations projected through the end of the 21st century (Figure 61). Figure 61 summarises the estimated risk levels for forest areas in NUTS3 regions across the Carpathian hotspots under the RCP8.5 climate scenario.

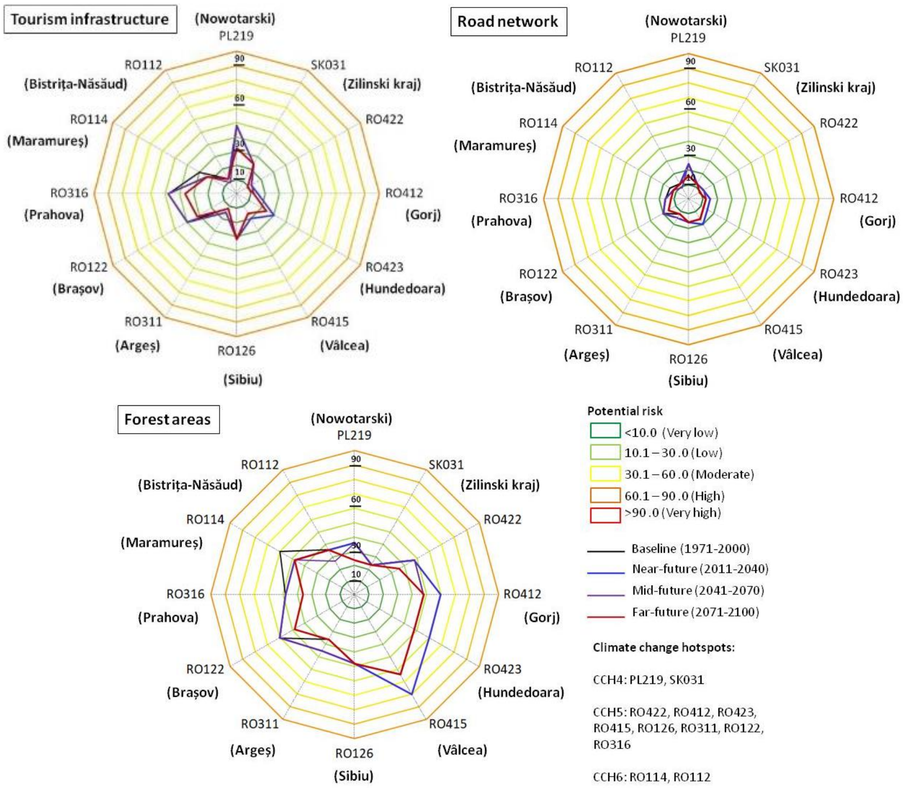

***Figure 61**: Potential risk to snow avalanches of tourism infrastructure (left), road network (middle) and forest areas (right) at NUTS3 level in climate change hotspot areas of the Carpathian Mountains in the baseline and future climate conditions (scenario RCP8.5).*

2.5.4. Challenges

Snow avalanche risk assessment in CSA 5 is constrained by the localised and weather-dependent nature of avalanches (Amihaesei et al., 2024; Micu et al., 2015), requiring reliance on climate-driven hazard indicators (H1–H7) and the composite hazard index (CHI) rather than precise event forecasting. Data limitations present a further challenge: inconsistent reporting, especially in under-monitored Carpathian regions, and the scarcity of dedicated socioeconomic indicators at the NUTS3 level restrict the accuracy of exposure and vulnerability estimate (Voiculescu et al., 2023) Finally, limited local stakeholder engagement, due to low perceived risk or competing priorities, hampers access to contextual knowledge and reduces co-production opportunities for adaptation planning.

2.5.5. Conclusions

CSA 5 highlights how climate change is altering snow avalanche hazard patterns across the European Alps and Carpathian Mountains, with implications for communities, tourism, transport, and forest ecosystems. Using composite climate hazard index, socio-economic indicators, and risk assessment frameworks, the study reveals persistent and emerging hotspots of risk, particularly under high-emissions scenarios (RCP8.5). The Alps show widespread moderate to high risk due to overlapping high exposure, sensitivity, and persistent hazard signals. In contrast, the Carpathians display lower risk profiles, largely driven by limited exposure and declining population trends, though vulnerability remains high in selected regions due to underdeveloped early warning systems. Historical snow avalanche events, documented through STLs, underscore the need for proactive adaptation, particularly in tourism-intensive zones. Adaptation strategies should prioritise strengthening early warning systems, updating hazard zoning, and enhancing cross-sectoral risk communication and planning, especially in newly exposed high-altitude zones. Overall, CSA 5 demonstrates the importance of integrating climate, socioeconomic, and topographic data for future-proofing risk management and territorial planning in Europe's mountain regions.

Therefore, CSA 5 introduces a dedicated assessment of snow avalanche risk, which was not addressed in COACCH or PESETA projects. It delivers a multi-hazard, sector-specific framework that integrates climate projections, terrain susceptibility, and NUTS3-level socio-economic indicators to evaluate risks to tourism, transport, forestry, and local communities. Key added values include: (i) first inclusion of the Carpathian region in a pan-European snow hazard context; (ii) use of a composite hazard index (CHI) combining 7 climate indicators with terrain features; (iii) integration of EUROSTAT population projections (2030, 2050, 2100) with climate hazard data; (iv) application of STLs and CCHs to contextualise the potential risks; (v) sector-specific focus reveals highly context-dependent climate change impacts and enables the baseline knowledge for adaptation analysis.

2.5.6. References

Amihaesei V, Micu D, Cheval S, Dumitrescu A, Sfica L, Birsan V-V (2024) Changes in snow cover climatology and its elevation dependency over Romania (1961–2020). Journal of Hydrology: Regional Studies, 51, 101637. https://doi.org/10.1016/j.ejrh.2023.101637.

Bąkowski R, Achimowicz J, Mazur A (2014). Current status of early warning systems for severe environmental threats in the Polish National Meteorological Service. Meteorology, Hydrology and Water Management, 2, p. 35-42. doi: 10.26491/mhwm/36432

Bélanger L, Cassayre Y (2004). Projects for past avalanche observation and zoning in France, after 1999 catastrophic avalanches. Environmental Science, Geography.

Bründl M, Etter J-H, Steiniger M, Klingler Ch, Rhyner J, Ammann WJ (2004). IFKIS– a basis for managing avalanche risk in settlements and on roads in Switzerland. Natural Hazards and Earth System Sciences (2004) 4: 257–262.

Chiambretti I, Chiaia B, Frigo B, Marello S, Maggioni M, Fantucci R, Bernabei M (2018). The 18th January 2017 Rigopiano avalanche disaster in Italy - Analysis of the applied forensic field investigation techniques, Environmental Science, Engineering, Geology.

Costa JE (1991). Nature, mechanics, and mitigation of the Val Pola landslide, Valtellina, Italy, 1987–1988. Zeitschrift fur Geomorphologie 35, 15–38, 1991.

Debernardi A, Roveyaz S, Borney E, Frigo B (2022). Land Planning and Extreme Snow Events: The Case of Buthier Avalanche in Aosta Valley – IT. International Journal of Environmental Sciences & Natural Resources 31(2). doi: 10.1908/IJESNR_2022.31.556312.

ESPON-Climate (2022). FINAL REPORT - Updating and Integrating CLIMATE Datasets and Maps. ESPON 2020 data and maps updates, European Commission, September 2022.

Glass B. et al. (2000). "Retour d'expérience sur l'avalanche du 9 février 1999 à Montroc, commune de Chamonix", Inspection Générale de l'environnement, Ministère de l'Aménagement du Territoire et de l'Environnement, Affaire n° IGE 00 002.

IPCC (2014). Climate Change 2014: Impacts, Adaptation, and Vulnerability. Part A: Global and Sectoral Aspects. Contribution of Working Group II to the Fifth Assessment Report of the Intergovernmental Panel on Climate Change (eds CB Field, VR Barros, DJ Dokken, et al.). Cambridge, United Kingdom and New York, NY, USA: Cambridge University Press.

Jakubis M, Jakubisová M (2023). Mountain Rescue Service - Inevitable help at recreational and sport activities in mountainous areas in Slovakia. Proceedings of the Conference Public recreation and landscape protection - with environment hand in hand?, doi: 10.11118/978-80-7509-904-4-0174

Lorenzoni N, Raich M (2021). Long-term impact of the Galtuer avalanche on the public health system. Journal of Emergency Management, 19(2):197-208, doi: 10.5055/jem.0570.

Ortner, G., Michel, A., Kropf, C.M. et al. (2025). Assessing the impacts of climate change on snow avalanche-induced risk in alpine regions. Nat Hazards. https://doi.org/10.1007/s11069-025-07229-9

Micu D, Dumitrescu A, Cheval S, Birsan M-V (2015) Climate of the Romanian Carpathians. Variability and Trends. Springer Atmospheric Sciences. 213 p.

Navarro D, Lizundia-Loiola J, Paz J, Abajo B, Cantergiani C, García G, Feliu E (2022). Updating and Integrating CLIMATE Datasets and Maps. Final Report. ESPON 2020.

Peters M, Pikkemaat B (2008). Crisis management in Alpine winter sports resorts—The 1999 avalanche disaster in Tyrol. Journal of Travel & Tourism Marketing Volume 19, 2006 - Issue 2-3. https://doi.org/10.1300/J073v19n02_02.

Pérez-Guillén C, Techel F, Volpi M, can Herwijnen A (2025). Assessing the performance and explainability of an avalanche danger forecast model, Nat. Hazards Earth Syst. Sci., 25, 1331–1351.

Rapisarda A, Pranzo AMR (2021). Mapping the avalanche risk: from survey to cartographic production. The avalanche bulletin of the Meteomont Service of the Alpine Troops Command. Proc. Int. Cartogr. Assoc., 4, 92, https://doi.org/10.5194/ica-proc-4-92-2021.

Sauermoser S (2006). Avalanche hazard mapping—30 years experience in Austria. In Proceedings of the 2006 International Snow Science Workshop in Telluride, Colorado, p. 1-6.

Valt M, Chiambretti I, Zasso R (2009). 1985 – 2009 Twenty-Five Years of Avalanche Accidents in Italy. Environmental Science.

Voiculescu M, Török-Oance M, Chiroiu P, Popescu F (2023). Snow avalanches in relation to tourism and transportation activities in the Făgăraş Mountains, Romanian Carpathians, Anthorpocene. 44, 100407. https://doi.org/10.1016/j.ancene.2023.100407.

Funded by the European Union

2.6. CSA 6 INDIRECT (Cross-sectoral multi-hazard risk)

2.6.1. Summary of climate change hotspots and event-based storylines

The Lower Danube region in Romania (Figure 62) is defined by an extensive floodplain that spans approximately 6,000 km², housing crucial ecosystems, agriculture, energy infrastructure, and human settlements.

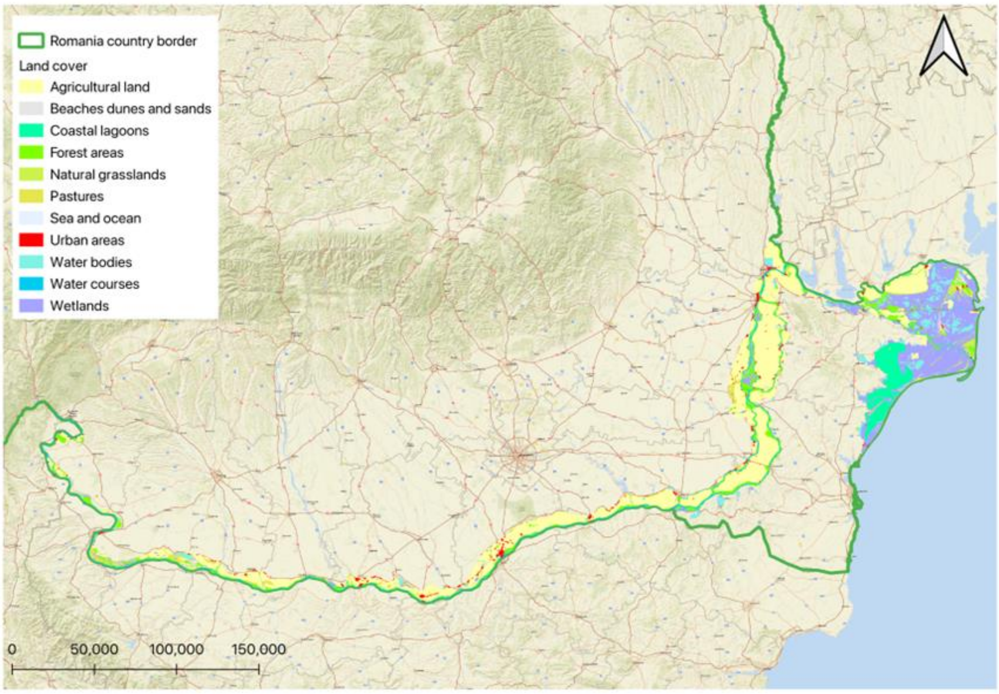

Figure 62: *Case study area - Lower Danube (land cover)*

The Lower Danube region (Romania) has experienced extreme floods (ICPDR, 2006; ICPDR, 2010; ROWATER, 2023) and droughts that highlight its status as a climate hotspot. In spring 2006, the Danube swelled to record levels, causing one of the worst floods in over a century. Dikes were overtopped or breached along the river, inundating tens of thousands of hectares, some 7,000 people were evacuated and over 700 homes were flooded. This catastrophic flood, lasting over two months, caused an estimated €343 million in damages in the Brăila region and adjacent areas. It also illustrated the vulnerability of low-lying islands and floodplain communities: for instance, the Great Brăila Island, a large, diked island devoted to agriculture, was under severe threat as emergency crews worked to reinforce levees and pump out seepage waters. In contrast, recent drought events have been equally alarming. The summer of 2022 brought Europe's worst drought in decades, pushing the Danube to its lowest levels in almost a century, hindering water transport as channels became too shallow for navigation, and historical relics emerged from the riverbed. This ultra-low flow event disrupted commerce and drew international attention to the Danube's vulnerability under extreme heat and scant rainfall. These storylines – the 2006 mega-flood and the 2022 mega-drought – underscore the climate extremes facing the region and set the stage for understanding future risks.

Characteristics of Selected Storyline Events

To illustrate the range of impacts, we summarise key characteristics of several extreme "storyline" events in the Lower Danube (Brăila) region (Table 15).

***Table 15:** Summary of Selected Extreme Events in the Lower Danube (Brăila) Region.*

Event	Type	Timing	Peak Magnitude	Duration	Area Affected	Notable Impacts
2006 Flood	Spring flood (snowmelt + rain)	Mar–May 2006	~15,800 m³/s @ Bazias; Brăila gauge > 7m	~69 days	Widespread Danube floodplain (>116k ha)	~7,000 evacuated [2]; €342.9M damage; ~3,000 houses affected; major navigation & ferry disruptions [6].
2010 Flood	Early-summer flood (rainfall)	June 2010	Brăila level 713 cm; ~13,350 m³/s inflow	~60 days	Local dike breach at Ciobanu-Garliciu (~3,500 ha flooded)	Dozens of homes and farms flooded; localized evacuations; highlighted dike vulnerabilities in rural areas.
2022 Drought	Severe drought & low flow	Apr–Aug 2022	Brăila flow <3,000 m³/s (est.); Tulcea level 51 cm [7]	~5+ months	Regional (Lower Danube & tributaries)	Navigation halted (Danube depth < min. clearance) [7]; shipping channel dredging required [7]; crop yields down 30–50%; power plant cooling risks; water use restrictions in villages.

2006 Extreme Flood: A prolonged spring flood (March–May 2006) with peak discharge >15,000 m³/s at the upstream Bazias gauge. Water levels at Brăila exceeded safety thresholds for 69 days, straining dikes. The flood affected an estimated 116,000 ha in Romania, including poldered farmland and several villages. Damages were catastrophic (over €340 million) and thousands were displaced. In Brăila city, the Danube waterfront was inundated, and critical infrastructure like ferries was shut down. This event tested emergency response and revealed weaknesses in flood defences – notably, the Great Brăila Island's levees barely held, and one dike section in a neighbouring county failed.

2010 Summer Flood: A severe early-summer flood peaking in June 2010 that mainly impacted localised stretches. For example, a dike breach at Ciobanu–Garliciu (Brăila–Constanța county border) inundated about 3,500 ha of agricultural land. The Danube at Brăila reached 713 cm (about 7 m), and upstream inflow peaked ~13,350 m³/s – high but not as extreme as 2006. This event caused fewer damages overall (the Damage column is blank in records, suggesting limited monetary losses) but highlighted the susceptibility of smaller dikes. It also underscored the cascade of minor flood events that regularly threaten rural communities even if the main cities stay safe behind major embankments.

2022 Extreme Drought: An exceptional drought from late spring through summer 2022 resulting in record low Danube levels. By August 2022, the water level at Tulcea (downstream of Brăila, in the Danube Delta) dropped to only 51 cm, about 6 cm below the minimum level for navigation. Large sections of the Lower Danube became unnavigable, stranding cargo vessels and forcing emergency dredging to reopen channels. At Brăila, the river's flow fell so low that wetlands disconnected from the main channel, threatening aquatic ecosystems. The drought's duration (several months) and breadth meant widespread agricultural damage – as noted, roughly half of Romania's farmland is impacted in such dry years, with the Brăila Plain among the worst-hit regions. This event had profound socioeconomic effects (crop failures, water rationing, energy production drops, navigation restrictions) indicative of climate extremes.

2.6.2.Application of the methodological framework

Step 1 Climate and socioeconomic scenarios

According to the CROSSEU Climate Data/Scenario Protocol, elaborated by WP1, the selected temporal slices used in hazard computation and analysis under CSA 6 are:

Aspect	Dataset / Source	Period
Present climatic data	ERA5, E-OBS, CERRA, national meteo data	1971–2000 / 1981–2010
Present climate hazard (CERRA)	CERRA high-resolution reanalysis	1984–2021
Future climate hazard	EURO-CORDEX, CMIP5/6, E-HYPE, LISFLOOD	Up to 2100 (RCP4.5, RCP8.5)
Present hydrological data	HYPE (Hydrological Predictions for the Environment) reanalysis for Danube River Braila station	1971–2000 / 1981–2010
Future hydrological data	HYPE (Hydrological Predictions for the Environment) reanalysis for Danube River Braila station	Up to Up to 2100 using (RCP4.5, RCP8.5)

Step 2: Spatial data aggregation

In CSA 6, spatial data aggregation follows a two-tiered approach: (i) All climatic data have been integrated in **HYPE (Hydrological Predictions for the Environment)** as a **semi-distributed** catchment-based hydrological model developed by the **Swedish Meteorological and Hydrological Institute (SMHI)**.

(ii) Socio-economic analyses — focusing on exposure and vulnerability — are based on data aggregated at the NUTS3 level, sourced from various repositories.

Method

Extreme Event Definition: two high-flow thresholds were analysed – 10,000 m³/s (major flood events) and 15,000 m³/s (extreme floods) – and two low-flow thresholds – 4,800 m³/s (critical for ecosystems) and 3,000 m³/s (critical for navigation). For each threshold, we identified discrete events (continuous days above or below the threshold) and computed their annual frequency, average duration, and timing. High-flow events typically correspond to flood waves, while low-flow events correspond to drought periods or navigation outages.

Trend & Seasonality Analysis: we calculated metrics per year and per future period, assessing changes in frequency and duration of events. Statistical trend analysis (Mann-Kendall test and linear regression on annual counts) was used to gauge significance of changes over time (though results are presented qualitatively). To examine seasonality shifts, we evaluated the distribution of event peak dates. Because timing within the year is circular, we employed techniques from circular statistics (computing mean event timing in a year). In practice, we compared the most frequent peak month historically vs. future. A “circular” shift is noted when events cluster in earlier or later parts of the year compared to the past. We also analysed multi-model agreement to ensure findings are robust across the ensemble.

Step 3 Sectoral Impact Analysis

Climate extremes in the Lower Danube have cascading **sectoral impacts**. We examine four key sectors – **Agriculture, Transport, Energy, and Human Health** – to understand how floods and droughts (both present-day and projected future events) affect each. We also performed an integrated socio-economic vulnerability analysis.

Step 4: Risk assessment

The risk-based assessment approach represents the sector-specific risk as a function of hazard intensity, the exposure of assets or populations, and their vulnerability. However, given the complexity and uncertainty associated with hazard estimation, the analysis reflects an assessment of a potential risk, rather than observed or fully quantifiable risk.

Table 16: Indicators for floods (examples)

Indicator (Definition, Year, Unit)	Dimension	Sectors	Data Source	New indicator
Population in flood-prone areas – Number of residents living within the modelled 100-year floodplain (e.g. 2020, persons)	Exposure	Communities, Socio-economic systems	JRC Flood Hazard Maps + GHSL population grid	Yes (derived from spatial data)
Area at risk of flooding – Land area exposed to a 100- year return period flood, as % of total county area (e.g. 2018, %)	Exposure	Nature & ecosystems, Agriculture, Communities	Copernicus flood extent maps; CORINE Land Cover	Yes (spatial analysis)
Agricultural land in floodplain – Arable and pastureland located in flood-risk zones (2018, hectares or % of farmland). A large value indicates significant agricultural assets exposed to flooding.	Exposure	Agriculture, Socio-economic systems	CORINE Land Cover (agricultural classes) overlaid with flood zones	Yes (derived indicator)
Urban areas in floodplain – Built-up area (towns/ cities) within flood hazard zones (2018, km²). High values mean major settlements lie in flood-prone areas.	Exposure	Communities, Socio-economic systems	CORINE; OpenStreet Map urban footprint + flood maps	Yes (derived indicator)
Infrastructure near rivers – Length of roads and number of bridges within 100 m of major rivers (2020, km and count). Indicates transport infrastructure directly exposed to flooding	Exposure	Communities, Transport (naval & road)	OpenStreet Map (roads, bridges) + river network	Yes (derived indicator)
Critical facilities in flood zone – Count of key facilities (e.g. hospitals, power plants including 1 nuclear plant at Cernavodă) located in the floodplain (2020, count). Highlights exposed critical infrastructure.	Exposure	Nuclear energy, Socio-economic systems, Communities, National infrastructure maps;	OpenStreet Map	Yes (new indicator; site-specific for nuclear)

2.6.3.Results

Climate Change Projections and Trends (Floods & Droughts)

Climate projections for the Lower Danube (Brăila region) under mid-century (2030, 2050) and late-century (2100) scenarios show a clear trend toward more frequent and intense extremes. Using an ensemble of hydrological model simulations (E-HYPE for the Danube at Brăila) forced by climate models under RCP4.5 (moderate emissions) and RCP8.5 (high emissions), we have compared future periods to a 1971–2000 baseline (Figure 63, 64; Table 17).

Projected changes include:

A) Flood Frequency Increase: High-discharge floods, above 10,000 m³/s (a threshold that historically corresponds to moderate flooding at Brăila), are projected to occur far more often. By the near-future (2021–2050), floods over 10,000 m³/s could increase by 50% (RCP4.5) to 75% (RCP8.5) in frequency. The trend analysis revealed distinct linear trends in annual de-seasonalised discharge across the three scenarios. Seasonality was removed using STL decomposition, enabling clearer detection of long-term changes: historical data shows a moderate increasing trend. RPC 4.5 and RPC 8.5 show stronger upward trends, with RPC 8.5 displaying the steepest increase.

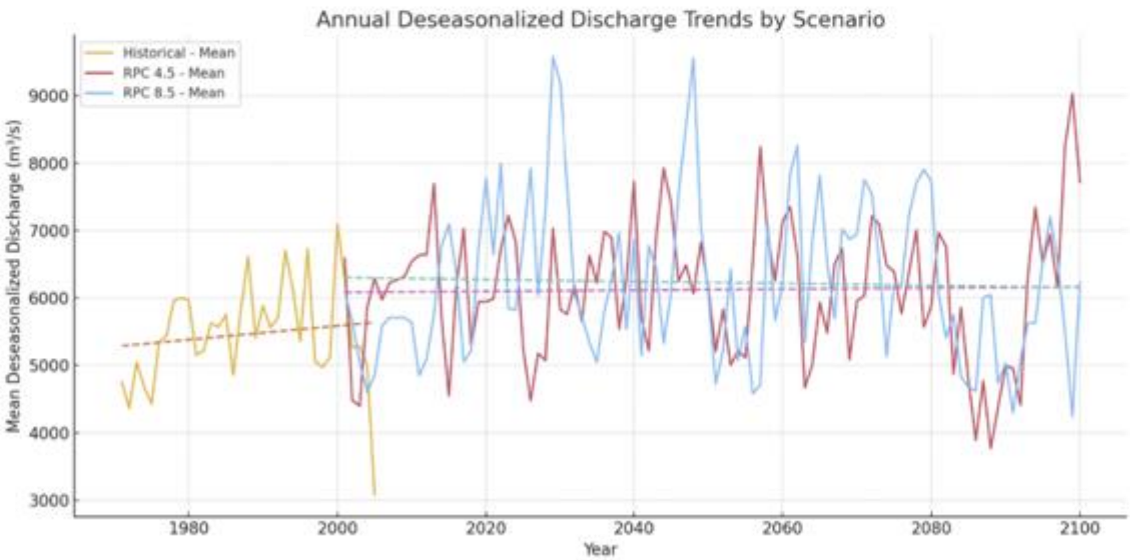

Figure 63: *Trend analysis of the de-seasonalised discharge by historical data and scenarios (RPC4.5 and RPC 8.5)*

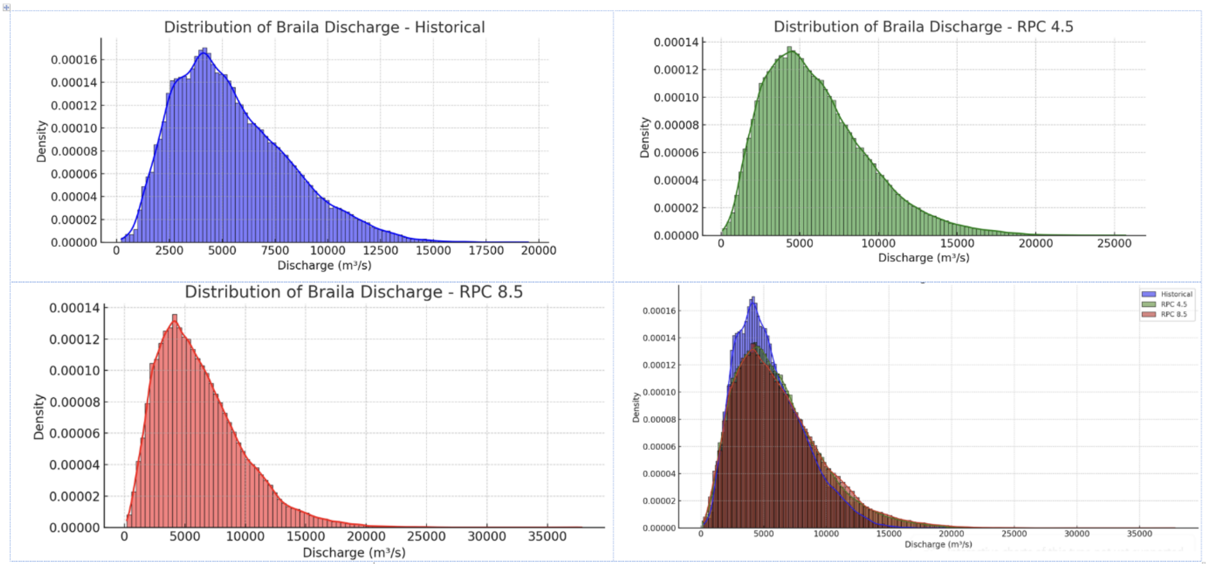

Figure 64: *Discharge distribution for the historical, RPC4.5 and RPC8.5 scenarios up to the year 2100.*

In concrete terms, the model ensemble indicates roughly 15–18 events per year exceeding 10,000 m³/s by mid-century, up from ~10.5 per year historically. Even more dramatic is the rise in extreme floods above 15,000 m³/s (flows of this magnitude were very rare in the 20th century, occurring only ~0.3 times per year on average).

Table 17: *Summary of the discharge data for historical and selected future scenarios (RPC4.5 and RPC8.5).*

Scenario	Mean (m³/s)	Median (m³/s)	Min (m³/s)	Max (m³/s)	Std Dev (m³/s)	Count
Historical	5472	5005	232	19482	2705	102272
RPC 4.5	6105	5528	98	25687	3351	277584
RPC 8.5	6251	5586	206	37821	3602	277584

High-Flow Extremes: Frequency, Duration & Timing

Historical context: Flood flows in the Lower Danube are already substantial – the Braila gauge saw peak discharges near 19,500 m³/s in the late 20th century. Historically (1971–2000), flows exceeded 10,000 m³/s about 10.5 times per year on average (i.e. roughly 10 days or events per year) and exceeded 15,000 m³/s only once every ~4 years on average (0.27 events/year). These large floods tended to occur in spring (March–April), driven by snowmelt from the Upper Danube and spring rainfall. Individual flood events typically lasted ~2–3 days above 10,000 m³/s, or ~2–7 days above 15,000 m³/s for the largest floods.

Increasing flood frequency: both climate scenarios project more frequent high flows, with a particularly dramatic rise for the most extreme floods. By the 2030 horizon, moderate floods (>10,000 m³/s) increase roughly 50% in frequency under RCP4.5 and 75% under RCP8.5 relative to historical. Specifically, in the 2021–2050 period the model ensemble shows ~15.3

events/year >10,000 m³/s under RCP4.5 and ~18.3 events/year under RCP8.5, compared to ~10.5 historically. The trend continues toward mid-century (2050): under RCP4.5 about 16.8 events/year, and under RCP8.5 about 17.9 events/year exceed 10,000 m³/s. Figure 65 illustrates this rise in high-flow event frequency.

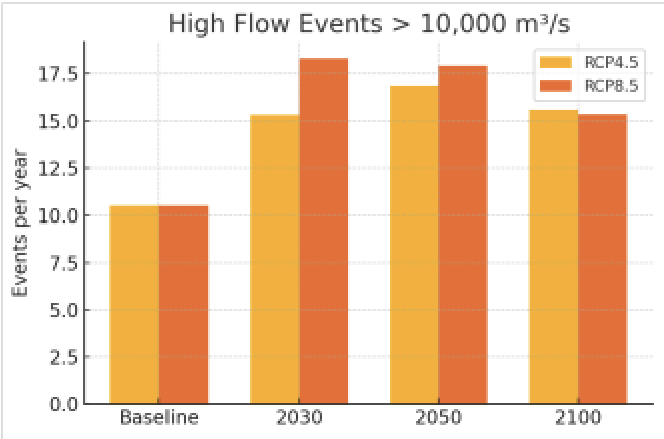

Figure 65: *Projected annual frequency of high-flow events (>10,000 m³/s) at Brăila. Bars show the average number of events per year for the historical baseline (1971–2000) vs. future horizons (2030, 2050, 2100) under RCP4.5 (yellow) and RCP8.5 (orange) scenarios. An "event" is a continuous period exceeding the threshold.*

By 2100, the frequency under RCP8.5 (~15.3 events/year) plateaus slightly, potentially reflecting drier summer conditions counteracting increased winter flows (discussed below). Still, all future periods remain well above the historical baseline in flood frequency. Such an increase aligns with basin-wide studies that show high certainty in more frequent flood events in the future, especially in large basins like the Danube where heavier precipitation events are expected. Under RCP8.5, such very large floods could become an annual or multi-annual occurrence by 2050.

The ensemble mean shows ~3.9 events/year >15,000 m³/s by mid-century under RCP8.5 – about a 14-fold increase over historical frequency. Even more striking is the change in **extreme floods >15,000 m³/s** (events that historically were quite rare). Under RCP8.5, these **once-in-several-years floods could become annual or multi-annual events by mid-century**. The ensemble mean indicates ~**3.9 events/year >15,000 m³/s by 2050 (RCP8.5)** – roughly a **14- fold increase** from the 0.27 events/year historically. RCP4.5 shows ~3.3 events/year by 2050 – still an order of- magnitude jump. In the near term (2030), RCP8.5 already shows ~4.3 events/year >15,000 (versus ~2.6 under RCP4.5), suggesting a front-loaded increase in extreme flood frequency under the highest emissions.

By 2100, frequencies in both scenarios converge to ~3.5 events/year for >15,000 m³/s events. Figure 66 illustrates this dramatic escalation.

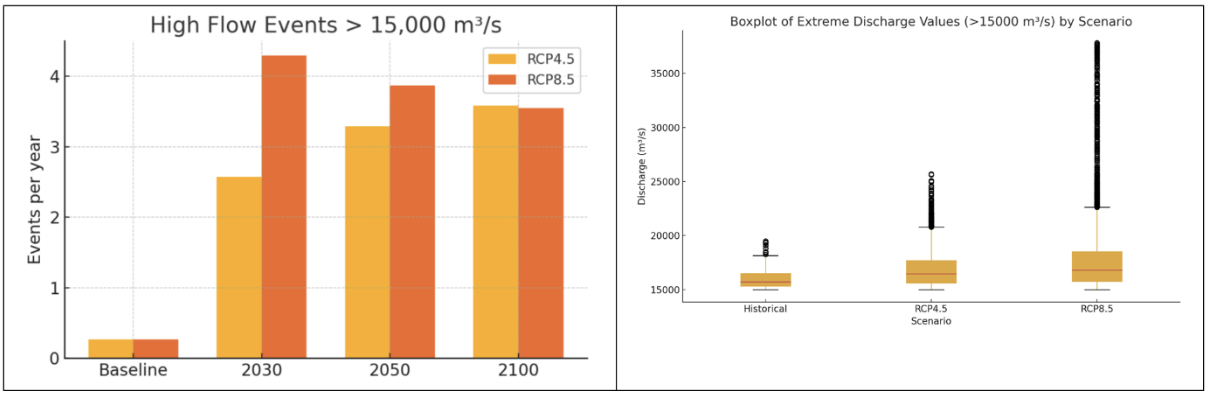

***Figure 66:** Same as Figure 65, but for extreme flood events >15,000 m³/s. Historically infrequent, such extreme discharges become much more common. By 2050, RCP8.5 projects ~4 events/year above 15,000 m³/ s on average (orange bar), versus ~0.3 historically. RCP4.5 (yellow) also shows a large increase. End-of-century projections suggest persistently elevated extreme flood risk in both scenarios.*

In practical terms, the **magnitude of floods experienced in 2006 or 1970 (which were >15,000 m³/s) could occur almost every year or even multiple times a year in coming decades** under climate change. This projection is consistent with research noting a general increase in extreme precipitation and flood hazard for the region, though the exact magnitude involves uncertainties. It's important to note the ensemble spread: some model runs yield up to ~5 events/year >15,000 m³/s at mid-century, while a few are lower, but the trend is robustly upward in all members (Figure 66). RCP4.5 also shows a steep rise (on the order of 1–3 events/year >15,000 m³/s by 2050). Such projections imply that the kind of flood seen in 1970 or 2006 (>15,000 m³/s at Brăila) might occur almost every year or even multiple times a year in coming decades. By late-century (2071, 2100), there is some indication that under RCP8.5 the extreme flood frequency may plateau or slightly decline (the ensemble average for >15,000 m³/s events settle to ~3.5/year by 2100). This could reflect drier summers offsetting further increases – an important nuance that suggests mid-century might see the peak flood hazard before a slight attenuation by 2100. Nonetheless, all projections maintain flood frequencies well above the historical baseline throughout the 21st century, in line with other studies projecting more heavy precipitation and flood risk in the region.

B) Flood Intensity & Duration: Not only are floods more frequent, but peak magnitudes of flood events are expected to grow. Under RCP8.5 in the near-future (2030 horizon), the average peak flow of >15,000 m³/s floods rise to ~19,300 m³/s, higher than any 20th-century recorded peak (~17,900 m³/s). Some model simulations even produce peaks above 20,000 m³/s (which would be unprecedented at Brăila).

This suggests new record floods are plausible by mid-century. Interestingly, by the late 21st century, peak magnitudes might stabilise or decrease slightly under RCP8.5 (average peaks ~17,100 m³/s by 2100), as extremely intense floods become a bit less extreme even though they are more frequent. In terms of duration, future high-flow events may last a bit longer: historically a >10,000 m³/s flood lasted ~2.5 days on average, whereas in projections this extends to ~3.0–3.3 days. This hints that multi-day rainstorms or successive runoff peaks will keep rivers high for longer. For >15,000 m³/s floods, the duration remains around 2–3 days (extreme peaks tend to be brief), but an increase in clustering of events could effectively prolong the flood season.

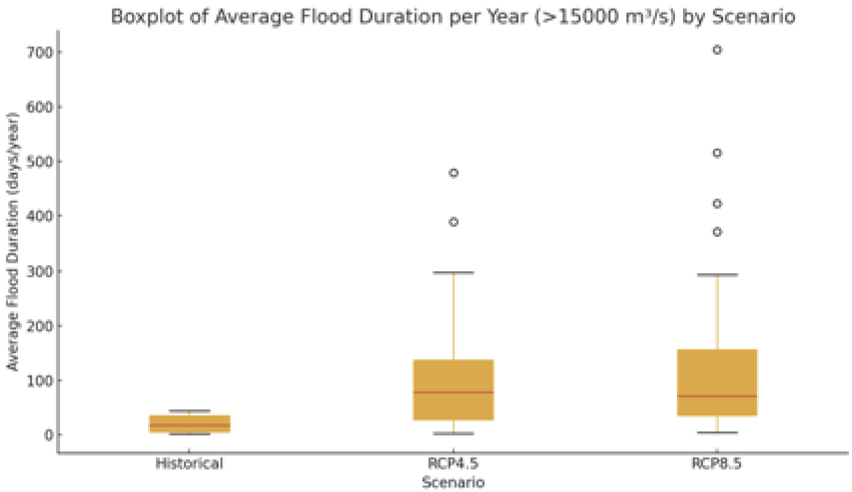

Figure 67: *Flood duration change (historical, RPC4.5 and RPC8.5) for the extreme values.*

Overall, the mid-21st century emerges as a period of both more frequent and more severe floods on the Lower Danube. Historically, a flood >10,000 m³/s lasted ~2.5 days on average. In future scenarios this grows to ~3.0–3.3 days, indicating that high flows may persist slightly longer (likely due to longer rain spells or successive peaks). For >15,000 m³/s events, average duration remains ~2–3 days (with many extreme peaks being brief), constrained perhaps by the transient nature of extreme storms. Flood magnitudes are projected to rise: under RCP8.5 near-future, the average peak flow of >15,000 m³/s events is ~19,300 m³/s, which is higher than historical extreme peaks (~17,900 m³/s) – suggesting new record floods are plausible.

For mid-century simulations there are peaks above 20,000 m³/s, a value virtually unseen in the 20th century at Brăila. This aligns with studies finding 10–30% increases in peak flows in parts of the Danube basin under high warming. However, by late-century, the peak magnitudes in our projections stabilise or even slightly reduce under RCP8.5 (the average peak drops to ~17,100 m³/s by 2100), potentially due to drier summers limiting the absolute flood heights despite more frequent events. In summary, mid-21st century may represent the peak hazard for flood intensity under current model assumptions, with a slight attenuation by 2100 – but still far above historical intensity.

C) Seasonal Shift of Floods: A pronounced shift in flood seasonality is anticipated. Historically, the largest Danube floods at Brăila came in spring

(March–May), fed by Alpine snowmelt and spring rains. Climate change, however, is expected to move the peak flood season to late winter. By 2100 under high emissions, January–February could replace spring as the period of most frequent high flows. The projections show that February will be the peak flood month by 2100 in RCP8.5. This is attributed to warming-driven changes: with warmer winters, snowpack in the upper Danube melts earlier and more precipitation falls as rain, resulting in higher winter flows, while spring/early summer floods diminish. Studies indeed project the traditional May–June snowmelt flood peak to weaken by 8–34% by 2060, accompanied by up to +40% higher accompanied by up to **+40% higher runoff in December–March** and **~20% lower runoff in May–September**. These shifts mean flood management will have to be on high alert in winter (when historically it was less of a concern), and it could lessen the Alpine snowmelt-driven spring flooding while increasing risk from winter rain-on-snow events. There is even some model evidence of **autumn flood** tendencies under certain scenarios (a few RCP4.5 simulations showed secondary peaks in November by late-century), though this is less consistent. Overall, by mid-century **floods are less tied to spring thaw** and more linked to **episodic heavy winter storms**, broadening the season of flood

D) Low-Flow (Drought) Trends: The projections for **droughts and low flows** are nuanced. On one hand, **low-flow extremes** (prolonged periods of very low discharge) are expected to become **more severe and prolonged by 2100**, especially under RCP8.5. We used several discharge: below 4,800 m³/s (critical for wetland ecosystems) and below 3,000 m³/s (critical for navigation) and in both cases will likely last longer and cause greater impacts by late-century.

However, in terms of **frequency of threshold-crossing events**, the near-term changes are not a simple linear increase. In fact, by 2030 (2021–2050), the *number* of low-flow events per year might *slightly decrease* compared to historical averages. The model ensemble shows flows <4,800 m³/s occurring ~28–27 times a year in 2021–2050 (down from ~31 historically), and events <3,000 m³/s dropping to ~14–17 per year (from ~20 historically). This counterintuitive short-term improvement is attributed to **increased winter flows** (fewer winter low-flow days due to warmer, wetter winters) partially compensating for more severe summer droughts. Essentially, climate change may **reduce winter low-flow incidents** (by reducing ice-related stoppages and increasing baseflow in warmer winters) even as it **intensifies summer low flows**. By mid- to late-century, as warming progresses, the summer drought signal dominates **longer and deeper summer low-flow periods** are projected by 2100, especially under RCP8.5. Model runs suggest that by late-century, the Danube could spend a significantly larger portion of the year below ecological and navigational flow thresholds, even if the count of distinct "events" doesn't skyrocket.

But for the more severe <3,000 m³/s events, mean duration lengthens from ~3.2 days to **~3.9 days by 2100 (RCP4.5)** and **~3.8 days (RCP8.5)**. That is a ~20%

increase in how long extreme low-flow spells persist. Consequently, the **total number of days per year below critical thresholds increases** markedly by late century. We calculated the ensemble-mean **days per year <3,000 m³/s**: historically ~65 days/year; by 2100 this grows to **~69 days (RCP4.5)** and **~79 days (RCP8.5)**. **Figure 68** shows this evolution. Notably, RCP8.5 near-term had fewer (~45 days/year) due to the winter effect, but by end-century it jumps to ~80 days (a ~20% increase over baseline). In effect, **the Danube could spend an extra 2–3 weeks per year below navigation-critical levels by 2100 in a high-emissions future**, relative to today. This indicates **more prolonged navigation outages and ecological stress** during dry months. It corroborates studies predicting **longer and more intense droughts/low flows in the southern and eastern Danube region.** Even under RCP4.5, total low-flow days slightly exceed historic levels by late century, implying that some worsening of drought impact is likely even with moderate climate action.

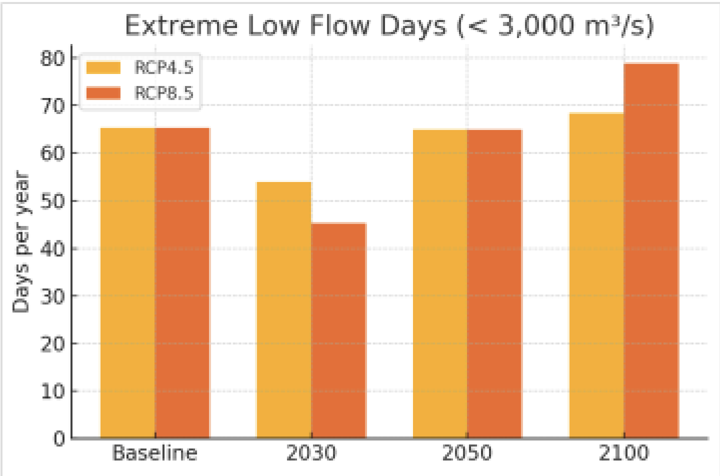

Figure 68: *Projected annual extreme low-flow duration (total days per year with discharge < 3,000 m³/s). Bars compare the historical baseline to future periods (2030, 2050, 2100) under RCP4.5 and RCP8.5. While near-term projections show a slight reduction in low--flow days (due to wetter winters), by 2100 the cumulative drought days increase, especially under RCP8.5 (nearly 80 days/year <3,000 m³/s).*

The **duration** of drought spells increases. Historically, a low-flow event (<4,800) lasted ~5.4 days on average; with climate change, not only could individual events lengthen, but they may also merge into **multi-week or multi-month dry periods**. Moreover, whereas historically the worst low flows came in late summer (August was the peak month for extreme lows), the future might see a **wider seasonal window of drought**. Some projections indicate **bimodal low-flow seasons** (one in winter when upstream freezing reduced flows, and a larger one in late summer due to drought) could shift to a more singular focus on **summer drought** by 2100, as winters get wetter and ice-free. The upshot is that **extreme drought risk increases later in the century**, primarily through more intense summer drying, even if winter low-flow problems ease in the interim.

In summary, **climate change is expected to amplify hydrological variability** on the Lower Danube. Moderate floods that were once infrequent will become common and very destructive floods that were once rare could occur every few years or even annually. Simultaneously, while near-term changes in drought frequency are subtle, the long-term outlook points to more severe **summer droughts**, with river levels staying dangerously low for longer periods. These projected trends directly translate into rising risks for various sectors and communities, as discussed next.

Agriculture

Agriculture is one of the most vulnerable sectors in Brăila County, heavily impacted by both floods and droughts. The county lies in Romania's fertile but climate-sensitive **Bărăgan Plain**, where farming is central to livelihoods. However, this area faces a **continental temperate climate with hot, dry summers** and periodic droughts.

- **Flood Impacts on Agriculture:** Major floods can devastate crops and livestock. When the Danube overtops levees, it can **inundate vast tracts of farmland.** For instance, the 2006 flood submerged tens of thousands of hectares right at the start of the growing season. Even areas protected by dikes suffer from water seepage and **high groundwater** during floods, which can waterlog root zones and delay planting. In Brăila's Great Island, a fully diked agricultural zone, a dike breach would be catastrophic – the flat island could fill like a "bathtub," ruining crops on tens of thousands of hectares in one event. Even without a breach, prolonged high water in 2006 caused pumping stations to operate continuously to keep fields drained. The **financial losses** from a big flood include lost harvests, soil erosion, and expensive recovery efforts like replanting and repairing farm infrastructure. For example, farmers in inundated villages may lose tractors or grain stores. The flood events of 2010 and 2014, though smaller, still saw thousands of hectares of pasture and forest flooded (Table 15) and required compensation for affected farmers. Floods can also deposit **silt and debris** on fields – occasionally beneficial as natural fertilizer, but often harmful if contaminated or too gravelly.
- **Drought Impacts on Agriculture:** Drought is a more chronic threat. In dry years, **crop yields plummet** and pastureland withers, hitting subsistence farmers and large agribusiness alike. **Half of Romania's farmland is affected by drought in severe dry years**, with Brăila's region among the worst-hit. Key crops like **maize, sunflower, and wheat** are highly sensitive to summer soil moisture deficits. In 2022 and 2023, for example, Brăila County recorded significant losses in maize and sunflower output due to extreme heat and minimal rainfall. Irrigation could buffer these impacts, but the local irrigation infrastructure has declined: on the Great Brăila Island, only ~21% of land was still irrigated by the 2010s, down from nearly 100% in the late 1970s. This decline, due to deteriorating pumps and canals, leaves many farmers at the mercy of rainfall. During droughts, even having the Danube nearby doesn't guarantee water for crops – **when river levels are low, pumps struggle to lift water** into canals, and energy

costs for irrigation soar. Livestock suffer as well; fodder crops and grazing lands dry up, forcing farmers to buy feed or cull herds. Prolonged drought also increases crop pest and disease pressures, further hitting yields. Looking ahead, climate projections of longer summer dry spells suggest **more frequent crop failures** and a need for drought-tolerant crop varieties. Drought insurance and state aid have become frequent needs in Brăila. In summary, **floods can deliver acute, immediate blows to agriculture**, while **droughts impose more diffuse but widespread stress**, directly threatening the main economic base of rural communities.

Transport (Navigation & Infrastructure)

The transport sector – including **river navigation, ferries, roads, and rail** – is directly affected by Danube water extremes:

- **River Navigation:** The Danube is a major **inland waterway** for commerce. Both floods and droughts disrupt navigation but in different ways. **High floods** create strong currents, high debris loads, and force authorities to impose restrictions for safety. During the 2006 flood, **maritime ships and boats were forbidden** between Sulina and Galați (downstream of Brăila) due to dangerous conditions. Port operations were also hampered; at Brăila, the ferry service across the Danube was suspended for weeks in 2006 because landings were underwater. Fast currents and floating logs make navigation risky in floods, and some river ports get inundated. Conversely, **low water levels** (droughts) pose perhaps an even greater challenge to navigation. In late 2022, parts of the Danube became effectively **unnavigable** – sections of the main channel had water depths below the minimum required for barge traffic. Vessels had to **lighten their loads** or wait, disrupting supply chains. At Tulcea and other points, emergency **dredging** was undertaken to deepen the channel and allow ships to pass. Low flows also revealed hazards (like submerged rocks or wrecks) that normally lie safely below the draft of ships. As climate change brings more frequent low-flow periods, the navigation sector may face regular summer interruptions. Already, the Danube Commission and national authorities are planning for more aggressive dredging and river training works at critical bottlenecks to maintain a navigable channel in drought conditions. However, such measures can be costly and have environmental trade-offs. **In summary**, floods cause short-term closures and damage to ports, while droughts cause sustained capacity reductions (e.g., ships can only load half their capacity) and higher transportation costs. Both extremes require adaptive management – from better forecasting and traffic regulation during floods to river engineering and fleet adjustments (using flat-bottom or smaller vessels) for low water.
- **Road and Rail Infrastructure:** The Lower Danube's floods threaten not only river traffic but also **land transportation** corridors that often

parallel the river. In Brăila County, many rural roads and even highways near the floodplain can be cut off by high water. For example, during a 2014 flood event on the Borcea branch (a Danube branch), authorities noted "danger for the nearby highway" between Fetești and Cernavodă. In 2006, dozens of kilometers of local roads were submerged or washed out. Bridges can also be affected; although major Danube bridges in Romania are high, approach viaducts and smaller bridge structures on tributaries can be damaged by floodwaters. Even when not overtopped, prolonged flooding saturates road base materials, causing potholes and collapses later. **Droughts**, on the other hand, can affect transport via indirect means like **wildfires along road/rail corridors** or thermal expansion on rails, but those impacts are less reported in this region. One notable drought-related issue is that as the Danube falls, some **ferries and river crossings become inoperable** (not just due to floods, but also when harbour ramps no longer reach the water). Additionally, extremely low groundwater during droughts can cause differential settling in road foundations, though this is a minor concern compared to flood erosion. Overall, ensuring connectivity during floods often requires investing in raised road embankments and robust drainage.

In essence, **transportation is a cross-cutting casualty of hydrological extremes** – river navigation is directly water-dependent, while roads/bridges suffer from the physical force of floods. The region has experienced both: e.g., **ferry closures and shipping halts in 2006 and 2022**, and **road outages in 2006 and 2014**. Adaptation measures (discussed later) like improved water level forecasting, dredging programs, and flood-proofing of critical routes will be increasingly important to keep people and goods moving.

Energy

The energy sector in the Lower Danube region intersects with water issues in multiple ways: through **hydropower generation, thermal power plant cooling, and electricity infrastructure** in flood-prone areas. Climate extremes are straining these links:

- **Hydropower:** While Brăila County itself does not host large hydropower stations, the Lower Danube's flow regime affects upstream plants like the **Iron Gates I & II dams** (at the Romania-Serbia border) and has implications for Romania's overall energy supply. **Droughts sharply reduce hydropower output**. In the severe 2022 drought, flows into Serbia's and Romania's hydropower reservoirs dropped by half, leading to an **at least 30% decrease in output at the Iron Gates hydropower plants** that year. Low river levels mean less water to turn turbines, and if levels fall below intake thresholds, generation must stop entirely. This was a major concern in 2022 as regional hydro reserves hit record lows and countries had to import electricity. For the future, prolonged summer low flows could diminish the reliable generation from the Iron Gates, which is a significant source in Romania's energy mix. **Floods**, conversely, usually don't limit hydropower (turbines can pass extra water, up to a point), but extremely high flows can force dam operators to spill water (bypassing turbines) or even shut gates to maintain stability, which in rare cases can reduce generation and stress the dam structures. Moreover, floods often carry debris that can threaten hydropower intakes.

- **Nuclear Energy:** the **Cernavodă Nuclear Power Plant** (**Cernavodă NPP**) uses Danube water for cooling. Both droughts and floods pose risks here. In extreme low-flow or heatwave conditions, **cooling water supply can become insufficient or too warm** to effectively cool the reactors. Indeed, by 2100 under a high-emissions scenario, severe droughts may **heighten operational risk for the Cernavodă plant**. There is concern that if Danube levels drop too far (or intake water temperature exceeds safe limits), the plant might have to curtail power output or shut down for safety. This is not just theoretical – during Europe's 2018 and 2022 heatwaves, some reactors in other countries were throttled due to warm cooling water, and Cernavodă closely monitored Danube conditions. On the flood side, an **extreme flood could threaten the plant's infrastructure** (e.g., flooding of pumps or auxiliary buildings). While the plant is designed for floods, the risk is non-zero during an event exceeding design level.
- **Electricity Infrastructure:** Floods can damage substations, power lines, and distribution networks. In 2014, a flood event led to impacts on the **electricity network**. This implies that floodwaters may have knocked out a transformer or forced a shutdown of power in that area. In rural floodplain villages, many electrical poles and wires are at risk when the ground is saturated or eroded. Conversely, **droughts and heat** can increase electricity demand (for cooling) while reducing generation (hydro, as noted above). They can also cause **overheating of transformers** and sagging of power lines, potentially leading to outages or the need for load reductions.

In summary, the energy sector faces a **double vulnerability**: **too much water** (flood) can be just as problematic as **too little water** (drought). Hydropower and cooling for power plants depend on stable river flows, which climate change threatens to destabilise. The **Cernavodă NPP** is a particular concern noted in risk assessments – ensuring its resilience (e.g., via backup cooling ponds or alternative cooling technologies) is critical. Additionally, maintaining reliable electricity during floods will require flood-proofing key grid components and having standby generation if hydropower falters.

Human Health

Floods and droughts also have important implications for **human health and wellbeing** in the Brăila region:

- **Flood-related Health Impacts:** during floods, immediate physical dangers include **drowning** and injuries from debris or collapsing structures. The 2006 flood fortunately saw few fatalities in Romania due to timely evacuations, but it generated thousands of **displaced persons** who had to stay in temporary shelters for weeks. Living in crowded conditions (like tent camps or gymnasiums) can lead to the spread of communicable diseases if not managed carefully. Floodwaters often contaminate drinking water wells with sewage and pollutants, raising risks of **water-borne diseases** such as gastrointestinal illnesses or hepatitis. Public health authorities in Romania have protocols to chlorinate wells and distribute clean water during such crises. Another health issue post-flood is **mold growth** in damp houses, which can exacerbate respiratory problems. Mental health is an under-recognised facet: the trauma of losing one's home or livelihood in a flood can lead to stress, anxiety, or depression. Community surveys after the 2006–2007 floods indicated that psychosocial support was needed for some displaced families, and that no major disease outbreaks occurred largely thanks to preventive measures (e.g. vaccinations, sanitation control). Nonetheless, each flood tests the healthcare system's ability to provide emergency medical services in isolated flood-hit areas. Hospitals themselves can be at risk: the Brăila County hospital is on high ground, but small clinics in villages have been flooded.

- **Drought and Heat-related Health Impacts:** droughts tend to be accompanied by **heatwaves** in this region, which can directly impact human health. Extended periods of high temperature and dry weather in Brăila can cause **heat exhaustion or heatstroke**, especially among the elderly and those working outdoors (like farmers). In urban Brăila, heat combined with dry conditions exacerbates **air quality issues** (dust, pollution) that affect respiratory health. Water scarcity during droughts can compromise **hygiene and sanitation**, particularly in villages where shallow wells dry up – some communities have faced shortages of drinking water in extreme cases. If people resort to unsafe water sources, it can lead to diarrheal diseases. Droughts also reduce food production, which in prolonged cases can influence nutrition; however, in Brăila, food insecurity is more an economic issue (loss of income to buy food) than immediate lack of food. Another health aspect is the potential for **wildfires** in parched reed beds or forests along the Danube, which release smoke harmful to nearby populations. Moreover, low river levels can lead to ecological changes that, for example, might increase mosquito breeding in stagnant pools – potentially affecting **vector-borne disease** dynamics (though a very wet year with many puddles can equally boost mosquitoes; the relationship is complex). One specific vector concern is **West Nile virus**: the Danube Delta region has seen

West Nile fever cases, and altered flood/drought patterns could shift mosquito habitats (floodwater mosquitoes versus stagnant water mosquitoes).

- In general, **rural communities are more vulnerable** on the health front, as they have less access to healthcare and are directly exposed to the elements. In Brăila's rural Danube villages, many residents are elderly (as younger people often migrate to cities), so they are at higher risk from heat and stress. Urban Brăila, with better infrastructure (like a centralised water supply that can buffer shortfalls) and healthcare facilities, is relatively resilient, but urban poor neighbourhoods (often low-lying and densely populated) would need special assistance if a major flood hits.

Floods and droughts carry significant **health risks**, from the immediate physical and mental health toll of disasters to the subtler effects of heat and water scarcity. Protecting human health in the face of these extremes will require robust disaster response (evacuations, medical care, water purification) and long-term measures (heat health action plans, ensuring safe water supplies, etc.) as part of climate adaptation.

Integrated Socioeconomic Vulnerability Analysis

Understanding risk in the Lower Danube is not just about the hazards (floods and droughts) but also about **who and what are exposed and vulnerable (in terms of sectors, communities)**. Lower Danube River area and in particular Brăila County exhibits complex pattern of socioeconomic vulnerability that, when overlaid on the floodplain hazard, reveals critical **hotspots**. A recent assessment of Danube-adjacent communities in Brăila County found a worrying overlap: the areas **nearest the Danube – roughly the eastern third of the county – are both the most flood-exposed and home to some of the most socio-economically vulnerable populations**. These vulnerable groups include low-income households, a high proportion of elderly residents, and communities with limited access to resources.

Notably, the **Great Brăila Island (Insula Mare)** and the communes along the left (west) bank (such as Mărașu, Frecăței, Berteștii de Jos, Stăncuța, Tufești) stand out. These areas are protected by earthen dikes (in fact a huge destruction of floodplain wetlands) but would face calamity if those defences fail. They also have **higher poverty and unemployment rates** than the county's urban centre, meaning lower capacity to recover from disasters. The analysis flagged **"hotspot" communes like Mărașu**, where **high hazard exposure coincides with high social vulnerability** – in practical terms, a large flood or intense drought here would harm many people who have few buffers or alternatives. Essentially, the **eastern strip of the county along the river – including the entire Danube floodplain – contains the most vulnerable populations (by age, income, etc.)**.

Why is vulnerability so concentrated here? Historically, these riverine communities depend heavily on **agriculture and fishing**, livelihoods that are inherently exposed to weather and water fluctuations. Many villages are partially within natural floodplain or deltaic areas and rely on pumping systems to stay dry. The housing stock tends to be older, with one-story homes that are not elevated – meaning even moderate floods can inundate homes, and residents may not have insurance or savings for repairs. Socially, these areas often have a **high elderly population** (as younger folks leave, leaving grandparents to tend farms), which increases sensitivity – for example, older individuals may have difficulty evacuating or coping with heat stress. There are also **female-majority households** (widows or women whose spouses work abroad) in some villages, which can indicate less physical capacity to recover from property damage without assistance. Meanwhile, cities (like Brăila), while having pockets of poverty, generally has better infrastructure, more diversified income sources, and services that confer greater resilience. An important concept emerging from this analysis is that **risk = hazard × exposure × vulnerability**. In cities like Brăila's case, hazard (flood/drought probability) is spatially highest by the river, and exposure (people and assets in harm's way) is also high there (all the villages and farms on the floodplain). When you multiply by vulnerability (capacity to cope or adapt), which is also high in those same places, you get **very high risk**. This integrated approach suggests that a purely physical flood model is not enough; one must incorporate a **Social Vulnerability Index** or similar metric for each locality. Indicators like age dependency ratio, poverty rate, education level, and population density in hazard zones can be combined to rank communities by vulnerability. For instance, if a 1-in-100-year flood would inundate two communes, but one has mostly wealthy, mobile residents and the other has mostly poor, elderly residents, the latter clearly faces a higher real risk in terms of human harm.

The integrated analysis for Brăila County recommended several priority actions. One is **targeting risk reduction investments to the most vulnerable communities**. For example, strengthening the dikes around clusters like **Berteștii de Jos – Stăncuța – Tufești** would directly protect thousands of high-vulnerability residents, but this is not a long-term solution. In fact higher dikes are the most dangerous of all the future solutions due, in principle, to the high probability of high flood pikes, the potential for catastrophic Similarly, focusing drought mitigation measures (like subsidised irrigation and drought insurance) on the Great Island of Brăila can safeguard livelihoods where they are most precarious. In effect, **spatial targeting** is key: maps and data pinpoint "who needs help where." Another insight is the difference between **urban and rural contexts**: Urban Brăila has more concentrated exposure (a lot of people, but behind strong flood defences) and higher coping capacity, whereas rural areas have diffuse exposure (spread-out villages, many directly on floodplain) and lower coping capacity. So, adaptation strategies must differ. Urban resilience might emphasise ensuring the city's flood defences hold, and having evacuation plans for dense neighbourhoods that might flood if defences fail. Rural resilience might emphasise **resilient agriculture (drought-tolerant crops, irrigation rehab, rainwater harvesting) and community-**

Funded by the European Union

based flood warning systems, as well as maintaining evacuation routes (like all-weather road access) for isolated villages.

In conclusion, the socioeconomic vulnerability analysis for the Lower Danube in Brăila highlights a classic problem of **inequity in climate risk**: those with the least resources often face the greatest threats. By integrating these findings into flood and drought risk management, authorities can prioritise **hotspots such as Mărașu commune** (high hazard, high vulnerability) for interventions. This might include reinforcing levees, elevating homes, improving emergency response, and diversifying livelihoods (so people aren't entirely dependent on climate-sensitive income) in those areas.

2.6.4. Challenges

Future Risks and Hotspots (2030, 2050, 2100 Projections)

Combining the climate and hydrological projections with the vulnerability landscape allows us to foresee how **risk patterns may evolve** by 2030, 2050, and 2100 in the Lower Danube region:

- **Near Future (~2030, or 2021–2050):** By the 2030 horizon, the climate models project a noticeable uptick in flood risk – e.g. **50–75% more frequent moderate floods** – which implies that the existing flood defences will be tested more often. Communities currently at risk will face **flooding not once in a generation, but multiple times**. This could erode resilience, as people have less time to recover between events. A 1-in-20-year flood historically might become more like a 1-in-10 or 1-in-5-year event. One concrete projection is a **50–75% increase in floods >10,000 m³/s by the 2020s–2040s**, which means places like Brăila city (protected to a certain design level) will see that design level exceeded more frequently. The implication is that **hotspots identified today remain hotspots in 2030, but with amplified hazard**. Great Brăila Island, for example, may need to fight back floodwaters every few years instead of every decade. On the drought side, changes by 2030 are more subtle; a slight decrease in frequency of low-flow events was noted, but this might be cold comfort as **summer drought intensity** shows signs of increase (longer dry spells-with huge impact on the remaining natural and future restored wetlands). Thus by 2030, **floods are the more immediate escalated threat**, while drought impacts will start to climb, particularly in the hottest summers.
- **Mid-Century (~2050, or 2041–2070):** Around 2050, the projections show further divergence between a moderate-emissions world (RCP4.5) and a high-emissions world (RCP8.5), though both see significant changes. Under RCP8.5, mid-century is projected to be the **peak of flood hazard**: an **order-of-magnitude increase in very large floods (>15,000 m³/s)** is expected by 2050. This means floods of the

2006 magnitude could be happening roughly every **2–3 years** on average. The flood season will also be shifting by then – we may see the **biggest floods in winter** (Jan–Feb) as the norm. For Brăila, a mid-winter Danube flood is unprecedented in modern times, so emergency preparations (traditionally geared to spring) will need adjusting. The mid-century period also likely brings the **maximum flood intensities**: new record peaks potentially above 20,000 m³/s could occur, unless adaptation measures are implemented to attenuate floods (like upstream reservoirs or restored floodplains). If such a mega-flood coincides with vulnerable conditions (e.g., a poorly maintained dike or a socioeconomic downturn limiting response), the disaster potential is huge. On the drought side, by 2050 under high emissions, summers will be much drier (as much as ~20% less summer runoff). *Multi-year droughts* might emerge – sequences like 2021–2022 back-to-back dry years could become more common. By mid-century, it's plausible that **2030s-level droughts might be the new average summers**. Therefore, mid-century risk hotspots include not just the flood-prone villages but potentially **broader swathes of agricultural land facing chronic water shortage**. The Great Island, if irrigation isn't improved, could become a chronic drought hotspot with large economic losses in farming every few years. Additionally, **navigation risks compound** by 2050 – longer low-flow periods mean the Danube shipping season could have regular interruptions each summer, affecting the regional economy.

- **End of Century (~2100, or 2071–2100):** Looking to 2100, the outcomes depend greatly on global climate action. Under RCP4.5 (which assumes emissions peaking mid-century and then declining), we might see some stabilization: flood frequencies remain elevated but perhaps not worsening beyond mid-century levels, and some flood metrics even slightly reduce (as noted, peak flood magnitudes in one analysis levelled off or dropped by late-century under RCP8.5 due to extremely dry summers limiting floods). Under RCP8.5 (continued high emissions), the climate by 2100 is far hotter; interestingly, the model ensemble suggested **flood frequencies under RCP8.5 might actually plateau or decrease slightly by 2100 compared to 2050**. This is thought to reflect that by 2100, summers are so dry that despite heavy winter rains, the overall year-round moisture available for flooding might not further increase. Even so, the flood risk in 2100 is still **well above historical** – perhaps similar to 2050 levels, meaning a permanently much higher baseline of flood likelihood. Importantly, the **seasonal shift is fully realised by 2100**: winters would firmly be the high-flow season springs relatively lower. For drought, by late-century under high emissions, this region could see **Mega-droughts**. Half the years might be what we consider "extremely dry" today. Low-flow extremes are expected to be **more prolonged and severe, especially under RCP8.5** – meaning the Danube could stay below 3,000 m³/s for many weeks, crippling navigation and stressing ecosystems. One projection noted "longer summer low-flow periods by late-century" as a key outcome. This could lead to fundamentally altered landscapes; for instance, some smaller wetlands might convert to dry land, and species distributions (fish, waterfowl) could shift without regular inundation. The **hotspots in 2100** would likely include all the current ones (because vulnerability won't disappear without socio-economic transformation) but under even greater stress. Mărașu commune, for example, might see perhaps a 1-in-100 year flood (by 1970-2000 standards) happening every 10–20 years *and* have to contend with annual severe drought impacts on farming – a compounding of risks. Urban Brăila by 2100 might largely be flood-protected with higher dikes, but if a flood exceeds those protections (which by then could be conceivable), the densely populated low-lying parts of the city could face catastrophe given the potential depth of flooding and number of people exposed.

It's also worth noting potential **new hotspots** or challenges by 2100. If climate change forces change in land use (e.g., some areas might be abandoned due to repeated flooding or drying), **migration and demographic shifts** could occur. People might move from vulnerable rural floodplain zones to the city or elsewhere, which could alleviate some exposure – or conversely, economic necessity might keep vulnerable populations in place even as risks rise. Additionally, **transboundary issues** become sharper: the Lower Danube is shared by Romania, Bulgaria, Ukraine (in the Delta) – coordinated management of floods (through, say, upstream reservoirs or emergency releases) and drought (water sharing agreements) will be vital. By 2050 or 2100, without cooperation, one country's adaptation (like building a dike or canal) could worsen another's risk.

In summary, **by 2050 we expect a peak in flood risk and by 2100 a peak in drought impact under high emissions**, with both significantly elevated from today. The geographic risk hotspots (Danube-adjacent communities, critical infrastructure like the Cernavodă NPP, key navigation choke points, large-scale irrigation zones) are identifiable now and will likely remain so. The difference is that by late-century, **the stakes are higher** – extreme events will be more frequent, and coping capacity could be eroded if we don't invest in adaptation. The next section discusses what those adaptation and risk mitigation measures could look like.

2.6.5.Conclusions

The Lower Danube River system in the Brăila region stands at the frontline of climate change impacts in Southeast Europe. This comprehensive analysis shows that what is at stake is not just an environmental shift, but a socio-economic challenge that will define the future of communities along the Danube. The storyline events – catastrophic floods like that of 2006 and unprecedented droughts like 2022 – are signals of a new normal where extremes are more frequent. Historic discharge data and future projections (RCP4.5 and RCP8.5 scenarios) jointly indicate a trend toward greater hydrological volatility: more frequent & intense floods on one hand, and longer & harsher droughts on the other. For Brăila County, the analysis identified that the highest risks concentrate in the Danube floodplain corridor, where both flood hazard and social vulnerability peak. Poor, rural communities behind aging dikes face the burden of floods, and the same communities suffer most in droughts due to their reliance on rain-fed agriculture. Without intervention, climate change could widen this vulnerability gap, hitting hardest those least able to cope.

2.6.6. References

ICPDR (2006). The Analysis of the Danube Floods 2006. https://www.icpdr.org/sites/default/files/The%20Analysis%20of%20the%20Danube%20Floods%202006%20FINAL.pdf

ICPDR (2010). 2010 Floods in the Danube River Basin. https://www.icpdr.org/sites/default/files/nodes/documents/icpdr_flood_report_2010.pdf

ROWATER (2023). Danube River flood risk management plan. https://rowater.ro/wp-content/uploads/2023/09/12-PMRI-Dunare-1.pdf

Funded by the European Union

2.7. CSA 7 INDIRECT (Power system)

2.7.1. Summary of climate change hotspots and event-based storylines

Climate Change hotspots

For this case study the focus is on France in the context of the European electricity system with a focus on how climate change will influence the role of renewable energy in the electricity systems. This focus is chosen, e.g., because in a broader European context France already has an energy production with a significant contribution of renewable energy, and experiences from France then provides valuable results for other member states to achieve ambitious decarbonization goals (International Energy Agency [IEA], 2025). While France is the main focus, energy indicators have been calculated throughout all the European domain and aggregated at different NUTS levels, providing the potential to inform stakeholders in other countries. Within France, the central and southern regions are, with their high shares of hydropower, wind and solar, especially exposed to compounded hazards of extreme weather events associated to a changing climate. Aggregated data and visualisations will, in the final part of the project, be delivered via the Teal Tool, tailored to EDF's and other potential stakeholders' needs for easy access and analysis.

Event-based storylines

We are focusing on analysing prolonged events of extreme weather, this can both be in relation to renewable energy generation and increased demand such as:

- The heatwave and drought in the summer of 2022 which affected many parts of southern Europe and France where many stations recorded temperatures of above 40 degrees and historic low amounts of precipitation. The resulting spike in cooling demand, coupled with reduced thermal-plant cooling efficiency at elevated intake temperatures, placed exceptional operational stress on the electricity grid, increasing the risk of shortages in energy (Copernicus, 2022).
- The wind drought event in 2021 which affected several parts of northwestern and central Europe, experiencing the lowest annual average wind speeds since at least 1979 and leading to a reduction in the potential for wind power generation in different European countries (C3S, 2022). Wind speed anomalies occurred over France during October to December 2021, a critical period for heating demand.

These events are used as a reference to define associated thresholds in terms of temperature and low wind speed in ERA5 and to detect such events in CMIP6 projections, analyse their evolution and potential impacts on the power system using plan4res tool. The upper part of Figure 69 below shows an example of how the limits of the past events is calculated in this case for spatial aggregated 3 month running mean wind speed anomaly over France from the ERA5 reanalysis dataset, focusing on the above-described wind drought for fall 2021. This is then used in the bias corrected CMIP6 model data as the limit for similar events in the future. Similarly, the lower plot shows the temperature anomaly, highlighting the heatwave of the summer of 2022.

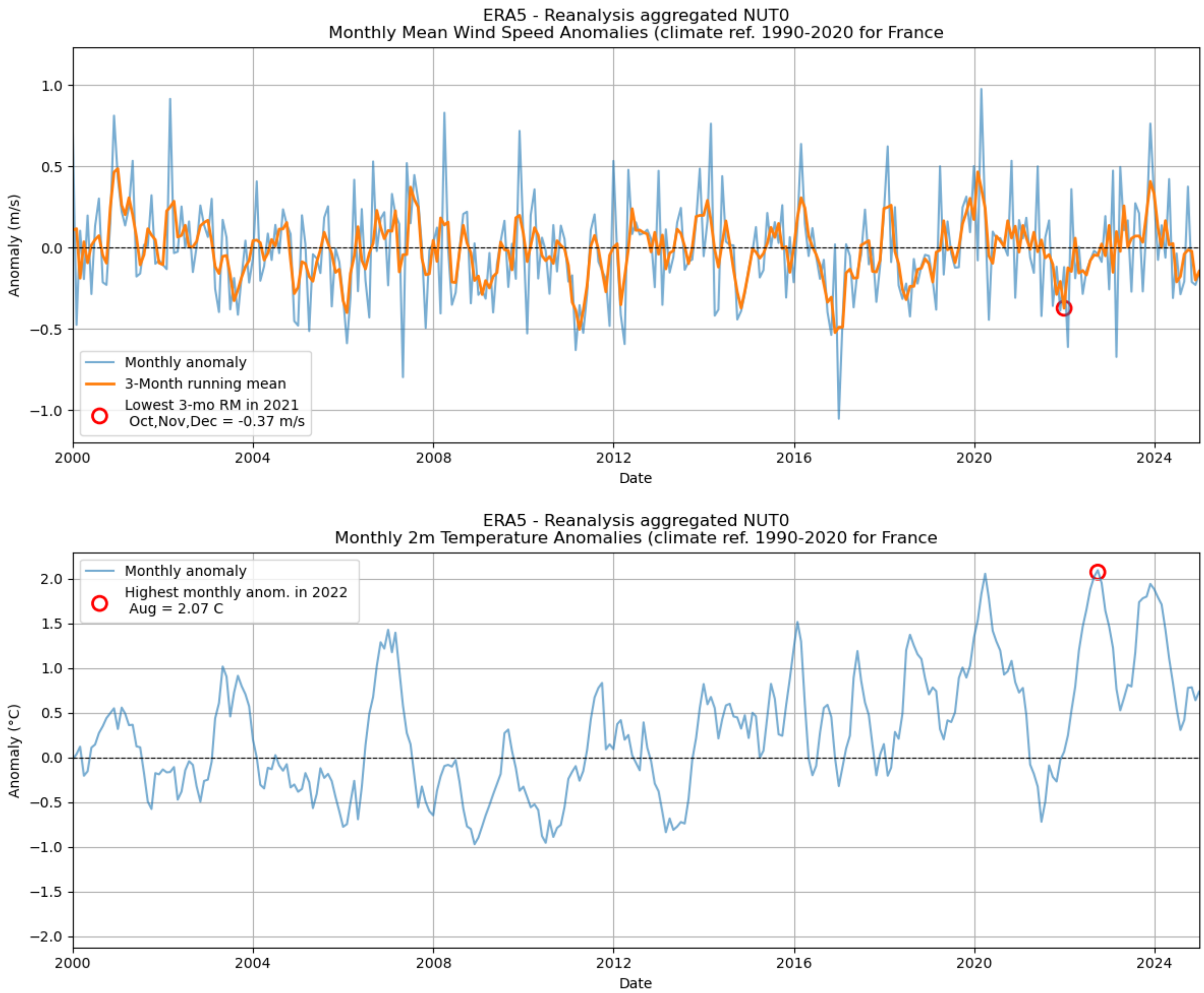

Figure 69: *ERA5 reanalysis data aggregated over France from the period 2000-2024 of monthly anomalies of wind speeds (upper) and 2 2 metre temperature (lower) with respect to the climate for each month over the years 1990-2020. In both plots the investigated events are highlighted with a red circle for the wind drought 2021 (upper) and 2022 heatwave (lower).*

Beside these events, we will also analyse the general trends in specific climatic conditions that are associated with difficulties for energy production, transmission and general grid management, such as concurring conditions leading to low production for several renewable energy sources and potentially also high demand. This will be done at different NUTS levels, for all the European domains. We will analyse the trend in the occurrence of these events for different times, models and scenarios.

2.7.2. Overview of general objectives.

The overall objectives of this case study are:

- To analyse the trend in and quantify the impacts of concurrent heatwaves, droughts and wind droughts on electricity production and demand.
- To (partly) estimate (part of) the cost of necessary operational adjustments and investments in mitigation and adaptation strategies for a renewable-dominated system under different climatic and socioeconomic scenarios.
- To analyse the dispersion of the marginal costs of electricity, and the risks of non-served energy events linked to the meteorological scenarios.

2.7.3. Application of the methodological framework

The work carried out so far for CSA 7 has focus on the large task of retrieval and preparation of the hourly CMIP6 data to be able to run the plan4res model for specific projected events with the extra "forcing" estimated from a changing climate. See Figure 70.

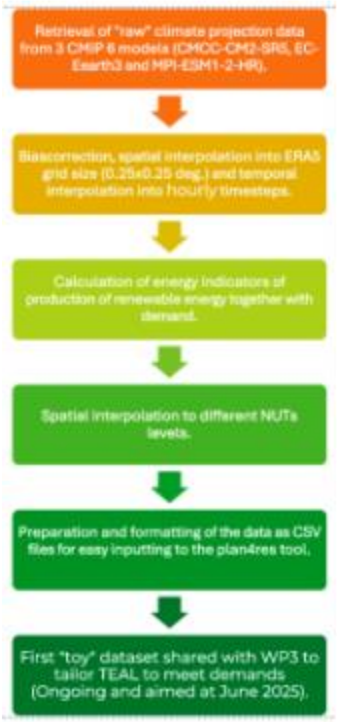

Figure 70: *Overview of workflow up untill now and next immediate step.*

Step 1 Climate and socioeconomic scenarios

The first step in the analysis was the selection of 3 climate projection models (see table 18) that all had a relative high spatial and temporal resolution. This allowed to downscale temporally to hourly resolution better capturing peak demands and impacts and spatially to a relative high resolution of 0.25x0.25 degrees matching the ERA5 data set used as reference for the downscaling/bias correction. Data was then retrieved for these three models for the necessary climate variables to process these and end up with the 4 main energy indicator categories:

- Wind energy both onshore and offshore production
- Solar energy for photo voltaic setups
- Hydro both reservoir and run of river
- Demand

The computation of energy generation and demand follows the methodologies provided by the C3S sectoral impact tool for energy (C3S Energy, 2024).

This is what is needed as input for the plan4res model which will be used as the main tool for the cost analysis of the implied impacts for the changing climate.

Table 18: *Overview of the three included CMIP6 models, origin, original atmospheric resolution and oceanic resolution (CMIP 2025).*

Model	Institution	Org. Atmosphere resolution	Org. Ocean resolution
CMCC-CM2-SR5	Fondazione Centro Euro-Mediterraneo sui Cambiamenti Climatici (CMCC), Italy	CAM5.3: 1° × 1° (~100 km; 288 × 192 grid; 30 levels) (wdc-climate.de)	NEMO 3.6 ORCA1: ~1° (~100 km; 362 × 292 grid; 50 levels) (wdc-climate.de)
EC-Earth3	EC-Earth Consortium (27 European research institutes)	IFS CY36r4: T255 (~80 km triangular truncation; 91 levels) (GMD)	NEMO 3.6 + LIM3 sea-ice: ~1° (~100 km) (GMD)
MPI-ESM1-2-HR	Max Planck Institute for Meteorology (MPI-M), Hamburg, Germany	ECHAM6.3: nominal 100 km grid (aerosol/atm/land) (wdc-climate.de)	MPIOM 1.6: nominal 50 km grid (ocean/sea-ice) (wdc-climate.de)

We have calculated the energy indicators for each of the three models for the scenarios SSP1-2.6, SSP2-4.5, SSP3-7.0 and SSP5-8.5 as seen in the table 19 below. The specific runs we are planning for the plan4res tool will focus on the higher forcing scenarios as current observed trend in global temperature have greater alignment with higher forcing scenarios. This also will give us a better understanding of the more challenging scenarios with respect to indirect impacts on the energy sector from a changing climate.

Table 19: *Radiative forcing in 2100, qualitative storyline of mitigation and adaptation challenges, CO_2 emissions trajectory, and projected global mean warming for 2081–2100 relative to 1850–1900, for the SSP1-2.6, SSP2-4.5, SSP3-7.0 and SSP5-8.5 scenarios.*

Scenario	Radiative forcing in 2100 (W/m²)	Storyline (mitigation/adaptation challenges)	Emissions trajectory	Projected warming (2081 – 2100 vs 1850 – 1900)
SSP1-2.6	2.6	Sustainability ("Taking the Green Road"): gradual shift to low-resource, inclusive development; low challenges	CO_2 cut to net zero around 2075	1.8 °C (very likely 1.3 – 2.4 °C)
SSP2-4.5	4.5	Middle of the Road: historical trends continue; moderate progress on sustainability; medium challenges	CO_2 near current levels until ~2050, then gradually declining (no net zero)	2.7 °C (2.1 – 3.5 °C)
SSP3-7.0	7.0	Regional Rivalry ("A Rocky Road"): resurgent nationalism, low cooperation, resource-intensive growth; high challenges	CO_2 emissions roughly double by 2100	3.6 °C (2.8 – 4.6 °C)
SSP5-8.5	8.5	Fossil-Fueled Development ("Taking the Highway"): rapid economic growth via abundant fossil fuels; high mitigation challenges	CO_2 emissions triple by ~2075	4.4 °C (3.3 – 5.7 °C)

For the specific runs with the plan4res tool the installed capacities, costs and annual demand will be those provided by the recently published energy transition scenarios ENVIS2060 (from the MANoEUVRE project). We will choose the "NECP Essentials" scenario as it is implementing the European NECPs (Löffler et al., 2025).

First statistics on trends in extreme events.

Currently ongoing is the first analysis of the calculated climate projections for the energy data. The following is documenting the procedure with projection data for onshore wind (WON), which were applied under the MPI-ESM SSP5-8.5 scenario for the NUTS0 domain. The final analyses will include more scenarios, domains and models.

First, we in this case define an "extreme" event as wind production to be lower than the 10th percentile for that specific day and hour of the year (using +-7 days to increase sample size) based on the period 2015-2025. For each month and all years for the period 2025-2100 it is then counted how often the wind speed is below their respective thresholds and the general linear trend is found. Looking at Figure 71, we can see that across much of Northern and Western Europe (SE, NO, FI and GB) the data reveal a clear seasonal signal with decreasing extreme low-wind events in spring and early summer whereas late fall and winter reveal the opposite as an increase in extreme low-wind events. At the same time in the Mediterranean area several countries (ES, IT, GR) show the opposite pattern.

During summer there is a decrease in the number of low-wind events and an increase in winter.

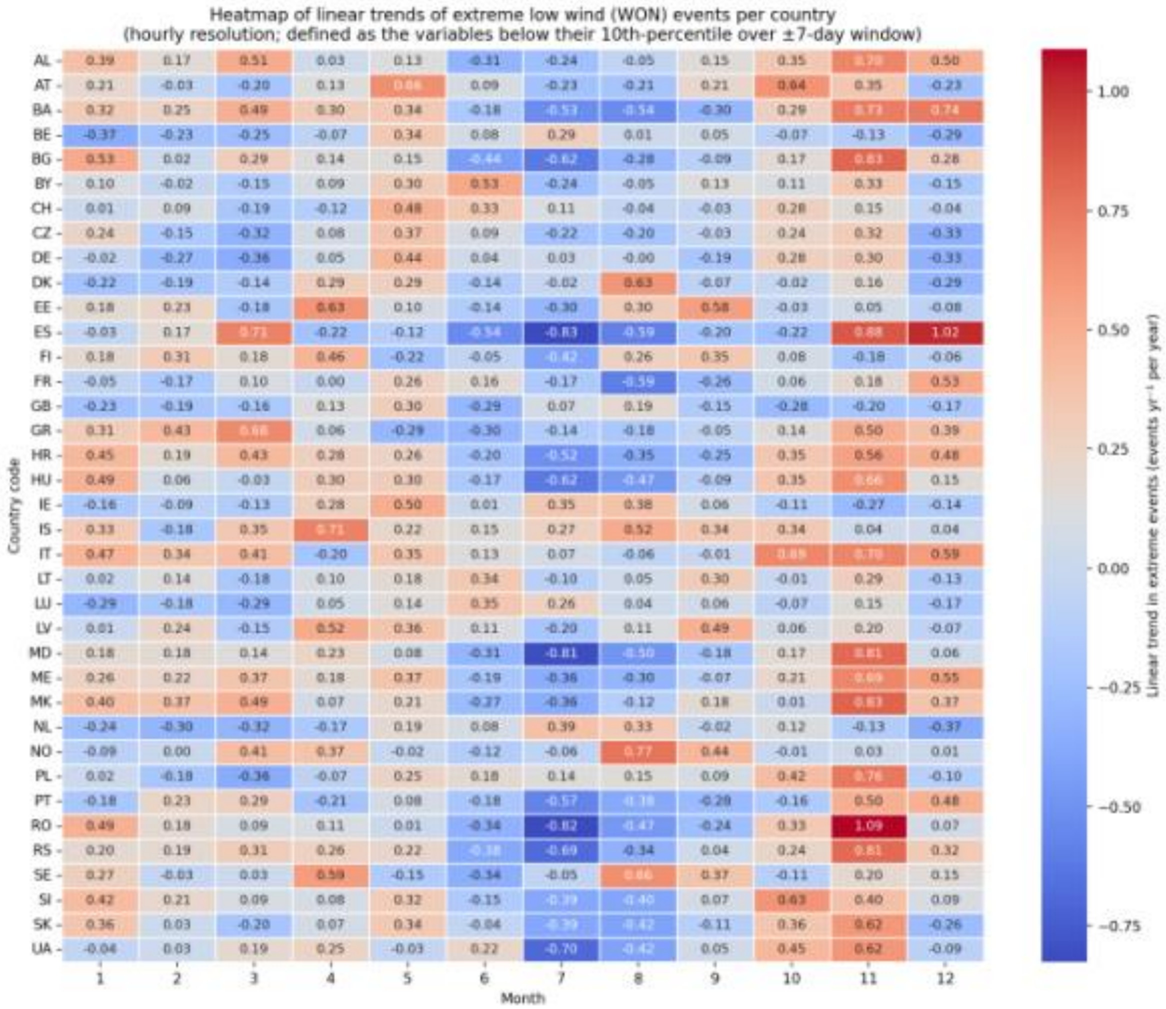

Figure 71: *Heatmap of linear trend in low wind speed events (lower than 10th percentile for the MPI-ESM SSP5-8.5 scenario.*

These patterns are even more clearly illustrated in Figure 72, highlighting the difference especially for central and southern Europe between late summer and early winter. In late summer the general signal in these areas is a decrease in extreme low-wind events and the opposite in early winter.

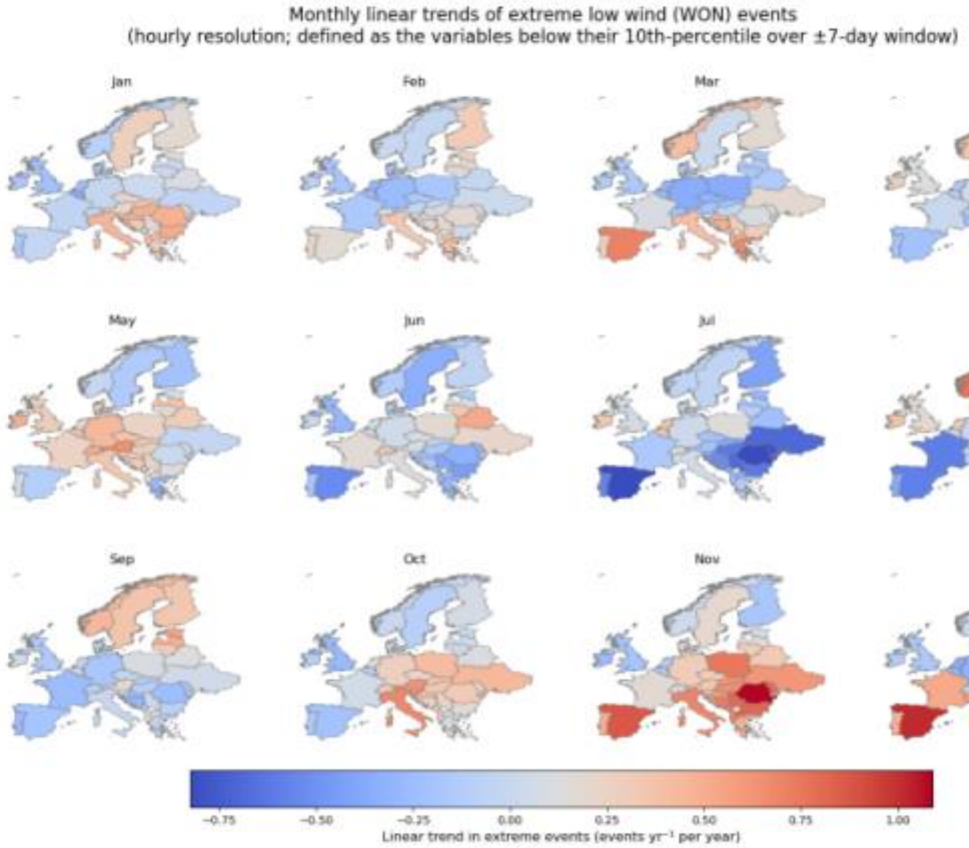

Figure 72: *Spatial map of linear trend in low wind speed events (lower than 10th percentile for the MPI-ESM SSP5-8.5 scenario.*

As a second step we have also analysed the trend in simultaneously occurring events with projected low onshore wind energy production and solar photovoltaic (SPV) production. For SPV the calculation is carried out in a similar fashion looking at events below the 10th percentile, however now the trend is found from the simultaneously occurring events where both WON and SPV are below the 10th percentile for that hour and day. Figure 73 and 74 below shows in a similar way the trend for each country for these low WON and SPV events for the same model and scenario as for WON only.

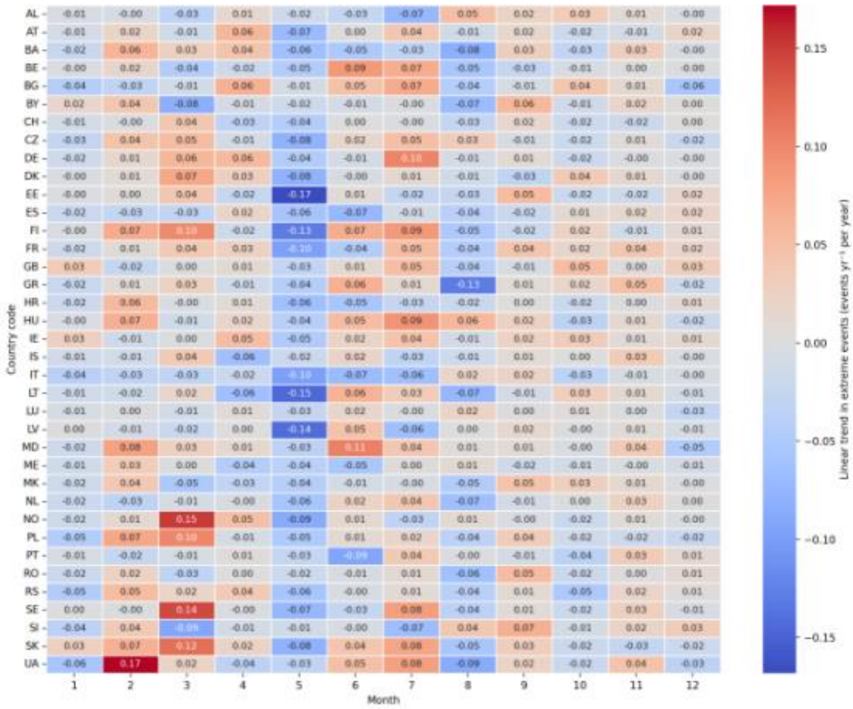

Figure 73: *Same as figure 71 Above, but for both simultaneous occurring low WON and SPV.*

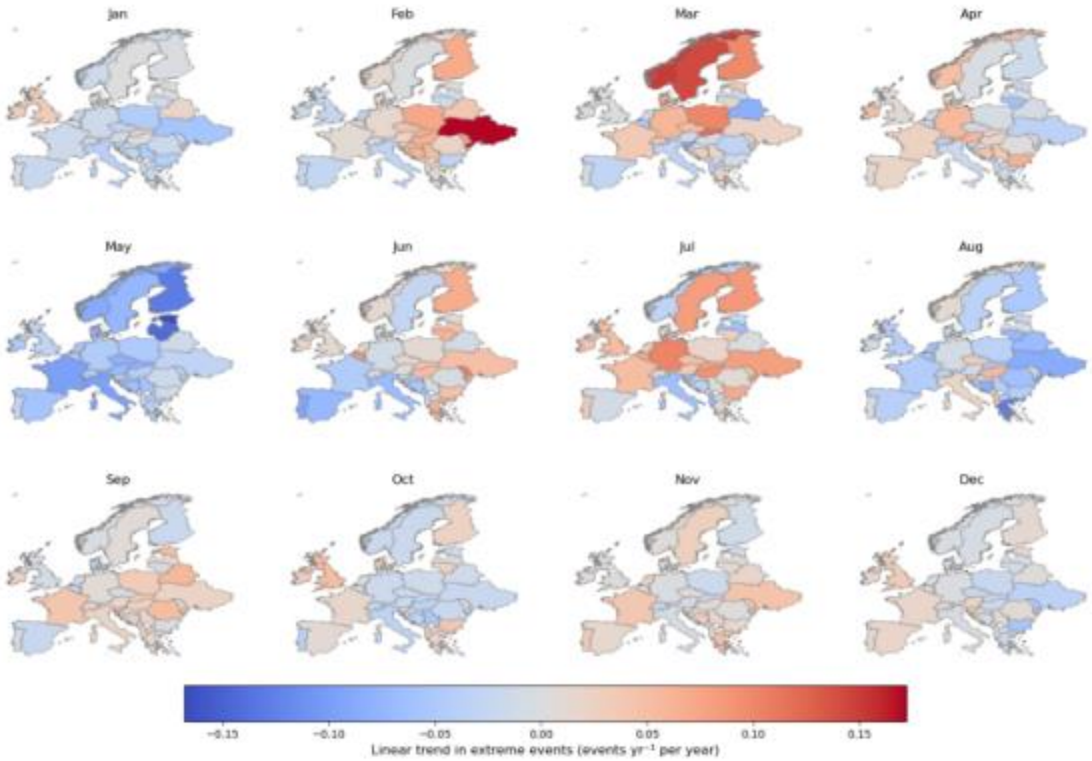

Figure 74*: Same as figure 72 above, but for both simultaneous occurring low WON and SPV.*

Finally, we have also looked at the linear trends in monthly cooling degree days (CDD). In this case looking at the trend in the absolute numbers and not specific occurrences of extremes. See Figure 75 and 76 below.

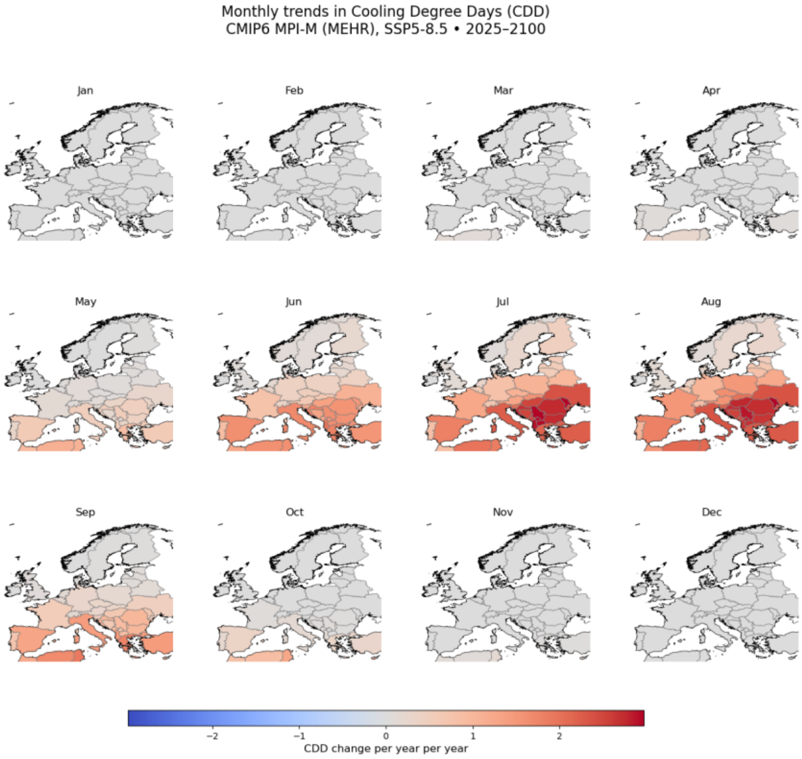

Figure 75: Monthly trend in Cooling degree days for the each month over the European region, calculated for the CMIP6 MPI-ESM1-2-HR model for SSP5-8.5.

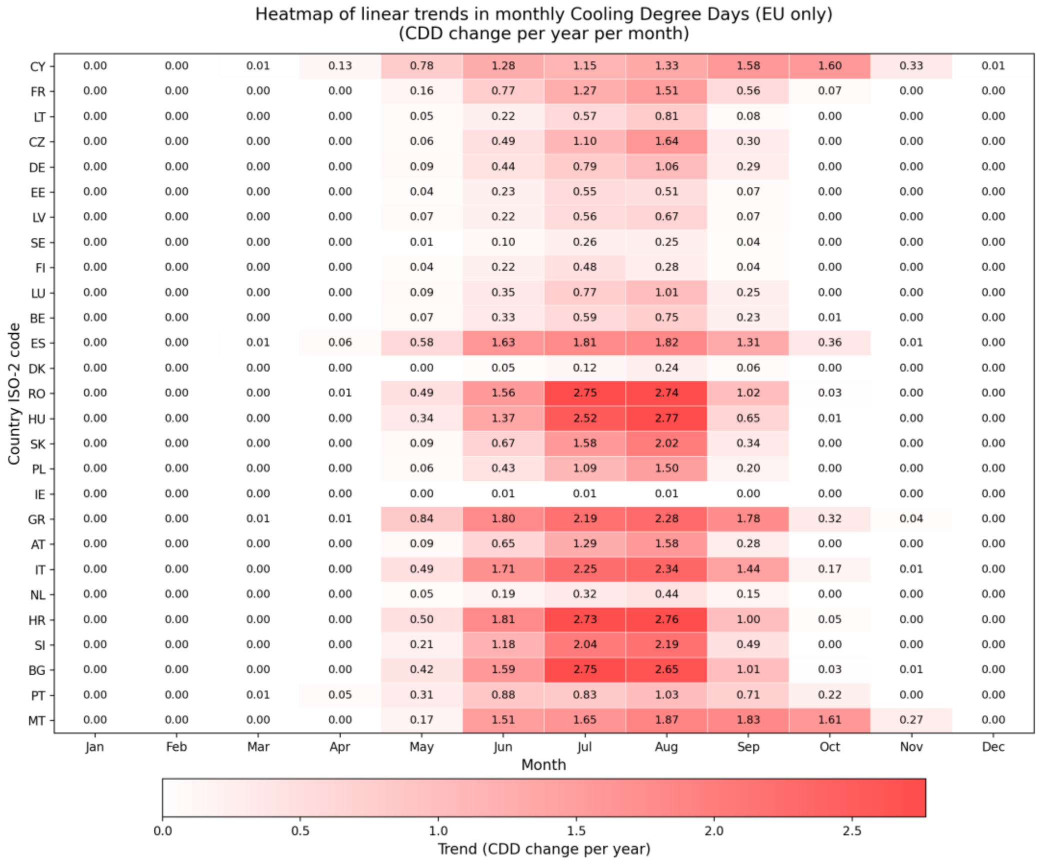

Figure 76: Heat map of the monthly trend in Cooling degree days for the each month over the European region, calculated for the CMIP6 MPI-ESM1-2-HR model for SSP5-8.5.

Funded by
the European Union

Southern and eastern member states show the strongest upwards trends, especially in July–August, where countries like Romania (≈2.75 °C·days yr^{-1}), Bulgaria (≈2.75 °C·days yr^{-1}), and Croatia (≈2.73 °C·days yr^{-1}) lead the pack.

France also exhibits significant increases in mid-summer (>1.2 °C·days yr^{-1} in July and August) and moderate rises in June and September. This will play an important in the yearly demand.

Even cooler climates (e.g. Germany, Czech Republic, Baltic states) register detectable upticks in late spring through early autumn.

Next step: Impact estimation with the plan4res model.

To fully estimate the impacts on the combined and connected energy system estimation of individual variables or combinations does not provide the full picture. Currently, we are in the final steps of preparing the climate projection data of the relevant energy indicators to be used with the plan4res model. This will give a complete estimate of the impacts on the combined energy system in Europe of the predicted climate changes. By having this it will furthermore estimate the cost of mitigating and adapting to cope with the changing climate. Outputs will be reported at the same NUTS0 level allowing allocating costs, reliability metrics and investment needs back to each region.

The plan4res model

plan4res is a power system model, which includes capacity expansion (adaptation of the generation and storage mix as well as of the existing interconnections of a given year), optimization of the strategies for managing seasonal storages, and simulation of the system operation.

plan4res focuses on electricity. It includes all power generation technologies, electricity storage technologies, a representation of the interconnections between regions (the transmission grid within one region is not represented, nevertheless, the granularity of regions can be adapted to the modelling needs); it can run on any geographic scope, provided that it is divided into a set of interconnected regions and that data are available at regional granularity; plan4res is usually ran on a chosen year, with hourly granularity.

plan4res is composed of the 3 following models:

- A Capacity expansion model (CEM) aimed at adapting the electricity mix
- A seasonal storage valuation model (SSV) aimed at optimizing the management of seasonal storages
- A simulation tool, based on a Unit Commitment model (UC), aimed at optimizing the short-term operation of the system

plan4res Inputs and Outputs

Main Inputs:

- **Electricity demand:**
  - Annual electricity demand per uses (heating, cooling, transport, others)
  - (scenarized) Hourly profiles per uses
- **System services requirements:** primary and secondary reserve
- **Interconnections:** characteristics of (existing) transmission lines between regions: capacity and investment cost
- **Generation mix:**
  - **Thermal generation** (mainly fossil and nuclear): installed capacity, variable and capital costs, system services capacity, etc.
  - **Hydro power**, including seasonal storage (reservoirs with large capacity, which are managed in general over one year), (short term) storage: this relates to small reservoirs, managed over 1 week or 1 day and run of river: installed capacity, volumes of reservoirs (if any), pumping efficiency,(scenarized) inflows timeseries, system services capacities, costs (for short term storage)
  - **Variable renewable generation** (other than hydro), mainly windpower and PV: installed capacity, system services capacities (if relevant), costs, (scenarized) hourly profiles which applied to the capacity give the hourly maximum power, depending on meteorological conditions
  - **(short term) storage** (apart from hydro): installed capacity, volume of the storage, charging / discharging efficiencies, costs

Main Outputs:

- Investment decisions: generation, storage, interconnections
- Power generation schedules
- System services mobilisation schedules
- Volume of reservoirs
- Marginal costs of electricity
- Marginal costs of system services and of interconnections
- Flows between regions

Methodology for CSA 7

In the case study, we will use the 3 layers of plan4res. In a first step the bellman values of the European seasonal storages will be computed. These Bellman values are defining the management strategies for the seasonal hydro reservoirs. Then a simulation run will allow to evaluate the (scenarized) operation costs of the electricity system on each chosen years, based on the strategies for hydro reservoirs. Finally, a capacity expansion run will allow to evaluate the investment cost which would be necessary to ensure that enough power is available to fit with the demand.

2 different runs will be done for each step:

1. A first run, denoted "reference" will include in the scenarized data, a "reference", without inclusion of the selected extreme scenarios
2. A second run will include a selected extreme scenario

Plan4res input data will consist of:

- Installed capacities, costs and annual demand will be those provided by the recently published energy transition scenarios ENVIS2060 (from the MANoEUVRE project). We will choose the "NECP Essentials" scenario as it is implementing the European NECPs. (see 10.5281/zenodo.13710868 and 10.5281/zenodo.14944682 for more details)
- All scenarized data (hourly profiles for the power demand, renewable generation potentials and hydraulic inflows) will be those computed in the first phase of the case study.
- The first step (simulation) will allow to evaluate the costs on the power system as defined by the NECP Essentials scenario. The following outputs will be used:
    - *Generation-$Region-$i.csv*: 1 csv file per region and per scenario representing the generation schedules from the different available technologies (1 column per technology, 1 row per hour in the year).
    - *Slack-$Region.csv*: 1 csv file per region representing the electricity not served (1 column per scenario, 1 row per hour in the year).
    - *nbHoursSlack.csv*: number of hours with non-served electricity per region and scenario.
    - *VariableCostPerScenario.csv*: represents the operation costs per scenario, region, and technology.
    - *meanTimeCmar.csv*: contains the average marginal cost over the year, for each region ans scenario.
    - *MarginalCostActivePowerDemand-$region.csv:* 1 csv file per region representing the marginal costs at each hour of the year, for all scenarios (1 column per scenario, 1 row per hour)
    - *ImportExport-$region-$i.csv*: import and exports schedules to/from the region for scenario $i. (1 column for import, 1 column for export, 1 row per time step.

Out of these raw results, different values could be computed:

- Comparison of the bellman values computed in the "reference" case (ie based on a set of scenarios not including the extreme scenario) and in the "reference+extreme" case (ie based on a set of scenarios including the extreme scenario)
- Comparisons of the simulation results:

Funded by
the European Union

- Percentage of variation of operation costs per regions in the chosen “extreme” scenario compared to the average operation costs (in the reference run and in the run including the extreme scenario)
  - Dispersion of the marginal costs per regions in the reference and reference+extreme cases
  - Percentage of variation of average non served electricity per regions in the chosen “extreme” scenario compared to the average (in the reference run and in the run including the extreme scenario)
  - Number of hours with non-served electricity
  - Average imports/exports
- Comparison of the capacity expansion results:
  - Comparison of the investment cost in the reference and reference+extreme cases
  - Analyses of the volume of invested technologies in both cases.

2.7.4. Challenges and conclusions

The main challenge we have encountered in our case study has been related to the generation and preparation of high-resolution (both temporal and spatial) energy indicator dataset with an hourly temporal resolution that we need in order to run the plan4res model. These calculations and adjustments are very consuming when it comes to computer power and result in several terabytes of data. However, we are now past that hurdle and are ready to start running the plan4res model in order to produce the data needed for our impact assessment.

Despite these hurdles of processing the data, the first analysis of the downscalled and bias-corrected datasets are all ready revealing important insights. The example from MPI-ESM1-2-HR SSP5-8.5 strongly indicates that conditions that historically has led to challenges for the energy production and distribution are expected to become more frequent and extreme under a changing climate. Especially looking at cooling-degree-day trends point to significant rises in mid-summer demand drivers. Southern France, for example, experiences increases exceeding 1.5 °C·days yr^{-1} for August, indicating elevated peak loads and stress on generation resources to increase. Analysis of simultaneous low-wind and low-solar events further underscores compound supply risks during critical demand periods. Further analysis on a broader selection of models and scenarios will be carried out and play a good background of the climate change driving the expected conclusions from the plan4res model.

Looking ahead, running the plan4res model with the prepared energy indicators as inputs will quantify the combined impacts of climate change on the electricity system in Europe. The outputs as described earlier will give estimates of costs of necessary mitigation and adaptation, enabling stakeholders the necessary information needed to ensure resilient infrastructure and allocate resources for the power generation and system accordingly.

2.7.5. References

Charousset, S., Oudjane, N., O'Reilly, R., Crespo del Granado, P., Barani, M., Perger, T., Zwickl-Bernhard, S., Auer, H., Olmos, L., Ramos, A., Graabak, I., Alvarez, E. F., Härtel, P., Frischmuth, F., Lepaul, S., Pinel, D., Wolfgang, O., Schledorn, A., Dominkovic, D. F., ... Belsnes, M. (2023). Open ENTRANDE deliverable 6.2: Case study results (Final). Zenodo. https://doi.org/10.5281/zenodo.8289103

Copernicus Climate Change Service. (2025). Low winds – European State of the Climate 2021. https://climate.copernicus.eu/esotc/2021/low-winds

Copernicus Climate Change Service. (2022). Extreme heat – European State of the Climate 2022. https://climate.copernicus.eu/esotc/2022/extreme-heat.

D. Beulertz, S. Charousset, D. Most, S. Giannelos and I. Yueksel-Erguen, "Development of a Modular Framework for Future Energy System Analysis," 2019 54th International Universities Power Engineering Conference (UPEC), Bucharest, Romania, 2019, pp. 1-6, doi: 10.1109/UPEC.2019.8893472. https://ieeexplore.ieee.org/document/8893472

International Energy Agency. (2025). France: Energy mix. https://www.iea.org/countries/france/energy-mix.

Intergovernmental Panel on Climate Change. (2021). Climate Change 2021: The Physical Science Basis. Summary for Policymakers. Contribution of Working Group I to the Sixth Assessment Report of the Intergovernmental Panel on Climate Change. Cambridge University Press. https://www.ipcc.ch/report/ar6/wg1/downloads/report/IPCC_AR6_WGI_SPM.pdf

Löffler, K., Moskalenko, N., Herpich, P., Hanto, J., Hainsch, K., Bornemann, J., Diesing, A., Dupke, R., & Barani, M. (2024). The European Energy Vision 2060 (EU EnVis-2060): Scenario Parametrization [Dataset]. Zenodo. https://doi.org/10.5281/zenodo.13710869

World Climate Research Programme. (2025). *CMIP Phase 6 (CMIP6)*. https://wcrp-cmip.org/cmip-phases/cmip6/

Funded by the European Union

2.8. CSA 8 SPILLOVER (Global agriculture)

2.8.1. Summary of climate change hotspots and event-based storylines

Event based storyline (STL)

Climate change is projected to affect agricultural systems in a spatially heterogeneous manner, primarily due to variation in baseline climatic conditions, geographic features, and agroecological zones across regions. While tropical regions are expected to be disproportionately affected by climate change, temperate and boreal regions may experience limited short-term benefits from moderate warming. However, the overall effect is predicted to be unfavourable, with global crop yields expected to decline at around 1 percent per decade (IPCC, 2022).

The uncertainty about the expected magnitude is also large. Projected impacts vary by crop, region, timeframe and RCP, depending on the current temperature level and degree of warming (Figure 77).

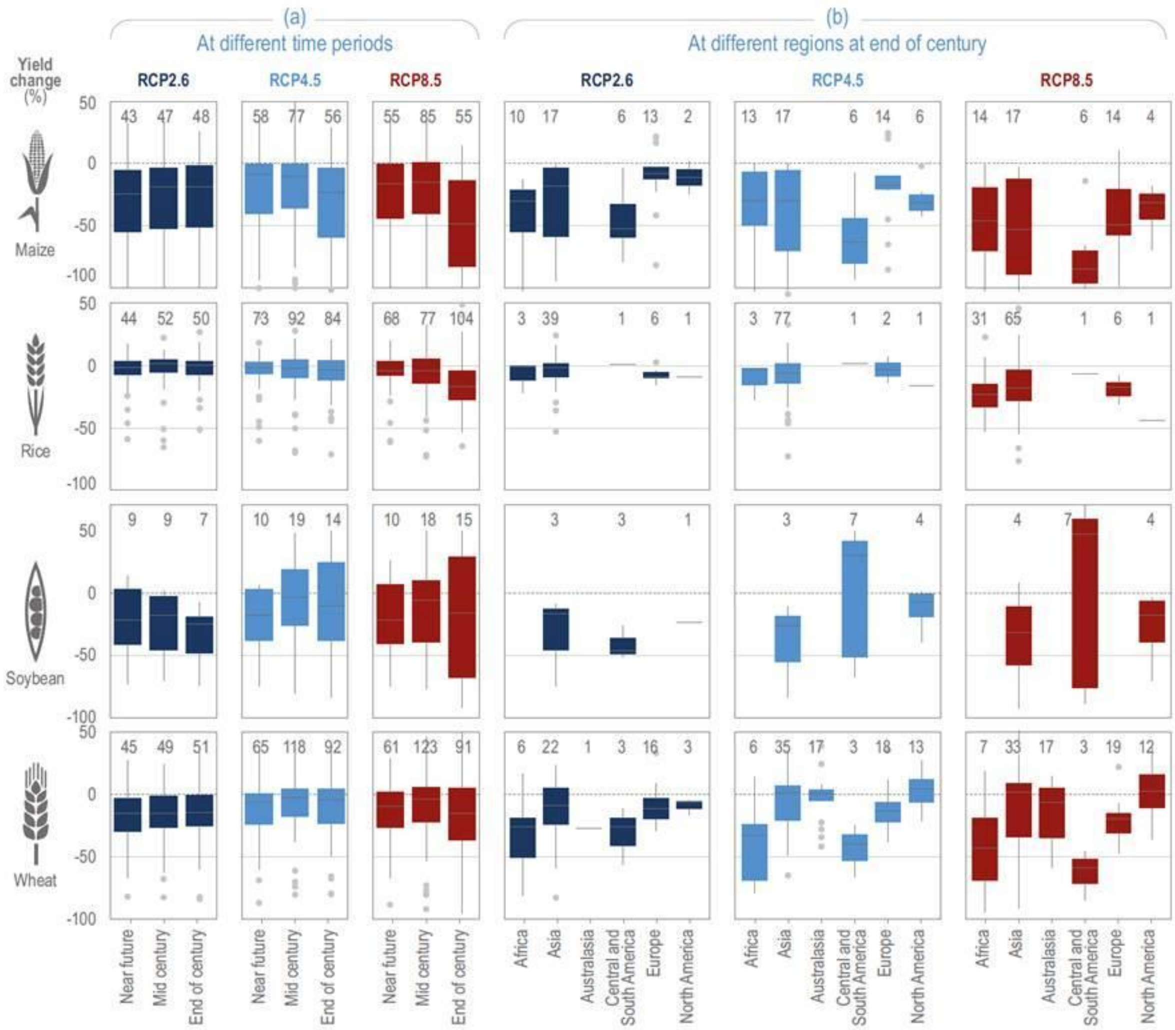

Figure 77: Projected yield changes relative to the baseline period (2001-2100) without adaption and with CO2 fertilisation effects. The box is the interquartile range (IQR), and the middle line in

the box represents the median. The upper and lower end of whiskers are median 1.5 × IQR ± median. Open circles are values outside the 1.5 × IQR. (a) At different time periods (near future, NF, baseline to 2039; mid-century, MC, 2040–2069; end-century, EC, 2070–2100) under three RCPs, and (b) at different regions at EC. Source: IPCC (2022).

Regions are not only affected by the direct impact of climate change on their agricultural yields, but they are also vulnerable to climate-induced changes in competitiveness. In fact, farmers in regions where climate change increases agricultural yields may produce more and experience greater access to markets, while farmers in regions adversely affected by climate change may lose their market share as they face lower yields and greater competition from elsewhere.

A comprehensive assessment of the climate change impacts on the global agricultural system must consider the effects on local crop production and markets, as well as the effect across national and international food supply chains.

Climate Change hotspots (CCH)

This case study examines the impacts of climate change on agriculture from a global perspective, with a focus on subnational-level analysis across EU27 and the UK, while also considering their main trade partners. A global economic model with spatial resolution at the NUTS2 level for the EU27 and the UK is currently under development and will be incorporated in subsequent phases of the project.

The analysis focuses on crop production, assessing how rising temperatures will affect both crop yields and labour productivity. It captures the dual pressure exerted by heat stress: limiting the physical capacity of agricultural workers and reducing crop output. Temperature projections under multiple climate scenarios inform these estimates, with particular emphasis on regions facing heightened climate exposure and socioeconomic vulnerability.

Rather than treating yield or labour shocks in isolation, the economy-wide model reflects intersectoral linkages and regional trade flows to simulate systemic effects. This comprehensive assessment supports policymakers in anticipating direct and indirect consequences of climate impacts—such as crop yield changes, shifts in supply chains, regional income disparities, increased pressure on trade systems, and changes in comparative advantages — and in crafting coordinated, cross-sectoral adaptation responses.

2.8.2. Application of the methodological framework

Modelling Framework and Analytical Approach

To assess the economy-wide implications of climate-induced impacts on agricultural outputs and labour productivity at NUTS2 level, we are developing a subnationally disaggregated version of the ENGAGE model

(ENvironmental Global Applied General Equilibrium). The development of the model is part of CROSSEU WP1 'Advancing the integration of bio-geophysical and socio-economic modelling in the climate change context'. The main analysis of the model, to be delivered in Month 30, will evaluate the direct and indirect impacts of climate change on global agriculture across sectors, NUTS2 regions and countries. It will cover 241 NUTS2 regions across the EU27 and the United Kingdom, capturing both regional detail and interregional trade flows (see Figure 78).

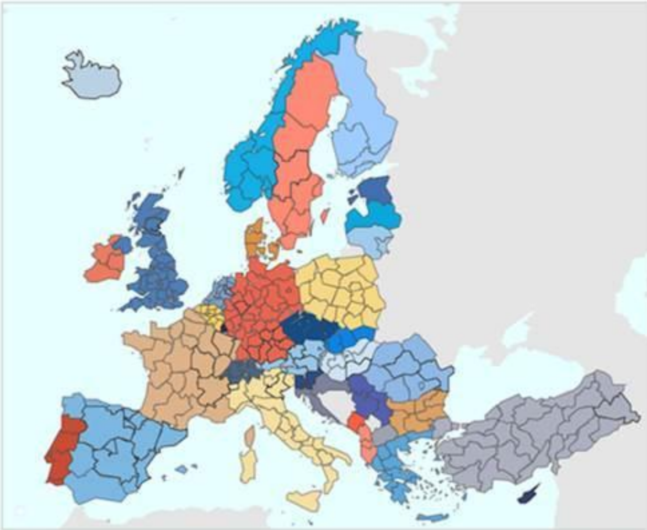

Figure 78: *NUTS2 regions across Europe. Source: Eurostat.*

The ENGAGE model, developed at University College London (UCL), is a standard multi-sectoral, multi-region, dynamic CGE model designed to evaluate the macroeconomic effects of energy, environmental, resource, and economic policies (Winning et al., 2017; Calzadilla & Carr, 2020; Nechifor et al., 2020). It is based on core general equilibrium assumptions, including market clearance, zero economic profits, and utility maximisation or cost minimisation by representative agents. All industries are modelled through representative firms operating in perfectly competitive markets and maximising profits. Sectoral output is produced using nested Constant Elasticity of Substitution (CES) functions to capture the substitutability of inputs.

The model also applies the Armington assumption to distinguish between domestic and imported goods, reflecting product differentiation across regions. On the demand side, a representative household in each region receives income defined by the value of national primary factors. This income is then allocated across household consumption, public consumption, and savings. This structural configuration allows ENGAGE to simulate the propagation of shocks—such as those induced by climate impacts—across interconnected economies and sectors over time.

The 'Subnational-ENGAGE' model is built upon the FIGARO (Full International and Global Accounts for Research in Input-Output analysis) database, produced by Eurostat in collaboration with the European Commission's Joint Research Centre (JRC). FIGARO provides harmonised supply-use and input-output tables at the national level for the EU27 countries and the United Kingdom. It covers 64 production sectors and 64 corresponding products, and includes detailed bilateral international trade flows, enabling a comprehensive representation of economic interlinkages across countries and sectors.

To achieve subnational resolution within the EU27 and the UK, the Subnational-ENGAGE model disaggregates the national-level FIGARO data by applying data-driven methods that allocate national economic activity to regions using regional accounts and subnational trade flow information. Regionalisation is performed using regional accounts data provided by Eurostat, including indicators such as gross value added (GVA) and employment by region, which are used as proxies to allocate national-level economic activity to subnational units. These are combined with bilateral subnational trade flow data to derive regional trade shares. The trade data are sourced from the PBL Netherlands Environmental Assessment Agency, which provides European regional trade flows from 2000 to 2010 (Thissen et al., 2013), and from a recent high-resolution dataset of subnational trade networks in Europe (Huang & Koutroumpis, 2023).

The Subnational-ENGAGE model is calibrated for the EU27 and the United Kingdom at the NUTS2 regional level, allowing for high-resolution analysis of climate and policy impacts across subnational European regions. The model places particular emphasis on the agricultural sector, with explicit representation of major crop commodities including maize, wheat, rice, and soybean, along with an aggregated category for other crops. In addition to agriculture, the model incorporates manufacturing sectors, extraction-related sectors—specifically mining and quarrying, electricity generation, gas supply, water supply, and waste management—as well as construction, private services, and public services. This sectoral breadth enables the model to capture cross-sectoral linkages and regional economic structures with a high degree of detail.

The same sectoral classification applies to production activities, allowing for consistency between the use of commodities and the output of economic sectors. This structure supports the analysis of supply chains (i.e., intermediate inputs), factor inputs, and value-added generation at the regional level.

The model includes a comprehensive treatment of fiscal instruments, represented through multiple tax accounts. These include sales taxes (levied on both domestic production and imports), factor use taxes (on labour, capital and land inputs), production taxes, and factor income taxes. This tax architecture allows for realistic modelling of public revenue mechanisms and their influence on production costs, consumption, and income distribution.

A central feature of the Subnational-ENGAGE model is its detailed representation of bilateral trade flows at the NUTS2 level for the EU27 and the UK. This enables precise tracking of interregional trade and value-added flows, which is essential for analysing trade dependencies and regional economic exposure to climate impacts occurring elsewhere. For countries outside the EU, the model differentiates between major 16 extra-European trading partners and a residual Rest-of-World (RoW) aggregate, allowing for enhanced resolution of bilateral trade patterns and value-added transmission beyond Europe. This structure improves the model's ability to simulate global economic linkages and feedback relevant to European regional economies. Leveraging its high spatial resolution, the Subnational-ENGAGE model produces a range of policy-relevant economic indicators under diverse climate scenarios, including projected changes in regional GDP; sectoral production, consumption, trade, and prices; household welfare; and other key economic variables across NUTS2 regions. Additionally, it supports the spatial identification of climate-vulnerable regions based on trade integration and supply chain exposure, enabling detailed assessment of how climate risks propagate through interregional trade, production, and supply chains.

For this specific report, we use the standard ENGAGE model which is implemented using the GTAP-10 Power database (Peters, 2016), as the version of the model calibrated to the FIGARO-based input-output framework is still under development. The GTAP-10 Power database represents the global economy for the reference year 2011, and offers detailed coverage of energy production technologies, energy-intensive sectors, and broader economic activities, making it suitable for analysing the systemic effects of climate and energy-related shocks.

The standard version of ENGAGE includes detailed representation of 27 economic activities across 16 global regions, with four factors of production (land, labour, capital, and natural resources). Within the agricultural domain, the model differentiates between two individual crops—wheat and rice—and two aggregated crop categories: cereals and other crops. In addition, a broader agriculture and food sector captures value-added processes across the food supply chain. This structure enables targeted analysis of climate-induced impacts on agricultural production, consistent with the objectives of this report. The detailed aggregation of the model is shown in Figure 79.

16 Regions	
AFR	Africa
AUS	Australia
CAN	Canada
CSA	Central and South America
CHI	China
EEU	Eastern Europe
FSU	Former Soviet Union
IND	India
JAP	Japan
MEA	Middle-east
MEX	Mexico
ODA	Other Developing Asia
SKO	South Korea
UK	United Kingdom
USA	USA
WEU	Western Europe

4 Factors of production	
LND	Land
LAB	Labour
CAP	Capital
RES	Natural resources

27 Sectors	
PDR	Paddy rice
WHT	Wheat
GRO	Cereal grains
OCR	Other crops
A_F	Agriculture and food
MIN	Minerals
PPP	Paper
CRP	Chemical
NMM	Non-metalic minerals
I_S	Iron and steel
MPR	Metal products
IND	Other industry
COA	Coal
OIL	Crude oil
GAS	Gas
P_C	Petroleum & Coke
NUP	Nuclear power
CFP	Coal-fired power
GFP	Gas-fired power
WIP	Wind power
HYP	Hydroelectric power
OFP	Oil-fired power
OTP	Other power
SOP	Solar power
TnD	Transmission and distribution
SER	Services
TRN	Transport

Figure 79: *Regional, sectoral and factoral aggregation in the standard ENGAGE model.*

Step 1: Climate and Socioeconomic Scenarios

Climate-induced changes in crop yields are incorporated into the model using region-specific damage estimates that vary by global temperature increase. These estimates are derived from a methodological framework developed in a World Bank Policy Research Working Paper "Estimation of climate change damage functions for 140 regions in the GTAP9 database" (Roson & Sartori, 2016), which provides regionally differentiated crop yield response functions for 140 global regions, consistent with the GTAP-10 database structure. Regional temperature increases used to simulate crop productivity impacts in the ENGAGE model are derived from gridded warming projections under the SSP framework, capturing spatial variability in climate exposure across countries and regions (see Figure 80).

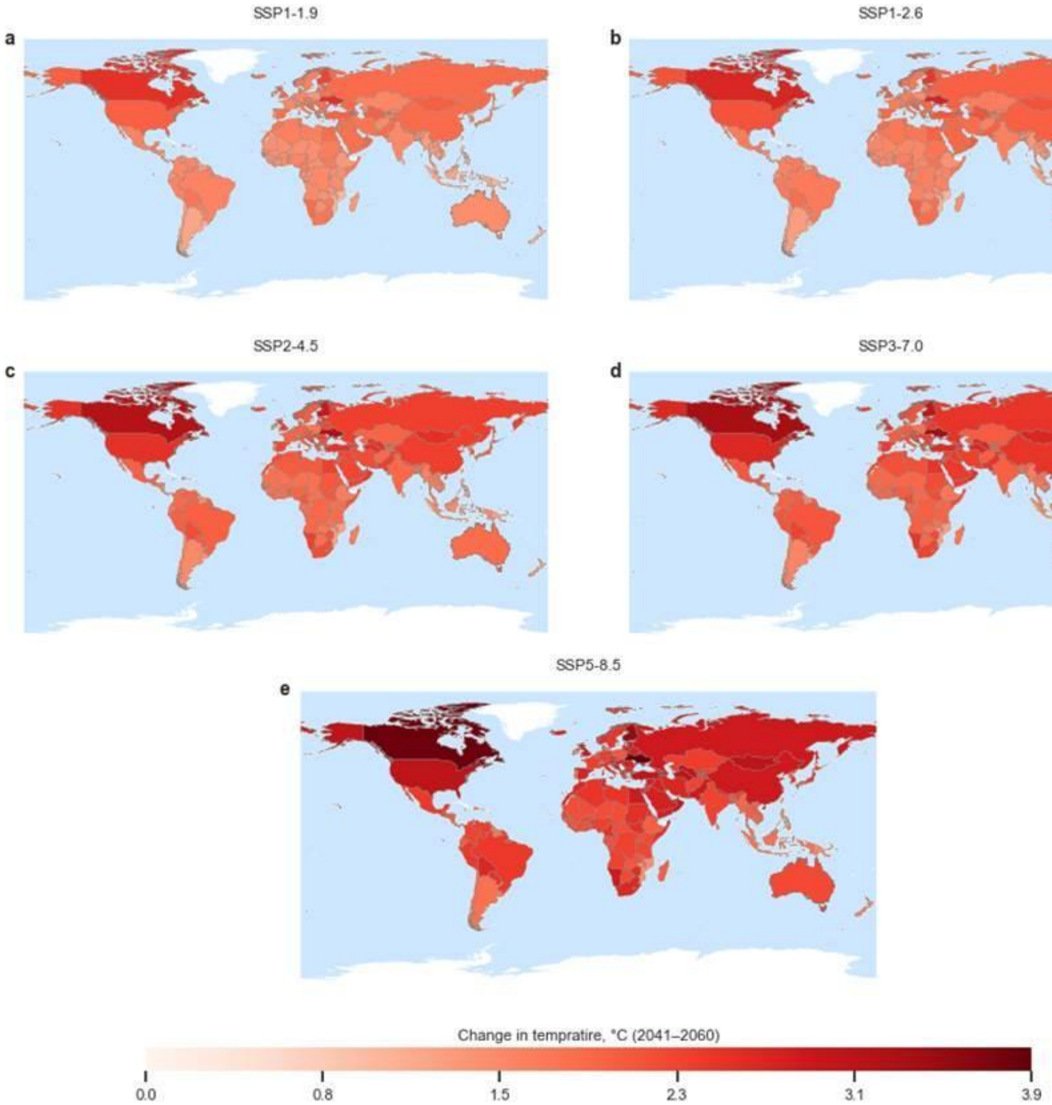

***Figure 80**: Projected regional warming by mid-century under five Shared Socioeconomic Pathways (SSPs).*

Notes: Panels (a)–(e) display projected changes in average surface temperature (Δ°C) between 2041–2060 relative to the average global surface temperature of the period 1850-1900, under scenarios SSP1-1.9 (a), SSP1-2.6 (b), SSP2-4.5 (c), SSP3-7.0 (d), and SSP5-8.5 (e). Colour intensity reflects the magnitude of regional warming, with pale yellow indicating lower warming levels and deep red indicating higher warming levels.

To assess the implications of warming on agricultural outputs, we use estimates of crop yield responses to temperature increases across the same set of scenarios (Figure 81). These estimates—used to parameterise yield shocks in the CGE model—reveal heterogeneous impacts across countries and crops, with wheat and cereal grains showing the highest sensitivity under mid- to high-end warming pathways (SSP2-4.5 and SSP5-8.5), which correspond to global surface temperature increases of approximately 2.0 °C and 2.4 °C, respectively. Both scenarios are compared against a 'Business-As-Usual' baseline, where crop yields are held constant to reflect current climate conditions.

Funded by
the European Union

All scenarios share the same SSP2-based socioeconomic assumptions—population-driven food demand, income- and diet-related shifts, and structural economic change as projected by the OECD—ensuring that only climate-induced yield shocks differ across scenarios. This design isolates the impact of warming on crop productivity and output, while holding demand and economic structure constant to facilitate clear attribution of production changes to climate effects alone.

Figure 81: *Projected changes in crop yields under five SSPs by 2050—yield changes reflect only climate-induced temperature shocks, with all socioeconomic inputs (population, income, dietary shares, labour and capital parameters) held constant at SSP2. Each panel illustrates yield change (fractional difference relative to baseline) across countries for rice, wheat, cereal grains, and other crops. Rows correspond to SSP2-4.5 and SSP5-8.5 scenarios, while columns list countries represented in the ENGAGE model. Africa (AFR), Australia (AUS), Canada (CAN), China (CHI), Central and South America (CSA), Eastern Europe (EEU), Former Soviet Union (FSU), India (IND), Japan (JPN), Middle-east (MEA), Mexico (MEX), Other Developing Asia (ODA), South Korea (SKO), United Kingdom (UK), USA (USA) and Western Europe (WEU). Estimated based on Roson and Sartori (2016).*

Step 2: Spatial Data Integration

For this report we use the standard version of the ENGAGE model represents the global economy through 16 aggregated world regions: Africa (AFR), Australia (AUS), Canada (CAN), China (CHI), Central and South America (CSA), Eastern Europe (EEU), Former Soviet Union (FSU), India (IND), Japan (JPN), Middle East (MEA), Mexico (MEX), Other Developing Asia (ODA), South Korea (SKO), United Kingdom (UK), United States (USA), and Western Europe (WEU). This spatial aggregation facilitates computational efficiency while maintaining sufficient regional resolution for global analysis.

We aggregate country crop yield data to regional crop yields by using crop harvested area as weighting factor.

Step 3: Impact Assessment

Climate change under both moderate (SSP2-4.5) and high-emission (SSP5-8.5) trajectories drives a broad reduction in rice and wheat production, while any potential gains in cereals and other crops production are largely confined to the coldest regions (Figure 82).

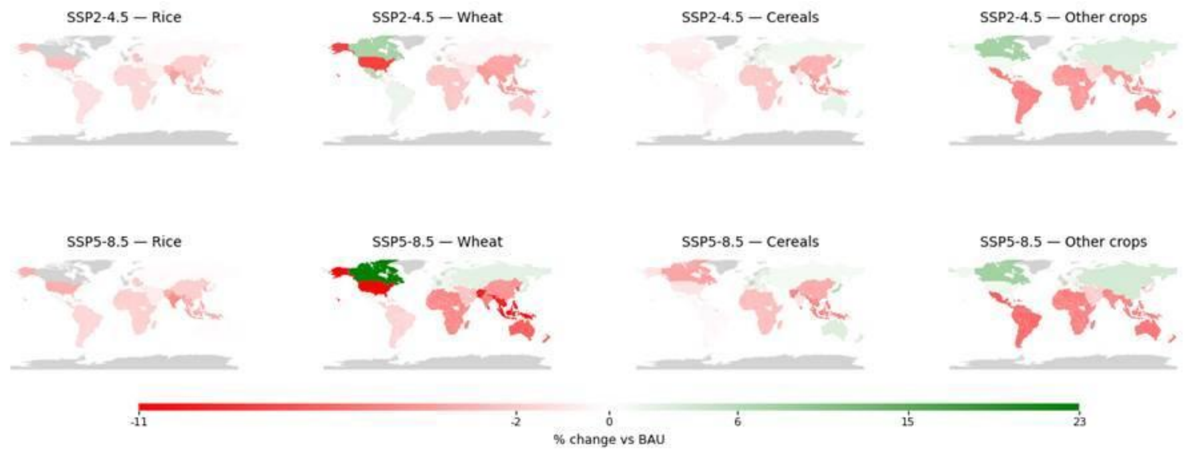

Figure 82: *Percentage change in crop production by 2050 relative to the business-as-usual baseline under two shared socioeconomic pathways (SSP2-4.5 and SSP5-8.5)*

Under SSP2-4.5, rice production declines everywhere, except in Mexico—Western Europe's losses are relatively mild compared with larger setbacks in India, South Korea, Other Developing Asia, North America and Eastern Europe—while wheat still manages gains in Canada, Mexico and Japan but contracts elsewhere in temperate zones (including Eastern Europe). Wheat production declines the most in the USA. While cereals and other non-cereal crops production is expected to decline in tropical and subtropical areas, they increase in cooler northern climates.

Under the stronger warming of SSP5-8.5, all these patterns intensify: rice production declines sharply worldwide, and Mexico's initial gains are reduced; wheat gains declines in Mexico and Japan, but intensifies in Canada, the Former Soviet Union, the UK and Western Europe; and cereal and other non-cereal crops gains intensify in northern latitudes, whereas losses in tropical regions become more pervasive.

Climate change is projected to reduce crop yields, exerting upward pressure on staple food prices worldwide. Under a warming trajectory of roughly 2.0 °C (SSP2-4.5), the aggregate crop price index rises by about 5.4%, climbing to 6.5% under 2.4 °C (SSP5-8.5). Price increases are unevenly distributed: regions with the most severe yield losses—Africa, Australia, India, the Middle East and Other Developing Asia—could see local price hikes exceeding 10% under the higher-warming scenario. In contrast, high-latitude producers such as Western Europe, Eastern Europe, the Former Soviet Union and the UK are likely to see comparatively smaller price increases (Figure 83).

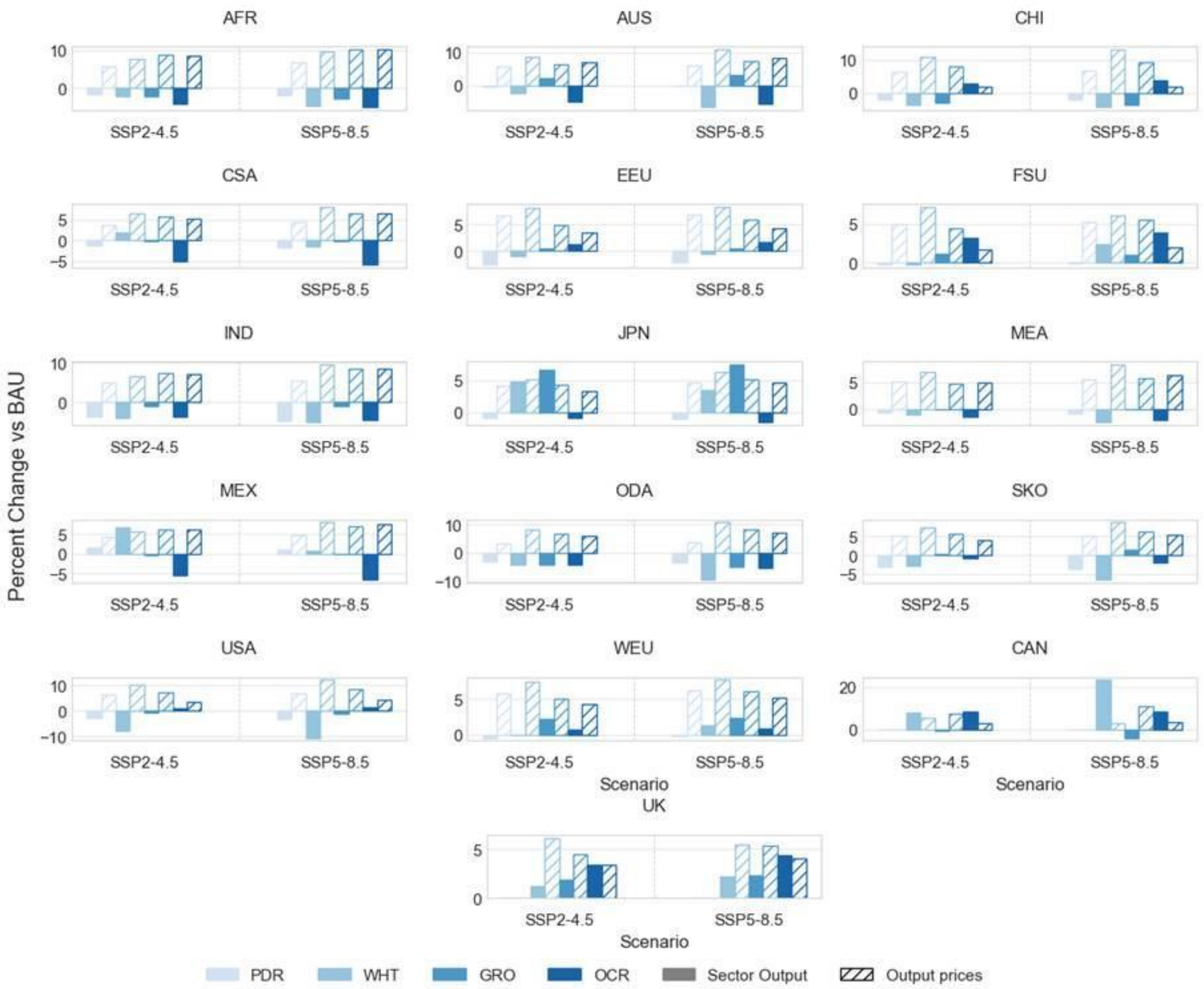

Figure 83: *Percent changes relative to a business-as-usual baseline in 2050 for four crop commodities (PDR – rice, WHT – wheat, GRO – cereals, OCR – other crops), showing output prices (hatched bars), and sectoral output (solid bars), under two mitigation scenarios (SSP2-4.5, SSP5-8.5). Scales on vertical axes are not uniform across subfigures. Africa (AFR), Australia (AUS), Canada (CAN), China (CHI), Central and South America (CSA), Eastern Europe (EEU), Former Soviet Union (FSU), India (IND), Japan (JPN), Middle east (MEA), Mexico (MEX), Other Developing Asia (ODA), South Korea (SKO), United Kingdom (UK), USA (USA) and Western Europe (WEU).*

Climate change is expected to reduce crop yields and trigger sharp price spikes that disproportionately affect tropical, lower-income regions, underscoring a widening global equity gap. While production losses and price increases reduce global income and welfare, their regional impacts creates both winners and losers.

Climate change under both SSP2-4.5 and SSP5-8.5 leaves global GDP largely unchanged (within ±0.02%) but masks substantial regional divergence. Under SSP2-4.5 (2.0 °C), GDP falls in most lower-latitude and developing regions—India by about 1.2%, Other Developing Asian countries by 1.0%, and China by 0.4%—while high-latitude and advanced economies record modest gains: Canada by around 1.8%, Western Europe 0.7%, Eastern Europe 0.6%, the USA 0.5%, and the UK 0.4%. Under SSP5-8.5 (2.4 °C), these trends intensify: losses grow to roughly 1.6% in India and 1.2% in Other Developing Asian countries, whereas Canada's GDP increase exceeds 2.2%, Western Europe rises to 0.8 %, Eastern Europe to 0.7%, the USA to 0.6%, and the UK to 0.5% (Figure 84).

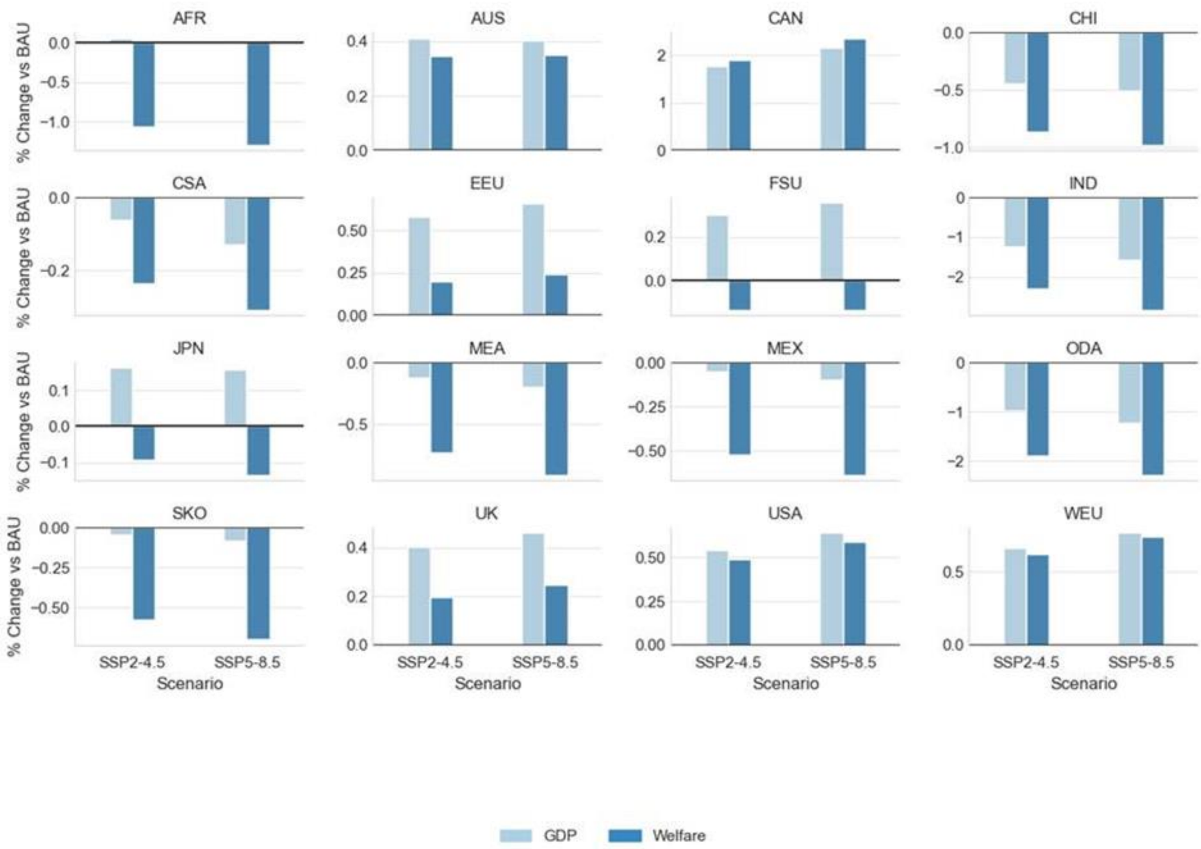

Figure 84: *Percentage changes in regional GDP (light bars) and welfare (dark bars) relative to a business-as-usual baseline in 2050 under the moderate-emissions SSP2-4.5 and high-emissions SSP5-8.5 scenarios. Scales on vertical axes are not uniform across subfigures. GDP is the Gross Domestic Product, defined as the sum of consumption, government expenditure, investment, exports and (minus) imports; welfare is defined as the change in regional household income at constant prices that is equivalent to the proposed change. Africa (AFR), Australia (AUS), Canada (CAN), China (CHI), Central and South America (CSA), Eastern Europe (EEU), Former Soviet Union (FSU), India (IND), Japan (JPN), Middle east (MEA), Mexico (MEX), Other Developing Asia (ODA), South Korea (SKO), United Kingdom (UK), USA (USA) and Western Europe (WEU).*

The impact on regional welfare is more pronounced, with larger reductions than GDP in high-latitude countries and smaller gains in tropical regions. The only exception is Canada, where welfare gains are larger than GDP gains. Northern regions—such as Canada, Western Europe, the USA, Eastern Europe and the UK—benefit from higher production and exports as warming reduces cold-season constraints. Moreover, their relative increase in exports exceeds that of production, indicating improved markets access and higher comparative advantage, which translates into positive welfare gains. The opposite trend is observed in tropical and subtropical regions such as India, Other Developing Asian countries, Africa and the Middle-east—where their decline in exports exceeds the decline in production, leading to welfare losses as these regions lose their market share in global food production (Figure 85).

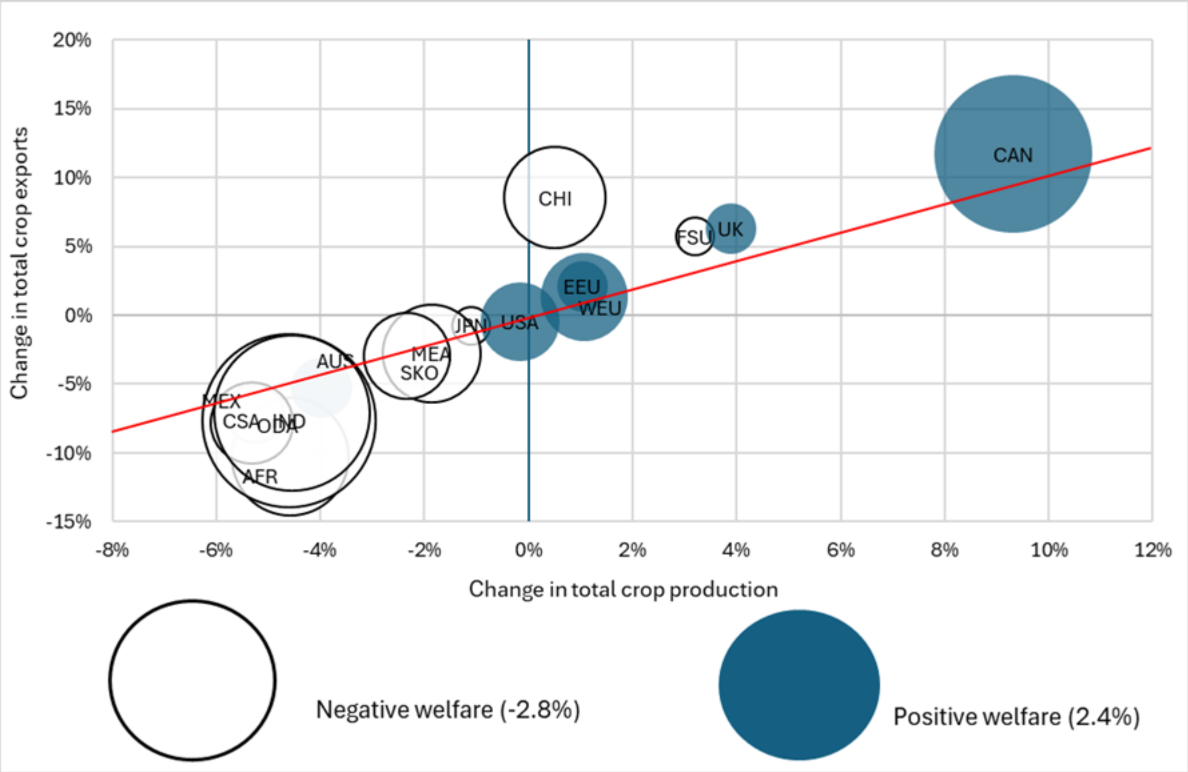

Figure 85: *Percentage changes in regional total crop production (x-axis), exports (y-axis) and welfare (circles) relative to a business-as-usual baseline in 2050 under the high-emissions SSP5-8.5 scenario. Africa (AFR), Australia (AUS), Canada (CAN), China (CHI), Central and South America (CSA), Eastern Europe (EEU), Former Soviet Union (FSU), India (IND), Japan (JPN), Middle east (MEA), Mexico (MEX), Other Developing Asia (ODA), South Korea (SKO), United Kingdom (UK), USA (USA) and Western Europe (WEU).*

The above results indicate that regions are not only affected by changes in local crop production conditions. They are also affected by climate-induced changes in competitiveness. Northern regions benefit from longer growing seasons, CO_2 fertilization, and reduced frost risk. The pattern underscores a growing geographical divide: Europe's modest but reliable gains contrast sharply with welfare losses elsewhere, underlining the need for targeted adaptation in vulnerable regions and the equity value of more ambitious global mitigation.

Step 4: Risk Assessment

Figure 86 illustrates how physical climate change risks (exogenous yield changes introduced to the economic model) are translated to economic risks (the resulting changes in production, export, and regional welfare produced by the model). Yield changes represent direct biophysical impacts to crop yields and agricultural productivity due to different levels of temperature increase, based on damage functions estimated by Roson and Sartori (2016). Production changes reflect both direct and indirect effects, as farmers reallocate resources among crops in response to yield shocks that vary across crop categories. These adjustments, influenced by relative changes in prices, productivity and intersectoral competitiveness, lead to region-specific gains or losses in agricultural output. Export responses reflect in addition changes in interregional competitiveness and trade patterns, as regions gain or lose the ability to produce certain crops more efficiently than others. These shifts in comparative advantage—a region's relative efficiency in producing a good—are influenced by how severely climate impacts local and international productivity and prices. Welfare impacts represent aggregate household utility effects, represented by changes in regional income.

	Physical risk				Economic risk								
	Yield changes				Production changes				Export changes				Welfare
Regions	Rice	Wheat	Cereals	Other crops	Rice	Wheat	Cereals	Other crops	Rice	Wheat	Cereals	Other crops	changes
AFR	-2.6%	-8.0%	-7.1%	-7.1%	-1.9%	-4.9%	-2.7%	-5.1%	-2.9%	-4.5%	-5.7%	-10.5%	-1.3%
AUS	-2.7%	-6.9%	-4.9%	-4.6%	-0.1%	-6.5%	3.0%	-5.4%	-1.9%	-7.8%	3.5%	-8.6%	0.3%
CAN		5.5%	-3.5%	5.5%		23.2%	-3.8%	8.4%		28.2%	-7.5%	9.5%	2.4%
CHI	-2.3%	-8.1%	-4.5%	1.6%	-2.0%	-4.3%	-3.4%	3.7%	-4.9%	-9.8%	-5.3%	9.2%	-1.0%
CSA	-2.7%	-6.9%	-5.6%	-5.2%	-1.6%	-1.5%	-0.2%	-5.9%	-0.3%	-1.2%	1.0%	-7.7%	-0.3%
EEU	-2.0%	-5.6%	-2.3%	0.1%	-2.2%	-0.6%	0.4%	1.6%	-3.3%	-0.7%	1.5%	3.0%	0.2%
FSU	-2.1%	-2.9%	-2.4%	2.5%	-0.1%	2.5%	1.0%	3.9%	0.4%	4.8%	3.2%	7.6%	-0.1%
IND	-2.7%	-7.6%	-5.7%	-5.4%	-4.8%	-5.2%	-1.1%	-4.6%	-4.3%	-5.7%	-2.5%	-8.3%	-2.8%
JPN	-2.6%	-7.3%	-4.4%	-3.2%	-1.0%	3.5%	7.4%	-1.6%	1.1%	6.0%	11.2%	-0.8%	-0.1%
MEA	-2.4%	-8.0%	-4.6%	-5.1%	-0.8%	-2.5%	0.0%	-2.0%	-1.1%	-1.4%	2.5%	-2.9%	-0.9%
MEX	-2.7%	-8.2%	-5.6%	-6.3%	1.1%	0.8%	-0.1%	-6.7%	3.5%	1.0%	0.0%	-8.2%	-0.6%
ODA	-2.3%	-8.9%	-6.1%	-5.5%	-3.3%	-9.5%	-4.9%	-5.1%	-0.9%	-10.8%	-5.2%	-7.1%	-2.3%
SKO	-2.5%	-7.2%	-4.1%	-3.1%	-3.6%	-6.6%	1.3%	-2.0%	-4.4%	-6.6%	3.5%	-2.9%	-0.7%
UK		-2.3%	-1.6%	0.7%		2.2%	2.3%	4.4%		5.9%	4.3%	6.5%	0.2%
USA	-2.4%	-8.1%	-4.6%	0.8%	-3.2%	-10.5%	-1.1%	1.4%	-4.5%	-12.3%	-1.6%	1.5%	0.6%
WEU	-2.4%	-5.7%	-2.6%	-0.8%	-0.2%	1.3%	2.4%	0.9%	-0.6%	1.7%	3.6%	1.0%	0.7%

Figure 86: *Percentage changes in regional welfare, and crop yield, production and exports relative to a business-as-usual baseline in 2050 under the high-emissions SSP5-8.5 scenario. Africa (AFR), Australia (AUS), Canada (CAN), China (CHI), Central and South America (CSA), Eastern Europe (EEU), Former Soviet Union (FSU), India (IND), Japan (JPN), Middle east (MEA), Mexico (MEX), Other Developing Asia (ODA), South Korea (SKO), United Kingdom (UK), USA (USA) and Western Europe (WEU).*

The results show that climate risks are unevenly distributed across the world, with some regions facing much greater impacts than others. High-risk regions—including Africa, India, and Other Developing Asia—experience substantial yield losses across all crop types. These physical impacts translate into pronounced production and export declines, with household welfare losses surpassing 2% in India and Other Developing Asia. Moderate-risk regions such as China, the Middle East, and South Korea exhibit mixed production responses, but experience persistent welfare declines of around 1%, due to trade dependencies and limited adaptive capacity. In contrast, low-risk or net-beneficiary regions—such as Canada, Western Europe, the USA, and the UK —may experience moderate yield improvements, particularly for temperate crops, leading to gains in exports and positive welfare outcomes.

Western Europe is projected to benefit from moderate increases in production, which, combined with strong trade infrastructure and adaptive capacity, translate into increased agricultural exports and improved regional welfare. These gains are primarily driven by favourable shifts in comparative advantage in food production within global markets. Eastern

Europe, while not experiencing the same level of benefit as Western Europe or the UK, shows larger production and exports of cereals and 'other crops'. The region's economic performance depends on the relative impact of climate change on crop yields and its ability to maintain competitiveness in key crop sectors.

The mismatch between physical impacts (yield losses) and economic outcomes (production, exports or income changes) in some regions highlights how interconnected and complex global agricultural markets are—and how climate risks spread through these systems. For instance, Africa exhibits larger declines in exports than in production across most crops, resulting in welfare losses due to reduced trade competitiveness. Conversely, the UK shows positive export and welfare outcomes, despite moderate yield or production shifts, reflecting enhanced competitiveness and trade positioning.

2.8.3. Challenges and conclusions

The analysis shows that climate change poses significant challenges to global agriculture, particularly under high-emission scenarios. Widespread declines in crop production is expected, with the most severe impacts concentrated in tropical and subtropical regions such as India, Africa, and Other Developing Asia. These regions not only face yield and production losses but also reduced export competitiveness, resulting in welfare losses. In contrast, high-latitude regions like Canada, Western Europe, and the UK benefit from longer growing seasons and reduced frost risk, leading to increased production, exports, and welfare gains.

This uneven distribution of gains and losses is expected to increase the global equity gap. While global GDP remains relatively stable, regional disparities in income and welfare intensify. The findings highlight the need for targeted adaptation strategies in vulnerable regions and reinforce the importance of ambitious global mitigation efforts to address the unequal distribution of climate risks.

2.8.4. References

Calzadilla, A., & Carr, T. (2020). Land degradation and food security: water erosion impacts and adaptation options. https://www.gtap.agecon.purdue.edu/resources/res_display.asp?RecordID=6088

ESA. (2013). European System of Accounts 2010. In Luxembourg.

Huang, S., & Koutroumpis, P. (2023). European multi regional input output data for 2008–2018. Scientific Data, 10(1), 1–9. https://doi.org/10.1038/S41597-023-02117-Y;SUBJMETA=253,66,703,706;KWRD=BUSINESS,INDUSTRY

Lobell, D. B., & Gourdji, S. M. (2012). The Influence of Climate Change on Global Crop Productivity. Plant Physiology, 160(4), 1686–1697. https://doi.org/10.1104/PP.112.208298

Mainar Causapé, A., Philippidis, G., & Caivano, A. (2018). BioSAMs for the EU Member States: Constructing Social Accounting Matrices with a detailed disaggregation of the bio-economy. https://doi.org/10.2760/811691

Nechifor, V., Calzadilla, A., Bleischwitz, R., Winning, M., Tian, X., & Usubiaga, A. (2020). Steel in a circular economy: Global implications of a green shift in China. World Development, 127, 104775. https://doi.org/10.1016/J.WORLDDEV.2019.104775

Peters, J. C. (2016). The GTAP-Power Data Base: Disaggregating the Electricity Sector in the GTAP Data Base. Journal of Global Economic Analysis, 1(1), 209–250. https://doi.org/10.21642/JGEA.010104AF

Roson, R., & Sartori, M. (2016). Estimation of Climate Change Damage Functions for 140 Regions in the GTAP 9 Data Base. Journal of Global Economic Analysis, 1(2), 78–115. https://doi.org/10.21642/JGEA.010202AF

Thissen, M., Oort, F. van, & Diodato, D. (2013). Integration and Convergence in Regional Europe: European Regional Trade Flows from 2000 to 2010. https://www.econstor.eu/handle/10419/124122

Winning, M., Calzadilla, A., Bleischwitz, R., & Nechifor, V. (2017). Towards a circular economy: insights based on the development of the global ENGAGE-materials model and evidence for the iron and steel industry. International Economics and Economic Policy, 14(3), 383–407. https://doi.org/10.1007/S10368-017-0385-3/FIGURES/6

3. Overarching CSA Conclusions

3.1. European Challenges in risk management

CROSSEU CSAs undertake a detailed climate hazard risk assessment at NUTS 3 levels for Europe. They provide information about how both physical and socioeconomic risks could develop from the present to 2100. Thereby, they allow new insights about climate risk for Europe beyond the assessment reported by the IPCC Seventh Assessment Report AR7 Working Group II Climate risks and Adaptation (IPCC, 2022). The IPCC risk assessment for Europe is illustrated in Figure 87. Key overarching results of the CSAs are provided in the following sections and discussed in relation to the IPCC conclusions.

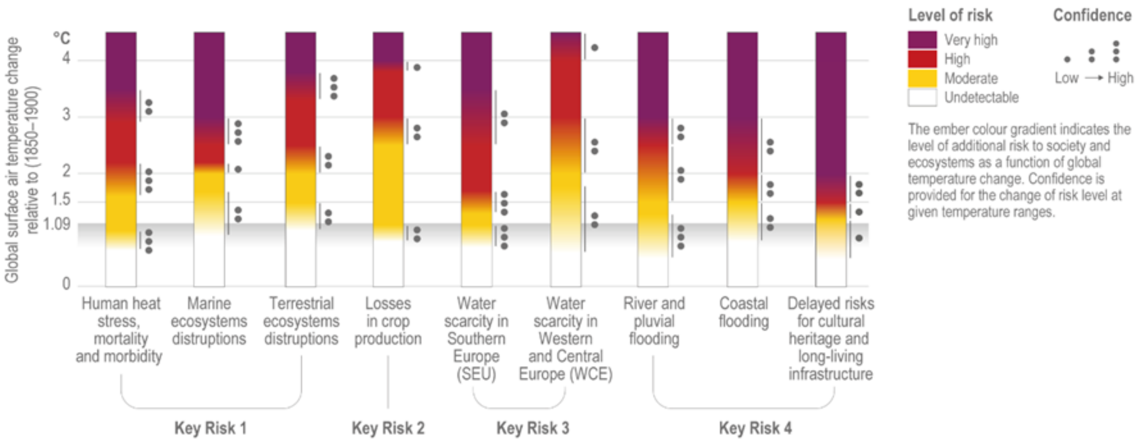

***Figure 87:** Key risks for Europe under low to medium adaptation, (IPCC, 2022).*

In Figure 87, the risk level associated with global temperature changes is illustrated by colours from undetectable (white) to very high (purple). Some regions and areas are exposed to relatively high risk levels already at a low level of global temperature change. These include human heat stress, mortality and morbidity, water scarcity, river and pluvial flooding, and coastal flooding. These areas are all included as foci of CSAs in CROSSEU. Other areas with high risks following Figure 87 that are not included in CROSSEU are cultural heritage and long-living infrastructure. The IPCC report includes detailed assessment of the climate risk literature for these areas.

CSA 1 Heat

The CROSSEU CSA 1 Heat has been conducting a detailed assessment of extreme heat events in the Czeck Republic. It provides an example of the escalating intensity, frequency, and duration of warm extremes (i.e., heatwaves) in Europe, which have been identified as being among the most certain impacts of climate change and a severe threat to human health (Cissé et al. 2022). The heightened risk of heat-related mortality and morbidity is particularly pronounced in Europe relative to other global regions. Europe is the fastest warming continent (C3S 2025; Van Daalen et al. 2024), and recent studies indicate concerning trends in both rising temperatures and impacts on human health (Lhotka & Kyselý 2022; Ballester et al., 2023). Attributional studies underscore the exacerbating role of climate change, with the likelihood of current European heatwave occurrences being approximately 30% higher compared to the counterfactual (without anthropogenic climate change) scenario (Ma et al., 2020; Vicedo-Cabrera et al., 2021). The direct implications of these heatwaves on human health are evidenced by empirical studies, such as the notable case of Prague, Czech Republic, where the risk of heat-related mortality doubled during the period from 2010 to 2019 compared to the previous three decades from 1982 to 2009 (Urban et al., 2022). These findings underscore the urgency of assessing the adaptive capacity of health sectors in individual regions.

The results of CSA 1 Heat suggests that the observed trend will continue if no adaptation takes place. Specifically, in Prague, a more than fourfold increase in annual heat-attributable deaths (230) is projected by the end of the century (2090s, RCP 8.5), compared to 55 annual heat-related deaths in the reference period (2000s). Nationwide, heat impact is projected to increase from the current 290 to as many as 1500 annual heat-related deaths by the 2090s (RCP 8.5) in the Czech Republic. In addition to climate change, about 15% of this increase is attributable to population aging (according to the EUROPOP2019 regional population projections).

Our findings suggest that estimates of the future mortality burden associated with extreme temperature events are highly sensitive to demographic changes within regions. As both intra- and inter-national migration will likely alter future population distributions and exposure patterns, a follow-up analysis will integrate alternative population scenarios based on migration storylines informed by the Shared Socioeconomic Pathways (SSPs) and will thus allow for more nuanced projections.

CSA 2 Drought

The CROSSEU assessment of drought risk across hotspots in Germany, Poland, Czech Republic and Romania, based on the EURO-CORDEX CMIP5 climate projections under RCP4.5 and RCP8.5 scenarios, reveals a significant increase in drought hazard intensity, especially towards the late 21st century. The analysis highlights spatial heterogeneity in projected changes; while certain areas in Austria and Poland may experience slight increases in precipitation and thus a minor wetting trend, southern and western Europe—including Greece, Italy, and regions in Romania—are expected to face more frequent, longer-lasting, and intense drought events. Socio-economic vulnerability factors differ notably among these hotspots. For example, agricultural labour force participation is higher in Romania and Poland, suggesting a greater dependence on agriculture and hence increased sensitivity to drought impacts on livelihoods; however, this will tend to decrease over time with efficiency improvements in agriculture following the trend in other countries around the world Conversely, Germany exhibits higher population densities and better-developed irrigation infrastructure, which could enhance its capacity to adapt and reduce vulnerability. Combining climatic hazard projections with socio-economic indicators in a risk matrix shows that drought risk is unevenly distributed, with some hotspots—particularly in southeastern Europe—facing extreme risks due to the convergence of high hazard levels and socio-economic sensitivity. These findings underscore the critical need for regionally tailored adaptation and mitigation strategies integrating both climatic projections and local socio-economic realities to effectively reduce drought risk and enhance resilience.

A trade-off analysis for Austria on combined adaptation of land use and management practices demonstrates that climate hazard risk reduction and the environmental performance jointly can be achieved for fairly small reductions in agricultural net benefits and at relatively low costs. These findings underscore the critical need for regionally tailored adaptation and mitigation strategies integrating both climatic projections and local socio-economic realities to effectively reduce drought risk and enhance resilience.

CSA 3 Storm

As illustrated by IPCC (Figure 85), risks from Coastal flooding are already causing frequent hazards at the global warming levels pertinent today. Among the highest risk areas are the Northern coast of Germany, the Netherlands, Belgium and the North-western part of France. CROSSEU has conducted a detailed assessment of economic damages of coastal flooding for the two Danish cities Aabenraa and Haderslev located in the Southeast of Jutland. The cities have been exposed to flooding events several times and most recenty in October 2023, when large areas of the Aabenraa harbour with industrial buildings and services and areas with holiday homes in Haderslev were flooded.

In particular, Aabenraa could expect a very steep increase in flood risks after 2050 if a high climate scenario is materializing. Then, the city area and large population groups could be affected. It is estimated that today a 100-year flooding event could impact around 150 people, but this could increase to between 2,000 and 2,300 by the end of the century, dependent on the climate scenario. Large damage costs are associated with flooding risks, but on the top of this, there is also a negative incidence on equity, since households with a relatively low income living in the city centre of Aabenraa could be at risk.

In Haderslev, flood damage costs are developing very gradually from today and into the future, and holiday homes are a high share of the assets at risk. 300 people are today expected to be at risk from flooding from a 100-year event, and climate change will gradually increase this number over time. However, the increase will be more moderate than in the case of Aabenraa. Low-income households could suffer from flooding risks in Haderslev like for Aabenraa, but the equity impacts of flooding in Haderslev are smaller than in the case of Aabenraa. This is particularly the case, because permanent houses in the major city area of Aabenraa are risk prone, while flooding risks in Haderslev is higher for holiday houses.

CSA 4 Flood

The risks of floods have been assessed for a Hotspot in the valley areas of the Trentino-Alto Adige region in Northeastern Italy. This Alpine territory is increasingly exposed to short-duration extreme precipitation events, a trend driven by climate change (see e.g. Libertino et al., 2019; Dallan et al., 2022). The combination of complex orography and geomorphological fragility makes the region particularly susceptible to hydrogeological hazards, especially flash floods and debris flows, whose frequency and intensity are expected to rise under future climate scenarios. Among others, the high concentration of alluvial fans across the territory significantly contributes to hydrogeological vulnerability. These geomorphological formations are highly susceptible to flash flood events, as they tend to accumulate debris flows and channel sudden water surges during episodes of intense rainfall.

High-resolution climate and hydrological modelling have been combined with stated preference methods to inform socially responsive adaptation strategies in flood-vulnerable regions. The willingness to pay for avoiding flooding events in the area has been estimated based on a survey targeted households and vulnerable sectors. The results underscore the relevance of flood projections in capturing vulnerability gradients and guiding spatially targeted interventions. The analysis reveals substantial public support for M&A investments, especially when aimed at protecting residential areas and critical productive areas and infrastructure. The heterogeneity in WTP estimates across income and gender groups highlight the importance of incorporating equity and distributional concerns into policy design.

CSA 5 Snow

A detailed assessment of past avalanche events and climate scenarios for future events highlights how climate change is altering snow avalanche hazard patterns across the European Alps and Carpathian Mountains, with implications for communities, tourism, transport, and forest ecosystems. Using a composite climate hazard index, socio-economic indicators, and risk assessment frameworks, the analyses reveal persistent and emerging hotspots of risk, particularly under high-emissions scenarios (RCP8.5). The Alps show widespread moderate to high risk due to overlapping high exposure, sensitivity, and persistent hazard signals. In contrast, the

Carpathians display lower risk profiles, largely driven by limited exposure and declining population trends, though vulnerability remains high in selected regions due to underdeveloped early warning systems.

Key takeaways of the CSA include: (i) first inclusion of the Carpathian region in a pan-European snow hazard context; (ii) use of a composite hazard index (CHI) combining 7 climate indicators with terrain features; (iii) integration of EUROSTAT population projections (2030, 2050, 2100) with climate hazard data; (iv) application of STLs and CCHs to contextualise the potential risks; (v) sectoral focus enables targeted adaptation strategies beyond macroeconomic modelling. In contrast to the broader, more generalised assessments in COACCH and PESETA, CSA 5 offers granular, location-specific insights essential for climate-resilient planning in Europe's mountain regions. Historical snow avalanche events, documented through STLs, underscore the need for proactive adaptation, particularly in tourism-intensive zones. Adaptation strategies should prioritise strengthening early warning systems, updating hazard zoning, and enhancing cross-sectoral risk communication and planning, especially in newly exposed high-altitude zones.

CSA 6 Indirect (Cross-sectoral multi-hazard risk)

Today and in the future, the lower Danube area faces several climate risks including both floods and drought periods. Combining the climate and hydrological projections with vulnerabilities points to a forecast of risk patterns 2030, 2050, and 2100 in the Lower Danube region. By 2030 it is expected that floods will occur frequently, and this will be accelerated over time, particularly in the case of high climate scenarios as RCP8.5. The flood events could change to be a higher frequency in the wintertime, while droughts could occur increasingly in the summertime.

Potential new hotspots or challenges could emerge by 2100. If climate change forces change in land use (e.g., some areas might be abandoned due to repeated flooding or drying), migration and demographic shifts could occur. People might move from vulnerable rural floodplain zones to the city or elsewhere, which could alleviate some exposure – or conversely, economic necessity might keep vulnerable populations in place even as risks rise. Additionally, transboundary issues become sharper; the Lower Danube is shared by Romania, Bulgaria, Ukraine (in the Delta). Coordinated management of floods (through, say, upstream reservoirs or emergency releases) and drought (water sharing agreements) will be vital. By 2050 or 2100, without cooperation, one country's adaptation (like building a dike or canal) could worsen another's risk.

In summary, by 2050 a peak in flood risk and by 2100 a peak in drought impact under high emissions could occur. The geographic risk hotspots (Danube-adjacent communities, critical infrastructure like the Cernavodă NPP, key navigation choke points, large-scale irrigation zones) are identifiable now and will likely remain so. By late-century, the stakes are higher – extreme events will be more frequent, and coping capacity could be eroded without investments in adaptation.

The Lower Danube River system in the Brăila region stands at the frontline of climate change impacts in Southeast Europe. The analyses show that what is at stake is not just an environmental shift, but a socio-economic challenge that will define the future of communities along the Danube. The storyline events – catastrophic floods like that of 2006 and unprecedented droughts like 2022 – are signals of a new normal where extremes are more frequent. Historic discharge data and future projections (RCP4.5 and RCP8.5 scenarios) jointly indicate a trend toward greater hydrological volatility: more frequent & intense floods on one hand, and longer & harsher droughts on the other. For Brăila County, the analysis identified that the highest risks concentrate in the Danube floodplain corridor, where both flood hazard and social vulnerability peak. Poor, rural communities behind aging dikes face the burden of floods, and the same communities suffer most in droughts due to their reliance on rain-fed agriculture. Without intervention, climate change could widen this vulnerability gap, hitting hardest those least able to cope.

CSA 7 Indirect (Power system)

No conclusions

CSA 8 Spillover (Global agriculture)

Climate change is expected to reduce crop yields and trigger sharp price spikes that disproportionately affect tropical, lower-income regions, underscoring a widening global equity gap. While production losses and price increases reduce global income and welfare, their regional impacts creates both winners and losers.

Climate change under both SSP2-4.5 and SSP5-8.5 leaves global GDP largely unchanged (within ±0.02%) but masks substantial regional divergence. Under SSP2-4.5 (2.0 °C), GDP falls in most lower-latitude and developing regions—India by about 1.2%, Other Developing Asian countries by 1.0%, and China by 0.4%—while high-latitude and advanced economies record modest gains: Canada by around 1.8%, Western Europe 0.7%, Eastern Europe 0.6%, the USA 0.5%, and the UK 0.4%. Under SSP5-8.5 (2.4 °C), these trends intensify: losses grow to roughly 1.6% in India and 1.2% in Other Developing Asian countries, whereas Canada’s GDP increase exceeds 2.2%, Western Europe rises to 0.8 %, Eastern Europe to 0.7%, the USA to 0.6%, and the UK to 0.5% (Figure 15).

Funded by
the European Union

4. Bibliography

Adinolfi, M., Raffa, M., Reder, A., & Mercogliano, P. (2020). Evaluation and expected changes of summer precipitation at convection-permitting scale with COSMO-CLM over Alpine space. Atmosphere, 12(1), 54.

Adler, M. D. (2016). Benefit-cost analysis and distributional weights: An overview. Review of Environmental Economics & Policy, 10, 264-285. https://doi.org/10.1093/reep/rew005.

Amihaesei, V., Micu, D., Cheval, S., Dumitrescu, A., Sfica, L., & Birsan, V-V. (2024). Changes in snow-cover climatology and its elevation dependency over Romania (1961–2020). Journal of Hydrology: Regional Studies, 51, 101637. https://doi.org/10.1016/j.ejrh.2023.101637.

Atkinson, A. B. (1970). On the measurement of inequality. Journal of Economic Theory, 2, 244-263. https://doi.org/10.1016/0022-0531(70)90039-6.

Bąkowski, R., Achimowicz, J., & Mazur, A. (2014). Current status of early-warning systems for severe environmental threats in the Polish National Meteorological Service. Meteorology, Hydrology and Water Management, 2, 35-42. https://doi.org/10.26491/mhwm/36432

Baldauf, M., Seifert, A., Förstner, J., Majewski, D., Raschendorfer, M., & Reinhardt, T. (2011). Operational convective-scale NWP with the COSMO model: Description and sensitivities. Monthly Weather Review, 139, 3887-3905.

Barichivich, J., Osborn, T. J., Harris, I., van der Schrier, G., & Jones, P. D. (2024). Monitoring global drought using the self-calibrating PDSI in State of the Climate 2023. Bulletin of the American Meteorological Society (in press).

Belušić D., de Vries H., Dobler A., Landgren O., Lind P., Lindstedt D., Pedersen R.A., Sánchez-Perrino J.C., Toivonen E., van Ulft B., Wang F., Andrae U., Batrak Y., Kjellström E., Lenderink G., Nikulin G., Pietikäinen J.-P., Rodríguez-Camino E., Samuelsson P., van Meijgaard E. & Wu M. (2020). HCLIM38: A flexible regional climate model applicable for different climate zones from coarse to convection-permitting scales. Geoscientific Model Development, 13(3), 1311–1333. https://doi.org/10.5194/gmd-13-1311-2020

Bélanger, L., & Cassayre, Y. (2004). Projects for past avalanche observation and zoning in France after the 1999 catastrophic avalanches. Environmental Science, Geography.

Berthou, S., Kendon, E. J., Chan, S. C., Ban, N., Leutwyler, D., Schär, C., & Fosser, G. (2020). Pan-European climate at convection-permitting scale: a model intercomparison study. Climate Dynamics, 55, 35-59.

Beulertz, D., Charousset, S., Most, D., Giannelos, S., & Yueksel-Erguen, I. (2019). Development of a modular framework for future energy system analysis. Proceedings of the 54th International Universities Power Engineering Conference (UPEC), 1-6. https://doi.org/10.1109/UPEC.2019.8893472

Böhm, O., Jacobeit, J., Glaser, R., & Wetzel, K. F. (2014). Flood history of the Bavarian Alpine Foreland since the late Middle Ages. Hydrology & Earth System Sciences Discussions, 11, –.

Boisson, E., Wilhelm, B., Garnier, E., Mélo, A., Anquetin, S., & Ruin, I. (2021). Geo-historical analysis of flood impacts in Alpine catchments (HIFAVa database, Arve River, France, 1850–2015). Natural Hazards and Earth System Sciences Discussions, 2021, 1-24.

Boere, E., Valin, H., Bodirsky, B. Baier, F., Balkovic, J., Batka, M., Folberth, C., Karstens, K., Kindermann, G., Krasovskii, A., Leclere, D., Wang, X., Weindl, I., Havlik, P., LotzeCampen, H. (2019). D2.2 Impacts on agriculture including forestry & fishery. Deliverable of the H2020 COACCH project.; available online from https://www.coacch.eu/wp-content/uploads/2020/05/D2.2_after-revision-to-upload.pdf

Bojariu R, Chitu Z., Dascălu SI, Gothard M, Velea L, Burcea R, Dumitrescu A, Burcea S, Apostol L., Amihaesei V., Marin L, Crăciunescu VS, Irimescu A, Mătreata M, Niţă A., Bîrsan MV (2021). Schimbările climatice – de la bazele fizice la riscuri și adaptare (Climate change – from physical bases to risks and adaptation, in Romanian with Summary in English), editie revăzută si adăugită. Editura Printech, București, 222 p, ISBN: 978-606-23-1275-6, https://doi.org/10.5281/zenodo.10517336

Bojariu R, Dascălu SI, Gothard M, Dumitrescu A, Crăciunescu V, Mătreață M, Chendeș V, Burcea S, Cică R, Birsan M, Boincean B, Velea L, Niță A, Irimescu A, Potopová V, Cazac V, Niță A. (2018). Variability and change in water cycle at the catchment level. In: Engineering and mathematical topics in rainfall, vol 7, pp 115–129. https://doi.org/10.5772/67933

Botzen, W. J. W., Aerts, J. C. J. H., & van den Bergh, J. C. J. M. (2013). Individual preferences for reducing flood risk to near zero via elevation. Mitigation and Adaptation Strategies for Global Change, 18, 229-244.

Bründl M, Etter J-H, Steiniger M, Klingler Ch, Rhyner J, Ammann WJ (2004). IFKIS– a basis for managing avalanche risk in settlements and on roads in Switzerland. Natural Hazards and Earth System Sciences (2004) 4: 257–262.

Busschaert, L., de Roos, S., Thiery, W., Raes, D., & De Lannoy, G. J. M. (2022). Net irrigation requirement under climate scenarios using AquaCrop over Europe. Hydrology and Earth System Sciences, 26, 3731-3752.

Caillaud C., Somot S., Alias A., Bernard-Bouissières I., Fumière Q., Laurantin O., Seity Y. & Ducrocq V. (2021). Modelling Mediterranean heavy precipitation events at climate scale: An object-oriented evaluation of the CNRM-AROME convection-permitting regional climate model. Climate Dynamics, 56(5-6), 1717–1752. https://doi.org/10.1007/s00382-020-05558-y.

Caldas-Alvarez, A., Feldmann, H., Lucio-Eceiza, E., & Pinto, J. G. (2023). Convection-permitting modelling of heavy precipitation in Alpine simulations with COSMO-CLM. Weather and Climate Dynamics, 4, 543-565.

Calzadilla, A., & Carr, T. (2020). Land degradation and food security: Water-erosion impacts and adaptation options. https://www.gtap.agecon.purdue.edu/resources/res_display.asp?RecordID=6088

Carter, J. G., Hincks, S., Vlastaras, V., Connelly, A., & Handley, J. (2018). European Climate Risk Typology. http://european-crt.org

Charousset, S., Oudjane, N., O'Reilly, R., Crespo del Granado, P., Barani, M., Perger, T., Zwickl-Bernhard, S., Auer, H., Olmos, L., Ramos, A., Graabak, I., Alvarez, E. F., Härtel, P., Frischmuth, F., Lepaul, S., Pinel, D., Wolfgang, O., Schledorn, A., Dominkovic, D. F., … Belsnes, M. (2023). Open ENTRANDE deliverable 6.2: Case study results (Final). Zenodo. https://doi.org/10.5281/zenodo.8289103

Chiambretti I, Chiaia B, Frigo B, Marello S, Maggioni M, Fantucci R, Bernabei M (2018). The 18th January 2017 Rigopiano avalanche disaster in Italy - Analysis of the applied forensic field investigation techniques, Environmental Science, Engineering, Geology.

Cissé, G., R. McLeman, H. Adams, P. Aldunce, K. Bowen, D. Campbell-Lendrum, S. Clayton, K.L. Ebi, J. Hess, C. Huang, Q. Liu, G. McGregor, J. Semenza, and M.C. Tirado (2022). Health, wellbeing, and changing community structures. In Climate Change 2022: Impacts, Adaptation, and Vulnerability (IPCC AR6 WG II, pp. 1041-1170). Cambridge University Press. https://doi.org/10.1017/9781009325844.009

Cobon, D. H., Williams, A. A. J., Power, B., et al. (2016). Risk-matrix approach useful in adapting agriculture to climate change. Climatic Change, 138, 173-189.

Conradt, T., Engelhardt, H., Menz, Ch., Vicente-Serrano, S., Farizo, B., Peña-Angulo, Dh., Domínguez-Castro, F., Eklundh, L., Jin, H., Boincean, B., Murphy, C., López-Moreno, J.. (2023). Cross-sectoral impacts of the 2018–2019 Central European drought and climate resilience in the German part of the Elbe River basin. Regional Environmental Change. 23. 10.1007/s10113-023-02032-3.

Copernicus Climate Change Service. (2022). Extreme heat – European State of the Climate 2022. https://climate.copernicus.eu/esotc/2022/extreme-heat

Copernicus Climate Change Service. (2025). Low winds – European State of the Climate 2021. https://climate.copernicus.eu/esotc/2021/low-winds

Copernicus Climate Change Service (C3S) & World Meteorological Organization. (2025). European State of the Climate 2024. https://doi.org/10.24381/14j9-s541

Costa, J. E. (1991). Nature, mechanics, and mitigation of the Val Pola landslide (Valtellina, Italy, 1987-1988). Zeitschrift für Geomorphologie, 35, 15-38.

Coppola, E., Sobolowski, S., Pichelli, E., Raffaele, F., Ahrens, B., Anders, I., Ban, N., Bastin, S., Belda, M., Belusic, D., Caldas-Alvarez, A., Cardoso, R. M., Davolio, S., Dobler, A., Fernandez, J., Fita, L., Fumiere, Q., Giorgi, F., Goergen, K., Güttler, I., Halenka, T., Heinzeller, D., Hodnebrog, Ø., Jacob, D., & Warrach-Sagi, K. (2020). A first-of-its-kind multi-model convection permitting ensemble for investigating convective phenomena over Europe and the Mediterranean. Climate Dynamics, 55, 3–34.

Cox, L. A. (2008). What's wrong with risk matrices? Risk Analysis, 28(2), 497-512.

Dallan, E., Borga, M., Fosser, G., Canale, A., Roghani, B., Marani, M., & Marra, F. (2024a). A Method to Assess and Explain Changes in Sub-Daily Precipitation Return Levels From Convection-Permitting Simulations. Water Resources Research, 60(5). https://doi.org/10.1029/2023WR035969

Dallan, E., Marra, F., Fosser, G., Marani, M., & Borga, M. (2024b). Dynamical Factors Heavily Modulate the Future Increase of Sub-Daily Extreme Precipitation in the Alpine-Mediterranean Region. Earth's Future, 12(12), e2024EF005185.

Dallan, E., Marra, F., Fosser, G., Marani, M., Formetta, G., Schär, C., & Borga, M. (2023). How well does a convection-permitting regional climate model represent the reverse orographic effect of extreme hourly precipitation? Hydrology and Earth System Sciences, 27(5), 1133–1149

Danish Meteorological Institute. (2024). Klimaatlas. https://www.dmi.dk/klimaatlas

Debernardi, A., Roveyaz, S., Borney, E., & Frigo, B. (2022). Land-planning and extreme snow events: The Buthier avalanche, Aosta Valley. International Journal of Environmental Sciences & Natural Resources, 31(2). https://doi.org/10.1908/IJESNR_2022.31.556312

Dee, D. P., Uppala, S. M., Simmons, A. J., Berrisford, P., Poli, P., Kobayashi, S., Andrae, U., Balmaseda, M. A., Balsamo, G., Bauer, P., Bechtold, P., Beljaars, A. C. M., van de Berg, L., Bidlot, J., Bormann, N., Delsol, C., Dragani, R., Fuentes, M., Geer, A. J., Haimberger, L., Healy, S. B., Hersbach, H., Hólm, E. V., Isaksen, L., Kållberg, P., Köhler, M., Matricardi, M., McNally, A. P., Monge-Sanz, B. M., Morcrette, J.-J., Park, B.-K., Peubey, C., de Rosnay, P., Tavolato, C., Thépaut, J.-N., & Vitart, F. (2011). The ERA-Interim reanalysis: Configuration and performance of the data assimilation system. Quarterly Journal of the Royal Meteorological Society, 137(656), 553–597.

Dolge, K., & Blumberga, D. (2021). Composite risk index for designing smart climate-energy policies. Environmental and Sustainability Indicators, 12, 100159.

Duijm, N. J. (2015). Recommendations on the design of risk matrices. Safety Science, 76, 21-31.

ESA. (2013). European System of Accounts 2010. Luxembourg.

ESPON-Climate. (2022). Updating and integrating climate datasets and maps (final report). European Commission.

European Commission, Joint Research Centre. (2020). EDO Combined Drought Indicator (v 1.6.1) [Dataset]. http://data.europa.eu/89h/e83b19ce-08c2-4e0c-b93a-5fd62be21e5e

European Parliament & Council of the EU. (2013). Regulation (EU) 1308/2013 establishing a common organisation of agricultural markets. Official Journal of the European Union.

Feyen L., Ciscar J.C., Gosling S., Ibarreta D., Soria A. (editors) (2020). Climate change impacts and adaptation in Europe. JRC PESETA IV final report. EUR 30180EN, Publications Office of the European Union, Luxembourg, ISBN 978-92-76-18123-1, doi:10.2760/171121, JRC119178.

George, J.-.-P., Bürkner, P.-.-C., Sanders, T.G.M., Neumann, M., Cammalleri, C., Vogt, J.V. and Lang, M. (2022). Long-term forest monitoring reveals constant mortality rise in European forests. Plant Biol J, 24: 1108-1119. https://doi.org/10.1111/plb.13469.

Glass, B., et al. (2000). Retour d'expérience sur l'avalanche du 9 février 1999 à Montroc. Inspection Générale de l'Environnement.

Gasparrini, A., Armstrong, B., & Kenward, M. G. (2010). Distributed lag non-linear models. Statistics in Medicine, 29, 2224-2234.

Gasparrini, A., Armstrong, B., & Kenward, M. G. (2012). Multivariate meta-analysis for non-linear and other multi-parameter associations. Statistics in Medicine, 31, 3821-3839.

Halsnæs, K., Dømgaard, M. L., Larsen, M. A. D., & Kaspersen, P. S. (2021). Modeldokumentation og vejledning for DTU SkadesØkonomi-modellen (in Danish).

Halsnæs, K., Kaspersen, P. S., & Drews, M. (2015). Key drivers and economic consequences of high-end climate scenarios. Climate Research, 64, 85-98.

Halsnæs, K., Larsen, M. A. D., Sunding, T. P., & Dømgaard, M. L. (2023). Value of advanced flood models and land-use data in cost-effective climate-change adaptation. Climate Services, 31.

Hanel, M., Rakovec, O., Markonis, Y., et al. (2018). Revisiting recent European droughts from a long-term perspective. Scientific Reports, 8, 9499.

Harris, I., Osborn, T. J., Jones, P., et al. (2020). Version 4 of the CRU TS high-resolution multivariate climate dataset. Scientific Data, 7, 109.

Hanley, N., Mourato, S., & Wright, R. E. (2001). Choice-modelling approaches for environmental valuation. Journal of Economic Surveys, 15, 435-462.

Hanley, N., Wright, R. E., & Adamowicz, V. (1998). Using choice experiments to value the environment. Environmental and Resource Economics, 11, 413-428.

Hempel, S., Frieler, K., Warszawski, L., Schewe, J., & Piontek, F. (2013). Trend-preserving bias correction—the ISI-MIP approach. Earth System Dynamics, 4, 219-236.

Hersbach, H., Bell, B., Berrisford, P., Biavati, G., Horányi, A., Muñoz Sabater, J., Nicolas, J., Peubey, C., Radu, R., Rozum, I., Schepers, D., Simmons, A., Soci, C., Dee, D., Thépaut, J-N. (2023): ERA5 hourly data on single levels from 1940 to present. Copernicus Climate Change Service (C3S) Climate Data Store (CDS).

Hess, S., & Palma, D. (2019). Apollo: Freeware for choice-model estimation. Journal of Choice Modelling, 32, 100170

Huang, S., & Koutroumpis, P. (2023). European multi-regional input–output data for 2008–2018. Scientific Data, 10(1), 1–9. https://doi.org/10.1038/s41597-023-02117-Y

ICPDR (2006). The Analysis of the Danube Floods 2006. https://www.icpdr.org/sites/default/files/The%20Analysis%20of%20the%20Danube%20Floods%202006%20FINAL.pdf

ICPDR (2010). 2010 Floods in the Danube River Basin. https://www.icpdr.org/sites/default/files/nodes/documents/icpdr_flood_report_2010.pdf

International Energy Agency. (2025). France: Energy mix. https://www.iea.org/countries/france/energy-mix

Intergovernmental Panel on Climate Change (IPCC). (2014). Climate Change 2014: Impacts, Adaptation, and Vulnerability (Working Group II, AR5). Cambridge University Press.

Intergovernmental Panel on Climate Change (IPCC). (2021). Climate Change 2021: The Physical Science Basis. Summary for Policymakers (Working Group I, AR6). Cambridge University Press.

Intergovernmental Panel on Climate Change (IPCC). (2022). Climate Change 2022: Impacts, Adaptation, and Vulnerability (Working Group II, AR6). Cambridge University Press. https://doi.org/10.1017/9781009325844

Jánoš, T., Ballester, J., Čupr, P., & Achebak, H. (2024). Country-wide analysis of heat- and cold-related mortality trends in the Czech Republic. Environmental Research, 53, 1–11.

Jakubis, M., & Jakubisová, M. (2023). Mountain Rescue Service—inevitable help at recreational and sport activities in mountainous areas in Slovakia. In Public Recreation and Landscape Protection – With Environment Hand in Hand? https://doi.org/10.11118/978-80-7509-904-4-0174

Junger, L., Hohensinner, S., Schroll, K., Wagner, K., & Seher, W. (2022). Land use in flood-prone areas and its significance for flood-risk management—A case study of Alpine regions in Austria. Land, 11(3), 392.

Karner, K., Mitter, H., & Schmid, E. (2019). The economic value of stochastic climate information for agricultural adaptation in a semi-arid region in

Austria. Journal of Environmental Management, 249, 109431. https://doi.org/10.1016/j.jenvman.2019.109431

Keuler, K., Radtke, K., Kotlarski, S., & Lüthi, D. (2016). Regional climate change over Europe in COSMO-CLM: Influence of emission scenario and driving global model. Meteorologische Zeitschrift, 25(2), 121-136.

Kind, J., Botzen, W. J. W., & Aerts, J. C. J. H. (2016). Accounting for risk aversion, income distribution and social welfare in cost–benefit analysis for flood-risk management. WIREs Climate Change, 8, e446.

Knutzen, F., Averbeck, P., Barrasso, C., Bouwer, L. M., Gardiner, B., Grünzweig, J. M., Hänel, S., Haustein, K., Johannessen, M. R., Kollet, S., Pietikäinen, J.-P., Pietras-Couffignal, K., Pinto, J. G., Rechid, D., Rousi, E., Russo, A., Suarez-Gutierrez, L., Wendler, J., Xoplaki, E., & Gliksman, D. (2025). Impacts and damages of the European multi-year drought and heat event 2018–2022 on forests: A review. Natural Hazards and Earth System Sciences. https://doi.org/10.5194/nhess-25-77-2025

Kottegoda, N. T., & Rosso, R. (2008). Applied Statistics for Civil and Environmental Engineers.

Lancaster, K. J. (1966). A new approach to consumer theory. Journal of Political Economy, 74(2), 132-157.

Leutwyler, D., Fuhrer, O., Lapillonne, X., Lüthi, D., & Schär, C. (2016). Towards European-scale convection-resolving climate simulations with GPUs: A study with COSMO 4.19. Geoscientific Model Development, 9(9), 3393-3412.

Libertino, A., Ganora, D., & Claps, P. (2019). Evidence for increasing rainfall extremes remains elusive at large spatial scales: The case of Italy. Geophysical Research Letters, 46(13), 7437-7446.

Li, J., & van de Lindt, J. (2025). Climate adaptation matrix concept for multidisciplinary community resilience. Natural Hazards Review, 26(2). https://doi.org/10.1061/NHREFO.NHENG-2122

Lobell, D. B., & Gourdji, S. M. (2012). The influence of climate change on global crop productivity. Plant Physiology, 160(4), 1686-1697. https://doi.org/10.1104/pp.112.208298

Löffler, K., Moskalenko, N., Herpich, P., Hanto, J., Hainsch, K., Bornemann, J., Diesing, A., Dupke, R., & Barani, M. (2024). The European Energy Vision 2060 (EU EnVis-2060): Scenario Parametrization [Dataset]. Zenodo. https://doi.org/10.5281/zenodo.13710869.

Lorenzoni, N., & Raich, M. (2021). Long-term impact of the Galtür avalanche on the public-health system. Journal of Emergency Management, 19(2), 197-208. https://doi.org/10.5055/jem.0570

Mainar Causapé, A., Philippidis, G., & Caivano, A. (2018). BioSAMs for the EU Member States: Constructing social accounting matrices with a detailed disaggregation of the bio-economy. https://doi.org/10.2760/811691

Manski, C. F. (1977). The structure of random-utility models. Theory and Decision, 8(3), 229-254.

MARD (Ministry of Agriculture and Rural Development). (2016). National Program for the Rehabilitation of the Main Irrigation Infrastructure in Romania. https://www.madr.ro/... (accessed 27 May 2025).

Marani, M., & Ignaccolo, M. (2015). A metastatistical approach to rainfall extremes. Advances in Water Resources, 79, 121-126.

Mariel, P., Hoyos, D., Meyerhoff, J., Czajkowski, M., Dekker, T., Glenk, K., Jacobsen, J. B., Liebe, U., Olsen, S. B., Sagebiel, J., & Thiene, M. (2021). Environmental valuation with discrete choice experiments: Guidance on design, implementation and data analysis (p. 129). Springer Nature.

Marra, F., Borga, M., & Morin, E. (2020). A unified framework for extreme sub-daily precipitation frequency analyses. Geophysical Research Letters, 47(18).

Marra, F., Zoccatelli, D., Armon, M., & Morin, E. (2019). A simplified MEV formulation to model extremes from multiple non-stationary processes. Advances in Water Resources, 127, 280-290.

Martel, J.-L., Mailhot, A., & Brissette, F. (2020). Projected changes in 100-yr sub-daily, daily, and multiday precipitation extremes. Journal of Climate, 33(3), 1089-1103.

McFadden, D. (1974). Conditional logit analysis of qualitative choice behaviour. In P. Zarembka (Ed.), Frontiers in Econometrics (pp. 105-142). Academic Press.

Meza, I., Hagenlocher, M., Naumann, G., Vogt, J., & Frischen, J. (2019). Drought-vulnerability indicators for global-scale drought-risk assessments. EUR 29824 EN.

Micu, D., Dumitrescu, A., Cheval, S., & Birsan, M.-V. (2015). Climate of the Romanian Carpathians: Variability and Trends. Springer Atmospheric Sciences.

Mitter, H., & Schmid, E. (2021). Informing groundwater policies in semi-arid agricultural regions under stochastic climate impacts. Ecological Economics, 177.

Nabat, P., Somot, S., Cassou, C., Mallet, M., Michou, M., Bouniol, D., Decharme, B., Drugé, T., Roehrig, R., & Saint-Martin, D. (2020). Modulation of radiative aerosol effects by atmospheric circulation over the Euro-Mediterranean region. Atmospheric Chemistry and Physics, 20(14), 8315-8349.

Navarro, D., Lizundia-Loiola, J., Paz, J., Abajo, B., Cantergiani, C., García, G., & Feliu, E. (2022). Updating and Integrating CLIMATE Datasets and Maps. Final Report. ESPON 2020.

Nechifor, V., Calzadilla, A., Bleischwitz, R., Winning, M., Tian, X., & Usubiaga, A. (2020). Steel in a circular economy: Global implications of a green shift in China. World Development, 127, 104775.

Noël, B., Van de Berg, W. J., Van Meijgaard, E., Kuipers Munneke, P., Van de Wal, R. S. W., & Van den Broeke, M. R. (2015). Evaluation of the updated regional climate model RACMO2.3: Summer snowfall impact on the Greenland Ice Sheet. The Cryosphere, 9(5), 1831-1844.

Ortner, G., Michel, A., Kropf, C. M., & Larcher, L. (2025). Assessing the impacts of climate change on snow-avalanche-induced risk in alpine regions. Natural Hazards. https://doi.org/10.1007/s11069-025-07229-9

Palmer, W. C. (1965). Meteorological Drought. Research Paper 45, U.S. Weather Bureau.

Papathoma-Koehle, M., Promper, C., Bojariu, R., Cica, R., Sik, A., Perge, K., Laszlo, P., Czikora, E. B., Dumitrescu, A., Turcus, C., Birsan, M. V., & Glade, T. (2016). A common methodology for risk assessment and mapping for South-East Europe: An application for heat-wave risk in Romania. Natural Hazards, 82, 89-109.

Peace, C. (2017). The risk matrix: Uncertain results? Policy and Practice in Health and Safety, 15(2), 131-144.

Pérez-Guillén, C., Techel, F., Volpi, M., & van Herwijnen, A. (2025). Assessing the performance and explainability of an avalanche-danger forecast model. Natural Hazards and Earth System Sciences, 25, 1331-1351.

Peters, J. C. (2016). The GTAP-Power database: Disaggregating the electricity sector in the GTAP database. Journal of Global Economic Analysis, 1(1), 209-250.

Peters, M., & Pikkemaat, B. (2008). Crisis management in Alpine winter-sports resorts—The 1999 avalanche disaster in Tyrol. Journal of Travel & Tourism Marketing, 19(2-3). https://doi.org/10.1300/J073v19n02_02

Potopová, V., Trnka, M., Vizina, A., Semerádová, D., Balek, J., Chawdhery, M. R. A., Musiolková, M., Pavlík, P., Možný, M., Štěpánek, P., & Clothier, B. (2022). Projection of 21st-century irrigation-water requirements for sensitive agricultural crops across the Czech Republic. Agricultural Water Management, 262, 107337.

Rapisarda, A., & Pranzo, A. M. R. (2021). Mapping the avalanche risk: From survey to cartographic production. The avalanche bulletin of the Meteomont Service of the Alpine Troops Command. Proceedings of the International Cartographic Association, 4, 92. https://doi.org/10.5194/ica-proc-4-92-2021

Reisner, G. (2014). Datenerhebung, Datenaufbereitung und fachliche Darstellung des Bewässerungsbedarfs der landwirtschaftlichen Beregnung (No. 9-W-1099/315-2014). Amt der Burgenländischen Landesregierung, Abt. 9 – Wasser- und Abfallwirtschaft, Eisenstadt.

Reynaert, S., De Boeck, H. J., Verbruggen, E., Verlinden, M., Flowers, N., & Nijs, I. (2021). Risk of short-term biodiversity loss under more persistent precipitation regimes. Global Change Biology, 27, 1614-1626.

Rockel, B., Will, A., & Hense, A. (2008). The regional climate model COSMO-CLM (CCLM). Meteorologische Zeitschrift, 17(4), 347-361.

Roson, R., & Sartori, M. (2016). Estimation of climate-change damage functions for 140 regions in the GTAP-9 database. Journal of Global Economic Analysis, 1(2), 78-115.

ROWATER, 2023. Danube River flood risk management plan (https://rowater.ro/wp-content/uploads/2023/09/12-PMRI-Dunare-1.pdf)

Sauermoser, S. (2006). Avalanche-hazard mapping—30 years' experience in Austria. In Proceedings of the 2006 International Snow Science Workshop, Telluride, Colorado (pp. 1-6).

Scarpa, R., Thiene, M., & Train, K. (2008). Utility in willingness-to-pay space: Addressing random-scale effects in destination choice to the Alps. American Journal of Agricultural Economics, 90(4), 994-1010.

Schönhart, M., Schmid, E., & Schneider, U. A. (2011). CropRota: A crop-rotation model to support integrated land-use assessments. European Journal of Agronomy, 34, 263-277.

Sen, A. (1986). Commodities and capabilities. The Economic Journal, 96(383), 820-822.

Sepulcre-Canto, G., Horion, S., Singleton, A., Carrão, H., & Vogt, J. (2012). Development of a combined drought indicator to detect agricultural drought in Europe. Natural Hazards and Earth System Sciences, 12, 3519-3531.

Sera, F., Armstrong, B., Blangiardo, M., & Gasparrini, A. (2019). An extended mixed-effects framework for meta-analysis. Statistics in Medicine, 38(29), 5429-5444.

Sørland, S. L., Brogli, R., Pothapakula, P. K., Russo, E., Van de Walle, J., Ahrens, B., Anders, I., Bucchignani, E., Davin, E. L., Demory, M.-E., Dosio, A., Feldmann, H., Früh, B., Geyer, B., Keuler, K., Lee, D., Li, D., van Lipzig, N. P. M., Min, S.-K., Panitz, H.-J., Rockel, B., Schär, C., Steger, C., & Thiery, W. (2021). COSMO-CLM regional climate simulations in the CORDEX framework: A review. Geoscientific Model Development, 14(8), 5125–5154

Stiglitz, J., Sen, A., & Fitoussi, J.-P. (2009). Report by the Commission on the Measurement of Economic Performance and Social Progress.

Strauss, F., Formayer, H., & Schmid, E. (2013a). High-resolution climate data for Austria (2008-2040) from a statistical climate-change model. International Journal of Climatology, 33, 430-443.

Strauss, F., Moltchanova, E., & Schmid, E. (2013b). Spatially explicit modelling of long-term drought impacts on crop production in Austria. American Journal of Climate Change, 2, 1-11.

Szymalski, W., & Kassenberg, A. (2022). Determining the climate risk in the city using the risk-matrix method—Examples from Poland. Studia Ecologiae et Bioethicae, 20(3), 75-90.

Thissen, M., van Oort, F., & Diodato, D. (2013). Integration and convergence in regional Europe: European regional trade flows 2000-2010. Working paper, Netherlands Environmental Assessment Agency.

Thurstone, L. L. (1927). A law of comparative judgment. Psychological Review, 34, 273-286.

Train, K. E., & Weeks, M. (2005). Discrete-choice models in preference space and willingness-to-pay space. In R. Scarpa & A. Alberini (Eds.), Application of Simulation Methods in Environmental and Resource Economics (pp. 1-16). Springer.

Urban, A., Fonseca-Rodríguez, O., Di Napoli, C., & Plavcová, E. (2022). Temporal changes of heat-attributable mortality in Prague, Czech Republic (1982–2019). Urban Climate, 44, 101197.

van Daalen, K. R., Tonne, C., Semenza, J. C., Rocklöv, J., Markandya, A., Dasandi, N., Jankin, S., Achebak, H., Ballester, J., Bechara, H., Beck, T. M., Callaghan, M. W., Carvalho, B. M., Chambers, J., Pradas, M. C., Courtenay, O., Dasgupta, S., Eckelman, M. J., Farooq, Z., … Lowe, R. (2024). The 2024 Europe report of the Lancet Countdown on health and climate change: unprecedented warming demands unprecedented action. The Lancet Public Health, 9(7), e495–e522. https://doi.org/10.1016/S2468-2667(24)00055-0.

van der Schrier, G., Barichivich, J., Briffa, K. R., & Jones, P. D. (2013). A scPDSI-based global dataset of dry- and wet-spell duration (1901-2009). Journal of Geophysical Research: Atmospheres, 118, 4025-4048.

Valt, M., Chiambretti, I., & Zasso, R. (2009). 1985–2009: Twenty-five years of avalanche accidents in Italy. Technical report.

Vautard, R., Van Aalst, M., Boucher, O., Drouin, A., Haustein, K., Kreienkamp, F., Van Oldenborgh, G. J., Otto, F. E. L., Ribes, A., Robin, Y., Schneider, M., Soubeyroux, J.-M., Stott, P., Seneviratne, S. I., Vogel, M. M., & Wehner, M. (2020). Human contribution to the record-breaking June and July 2019 heatwaves in Western Europe. Environmental Research Letters, 15(9), 094077.

Vésier, C., & Urban, A. (2023). Gender inequalities in heat-related mortality in the Czech Republic. International Journal of Biometeorology, 67(8), 1373-1385.

Vicedo-Cabrera, A. M., Sera, F., & Gasparrini, A. (2019). Hands-on tutorial on modelling frameworks for projections of climate-change impacts on health. Epidemiology, 30(3), 321-329.

Vicedo-Cabrera, A. M., Scovronick, N., Sera, F., Royé, D., Schneider, R., Tobias, A., Åström, C., Guo, Y., Honda, Y., Hondula, D. M., Abrutzky, R., Tong, S., Coelho, M. de S. Z. S., Saldiva, P. H. N., Lavigne, E., Correa, P. M., Ortega, N. V., Kan, H., Osorio, S., Kyselý, J., Pascal, M., Nunes, B., Ragettli, M. S., Weisskopf, M. G., Zanobetti, A., Schwartz, J., Lee, W., Chen, B.-Y., Yang, J., Chen, R., Xu, Z., Vardoulakis, S., Golding, N., Arbuthnott, K. G., Kinney, P. L., Tirado, M. C., Lowe, R., & Gasparrini, A. (2021). The burden of heat-related mortality attributable to recent human-induced climate change. Nature Climate Change, 11(6), 492–500.

Voiculescu, M., Török-Oance, M., Chiroiu, P., & Popescu, F. (2023). Snow avalanches in relation to tourism and transportation in the Făgăraş Mountains, Romanian Carpathians. Anthropocene, 44, 100407. https://doi.org/10.1016/j.ancene.2023.100407

Weiss, F., von Wehrden, H., & Linde, A. (2024). Long-term drought triggers severe declines in carabid beetles in a temperate forest. Ecography.

Wells, N., Goddard, S., & Hayes, M. J. (2004). A self-calibrating Palmer Drought Severity Index. Journal of Climate, 17, 2335-2351.

Williams, J. P. (1995). The EPIC model. In V. P. Singh (Ed.), Computer Models of Watershed Hydrology (pp. 909-1000). Water Resources Publications.

Winning, M., Calzadilla, A., Bleischwitz, R., & Nechifor, V. (2017). Towards a circular economy: Insights from the ENGAGE-materials model for the iron and steel industry. International Economics and Economic Policy, 14(3), 383-407.

Wood, S. (2006). Generalized Additive Models: An Introduction with R. Chapman & Hall/CRC.

World Climate Research Programme. (2025). CMIP Phase 6 (CMIP6). https://wcrp-cmip.org/cmip-phases/cmip6/

Funded by
the European Union

CROSSEU Partners

Meteo Romania	UEA University of East Anglia	WORLD METEOROLOGICAL ORGANIZATION
Università degli Studi di Padova TESAF	UCL	K&I Conoscenza e Innovazione
Helmholtz-Zentrum hereon	LGi sustainable innovation	eDF
BOKU	DTU	WEMC World Energy & Meteorology Council
UK Research and Innovation	University of Bucharest	CZU

Funded by the European Union